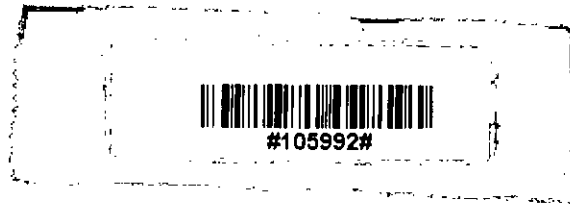# Contact Stresses in Conical Rollers under Normal and Tangential Loads

by

Mohammad Wasim Akram

#105992#

MASTER OF SCIENCE IN MECHANICAL ENGINEERING

Department of Mechanical Engineering

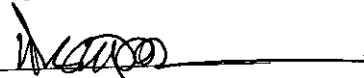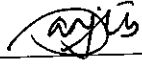BANGLADESH UNIVERSITY OF ENGINEERING AND TECHNOLOGY

DHAKA, BANGLADESH

2008

Certificate of Approval

The thesis titled "Contact Stresses in Conical Rollers under Normal and Tangential Loading", Submitted by Mohammad Wasim Akram, Roll No.:100610015P, Session: October, 2006 to the Department of Mechanical Engineering of Bangladesh University of Engineering and Technology has been accepted as satisfactory for partial fulfillment of the requirements of the degree of Master of Science in Mechanical Engineering on 25.11.2008.

BOARD OF EXAMINERS

1.   Chairman

Dr. Abu Rayhan Md. Ali
Professor and Head
Department of Mechanical Engineering
BUET, Dhaka-1000
(Supervisor)

2.   Member

Dr. Dipak Kanti Das
Professor
Department of Mechanical Engineering
BUET, Dhaka-1000

3.   Member

Dr. Sanjib Chandra Chowdhury
Assistant Professor
Department of Mechanical Engineering
BUET, Dhaka-1000

4.   25-11-2008   Member
(External)

Dr. Mohammed Alauddin
Professor and Head
Department of Mechanical Engineering
DUET, Gazipur

ii

CANDIDATE'S DECLARATION

It is hereby declared that this thesis or any part of it has not been submitted elsewhere for the award of any degree or diploma.

Signature of the candidate

Wasim Akram

Mohammad Wasim Akram

Table of Contents

List of Figures

List of Symbols used in this paper

Symbols

a	Half Width of Contact area
A,B	Major and Minor axes respectively of the ellips
b	Geometric constant
E_1	Young Modulus of first roller
E_2	Young Modulus of first roller
F	Length of the section, perpendicular to the cone surface, at t projected on the Y-Z plane passing through the axis of the cone
F	Applied Force
K	Constant
σ_x	Stress Component in X direction
σ_z	Stress Component in Z direction
σ_y	Stress Component in YX direction
τ_{xz}	Shear Stress in X- Z Plane
ε_x	Strain in X direction
ε_z	Strain in Z direction
γ_{xz}	Shear Strain in X-Z plane
t	Position of cut plane from apex of the cone
φ	Vertex Angle
R	Radius of Curvature
m_1	Material Constants of the first cone
m_2	Material Constants of the first cone
v	Poisson's Ratio
μ	Coefficient of Friction

$P(x)$	Normal Pressure Distribution
$Q(x)$	Tangential Traction Distribution
l	Contact length
r_1	Radius of the each conical roller at tip
r_2	Radius of the each conical roller at bigger end
P_{max}	Maximum Pressure
S	Distance from cone apex

ACKNOWLEDGEMENT

Abstract

Load transfer between components in engineering assemblies often causes very high localized stresses generally called contact stresses. The contact stresses are highly concentrated close to the contact region and decrease rapidly in intensity with distance from the point of contact, so that the region of practical interest lies close to the contact interface. The nature of stresses arising from the contact between two bodies is of great importance and attracted the attention of many researchers. But most of them were analyzed using simple geometries i.e. sphere on plane, sphere on sphere, and cylinder on cylinder. This work has focused on complicated geometries rather than simple geometries by considering conical rollers in contact. When two geometrical and materially identical conical rollers come into contact with each other under the application of a uniform compressive load in rolling, the contact patch appears in the form of a trapezoid, in contrast with two cylinders where the contact area is rectangle. The trapezoid shape of the contact area arises because the radius of curvature of either cone varies along the axial direction and contact length. So, radius of curvature will be a function of vertex angle as well as length of the contact, where in the case of cylindrical contact it is same through out the cross section of the contact. The work has also considered tangential loading along with normal loading. The stress functions have been solved numerically to find stress distribution with variation of contact geometries. Stress components in different axes have been investigated with variation of contact geometries for both normal and tangential loading. Half width distribution, pressure distribution and stress distribution along the length have been also investigated for different vertex angle as well as for different materials. The validity of numerical results has been done using a commercial finite element simulating software, Ansys. The results of the numerical technique are found to be consistent with the finite element simulations in predicting pressure, its distribution and the contact stresses in conical rollers.

CHAPTER ONE
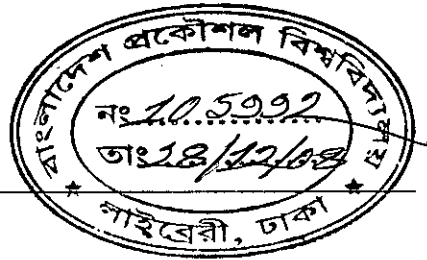
INTRODUCTION

1.1 General

Mechanical design is one of the most important problems which can confront a practicing engineer. The critical task of synthesis can be both distasteful and elusive because of the complex relationship existing among factors associated with the definition of design itself. Mechanical design can be defined as the selection of material and geometry which satisfies specified and implied functional requirements while remaining within the confines of inherently unavoidable limitations. Hence the basic problem of mechanical design is considerably more difficult that the problem of mechanical analysis, since generally for the later both geometry and materials are assumed to be constants and limitations such space restrictions are of no significance. The problem is much more difficult if there is any stress raiser or crack propagation parameters. The mechanical design as stated above may need specify its utilization. So for mechanical design objectives and justification is important issues.

This chapter includes overview of the thesis work, objectives of the thesis work, justification of the work as well as outline of the thesis paper.

1.2 Introduction

Load transfer between components in engineering assemblies often causes very high localized stresses, generally called contact stresses, which lead to component failure by different forms of surface contact fatigue. Consequently, the evaluation of contact area geometries, pressure distribution, stresses is imperative to prevent premature failure such as pitting, spalling, false brinelling.

The analysis of contact stresses between cylindrical elements or spherical elements has attracted the attention of many researchers. There are lots of works on these simple geometries. However with advent of more intricate components in machines,

1

the importance of understanding the contact problems for complex geometries evolved. This thesis work is based on more complex geometries rather than simple geometries by considering conical rollers are in contact. The shape of deformed contact area has been in trapezoid form which is in contrast with cylindrical contact where deformed shape is rectangular. For this reason, the radius of curvature is a function of vertex angle and length from tip, where it has been considered. So, equations used for cylindrical contact are not sufficient to describe the stresses raised from contact of conical rollers. There is variable half width and radius of curvature in this case. On the hand, in case of contact there is always some sliding which leads to tangential traction between interfaces of conical rollers. So the system has become more complex with both normal and tangential loading. In this work, the stresses due to conical rollers in contact with application of both normal and tangential loading have been solved using numerical technique. The results obtained from numerical technique has been verified a commercially available finite element simulating software ANSYS. The distribution of stresses has been observed for different contact geometrical parameters, materials and loading conditions.

1.3 Objectives Of The Thesis Work

The main objectives behind this thesis paper are listed below:

1) To develop a mathematical model for solve contact problems between two conical rollers under normal and tangential loads to obtain maximum contact pressure, contact stresses and their distribution along different axes.

2) To solve the above mentioned analytical models, a numerical method will be used.

3) The above mentioned results will be verified using a commercial finite element simulating software, ANSYS for similar loading conditions.

4) The above mentioned methods will be used for different vertex angle and for different materials.

1.4 Justification Of The Thesis Work

Contact problems are very common in engineering application. As a result, there is a lot of researches available on this. Most of them are based on approximation of simple geometries like sphere to sphere contact, cylinder to cylinder contact, and cylinder to

plane contact. But there are very few researches available on complex geometries like conical rollers. The previous researches only consider normal loading for their analysis, no tangential traction has been considered yet. This paper mainly focused on stress fields those obtained from combination of normal and tangential loading. On the hand, this work has also considered finite element simulation, which is also new.

Another fundamental reason for studying 'conical member in contact' is to address the contact problems in various applications such as rolling mills, gears, and tapered rollers bearings and in particular, traction drives. Earlier researches on these were based on simple geometries, though these are not. So, more accurate results will be if this work is being put into implementation.

1.5 Previous Works on Conical Contact Rollers

'We can confine our attention to that part of each body which is very close to the point of contact, since here the stresses are extremely great compared with those occurring elsewhere, and consequently depend only to the smallest extent on the forces applied to other parts of the bodies.' - Heinrich Hertz [1], the leading researcher in the field of contact mechanics. The subject of contact mechanics may be said to have started in 1882 with the publication by Hertz of his classic paper *"On the contact of elastic solids"*. His interest in the problem was aroused by experiments on optical interference between glass lenses. The question arose whether elastic deformation of the lenses under the action of the force holding them in contact could have a significant influence on the pattern of interference fringes. He computed the load distribution over the contact area and provided the mathematical models for the stress field using a potential function for the case of spherical contact. He deduced that an ellipsoidal distribution of pressure would satisfy the boundary conditions of the problem for the case of spherical contact. He verified his analytical results by running a series of experiments.

However, Hertz only considered spherical contact for his analysis. And for a long time there was no research on contact problems. Every contact problems were solved on Hertz spherical contact theory. In 1936, Lundberg [2] analyzed the problem when two bodies of different geometries come in contact. He calculated the stresses for the

case of a cylinder and a spherical ball pressed on a flat plate and verified his findings by photo elastic technique.

Hertz and Lundberg considered only normal loading for their analysis. But for case of contact between two rotating elements, there is always tangential traction except pure rolling. So in that case there exist some tangential loading. Mindlin [3] investigated the stress distribution due to tangential load when one elastic body slides over the other across the contact area for the case of cylindrical contact. Mindlin found that the stresses on the bounding curve of the contact area due to bounding curve are infinite and consequently a state of impending slipping prevails.

In 1953 Smith and Liu [4] studied the contact between parallel rollers in combined rolling and sliding for spherical contact only. Though there are lots of works on gear contact, cam – follower contacts and so on, but all of theses were based on simple contact geometries. With advent of time more complex geometries evolved and hence researches were needed on complex geometries. Al In 2004 Al Zain [5] analyzed the contact problem between two conical rollers under the normal load for first time In 2006 Shakoor [6] also agreed with Zain's proposal while he was doing research on special cam follower contact problems. Later Litvin [7] has used Zain's proposal for his research of bevel gear.

1.6 Outline Of Thesis Work

The thesis paper essentially consists of a brief introduction of contact, elasticity and stress distribution and maximum pressure distribution due to contact.

In chapter two some literature background are included in regard to contact mechanics. Necessary theories have been discussed and also useful mathematical relations have been derived for using in numerical techniques.

In chapter three Numerical technique and Finite Element Simulation have been discussed involving geometrical models, loading conditions and boundary conditions. For FE analysis

In chapter four, results obtained from numerical and FE analysis have been included with discussions. The results have been shown graphically, including stress

4

distribution vs. contact geometries for numerical solution. The validity of the numerical results also has been shown in compare with results from ANSYS.

In chapter five a conclusion was drawn in regard to whole thesis work. In this chapter there have been some further recommendations for research on same in future.

CHAPTER TWO

THEORETICAL BACKGROUND

2.1 General

This chapter is concerned with the some theoretical aspects which have been used for this thesis work. Derivations of the formulas, definition of some basic concepts have been described in this chapter. All of these have been concerned with the stresses which arise when the surface of two bodies are brought into contact.

2.2   Elasticity

Almost all engineering materials possess to a certain extent the property of elasticity. If the external forces producing deformation do not exceed a certain limit, the deformation disappears with the removal of the forces. Throughout the present work it has been assumed that the bodies undergoing the action of external forces are perfectly elastic i.e. that they resume their initial form completely after removal of the forces.

Atomic structure will not be considered here. It will be assumed that the matter of an elastic body is homogenous and continuously distributed over its volume so that the smallest element cut from the body possesses the same specific physical properties as the body. It has also been assumed that materials are isentropic, i.e. that the elastic properties are same in all directions.

2.3   Components of Stress and Strains

In discussing the deformation of an elastic body it will be assumed that there are enough constraints to prevent the body from moving as a rigid body so that so displacements of the particles of the body are possible without a deformation of it.

The small displacement of a particles of a deformed body will first resolve into components u, v, w parallel to the coordinate axes x, y, z respectively. It has been assumed that the components are very small quantities varying continuously over the

volume of the body. Consider a small element dx dy dz of an elastic body (Figure 2.1).

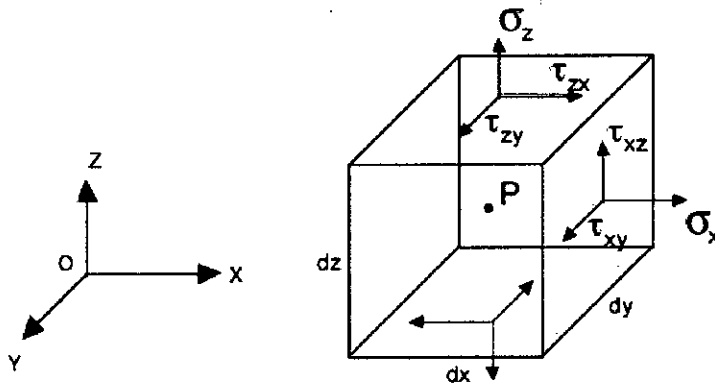

Figure 2.1: Components of stress

If the body undergoes a deformation and u, v, w are the component of the point P, the displacement in the x direction f an adjacent point A on the axis is to the first order in dx,

$$u + \frac{\delta u}{\delta x} dx$$

due to increase ($\delta u / \delta x$)dx of the function u with increase of the coordinate x. The increase in length of the element PA due to deformation is therefore ($\delta u / \delta x$)dx. Hence the unit elongation at point O in the x direction is $\delta u / \delta x$.
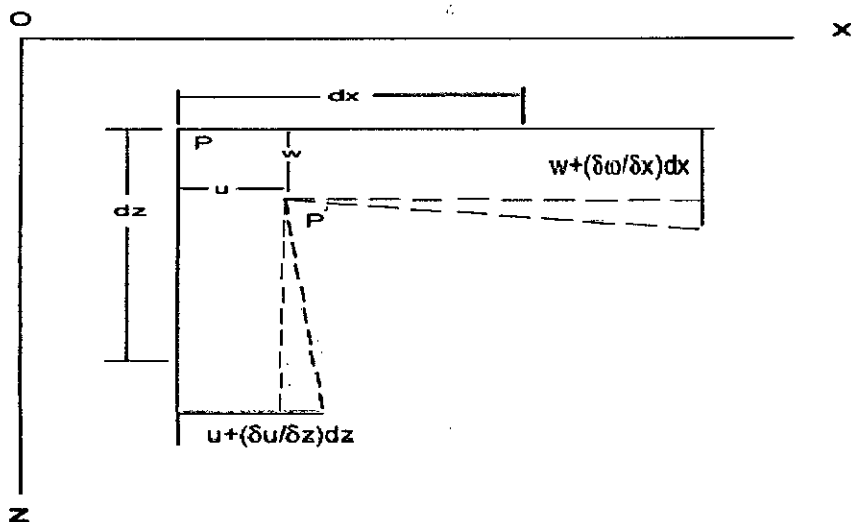
Figure 2.2: Components of strains

In the same manner it can be shown that the unit elongation in z direction is $\delta w / \delta z$. From figure 2.2, it has also been shown that shearing strain in xz plane –

7

$$\gamma_{xz} = \frac{\delta u}{\delta z} + \frac{\delta w}{\delta x} \qquad \text{-------- (2.1)}$$

2.4   Plane Stress and Plane Strain

If a thin plate is loaded by the forces applied at the boundary, parallel to the plane of the plate and distributed uniformly over the thickness (Figure 2.3), the stress components σ_y, τ_{xy}, τ_{zy} are zero on both faces of the plate, and it may be assumed tentatively, that they are zero also within the plate. The state of stress is then specified by the σ_x, σ_z and τ_{xz} only and called Plane Stress.
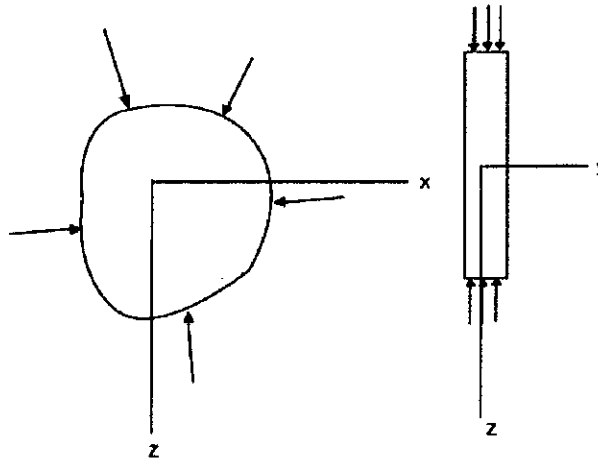
Figure 2.3: Example of Plane Stress

A similar simplification is possible at the other extreme when the dimension of the body in 'y' direction is very large. In this case strain in 'y' direction is assumed zero and following relation can be written –

$$\sigma_y = v \left(\sigma_x + \sigma_z \right) \text{-------- (2.2)}$$

The contact stress for conical roller will be solved based on Plane Strain approximation as the contact length is very large so strain in that direction has not been considered.

2.5   Hooke's Law

Linear relation between the components of stress and the components of strain are known generally as **Hooke's Law.** Imagine an elemental rectangular parallelepiped with the sides parallel to the coordinate axes and submitted to the action of normal stress σ_x uniformly distributed over two opposite sides as in the tensile test. The unit elongation of the element up to the proportional limit is given by

$$\varepsilon_x = \frac{\sigma_x}{E} \qquad \text{------- (2.3)}$$

in which E is the modulus of elasticity in tension. This extension of the element in the x direction is accompanied by lateral strain components (contraction)

$$\varepsilon_y = -v\frac{\sigma_x}{E} \qquad \varepsilon_z = -v\frac{\sigma_x}{E} \qquad \text{---------- (2.4)}$$

in which **v** is a constant called Poisson's ratio. Now if the above element is submitted simultaneously to the action of normal stresses σ_x and σ_z over the sides, the resultant components of strain can be obtained from equation (2.3) and (2.4) for the case of plane strain –

$$\varepsilon_x = \frac{1}{E}\left[\sigma_x - v\left(\sigma_y + \sigma_z\right)\right]$$

$$\varepsilon_z = \frac{1}{E}\left[\sigma_z - v\left(\sigma_x + \sigma_y\right)\right] \text{------------- (2.5)}$$

$$\gamma_{xz} = \frac{1}{G}\tau_{xz}$$

From here we can write -

$$\epsilon_x = \frac{1}{E}\{(1 - v^2)\sigma_x - v(1 + v)\sigma_z\}$$

$$\epsilon_z = \frac{1}{E}\{(1 - v^2)\sigma_z - v(1 + v)\sigma_x\} \qquad \text{------- (2.6)}$$

$$\gamma_{xz} = \frac{1}{G}\tau_{xz} = \frac{2(1 + v)}{E}\tau_{xz}$$

2.6   Equations of Equilibrium

The equilibrium of a small rectangular block edges h, k and unity. The stresses acting on the faces 1, 2, 3, 4 and their positive directions are indicated in the figure. On account of the variation of stress throughout the material, the value of, for instance, σ_x, σ_z, τ_{xz} refer to the point x, z, the midpoints of the faces are denoted by $(\sigma_x)_1$, $(\sigma_x)_2$ etc. Since the faces are very small, the corresponding forces are obtained by multiplying these values by the areas of the faces on which they act.
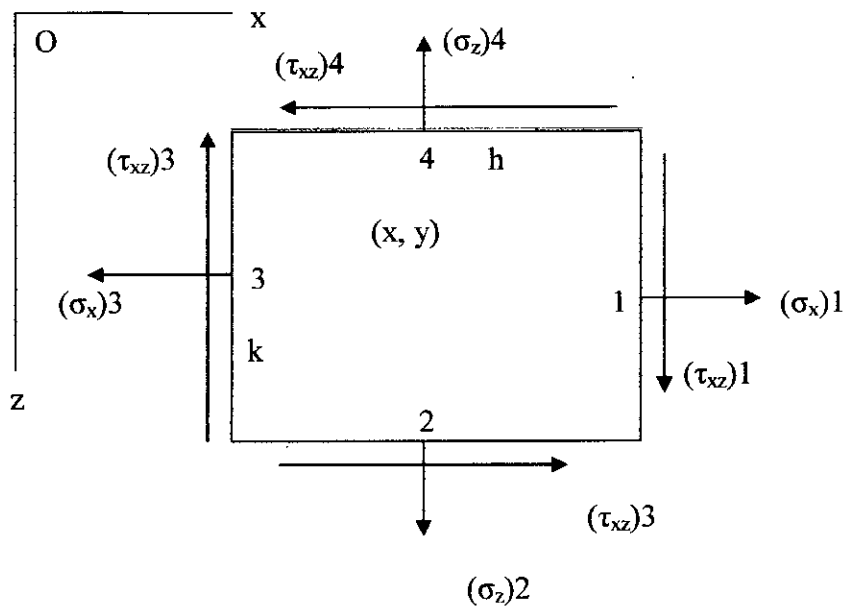
9

Figure 4: Derivation for Equations of equilibrium

Neglecting body force, we can write the equation of equilibrium for forces in x direction is

$$(\sigma_x)_1 k - (\sigma_x)_3 k + (\tau_{xz})_2 h - (\tau_{xz})_4 h = 0 \ \text{------} \ (2.7)$$

Dividing by **hk**,

$$\frac{(\sigma_x)_1 - (\sigma_x)_3}{h} + \frac{(\tau_{xz})_2 - (\tau_{xz})_4}{k} = 0$$

If now the block is taken smaller and smaller, that is $h \to 0, k \to 0$ the limit of

$\dfrac{(\sigma_x)_1 - (\sigma_x)_3}{h}$ is $\dfrac{\delta \sigma_x}{\delta x}$ by the definition of such a derivative. Similarly

$\dfrac{(\tau_{xz})_2 - (\tau_{xz})_4}{k}$ becomes $\dfrac{\delta \tau_{xz}}{\delta z}$. The equation of equilibrium for forces in z direction

is obtained in the same manner. Thus –

$$\frac{\delta \sigma_x}{\delta x} + \frac{\delta \tau_{xz}}{\delta z} = 0$$
$$\frac{\delta \sigma_z}{\delta z} + \frac{\delta \tau_{xz}}{\delta x} = 0$$
--------- (2.8)

2.7 Compatibility Equations

The mathematical formulation of the condition for compatibility of stress distribution with the existence of continuous function u, v, w defining the deformation will be obtained from Eqs. (2.1). for two dimensional problems we consider three strain components, namely –

$$\varepsilon_x = \frac{\delta u}{\delta x} \qquad \varepsilon_z = \frac{\delta w}{\delta z} \qquad \text{and} \qquad \gamma_{xz} = \frac{\delta u}{\delta z} + \frac{\delta w}{\delta x} \qquad \text{------- (2.9)}$$

These three strain components are expressed by two functions 'u' and 'w' hence they can't be arbitrarily taken, and there exists a certain relation between the strain components that can be easily obtained from (2.9) . Differentiating the first Eqs (2.9) twice with respect to z, and third one with respect to x. and once with respect to z we find –

$$\frac{\delta^2 \varepsilon_x}{\delta z^2} + \frac{\delta^2 \varepsilon_z}{\delta x^2} = \frac{\delta^2 \gamma_{xz}}{\delta x \delta z} \qquad \text{------ (2.10)}$$

This is the compatibility equation.

2.8 Conforming and Non Conforming Contact

A contact is said to be conforming if the surfaces of the two bodies 'fit' exactly or even closely together without deformation. Flat slider bearings and journal bearings are examples of conforming contact.

Bodies which have dissimilar profiles are said to be non-conforming. When brought into contact without deformation they will touch first at a point - 'point contact' - or along a line - 'line contact'. For example, in a ball-bearing the ball makes point contact with the races, whereas in a roller bearing the roller makes line contact. Line contact arises when the profiles of the bodies are conforming in one direction and non-conforming in the perpendicular direction. The contact area between non- conforming bodies is generally small compared with the dimensions of the bodies themselves; the stresses are highly concentrated in the region close to the contact zone and are not greatly influenced by the shape of the bodies at a distance from the contact area.

2.9   Elastic Half Space

Non-conforming elastic bodies in contact whose deformation is sufficiently small for the linear small strain theory of elasticity to be applicable inevitably make contact over an area whose dimensions are small compared with the radii of curvature of the undeformed surfaces. The contact stresses are highly concentrated close to the contact region and decrease rapidly in intensity with distance from the point of contact, so that the region of practical interest lies close to the contact interface. Thus, provided the dimensions of the bodies themselves are large compared with the dimensions of the contact area, the stresses in this region are not critically dependent upon the shape of the bodies distant from the contact area, nor upon the precise way in which they are supported. The stresses may be calculated to good approximation by considering each body as a semi-infinite elastic solid bounded by a plane surface: i.e. an elastic half-space. This idealization, in which bodies of arbitrary surface profile are regarded as semi-infinite in extent and having a plane surface, is made almost universally in elastic contact stress theory. It simplifies the boundary conditions and makes available the large body of elasticity theory which has been developed for the elastic half-space. In this chapter, therefore, we shall study the stresses and deformations in an elastic half-space loaded one-dimensionally over a narrow strip ('line loading'). In our frame of reference the boundary surface is the x-y plane and the z-axis is directed into the solid. The loaded strip lies parallel to the y axis and has a width (a + b) in the x-direction; it carries normal and tangential tractions which are a function of 'x' only. We shall assume that a state of plane strain ($\varepsilon_y = 0$) is produced in the half-space by the line loading. For the assumption of plane strain to be justified the thickness of the solid should be large compared with the width of the loaded region, which is usually the case.

The elastic half-space is shown in cross-section in Figure 2.5. Surface tractions P(x) and Q(x) act on the surface over the region from x = — b to x = a while the remainder of the surface is free from traction. It is required to find the stress components σ_x, σ_z and τ_{xz} at all points throughout the solid.

12
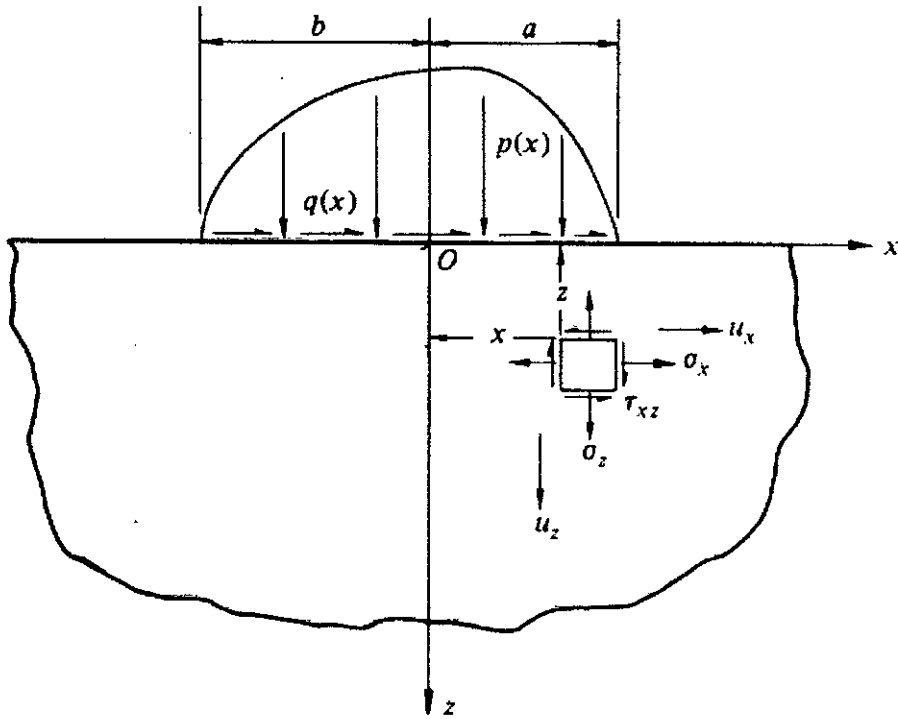
Figure 2.5: Elastic Half space

The stress component must satisfy the equilibrium equations throughout the solid-

$$\frac{\delta \sigma_x}{\delta x} + \frac{\delta \tau_{xz}}{\delta z} = 0$$

$$\frac{\delta \sigma_z}{\delta z} + \frac{\delta \tau_{xz}}{\delta x} = 0$$

The corresponding strains $\varepsilon_x, \varepsilon_z, \gamma_{xz}$ must satisfy the compatibility condition:

$$\frac{\delta^2 \varepsilon_x}{\delta z^2} + \frac{\delta^2 \varepsilon_z}{\delta x^2} = \frac{\delta^2 \gamma_{xz}}{\delta x \delta z}$$

Hooke's law relating the stresses to the strain, may be written –

$$\epsilon_x = \frac{1}{E} \left\{ (1 - \nu^2) \sigma_x - \nu(1 + \nu) \sigma_z \right\}$$

$$\epsilon_z = \frac{1}{E} \left\{ (1 - \nu^2) \sigma_z - \nu(1 + \nu) \sigma_x \right\}$$

$$\gamma_{xz} = \frac{1}{G} \tau_{xz} = \frac{2(1 + \nu)}{E} \tau_{xz}$$

13

If a stress function φ (x,z) is defined by –

$$\sigma_x = \frac{\delta^2 \varphi}{\delta z^2} \qquad \sigma_z = \frac{\delta^2 \varphi}{\delta x^2} \qquad \tau_{xz} = -\frac{\delta^2 \varphi}{\delta x \delta z} \quad \text{------- (2.11)}$$

Then Eqs of equilibrium, compatibility and Hooke's law are satisfied provided φ (x,z) satisfied the biharmonic function

$$\left\{ \frac{\delta^2}{\delta x^2} + \frac{\delta^2}{\delta z^2} \right\}\left\{ \frac{\delta^2 \varphi}{\delta x^2} + \frac{\delta^2 \varphi}{\delta z^2} \right\} = 0 \quad \text{--- (2.12)}$$

2.9.1 Boundary Conditions

The stress function must be satisfied the boundary condition. The boundary conditions for the half space in Figure – 2.5 are as follows.

On the boundary z = 0, outside loaded region, the surface is free of stress i.e.

$$\sigma_z = \tau_{xz} = 0 \qquad\qquad \text{x < - b and x > +a} \qquad \text{------ (2.13a)}$$

Within the loaded region –

$$\left.\begin{array}{l} \sigma_z = -p(x) \\ \tau_{xz} = -q(x) \end{array}\right\} \qquad -b \le x \le a \quad \text{----- (2.13b)}$$

At $x, z \to \infty$ $\qquad\qquad \sigma_x, \sigma_z, \tau_{xz} \to 0 \qquad \text{---- (2.13c)}$

For this thesis the contact has been considered in corporation with sliding. So tangential force has been raised which is the result from normal forces and related with friction. So another boundary condition has been considered –

$$q(x) = \pm \mu p(x) \qquad \text{------ (2.14)}$$

Stress distribution for concentrated normal force and for concentrated tangential traction has been required to develop mathematical model for numerical solution. So, stress distribution for concentrated normal and tangential force has been discussed in the following article.

2.10.1 Concentrated Normal Force

Stresses produced by a concentrated force of intensity 'P' per unit length distributed along the y-axis and acting in a direction normal to the surface has been discussed here. This loading may be visualized as that produced by a knife-edge pressed into contact with the half-space along the y-axis (Fig. 2.5 absence of tangential load and distributed load).

Stresses for concentrated normal forces are as follows –

$$\sigma_x = -\frac{2P}{\pi}\frac{x^2 z}{\left(x^2+z^2\right)^2}$$

$$\sigma_x = -\frac{2P}{\pi}\frac{z^3}{\left(x^2+z^2\right)^2} \qquad \text{---- (2.15a)}$$

2.10.2 Concentrated Tangential Force

A concentrated force 'Q' per unit length of the y – axis, which acts tangentially to the surface at O as shown in figure 2.5 produces stress distribution in x and z direction.

Stresses for concentrated tangential forces are as follows –

$$\sigma_x = -\frac{2Q}{\pi}\frac{x^3}{\left(x^2+z^2\right)^2}$$

$$\sigma_x = -\frac{2Q}{\pi}\frac{xz^2}{\left(x^2+z^2\right)^2} \qquad \text{----- (2.15b)}$$

2.10.3 Distributed normal and tangential force

An elastic half surface loaded over the strip (-b < x < a) by a normal pressure p(x) and tangential force q(x) is distributed is any arbitrary manner shown in figure 2.6. We wish to find the stress distribution under normal and tangential loading at any point A in the body of the solid.
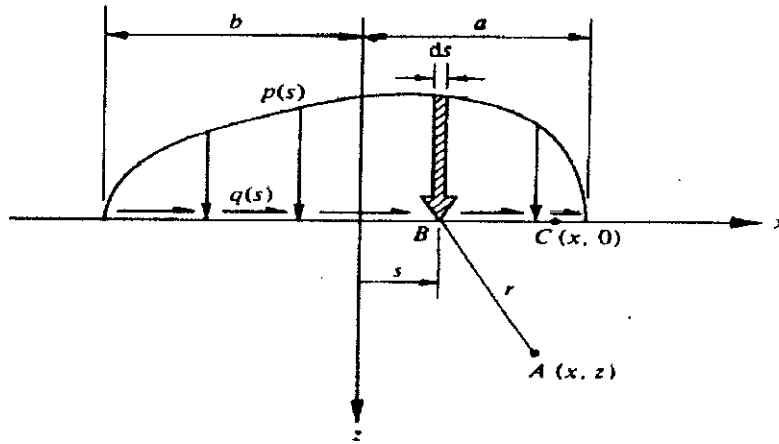
Figure 2.6: Distributed Load over elastic half space

As we have already discussed about stresses due to point loading, so to get stresses for distributed loading we had to implement superposition approximation and hence integrated over the entire loaded area.

The traction acting on the surface at B, distance s from O, on an elemental area of width 'ds' can be regarded as concentrated forces of magnitude **pds** acting normal to the surface and **qds** tangential to the surface. The stress at A due to these forces are given by the stress distribution of concentrated normal and tangential forces given by equations (2.15a) and (2.15b) in which x is replaced by (x-s). Integrating over the the loaded region gives the stress components at P due to complete distribution of p(x) and q(x)

The stress distribution hence as follows –

$$\sigma_x = -\frac{2z}{\pi} \int_{-b}^{a} \frac{p(s)(x-s)^2 \, ds}{\left\{(x-s)^2+z^2\right\}^2} - \frac{2z}{\pi} \int_{-b}^{a} \frac{q(s)(x-s)^3 \, ds}{\left\{(x-s)^2+z^2\right\}^2}$$

$$\sigma_z = -\frac{2z^3}{\pi} \int_{-b}^{a} \frac{p(s) \, ds}{\left\{(x-s)^2+z^2\right\}^2} - \frac{2z^2}{\pi} \int_{-b}^{a} \frac{q(s)(x-s) \, ds}{\left\{(x-s)^2+z^2\right\}^2}$$

-- (2.16)

If the stress distributions of p(x) and q(x) are known then the stress can be evaluated although the integration in closed form may be difficult. In this work, the distribution

of p(x) has been considered as Hertz Pressure Distribution and to solve these equations numerical technique has been evolved.

2.11 Hertz Theory

When two non-conforming solids are brought into contact they touch initially at a single point or along a line. Under the action of the slightest load they deform in the vicinity of their point of first contact so that they touch over an area which is finite though small compared with the dimensions of the two bodies. A theory of contact is required to predict the shape of this area of contact and how it grows in size with increasing load; the magnitude and distribution of surface tractions, normal and possibly tangential, transmitted across the interface. Finally it should enable the components of deformation and stress in both bodies to be calculated in the vicinity of the contact region.

In this work, pressure distribution has been assumed according to Hertz. He proposed pressure distribution for any contact region is elliptical while normal loading has been applied in the contact region. So, in this work we have been used elliptical pressure distribution –
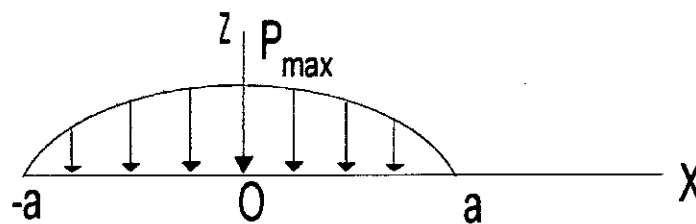
Figure 2.7: Distribution of Pressure according to Hertz theory

$$p(x) = \sqrt{1 - \frac{x^2}{a^2}} \qquad \text{---- (2.17)}$$

where 'a' is the half width of the contact region. According to Hertz, this contact region is very small in compare to overall dimension of the body. The contact region has shape of rectangular but for the conical roller it has shape of a trapezoid. So, half

width is not fixed like cylindrical contact. It has been changed according to line of consider ration from tip.

2.12 Relation between Normal and Tangential Traction

As this thesis work has been done considering normal and tangential load. In this work tangential force is related with normal force according to **Amonton's Law.** But this relation is valid only when there is sliding but not larger scale. It is noted that, there will be no tangential traction if there is absent of normal force. As in this work pressure distribution has been considered only function of 'x', hence tangential traction will be function of 'x' only. The relation is

$$\frac{|q(x)|}{p(x)} = \mu$$

where μ is a constant coefficient of kinetic friction whose value is determined by the materials and the physical conditions of the interface. For our approximation we assume it 0.30. It is also found to be approximately valid when non conforming sliding surfaces are separated by thin lubricating films. Experimental confirmation that the tangential traction is distributed in direct proportion to normal pressure is provided by photo- elastic work of Ollerton and Haines.

2.13 Effect on Normal Pressure Distribution and Half Width

A question may be raised, in presence of tangential load is there any change in normal pressure distribution or half width i.e. contact shape? To demonstrate this by considering figure 2.8 , the tangential force Q is proportional to (1-2v)/G.
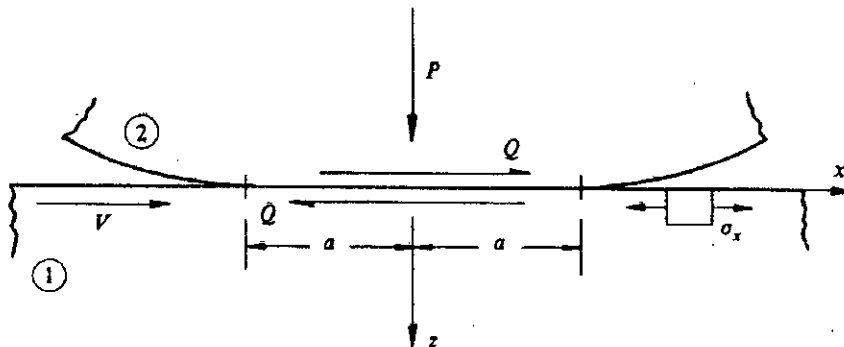
Figure 2.8: Combination of Normal and Tangential Load

The tangential traction acting on each surface at the interface are equal in magnitude and the opposite in sign,

$$q_1 (x, y) = -q_2 (x, y) \text{ --------(2.18)}$$

Hence normal displacement due to these tractions are proportional to the respective values of $(1-2v)/G$ of each body and are of opposite sign.

$$\frac{G_1}{1 - 2v_1} \bar{u}_{z1}(x,y) = - \frac{G_2}{1 - 2v_2} \bar{u}_{z2}(x,y)$$

where u_{z1} and u_{z2} is the normal displacement. If the two solids have the same elastic constants, any tangential traction transmitted between them gives rise to equal and opposite normal displacements of any point on the interface. Thus the warping of one surface conforms exactly with that of the other and does not disturb the distribution of normal pressure. The shape and size of the contact area are then fixed by the profiles of the two surfaces and the normal force, and are independent of the tangential force.

2.14 Radius of Curvature

When two geometrically and materially identical conical rollers come into contact with each other under the application of a uniform compressive normal load in rolling, the contact patch appears in the form of trapezoid, in contrast with two cylinders where the contact area is a rectangle. The trapezoid shape of the contact area arises because the radius of curvature of either cone varies along the axial direction of contact length.

Unlike cylinders where the radius of curvature is equal to the radius of a cylinder, the radius of curvature of a conical roller is equal to the radius of curvature of an ellipse formed by a cut plane normal to the external surface of the conical roller. This radius of curvature varies as the cut plane moves along the contact length. Figure -2.9 shows two ellipses in a side view formed by sectioning conical rollers by the cut plane at t.
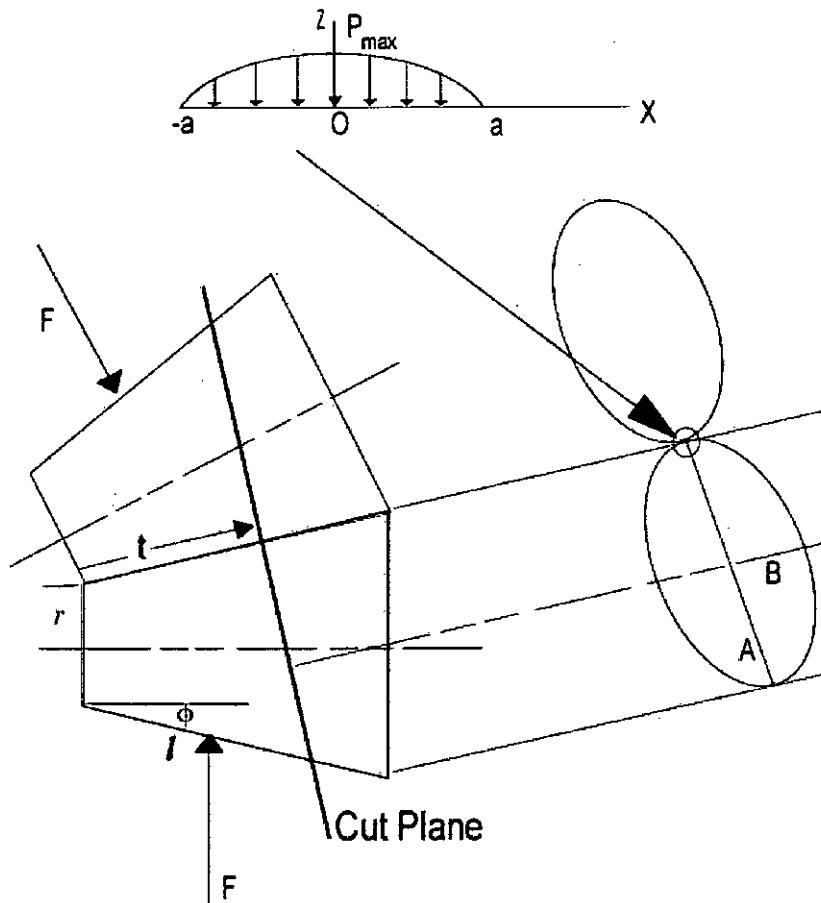
Figure 2.9: Side Cross sectional view of two conical rollers in contact

The radius of curvature of the osculating rollers for the section at t is –

$$R_1 = R_2 = R = f(t) = \frac{B^2}{A} \qquad o \le t \le l \qquad ----\ (2.20a)$$

Equation (2.20a) is a parametric form of radius R of curvature, where all values of R along the contact length can be determined as t increases from 0 to l. A and B are the lengths of the manor and minor axis respectively of the ellipses of osculating rollers 1 and 2 at t, when viewed perpendicular to the section, as shown in figure 2.9. The lengths of the major and minor axes, which are also function of t, are determined by visualizing the cone in a three dimensional space. From figure 2.10 the length of the minor axis of each cone is –
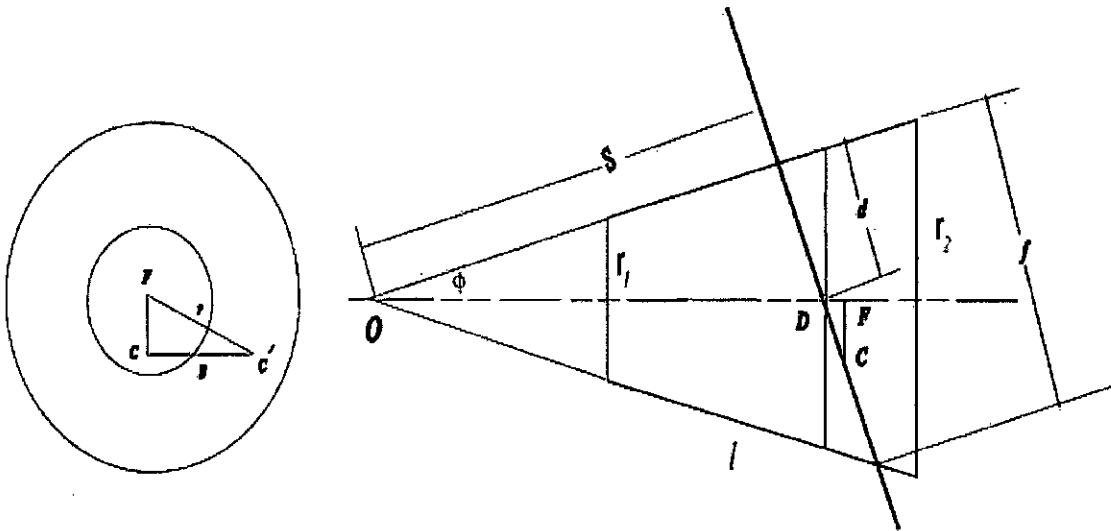
Figure 2.10: Front side view of conical cylinder

$$B = \sqrt{r^2 - FC^2} = \sqrt{(OD+DF)^2 \tan^2 \varphi - DC^2 \cos^2 \varphi} \quad 0 < \varphi < 45 \quad (2.20b)$$

Where r is the radius of each cone at t and φ is the vertex angle. The application of the above equation requires a vertex angle greater than $0°$ and less than $45°$. At 0, the cone reduces to a line and at-45 the cutting plane t becomes parallel to the side l.

Putting the values of OD, DF and DC in the above equation gives

$$B = \sqrt{\left\{ \frac{S^2}{\cos^2 \varphi} + \left[\left(\frac{f}{2} - d\right)^2 \sin^2 \varphi\right] + 2\left(\frac{S}{\cos \varphi}\right)\left(\frac{f}{2} - d\right)\right\} \tan^2 \varphi - \left(\frac{f}{2} - d\right)^2 \cos^2 \varphi}$$

$$0 < \varphi < 45 \qquad (2.20c)$$

where S is the distance from the apex, and f is length of the section, perpendicular to the cone surface, at t projected on the Y-Z plane passing through the axis of the cone. The above equation can be written in terms of t as

$$B = K\left(\frac{r_1}{\sin \varphi} + t\right) \qquad 0 \le t \le l, \qquad 0 < \varphi < 45° \qquad \text{------} (2.20d)$$

21

where K is a constant which is given by

$$K = \sqrt{\left(\frac{1}{\cos^2\varphi} + H^2\sin^2\varphi + \frac{2H}{\cos\varphi}\right)\tan^2\varphi - H^2\cos^2\varphi}$$ ----- (2.20e)

$$H = \frac{\tan(2\varphi)}{2} - \tan\varphi$$

The length of the major axis of each cone is –

$$A = \left(\frac{r_1}{\sin\varphi} + t\right)\frac{\tan(2\varphi)}{2} \qquad 0 \le t \le l \qquad 0 < \varphi < 45^\circ \qquad ----- (2.20f)$$

Putting the values of equations (2.20d) and (2.20f) in equation 2.20a gives –

$$R = \frac{2K^2}{\tan(2\varphi)}\left(\frac{r_1}{\sin\varphi} + t\right) \qquad 0 \le t \le l \qquad 0 < \varphi < 45^\circ \qquad ------- (2.20g)$$

The conical roller geometric constant b that depends only on the radii of curvature of two cones at t is –

$$b = \frac{1}{2}\left(\frac{1}{R} + \frac{1}{R}\right) = \frac{1}{R} \qquad 0 \le t \le l \qquad 0 < \varphi < 45^\circ \qquad ---(2.20h)$$

It may be noted that like b, has a unique value for each value of t as long as long radius of curvature is not infinite or undefined.

CHAPTER THREE

NUMERICAL SOLUTION AND FINITE ELEMENT SIMULATION

3.1 General

In the field of engineering sometimes we have to face some sort of problems which is not possible by analytical methods or equations. In such case we have to use various Numerical Techniques to fine the results. The numerical technique hence required validation using another comparison with that finding in the numerical analysis. In this chapter we have discussed about numerical techniques including governing equations, boundary conditions, coding used and comparison of the results with a commercially available software ANSYS.

3.2 Physical Description

The definition sketch of the problem and the boundary conditions are shown in the figure 3.1. There are two conical rollers in contact. The two rollers have materials with same elastic constant and poisson's ratio. The boundary surface is X-Y plane and Z axis is directed into the solid. The loaded strip lies parallel to the Y axis and has a width of 2a in X direction. The length of the conical roller has been taken 20 mm. The vertex angles have been taken as 5°, 20°, 30°, 45°. The material properties have been taken as Young modulus, E = 200 GPa and Poisson's ration, υ = 0.3 for steel and for aluminum it has been taken as 70 GPa and 0.25 respectively. The loading has been given perpendicular to Z axis and value is 1000 N/mm.
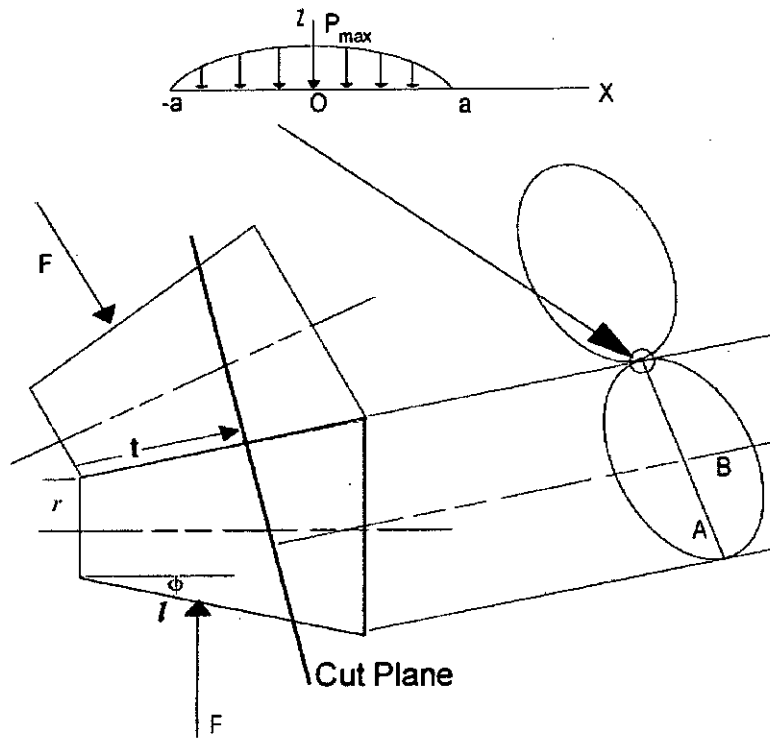
Figure 3.1: Physical Model for numerical solution

3.3 Mathematical Modeling

The governing equations and boundary conditions of the system to get the stress distribution are as follows –

Governing Equations

$$\sigma_x = -\frac{2z}{\pi}\int_{-b}^{a}\frac{p(s)(x-s)^2\,ds}{\left\{(x-s)^2+z^2\right\}^2} - \frac{2z}{\pi}\int_{-b}^{a}\frac{q(s)(x-s)^3\,ds}{\left\{(x-s)^2+z^2\right\}^2}$$

$$\sigma_z = -\frac{2z^3}{\pi}\int_{-b}^{a}\frac{p(s)ds}{\left\{(x-s)^2+z^2\right\}^2} - \frac{2z^2}{\pi}\int_{-b}^{a}\frac{q(s)(x-s)\,ds}{\left\{(x-s)^2+z^2\right\}^2}$$

$$\sigma_y = v.(\sigma_x + \sigma_z)$$

$$\tau_{xz} = \left|\frac{\sigma_1 - \sigma_3}{2}\right|$$

$$q(x) = \pm\mu p(x)$$

24

Radius of Curvature

$$R = \frac{2K^2}{\tan(2\varphi)}\left(\frac{r_1}{\sin\varphi} + t\right)$$

Pressure Distribution

$$p(x) = \sqrt{1 - \frac{x^2}{a^2}}$$

Boundary Conditions

On the boundary z = 0, outside loaded region, the surface is free of stress i.e.

$$\sigma_z = \tau_{xz} = 0 \qquad\qquad x < -b \text{ and } x > +a$$

Within the loaded region –

$$\left.\begin{array}{l}\sigma_z = -p(x) \\ \tau_{xz} = -q(x)\end{array}\right\} \qquad -b \leq x \leq a$$

At $x, z \to \infty$ $\qquad \sigma_x, \sigma_z, \tau_{xz} \to 0$

To solve above integration associated with pressure distribution, half width and boundary condition a programming has been written in MATLAB.

3.4   Steps Involved in MATLAB

Step 1: Input Material Properties and Physical Dimension of the rollers.

Step 2: Solving of Radius of Curvature

Step 3 : Solving Half width of contact

Step 4: Input Normal Loading F = 1000 N/mm

Step 5: Input Pressure Distribution according to Hertz Contact Stress

Step 6: Input Boundary Conditions

Step 7: Solve Stress Distribution For this Set of value using **Integration Technique**

Step 8: Solve half width for next iteration and repeat step 4 to 7

Step 9: Output results

3.5　Basic Procedure for Finite Element Analysis

To solve any problems using ANSYS, there are three steps to proceed. These steps are-

- Pre-processor: In this pre-processor, the model geometry is defined (for example, defining elements along with their real constant values, material properties and modeling of given specific structure).

- Solution mode: In this solution mode, boundary conditions and loads are applied to the model and analysis is run for the solution.

- Post processor: In this phase, results are examined.

3.6　Preprocessing Phase

The steps involved in this phase have been discussed from the following articles

3.6.1.　Element Description

Tetrahedral 10-Node element (SOLID 187) is used for 3-D modeling of solid structures. SOLID187 element is a higher order 3-D, 10-node element. SOLID187 has a quadratic displacement behavior and is well suited to modeling irregular meshes (such as those produced from various CAD/CAM systems). As the drawing has been completed in SOLID WORKS and then it has been imported to ANSYS interface, so this type of element is very useful for such analysis.

The element is defined by 10 nodes having three degrees of freedom at each node: translations in the nodal x, y, and z directions. The element has elasticity, plasticity, hyperelasticity, creep, stress stiffening, large deflection, and large strain capabilities. It also has mixed formulation capability for simulating deformations of nearly incompressible elastoplastic materials, and fully incompressible hyperelastic materials.

26
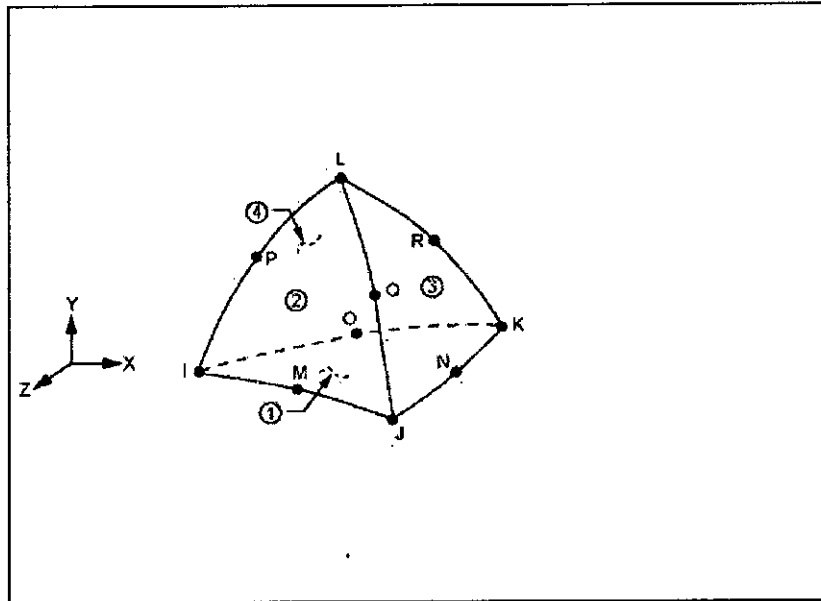
Figure 3.2: Tet 10 nodes using for meshing

The geometry, node locations, and the coordinate system for this element are shown in Figure- 3.2

In addition to the nodes, the element input data includes the orthotropic or anisotropic material properties. Orthotropic and anisotropic material directions correspond to the element coordinate directions. The element coordinate system orientation is as described in Linear Material Properties.

Linear material properties that are required for an element, but which are not defined, use the default values as described below (except that EX and KXX must be input with a nonzero value where applicable). Any additional material properties are ignored.

3.6.2   Material Specifications

As material properties are assumed as linear, so in ANSYS there are only two values for properties has been given as input. These are Young Modulus and Poisson's ratio. The other values of properties have been adjusted accordingly. No input has been given for thermal expansion. The material properties, that have been used are-

For steel, Young Modulus = 205 GPa and Poisson's ratio = 0.3

For Aluminum, Young Modulus = 70 GPa, Poisson's ratio = 0.25

3.6.3 Modeling

Three models are constructed to verify the validity of the mathematical model that has been solved numerically and to understand the effect of vertex angle, load and material on the maximum pressure and it's distribution. In order to alleviate the complexity of the problem each model uses cones of the same dimensions, material and boundary conditions.
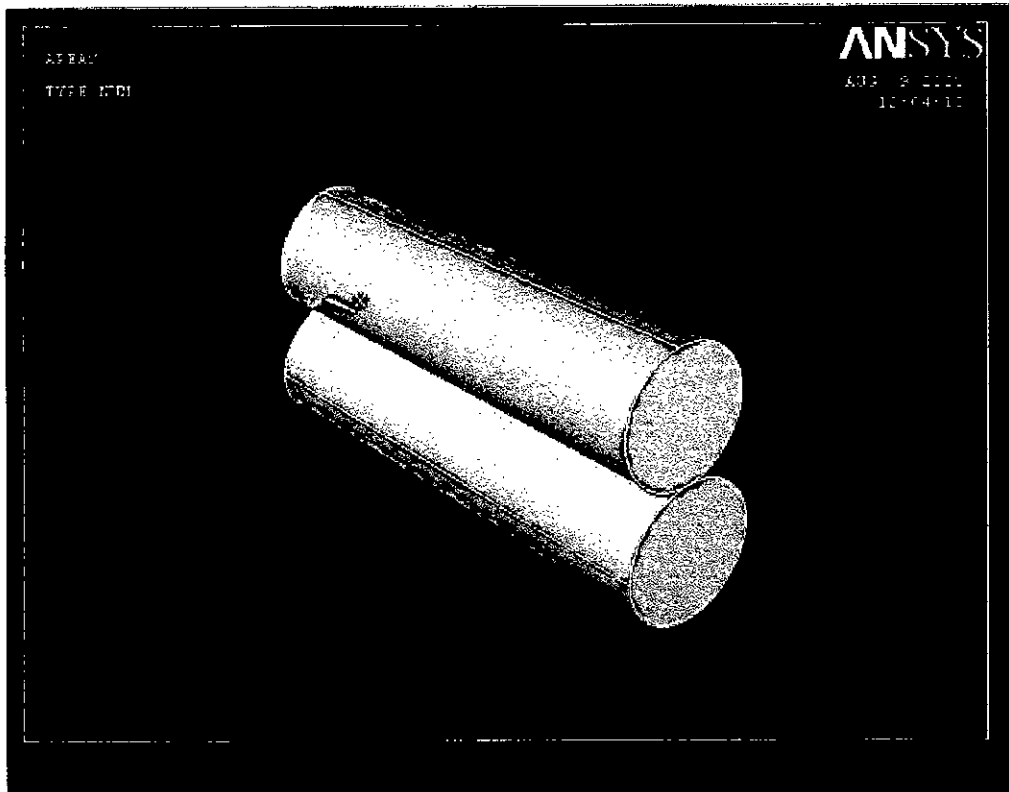
Figure 3.3: Model Imported from Solid Works

Model 1 consists of two three dimensional deformable conical rollers of vertex angle and axial length 20 mm. The model has been shown in figure 3.3. Then it has been saved in such format that ANSYS supports that.

3.6.4 Meshing

For finite element simulation meshing is the most important task. As in case of contact problems stress are concentrated close to contact region. So, fine mesh is required in the contact region. To do so, first all the geometrical models have been meshed freely. Then the contact surface has been **mapped mesh** to finer the meshing. After meshing the conical rollers are shown in figure 3.4-3.7

28
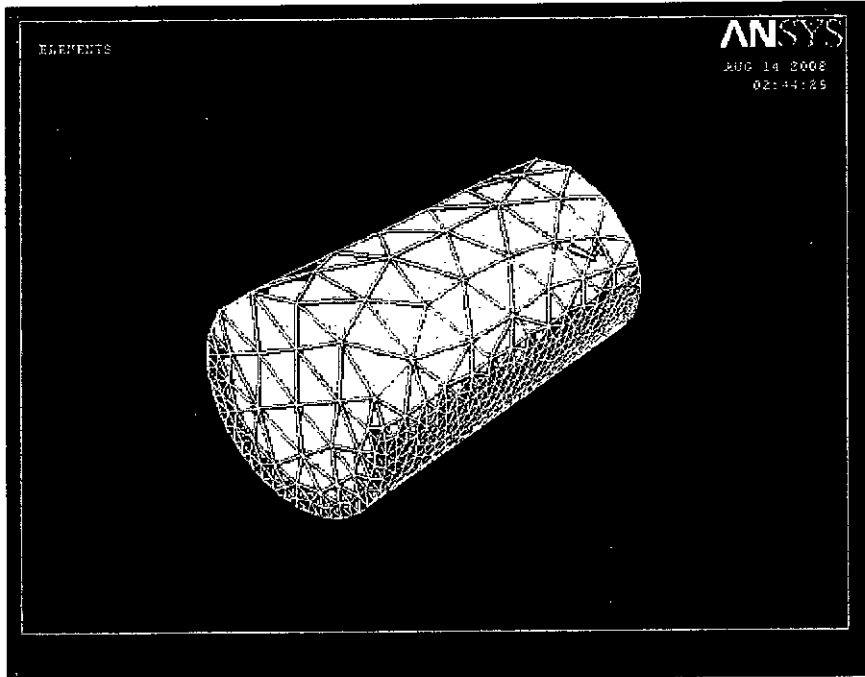
Figure 3.4 : Meshing of Single Conical Roller
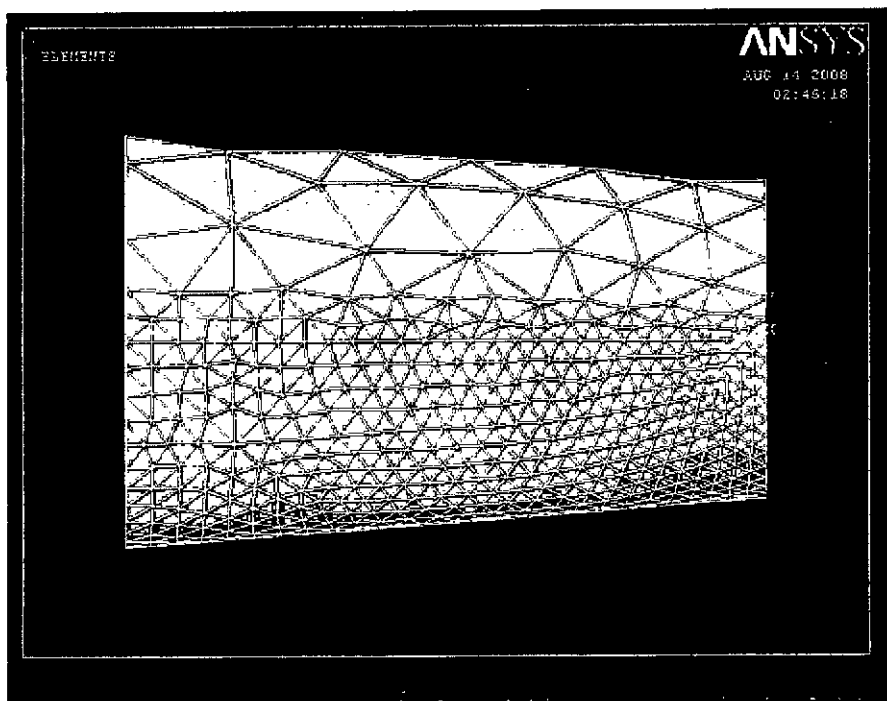
Figure 3.5: Side view of conical roller with mesh.
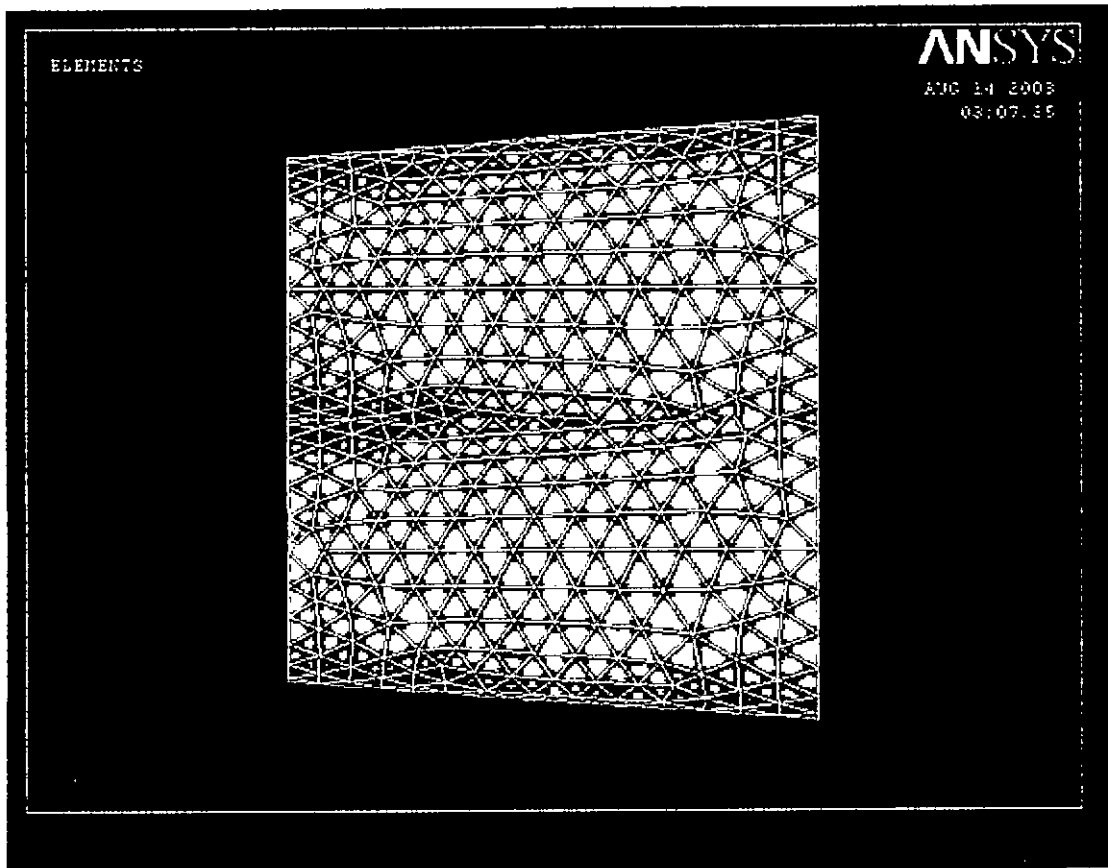
Figure 3.6: Tow conical rollers in mesh
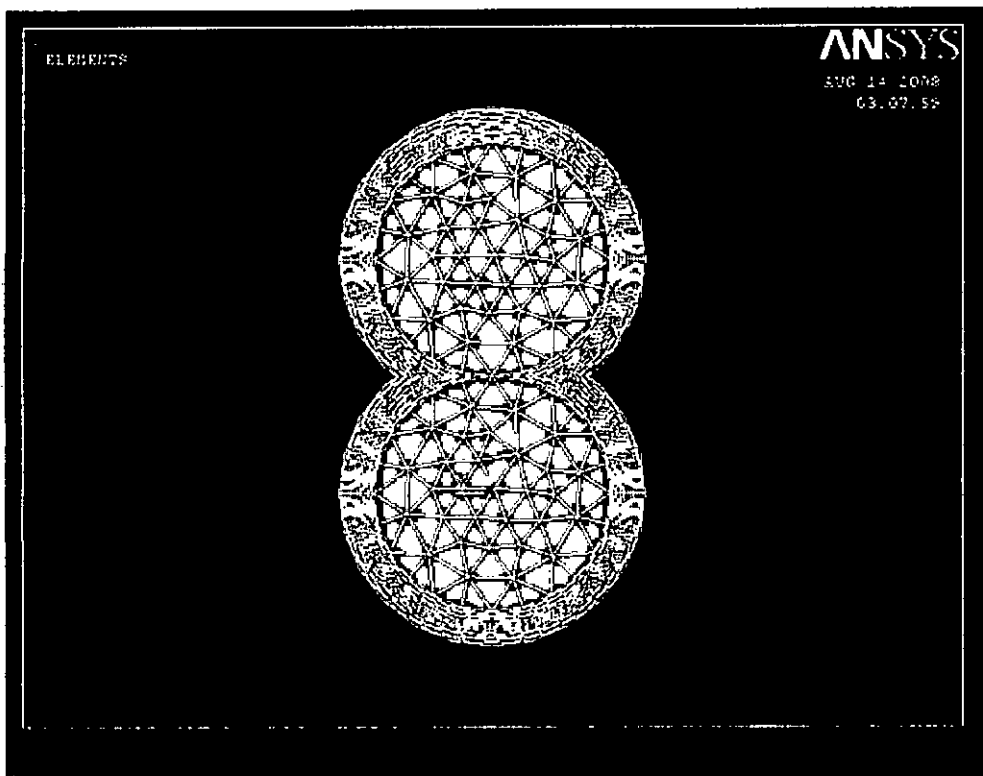
Figure 3.7: Front view of two conical rollers in mesh

30

3.6.5 Type of Contact Element

In this analysis, CONTAC175 (Contact, Surface-to-Surface) element is used to develop a contact pair between the two rollers. CONTAC175 is a surface-to-surface contact element. It supports small sliding, small deformation, and different meshes between the contacting components. Contact occurs when the element penetrates the target segment element (TARGE 169) on a specified target surface. CONTA175 is used to represent contact and sliding.. The element is applicable to 2-D or 3-D structural and coupled field contact analyses.
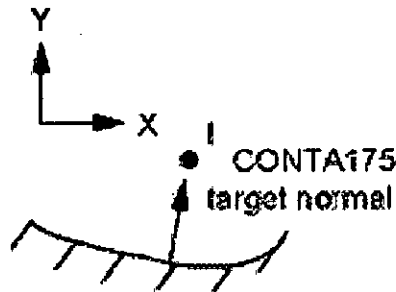
Figure 3.8: Contact element type with target

3.6.6 Graphical user interface (GUI)

Several GUI aids are available to create and manage contact pairs.

3.6.6.1 Contact Manager

The Contact Manager allows to define, view, and edit contact pairs. It provides a convenient way to manage all contact pairs for entire model. The Contact Manager Toolbar provides an intuitive interface for the creation and management of contact pairs. The manager supports surface-to-surface contact analysis (using CONTA175).
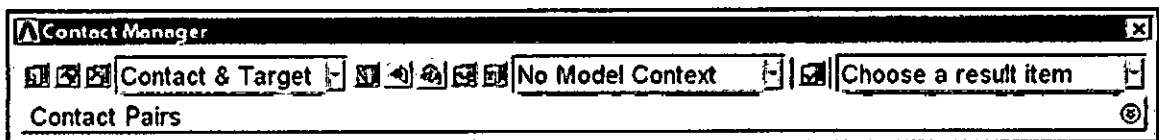
Figure 3.9: Contact Manager Toolbar

3.6.6.2 The Contact Wizard

This Contact Wizard leads through the process of manually creating contact pairs. The wizard supports rigid-flexible (with optional pilot node) and flexible-flexible contact, and supports both surface-to-surface and node-to-surface configurations. The wizard does not support rigid target primitives. The Contact Wizard also supports surface-based constraint contact pairs.

The Contact Wizard remains unavailable (dimmed) if any portion of the model is not meshed. To create a rigid-flexible model, only the parts of the model which will be used as flexible contact surfaces are meshed before launching the wizard(Rigid Target Surfaces are not meshed) and to create a flexible-flexible model, all parts of the model which will be used as contact surfaces (including target surfaces) before launching the wizard are meshed.

Target and contact surfaces are specified using lines, areas, volumes, selected set of nodes, or node components. The wizard allows choosing more than one area for the target and contacting surfaces, thus allowing multiple areas to form a single contact surface. If a rigid target surface is specified, a pilot node for that contact pair is defined. After the target and contact surfaces are specified, properties of the contact pair before creating the contact pair are specified. After all the required data is specified, the contact and target element types are created
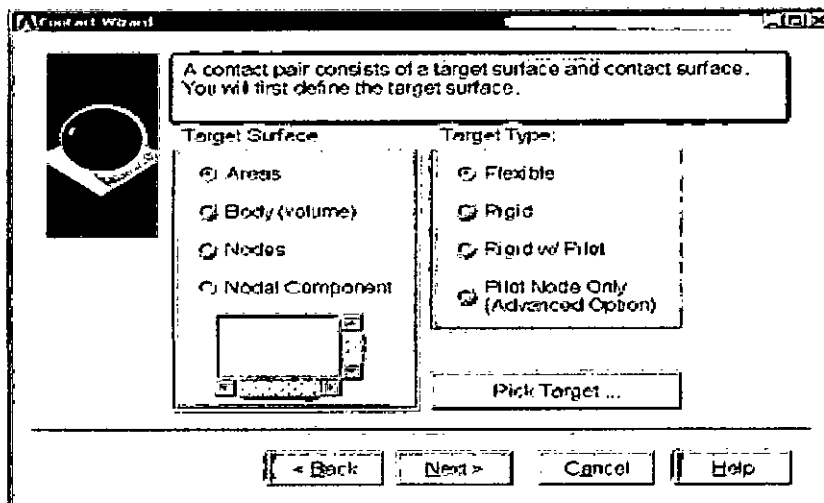
Figure 3.10: Contact Wizard Tool

3.6.6.3 Managing contact pairs

It is paramount that the contact elements be oriented correctly for proper contact detection. The contact manager provides to display one or more contact pairs on which to perform the below listed operations.

(i)   To verify that the normal of the contact and target surfaces are in the correct direction

(ii)   To reverse normal of elements those are not oriented correctly

(iii)   To edit the properties of the contact pair(s) as needed. The properties include real constant values and key option values.

The options that are considered for Contact175 element type are shown in the window below:-
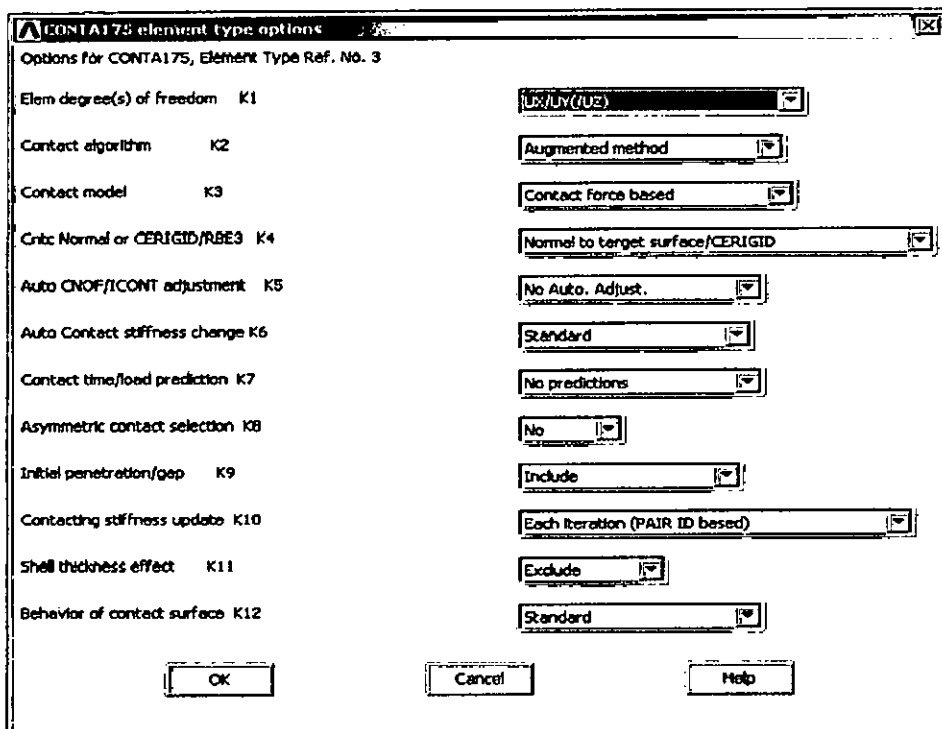
Figure 3.11: Managing Contact Pairs Tool

3.7   Solution Phase

In this phase loads and boundary conditions are applied to the system to get the results. The loads are applied 1000 N/mm in Y direction and tangential traction in X direction has been applied. Boundary conditions have been applied as it has been assumed. After applying load the figures has been shown from 3.12 to 3.13.
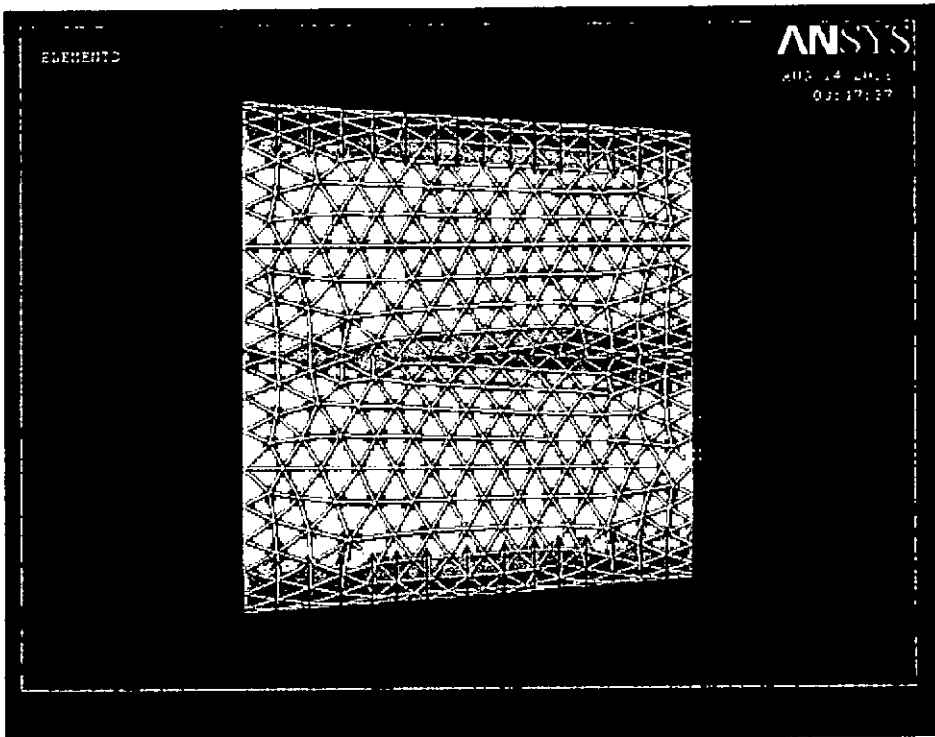
Figure 3.12: Applying Normal and Tangential Load
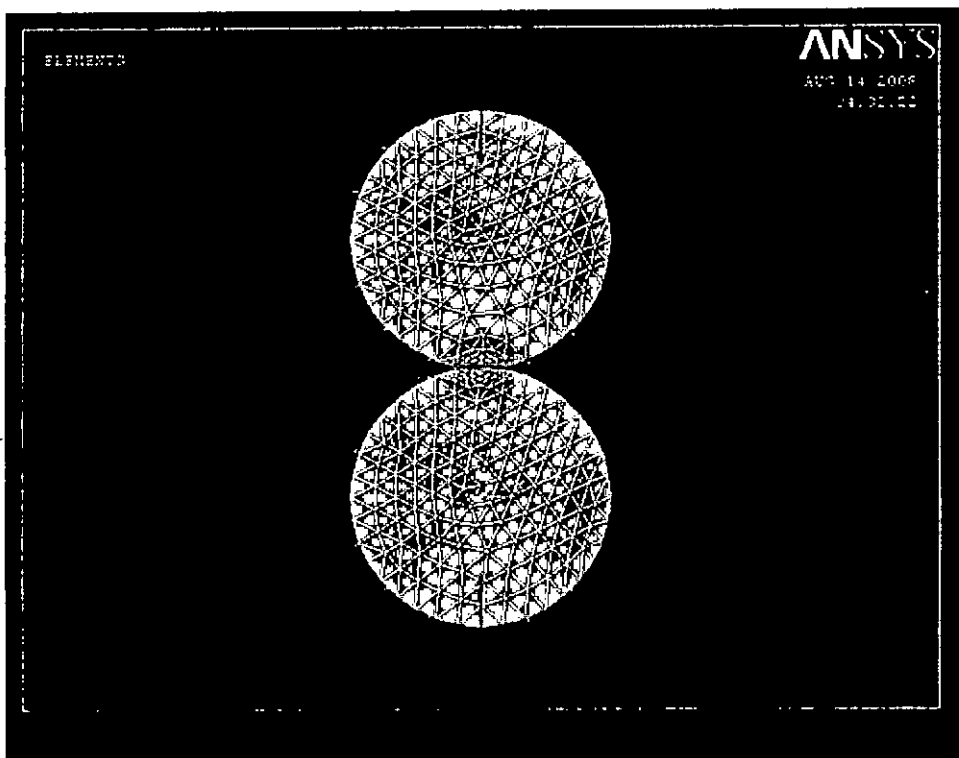
Figure 3.13: Applying Boundary Conditions

After applying loads and boundary conditions the system is then solved for current load set up.

3.8 Post Processor

In this phase results are plotted for given materials, meshing, applied load and boundary conditions. Here stress in X, Y, Z direction and Von Mises Shear stress have been observed at the portion where highest values have been found in numerical technique.

CHAPTER FOUR

RESULTS AND DISCUSSIONS

4.1 General

In this chapter, results on this thesis work from numerical solution and finite element analysis have been discussed. The results have been shown graphically relating contact stresses in different axes with contact geometries. Stress distribution, pressure distribution and comparison of results also have been shown.

4.2   Stress in X direction

With application of both normal and tangential load, the elements under the contact region have been in stressed. The component of stress in X- direction (σ_x) varies with contact geometries as well as length of the conical rollers. On the other hand, this stress also varies with different vertex angle. The following article includes the results from this stresses and discussion on that.

4.2.1 σ_x vs. x/a

Distribution of stresses in X- direction i.e. σ_x under normal load along x/a varies according to pressure distribution p(x). The maximum stress has been found when z=0 that is at the surface of contact. It decreases with increasing of distance from contact surface. In all cases i.e. at any depth from contact surface the variation of stress is elliptical. And the value of maximum stress is exactly same as the maximum pressure i.e. stress ratio is -1. It is noted that the stress component is compressive. The maximum pressure has been found at contact surface i.e. z=0 and at line of symmetry i.e. x/a=0.
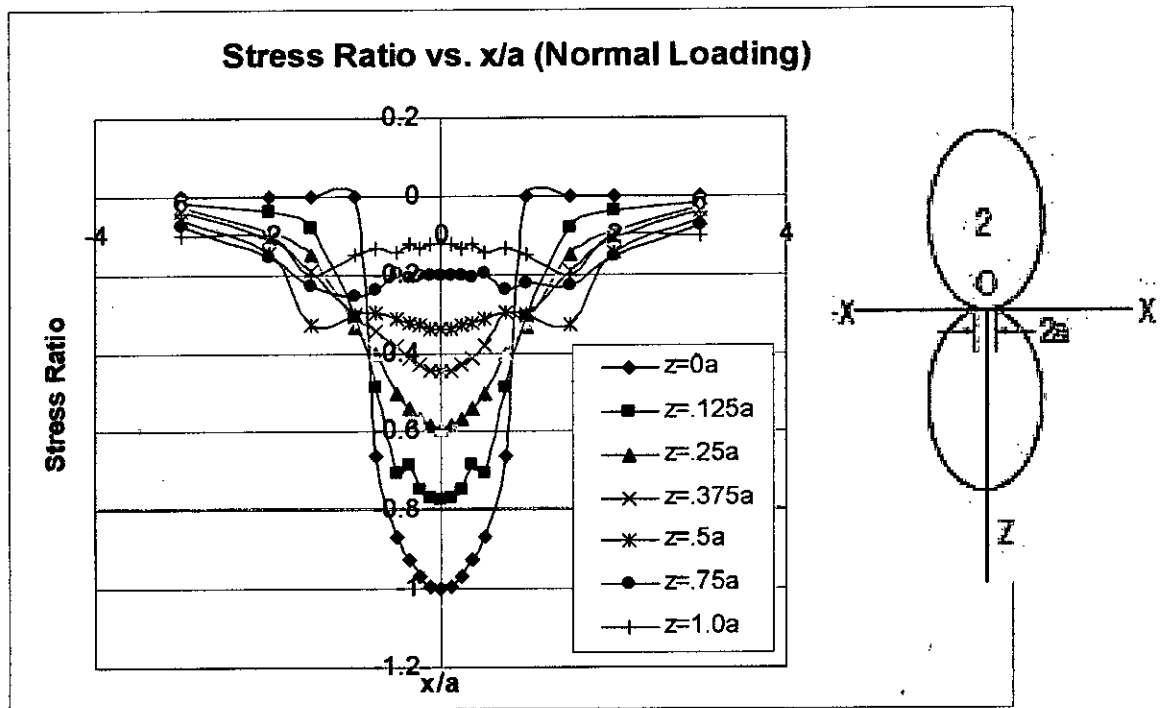
Figure 4.1: Stress distribution in X axis vs. x/a for normal loading

Distribution of stresses in X-direction is linear along x/a. The value is zero at the origin and is in compression at the leading edge of contact. But as the tailing edge the stress is in tension. In this case, the stress has maximum value at the contact surface and it is decreasing with increasing from the surface.
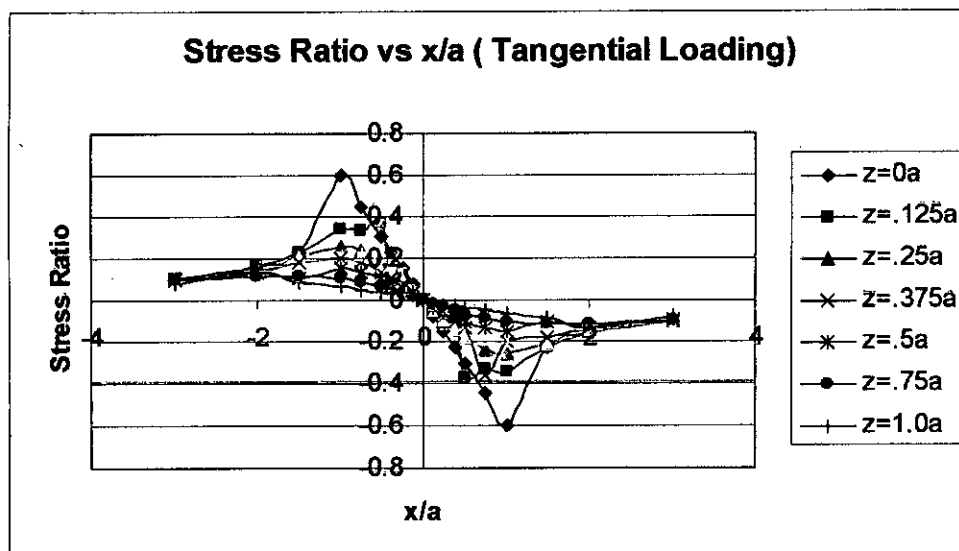
Figure 4.2: Stress distribution in X axis vs. x/a for tangential loading

To find the stress distribution for combined loading that is normal and tangential, here superposition approximation has been used. So, stresses from normal loading and

tangential loading have been superposed with a kinetic friction factor 0.3. As, the stress distribution for normal loading is elliptical and that for tangential loading is linear, so combined stress in X- direction has been skewed to the leading edge. It means, the maximum value of compressive stress has been found in the leading edge of roller and its value is higher than that for maximum pressure. As, for both case at surface (z=0) the stresses are higher, so combination of both also has higher value at contact surface. The distribution of stress in X direction for combined loading has been shown from figure 4.3.1 to 4.3.3 in dimensionless form as well as actual form for both steel and aluminum
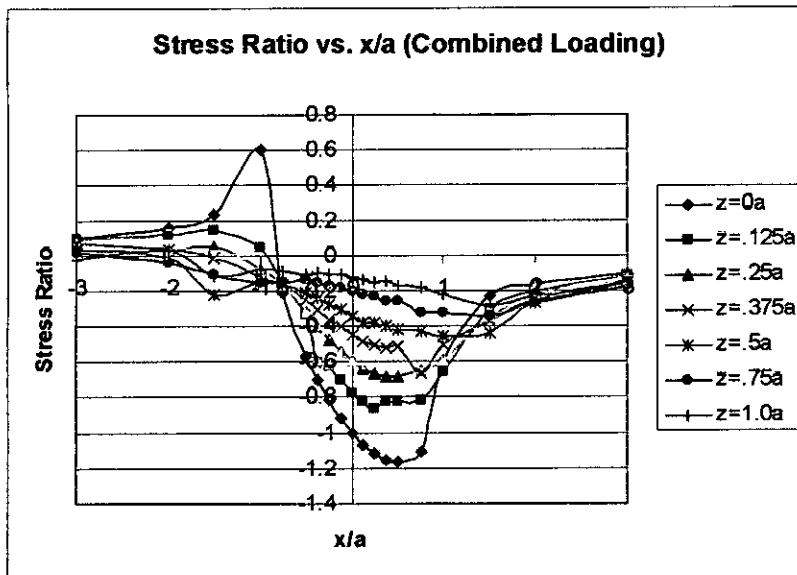
Figure 4.3.1: Stress distribution in X axis vs. x/a for combined loading
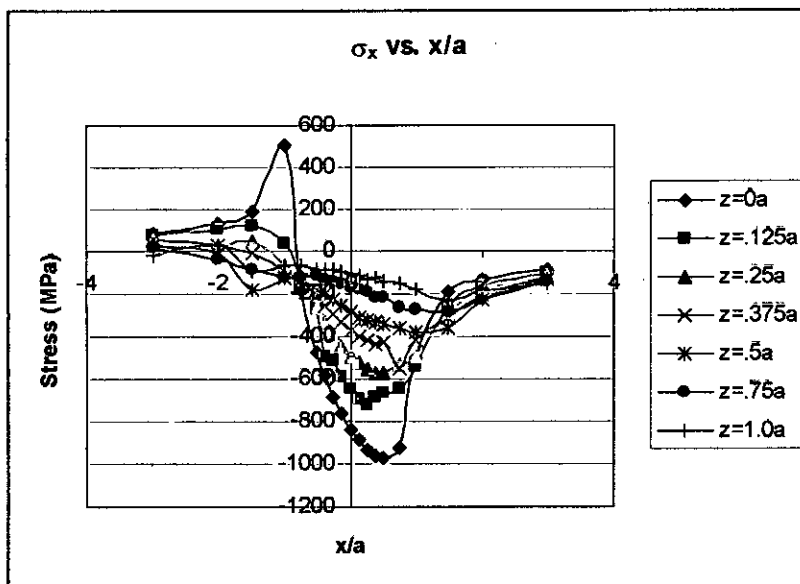
Figure 4.3.2: Stress Distribution vs. x/a for vertex angle $5°$ at t = 0l (steel)

38
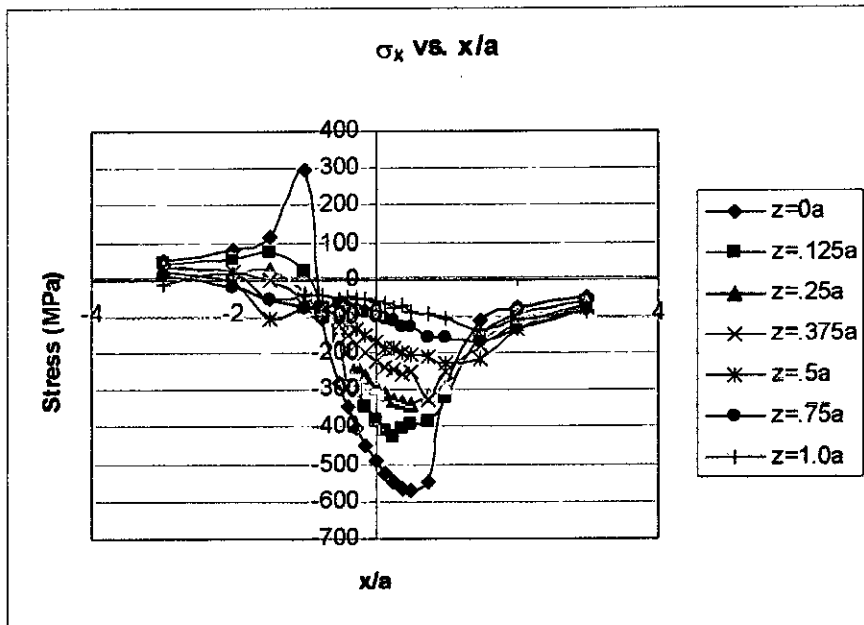
Figure 4.3.3: Stress Distribution vs. x/a for vertex angle $5°$ at t = $0l$ (aluminum)

4.2.2 σ_x vs. z/a

Stress distribution in X- axis along z/a direction for normal loading has maximum value for x/a = 0 i.e. at the center line of contact region and the value is -1. It is decreasing with increasing distance from the origin. Another matter is that at a large distance from contact surface as well as form center line the stress ratio has very low value, which satisfies the boundary conditions.
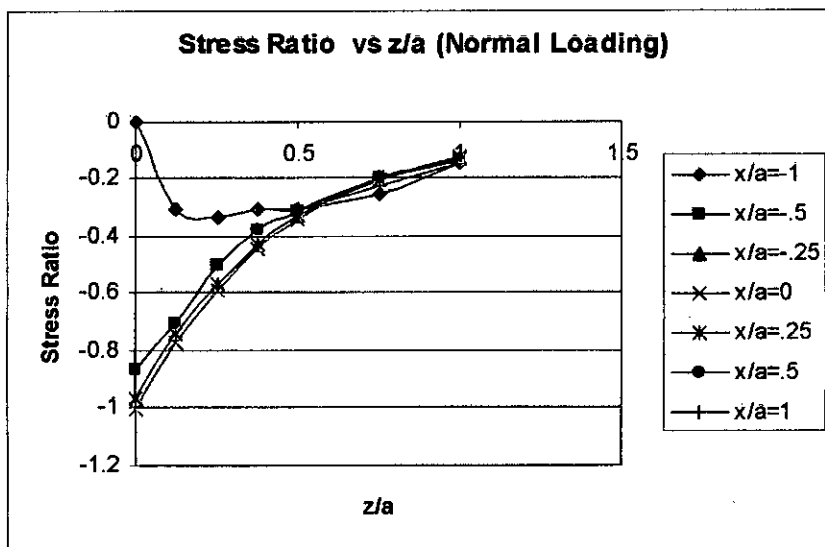
Figure 4.4: Stress distribution in X axis vs. z/a for normal loading

Stress distribution along z/a direction shows that the stresses are symmetrical about x/a =0 line i.e. center line. It has been shown that the maximum value has been found

at x/a = -1 which is 0.6 i.e. tension. On the other hand maximum value in compression has been found at x/a=1 which is 0.6.
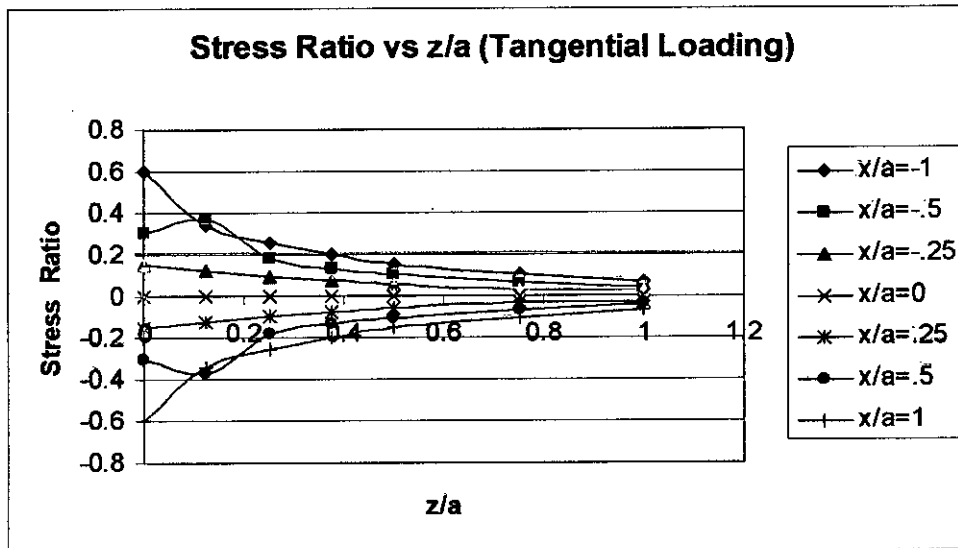
Figure 4.5: Stress distribution in X axis vs. z/a Tangential Loading

Stress distribution in X-direction for combined loading shows that the maximum value of compressive stress has been found at x/a = 0.5 i.e. some value tilted from the origin toward the leading edge. The reason behind this is, as the stresses are superposed to find the combined stresses. The stress for normal loading is always compressive on the other hand the stress for tangential loading is compressive only on the leading edge side. So combining these two stresses gives higher stress at x/a=0.5. The stress distribution in X direction vs z/a have been shown from figure 4.6.1 to 4.6.3 in case of both dimensionless form and different materials.
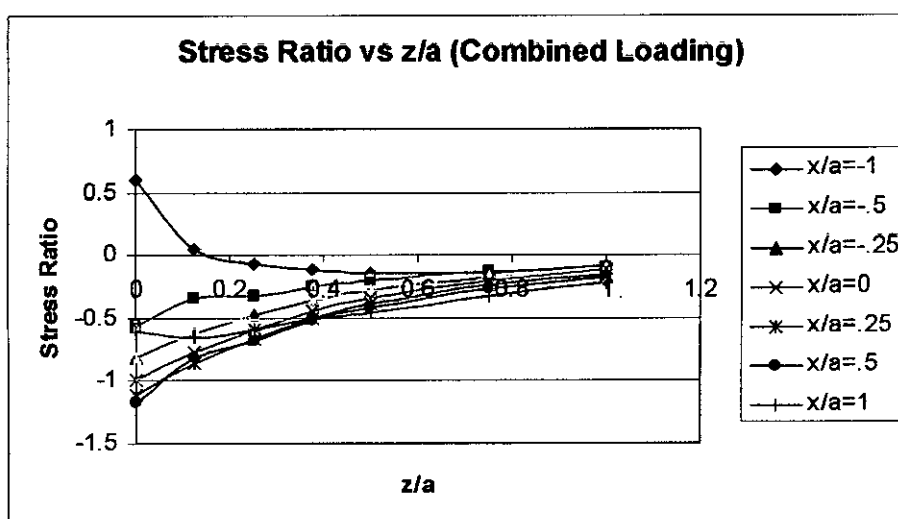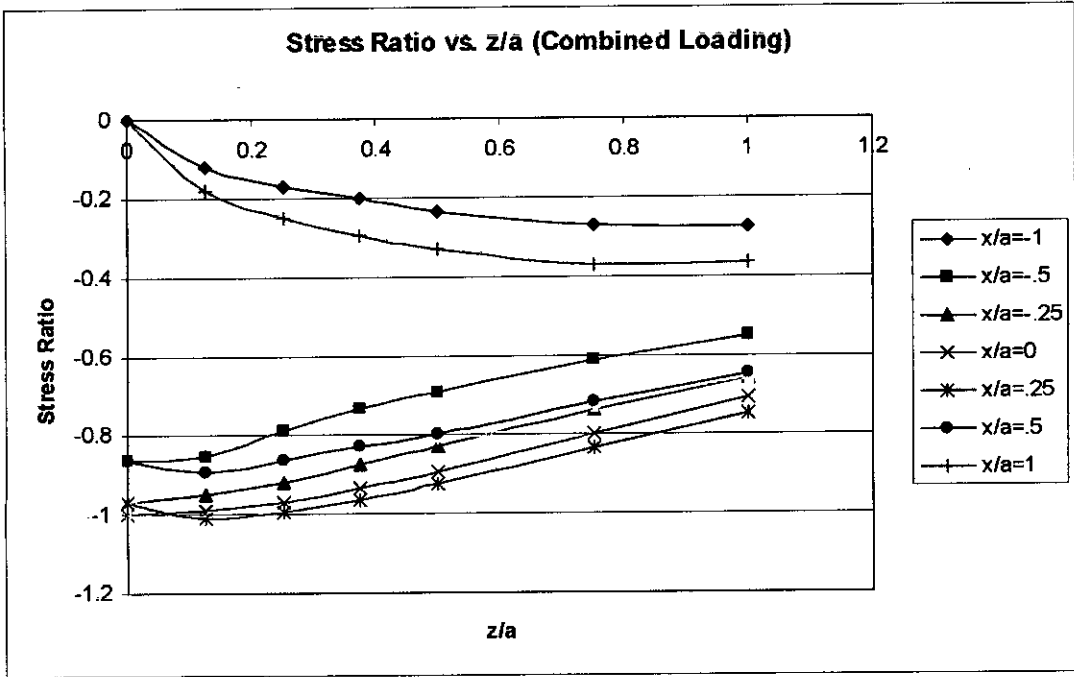

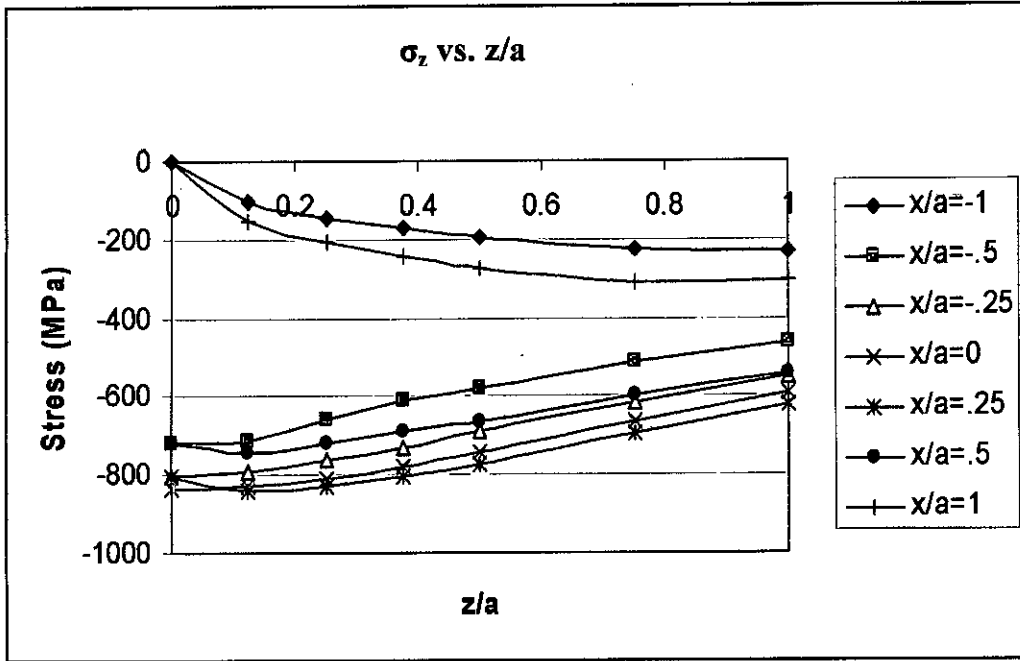Figure 4.6.1: Stress distribution in X axis vs. z/a for combined loading
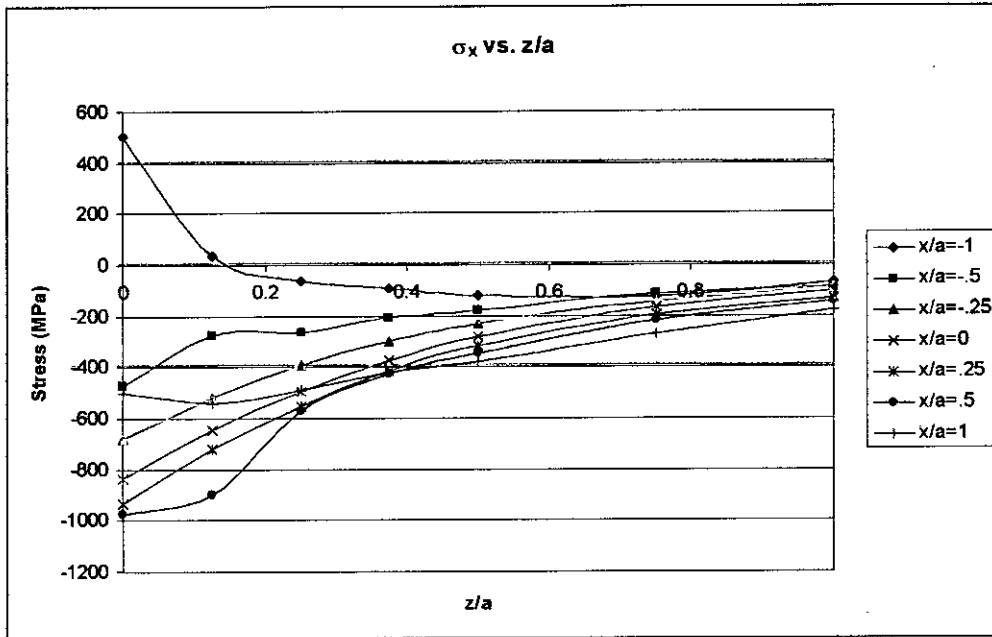
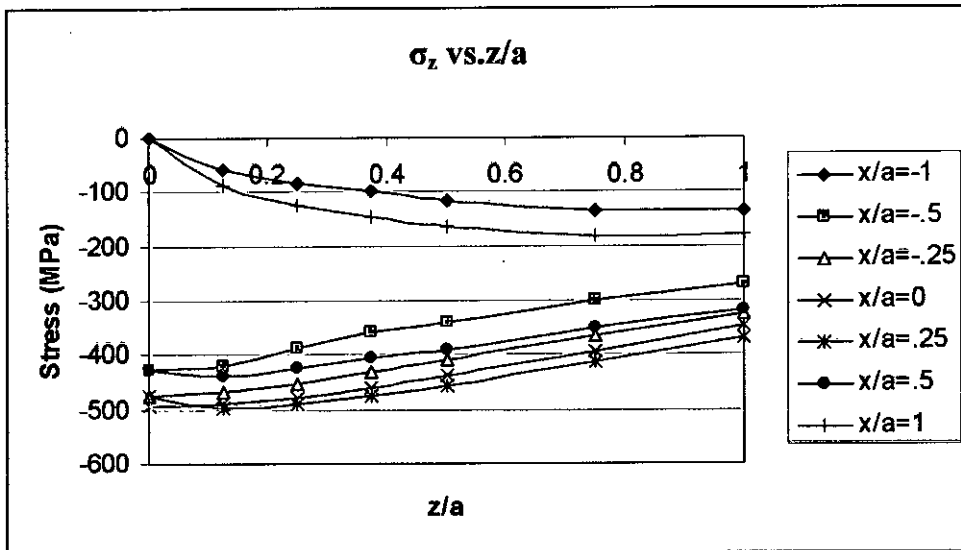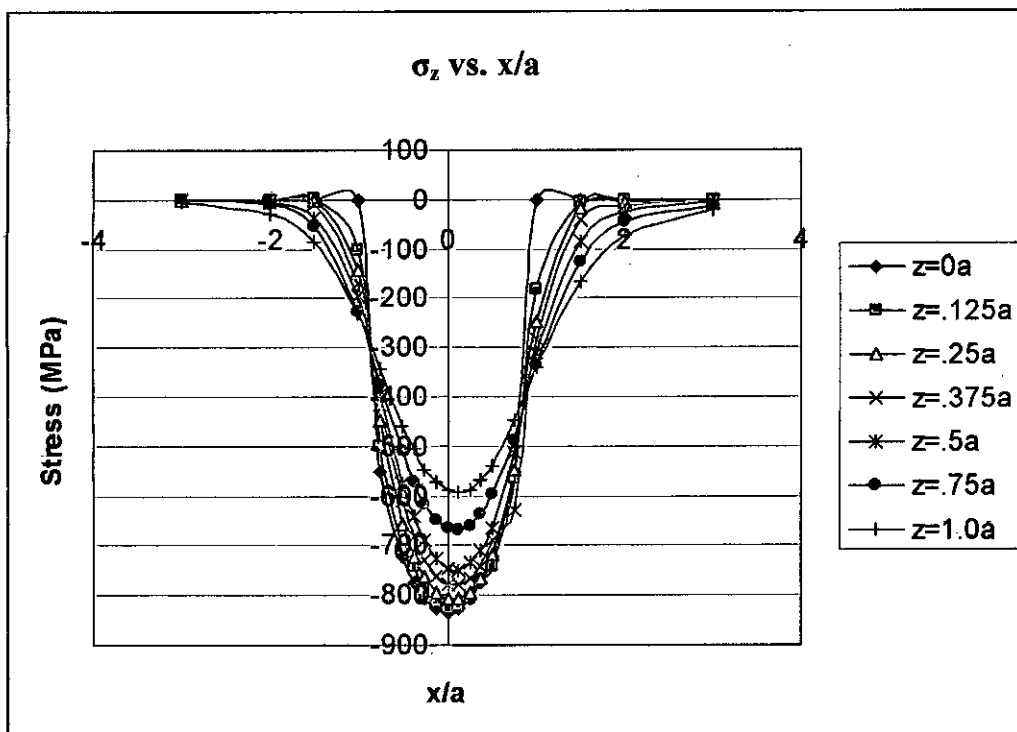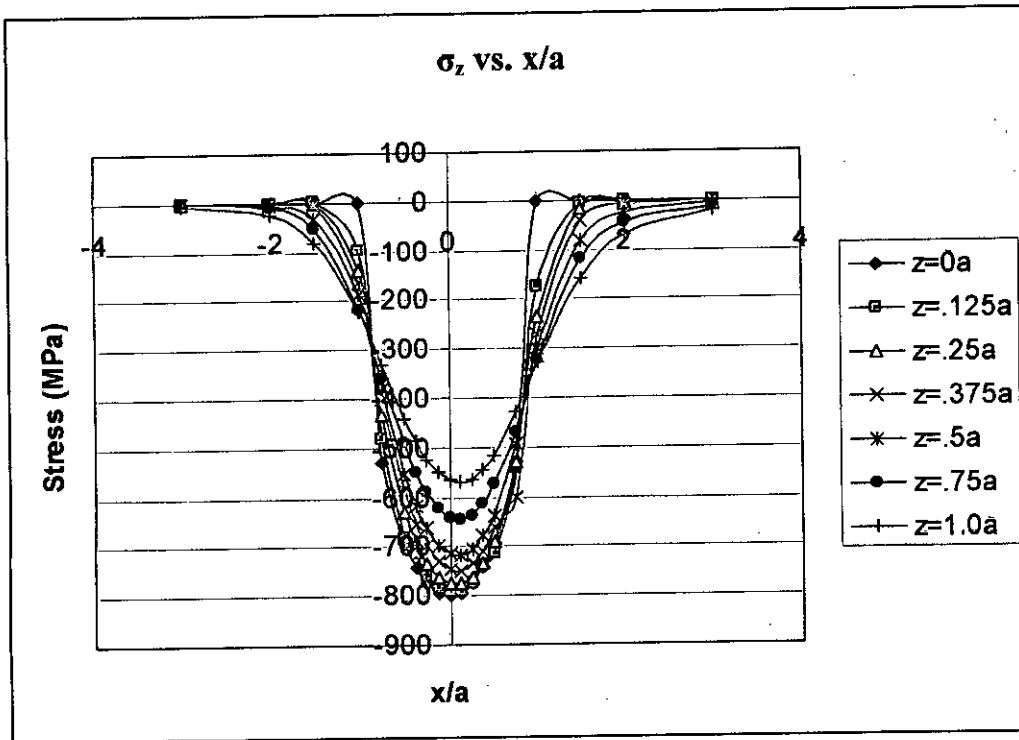Figure 4.6.2: Stress Distribution vs. z/a for vertex angle 5° at t = 0l (Steel)
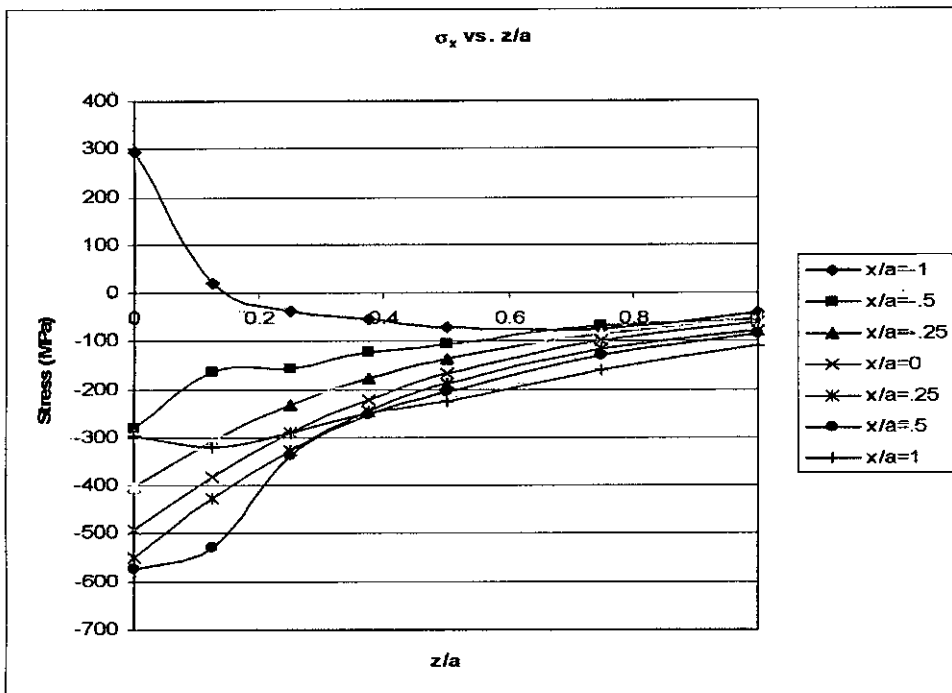
Figure 4.6.3: Stress Distribution vs. z/a for vertex angle 5° at t = 0l (Aluminum)

4.2.3. Distribution σ_x at different length

In the above paragraphs and graphs we have seen the variation of stress ratio at any cross section of the contact. As this thesis is based on contact in conical rollers, so it's cross section is not same at all section, hence there are different values for σ_x at different section and it varies along with length of the contact. As maximum contact pressure is higher at the tip of the conical roller, so stress will be high at the tip. It

41

decreases in value with the increases the length from the tip. In the following figure these has been shown for four different cross sections with different angles. As stress is higher at the surface so the distribution has been shown for z/a=0. The distributions of stresses for different length for combined loading have been shown from figure 4.7.1 to 4.7.10 for combined loading. The stress distributions vs. z/a have been shown from figure 4.8.1 to 4.8.9 for combined loading.
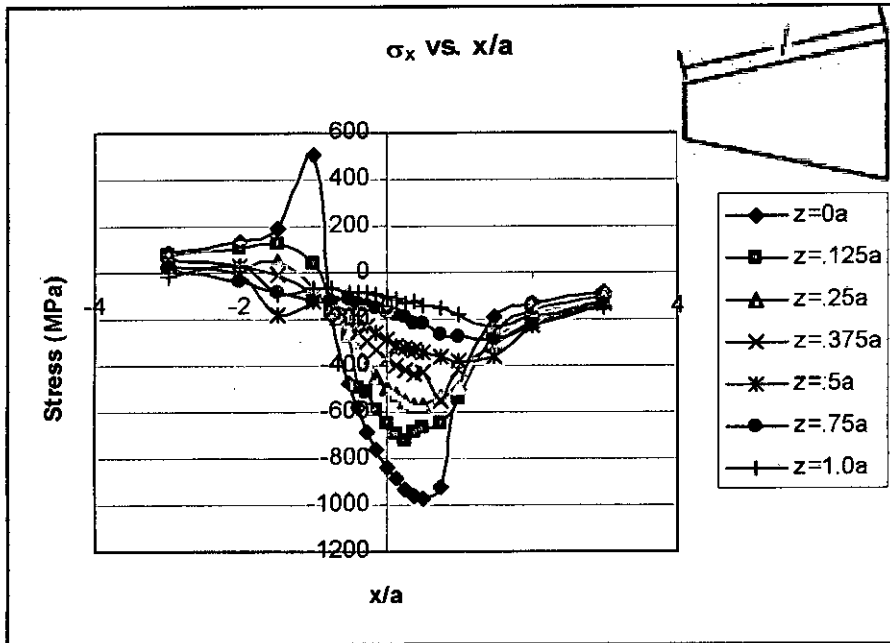
Figure 4.7.1: Stress Distribution vs. x/a for vertex angle 5° at t = 0*l* (Steel)
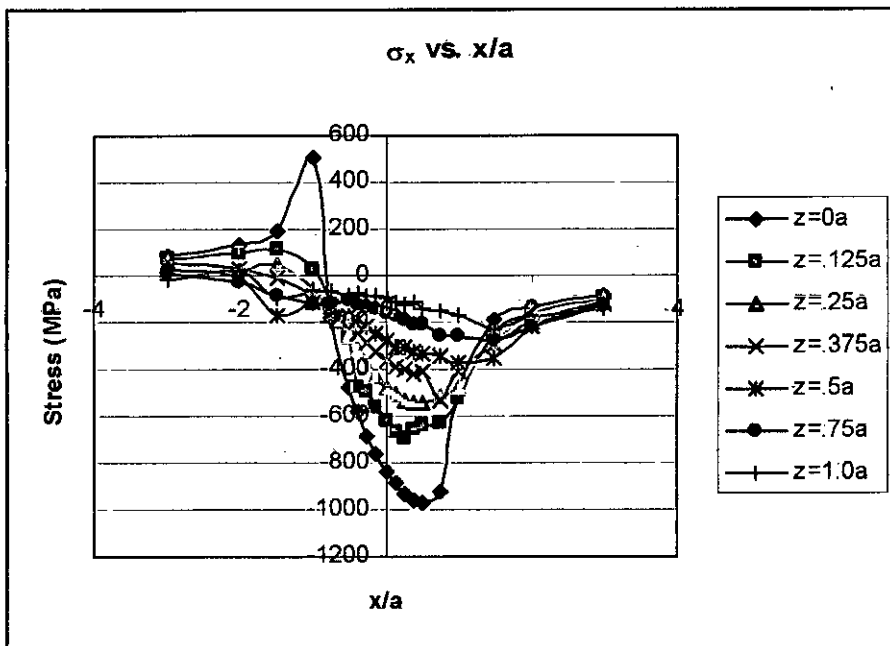
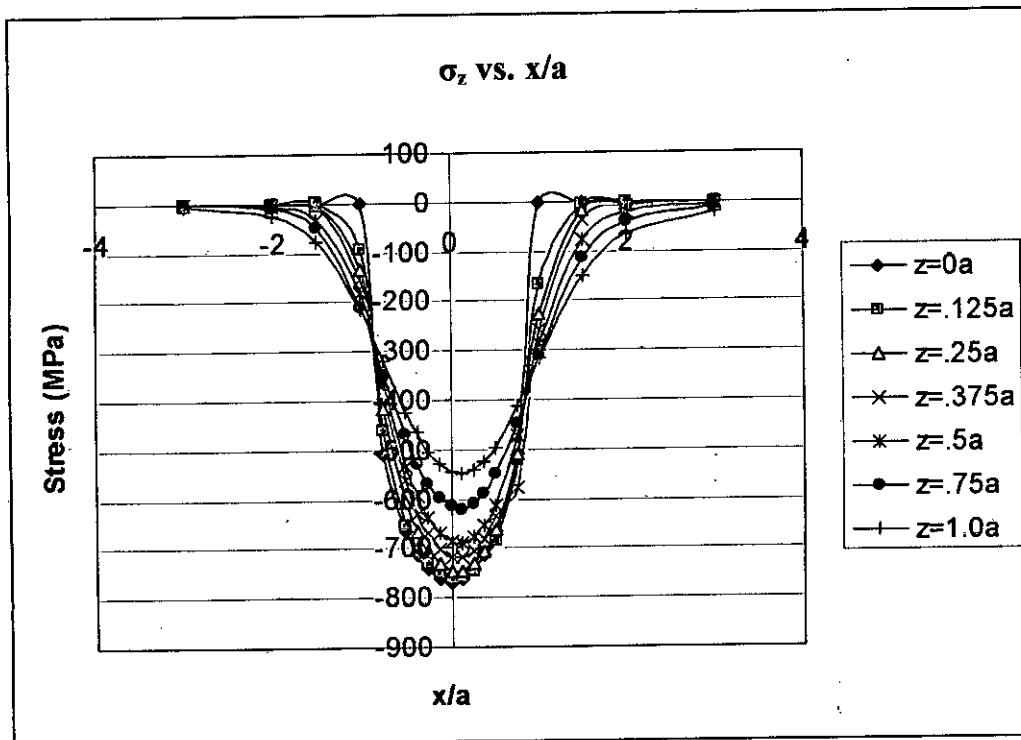Figure 4.7.2: Stress Distribution vs. x/a for vertex angle 5° at t = 0.25*l* (Steel)

42
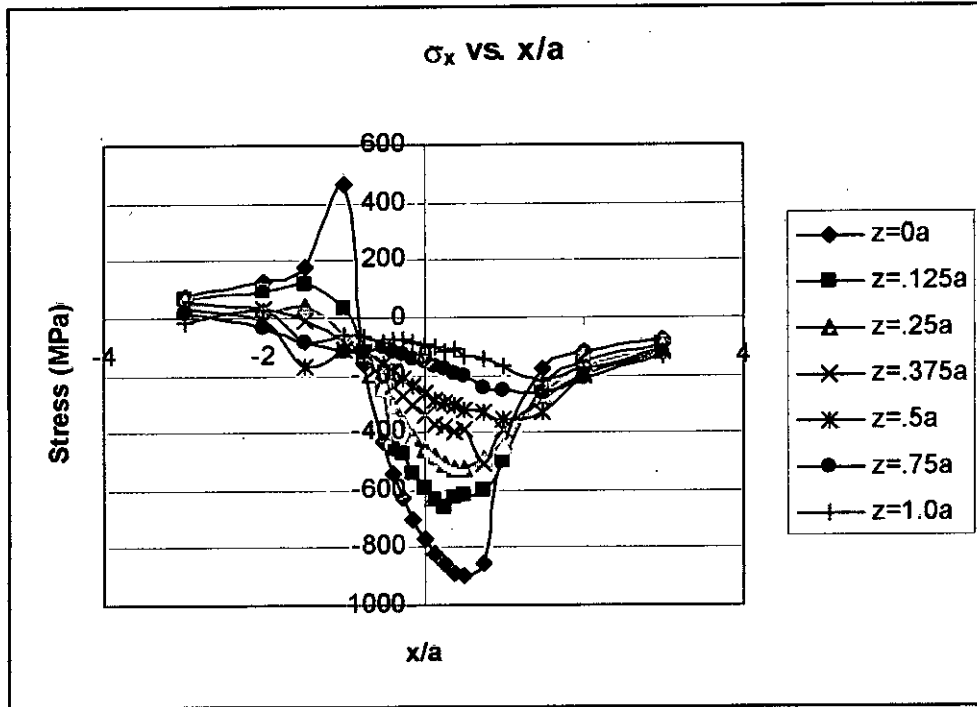
Figure 4.7.3: Stress Distribution vs. x/a for vertex angle 5° at t = 0.5*l* (Steel)
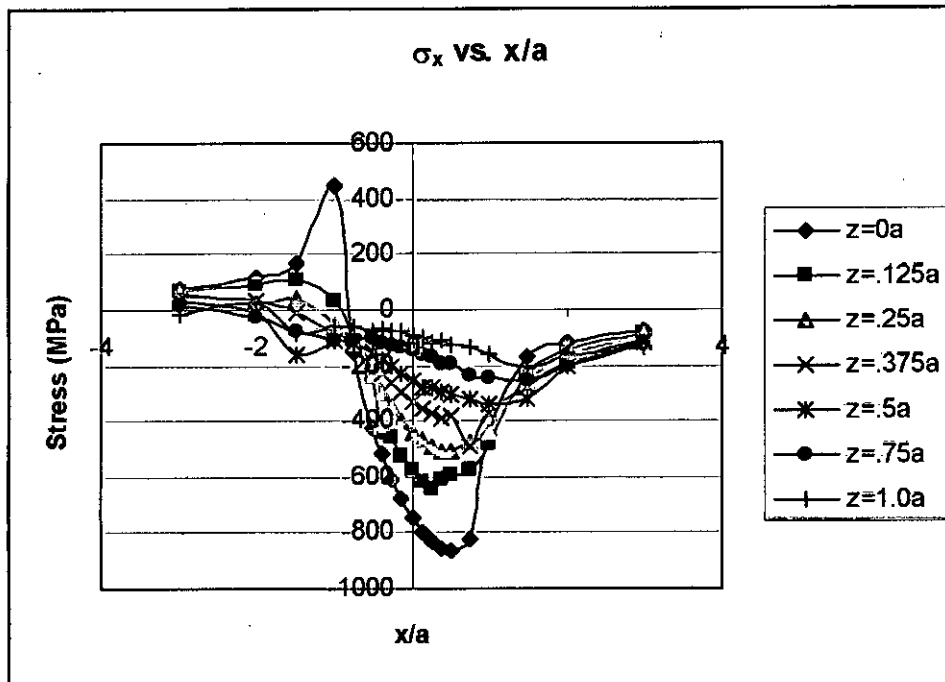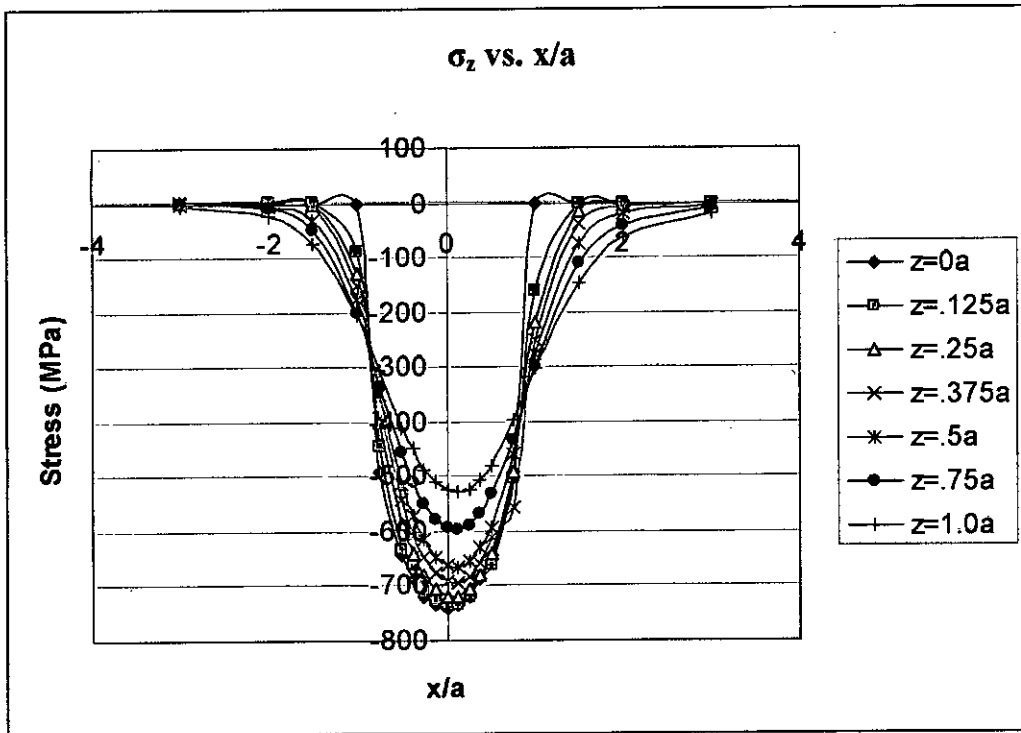

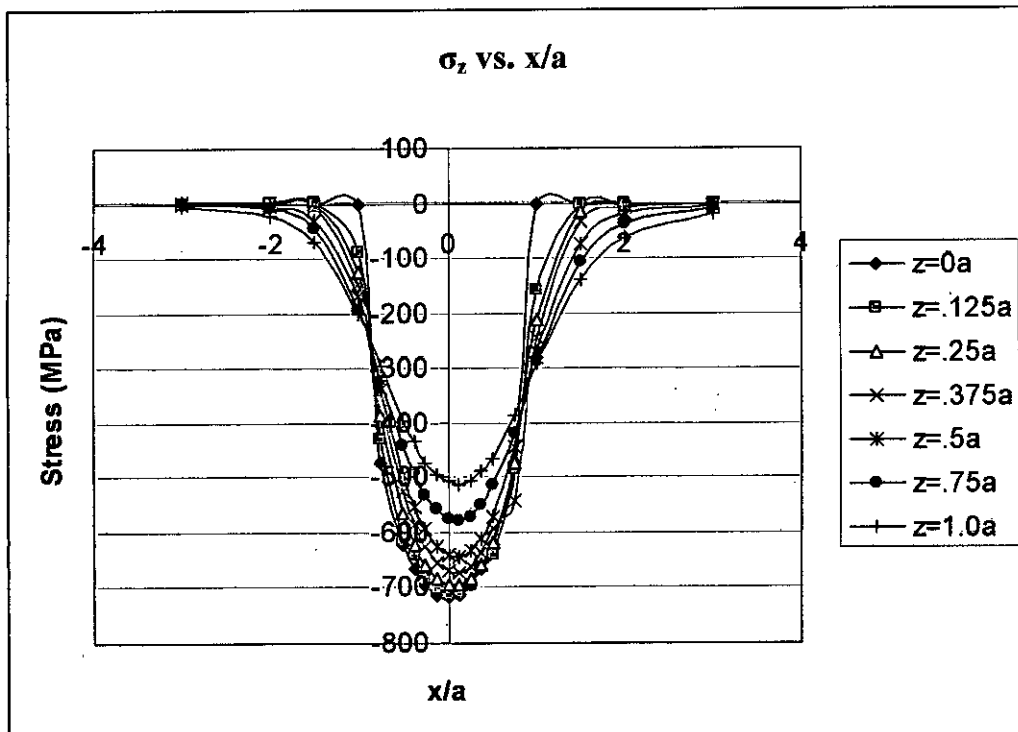Figure 4.7.4: Stress Distribution vs. x/a for vertex angle 5° at t = 0.75*l* (Steel)
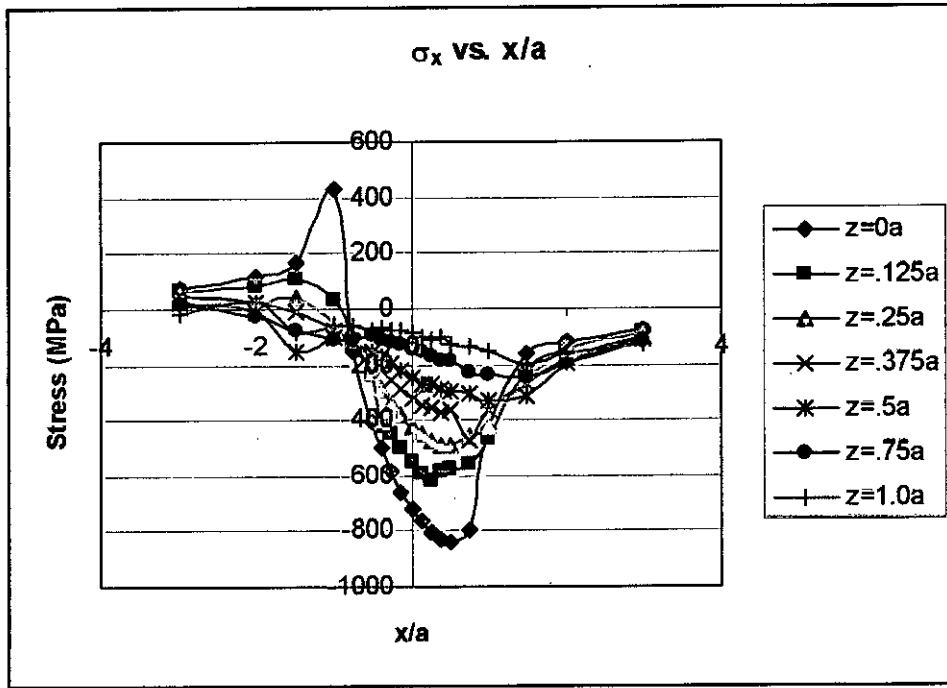
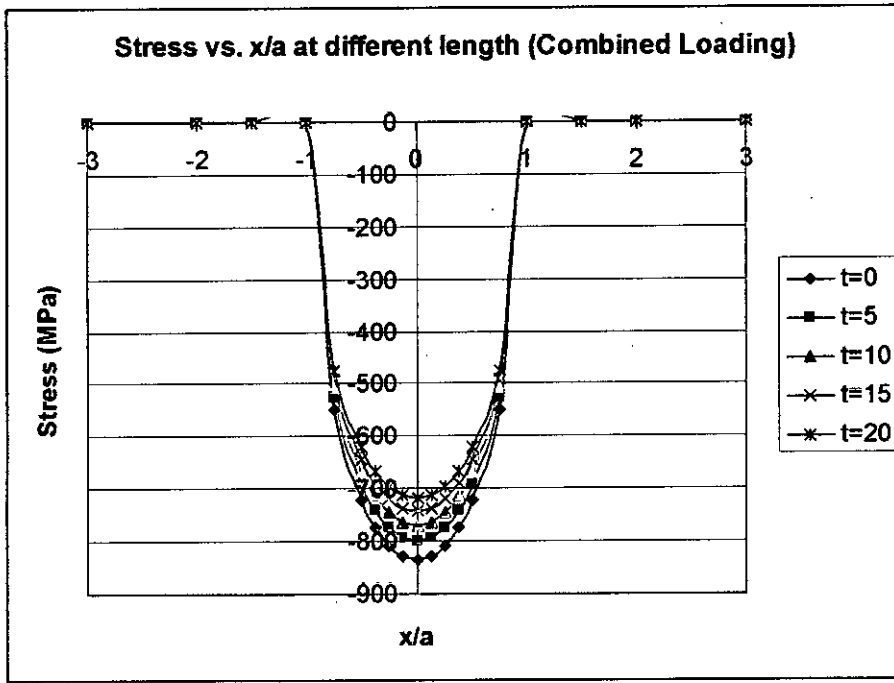Figure 4.7.5: Stress Distribution vs. x/a for vertex angle 5° at t =1*l* (Steel)
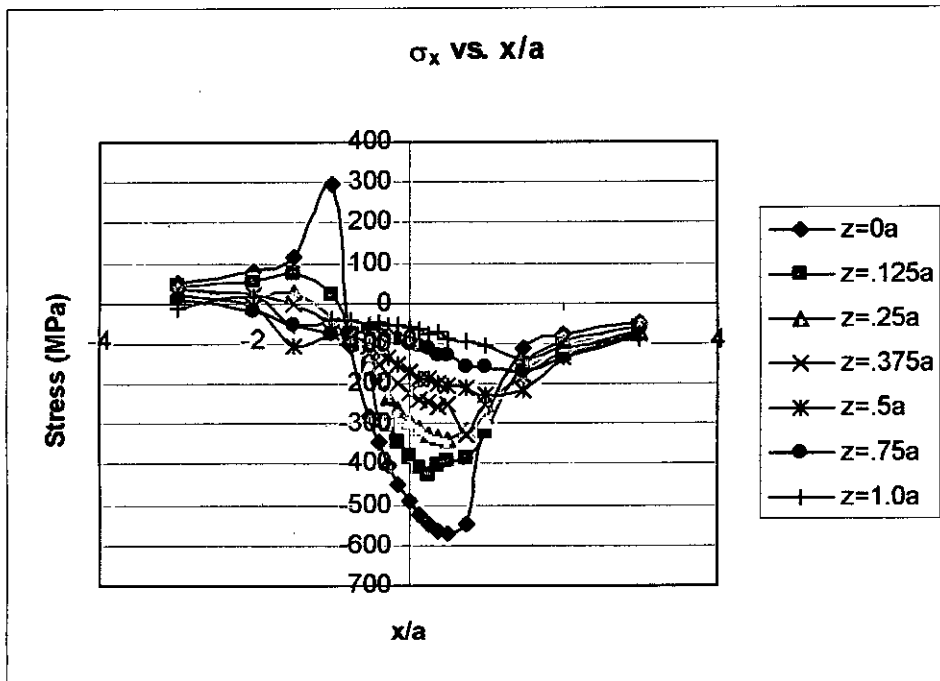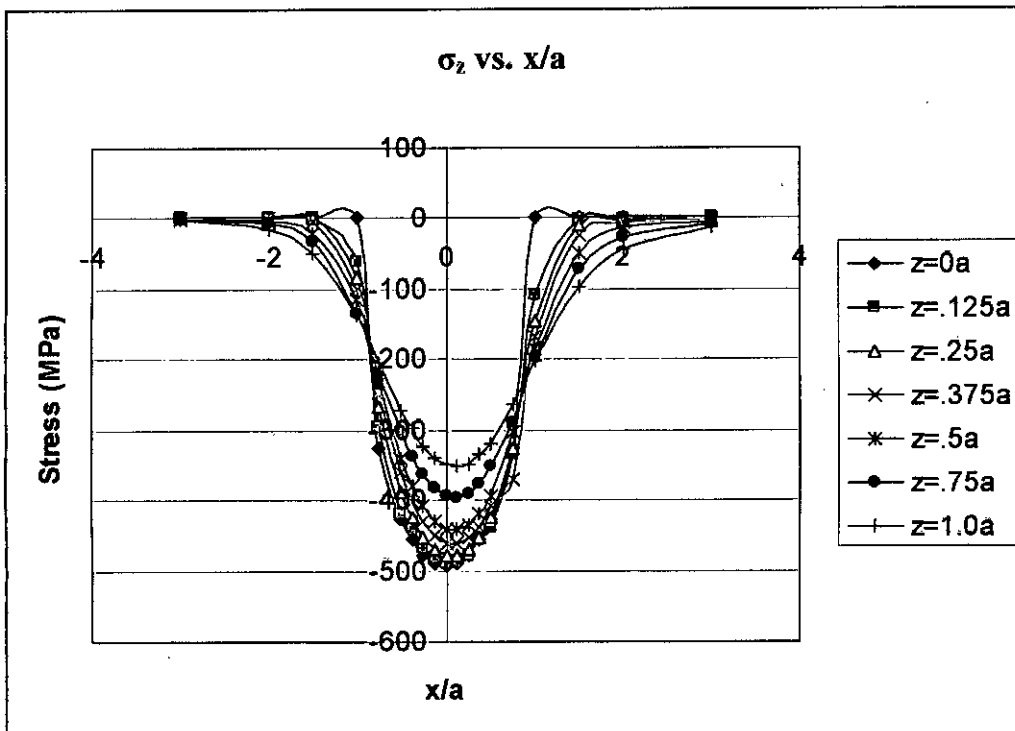

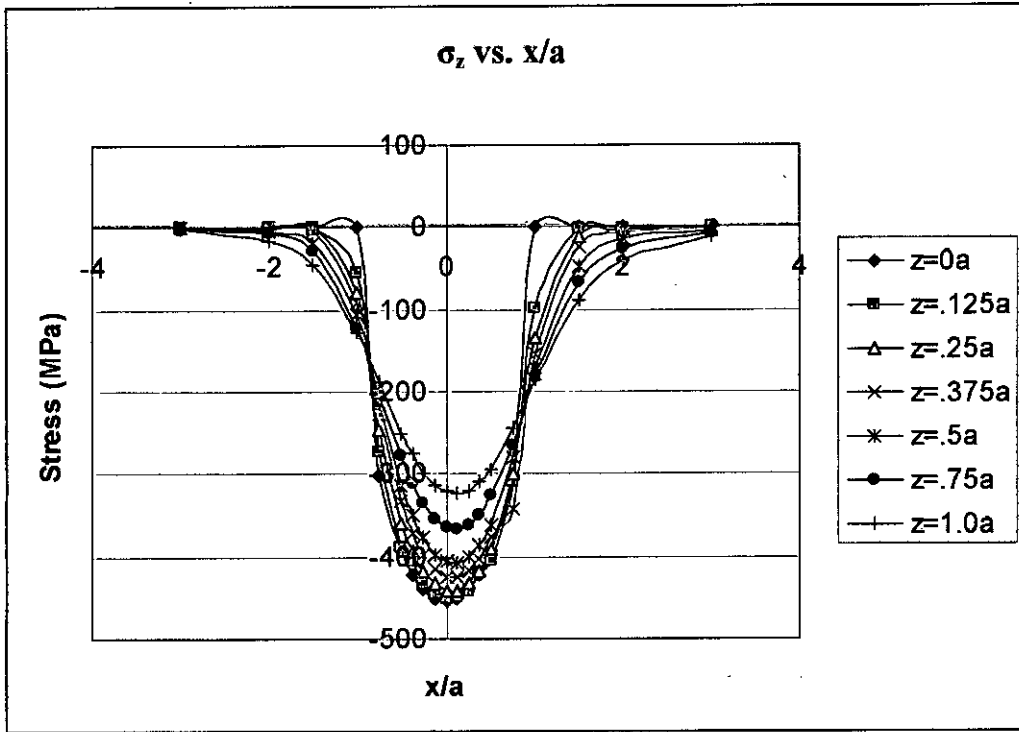Figure 4.7.6: Stress Distribution vs. x/a for vertex angle 5° at t =0*l* (Aluminum)
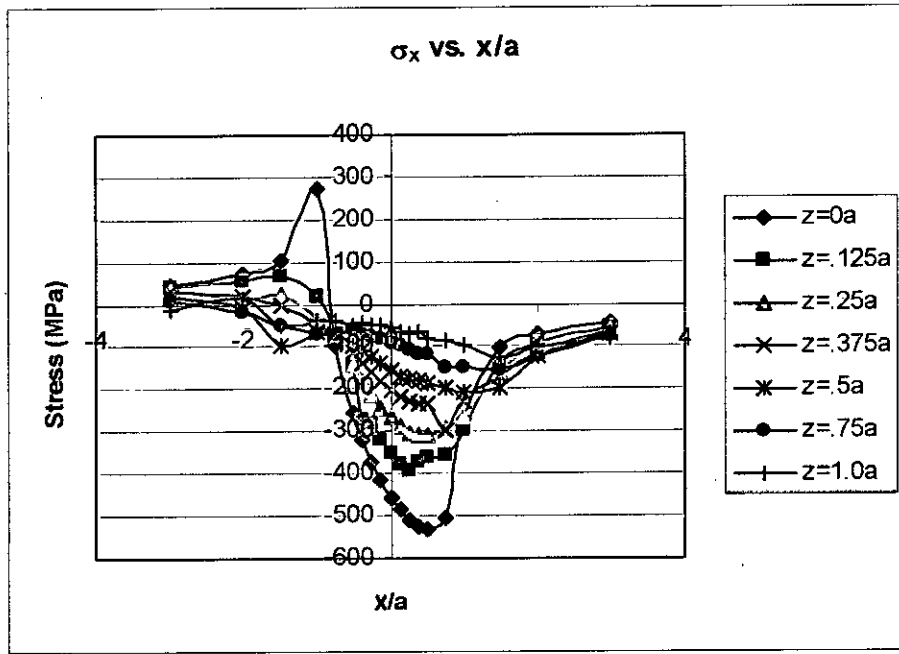
Figure 4.7.7: Stress Distribution vs. x/a for vertex angle 5° at t =0.5l (Aluminum)
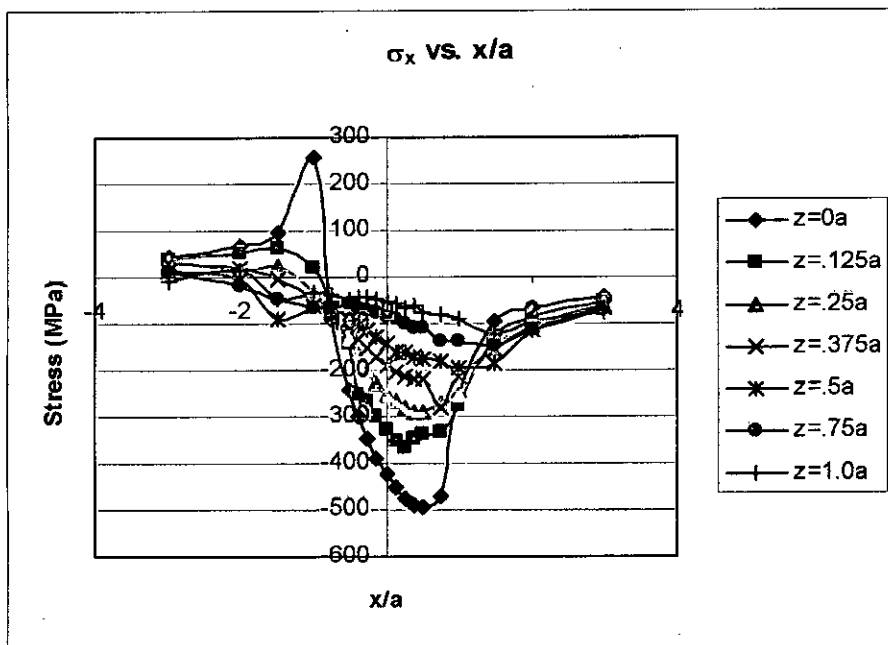
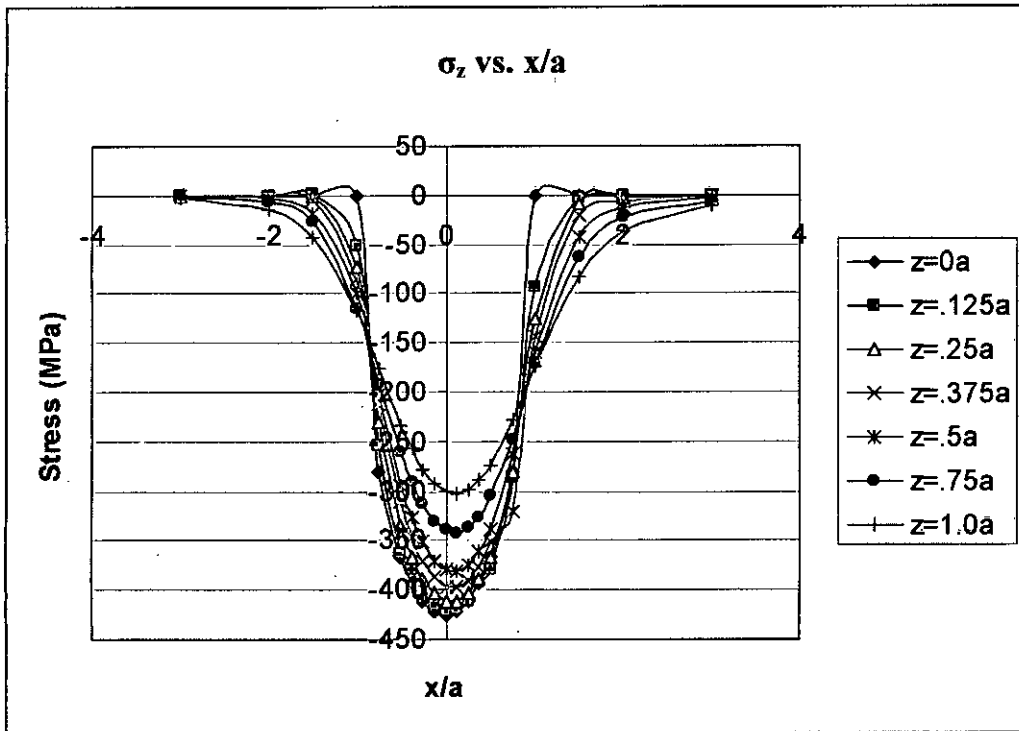Figure 4.7.8: Stress Distribution vs. x/a for vertex angle 5° at t =1l (Aluminum)
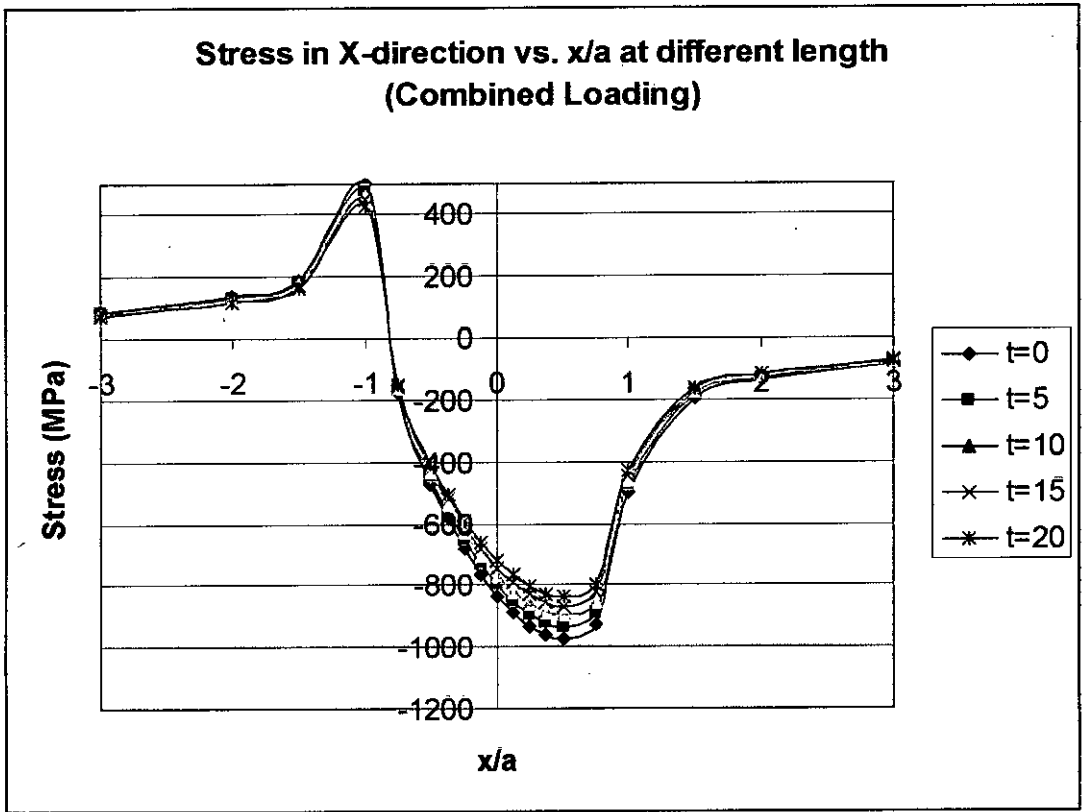
Figure 4.7.9: Stress distribution in X direction at different length at z/a=0 with vertex angle 5° (Steel)
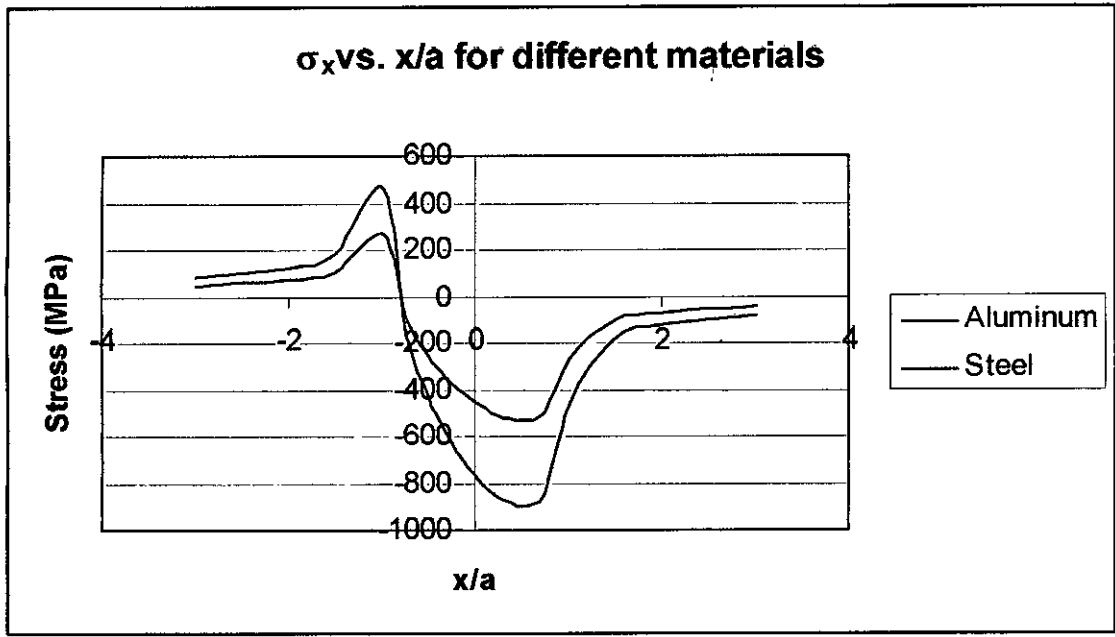
Figure 4.7.10: Stress Distribution vs. x/a at t = 0.5*l* for vertex angle 0° for different materials
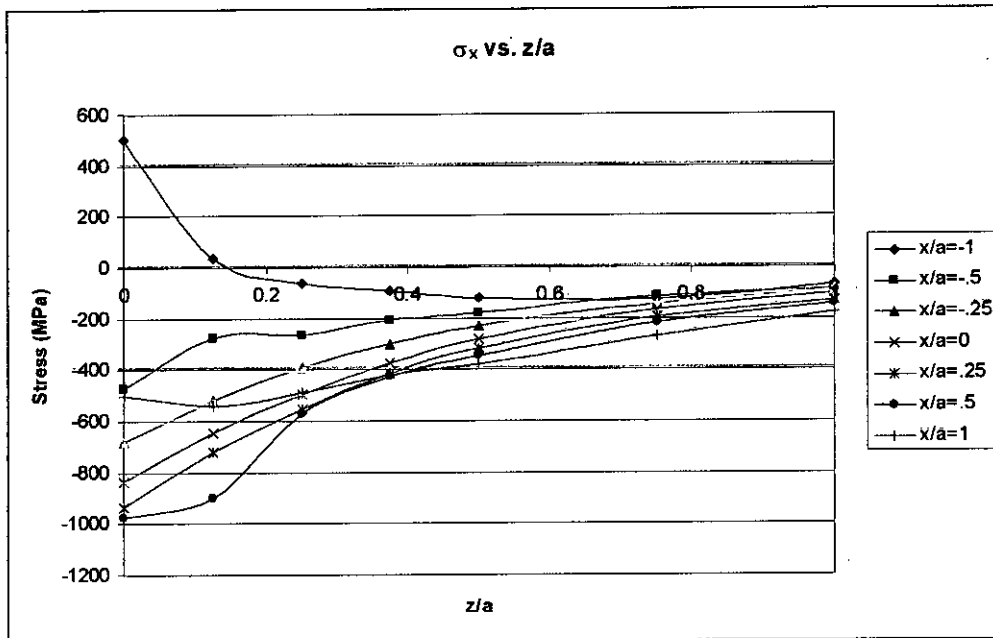
Figure 4.8.1 Stress Distribution vs. z/a for vertex angle $5°$ at t = 0l (steel)
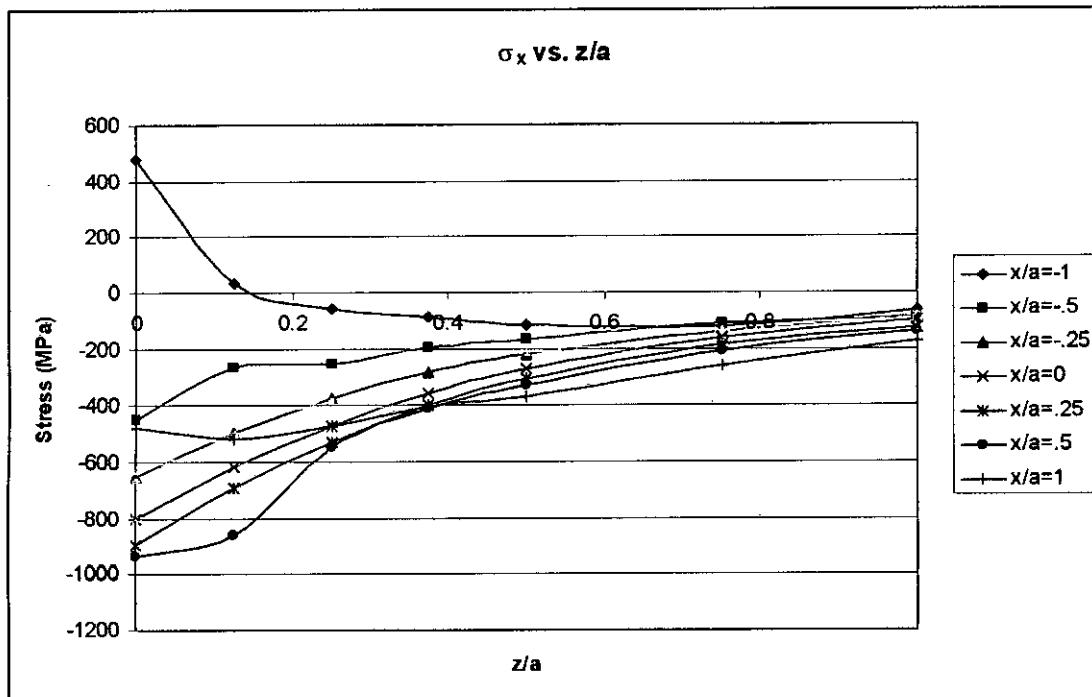
Figure 4.8.2 Stress Distribution vs. z/a for vertex angle $5°$ at t = 0.25l (steel)
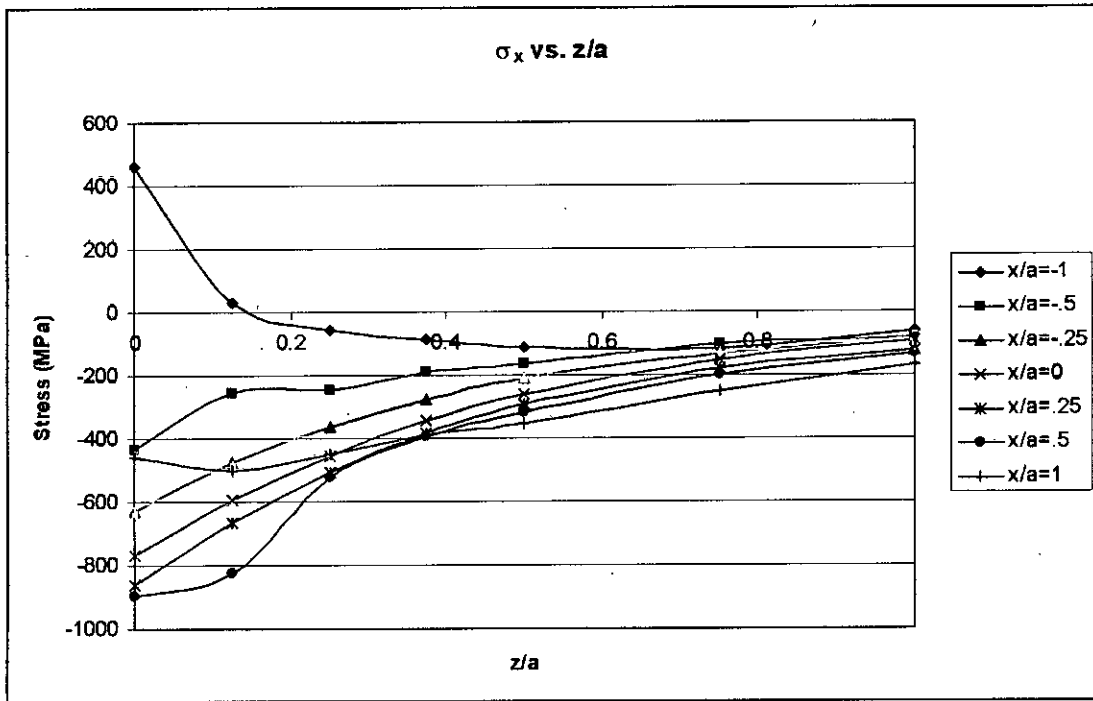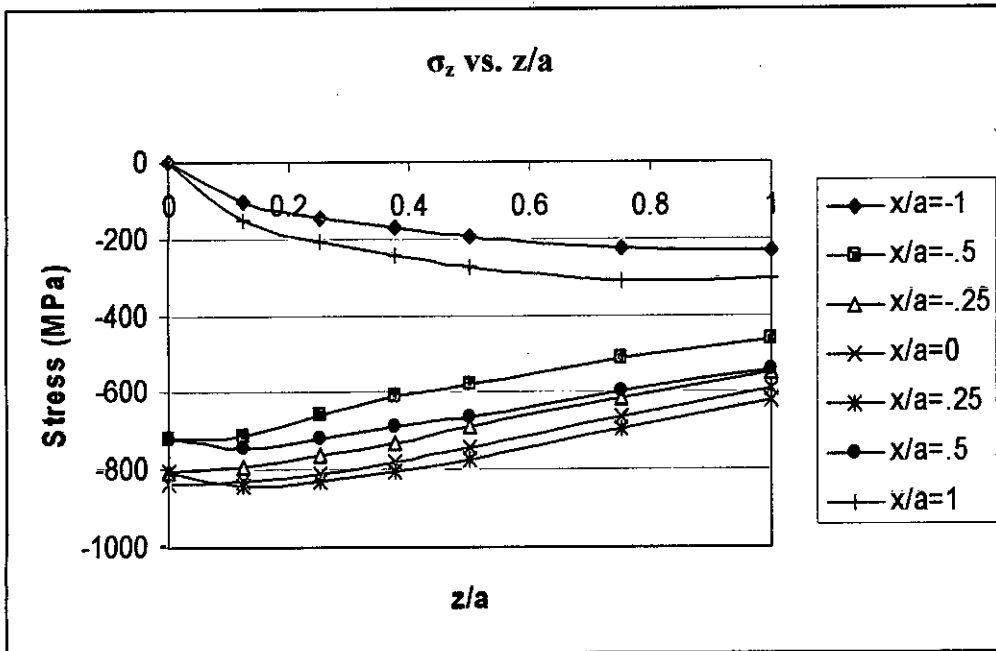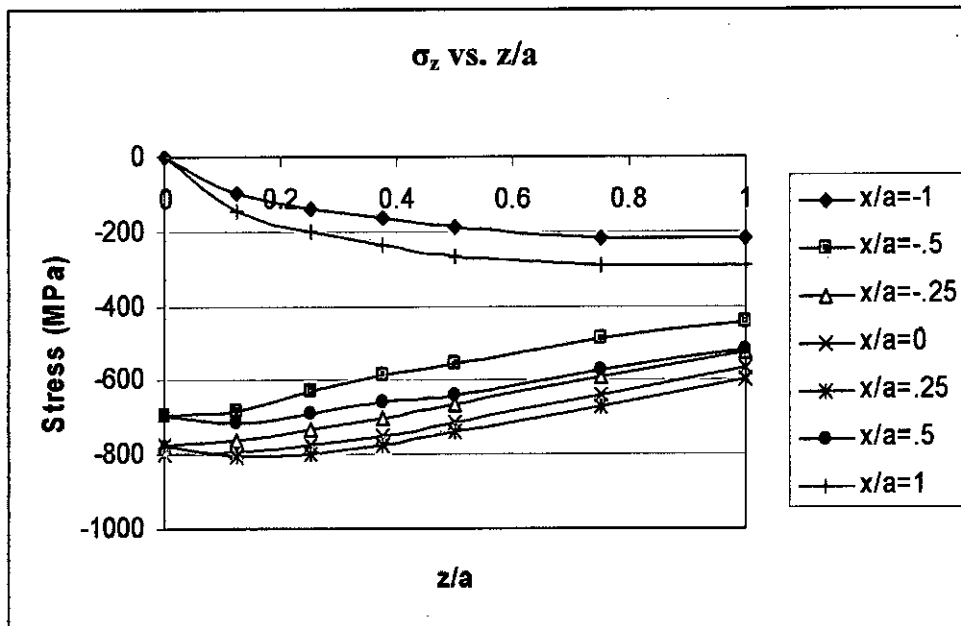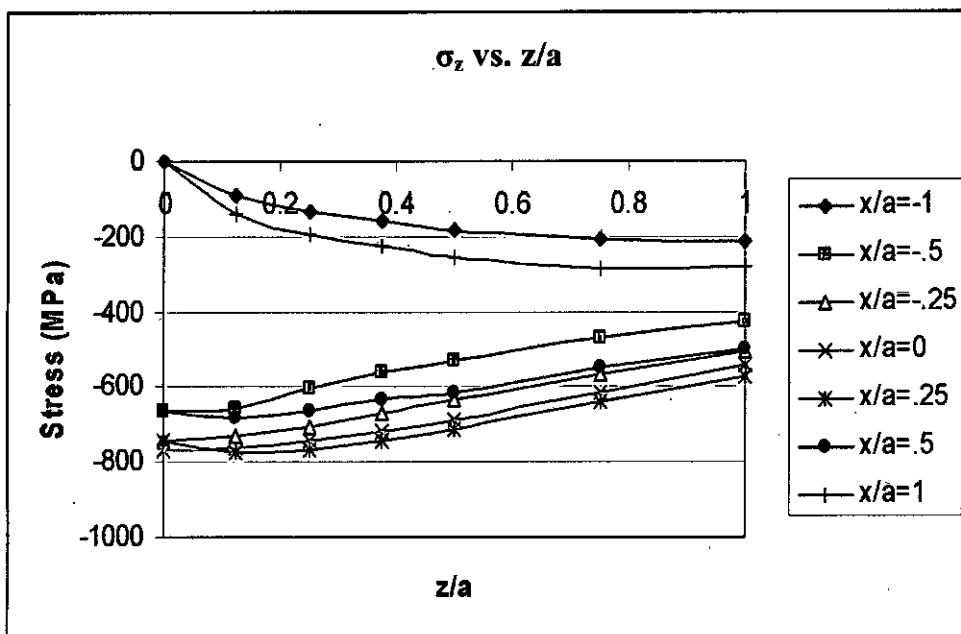
Figure 4.8.3: Stress Distribution vs. z/a for vertex angle 5° at t = 0.5l (steel)
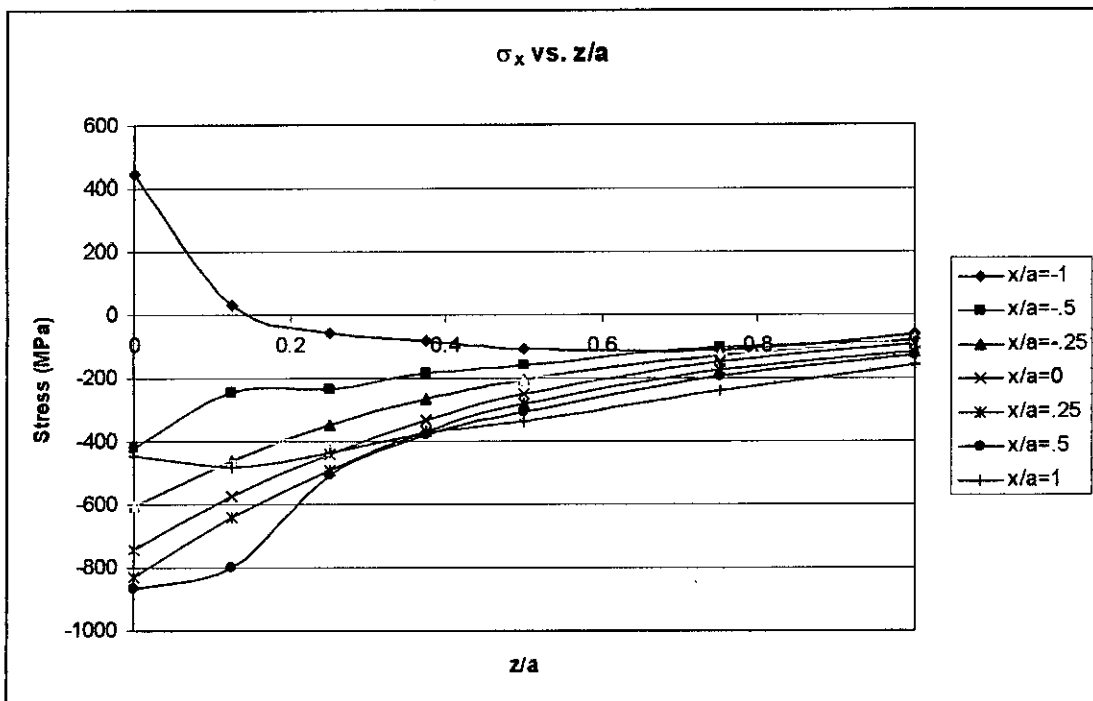
Figure 4.8.4: Stress Distribution vs. z/a for vertex angle 5° at t = 0.75l (steel)
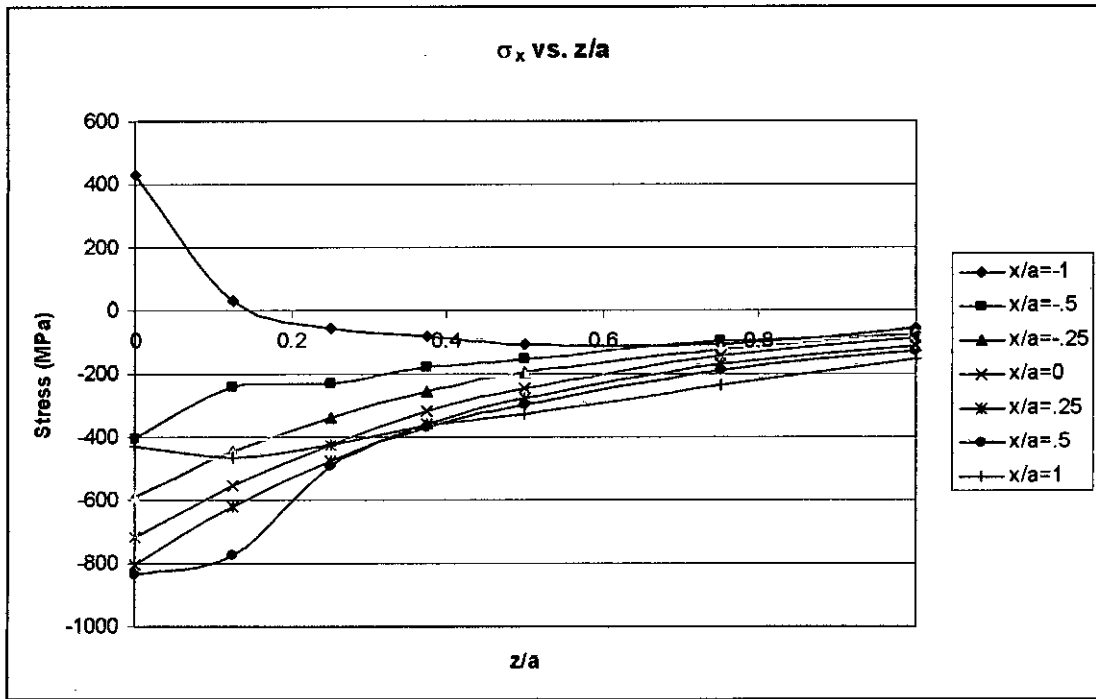
Figure 4.8.5: Stress Distribution vs. z/a for vertex angle 5° at t = 1*l* (steel)
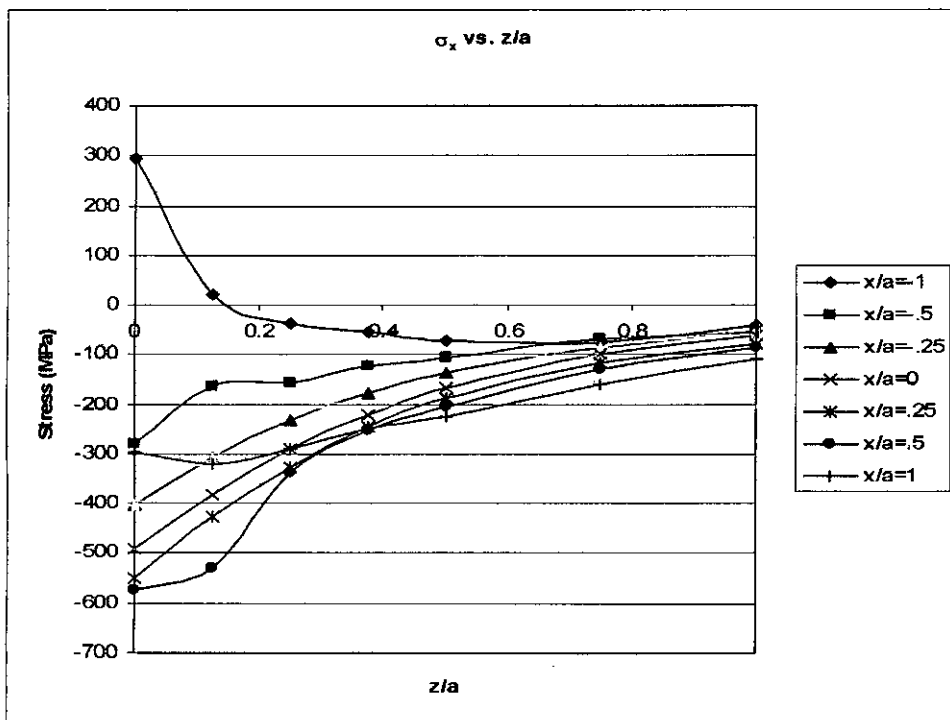
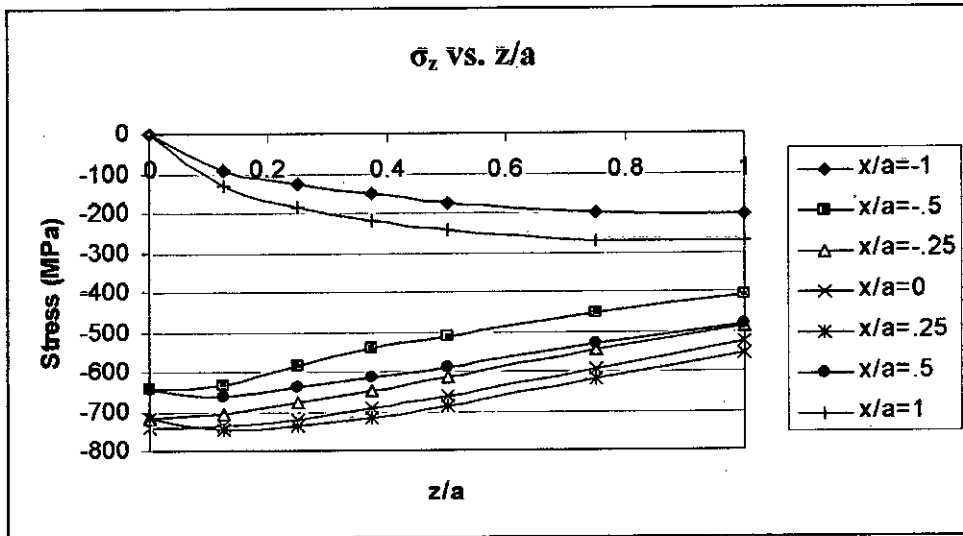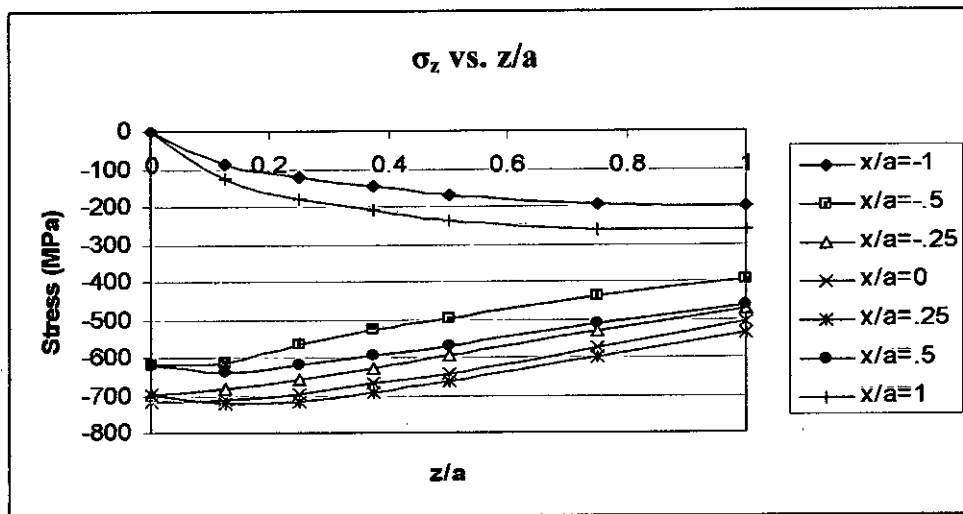Figure 4.8.6: Stress Distribution vs. z/a for vertex angle 5° at t = 0*l* (Aluminum)
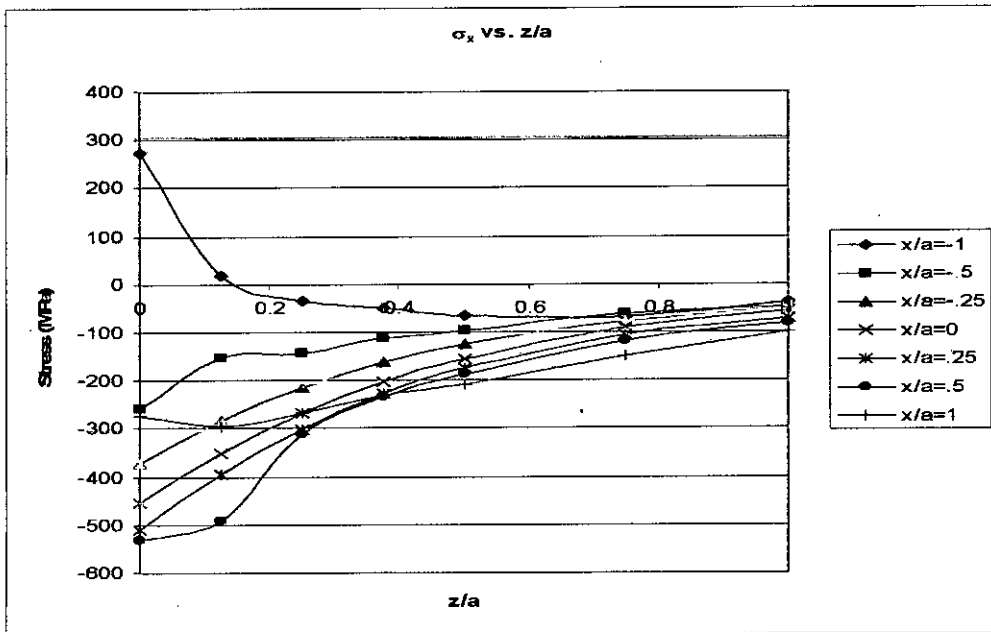
Figure 4.8.7: Stress Distribution vs. z/a for vertex angle 5° at t = 0.5*l* (Aluminum)
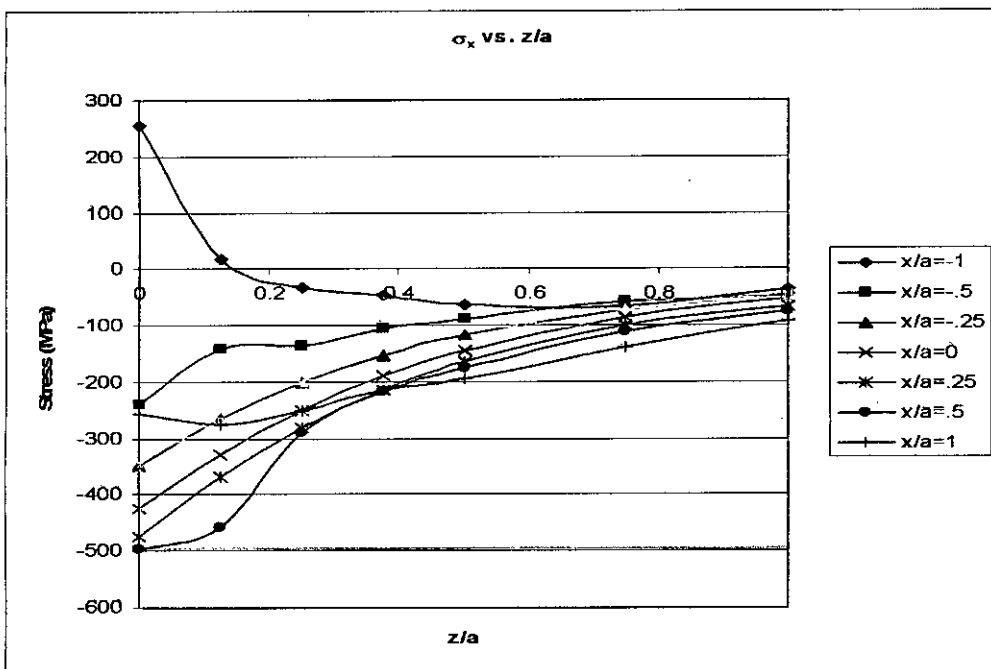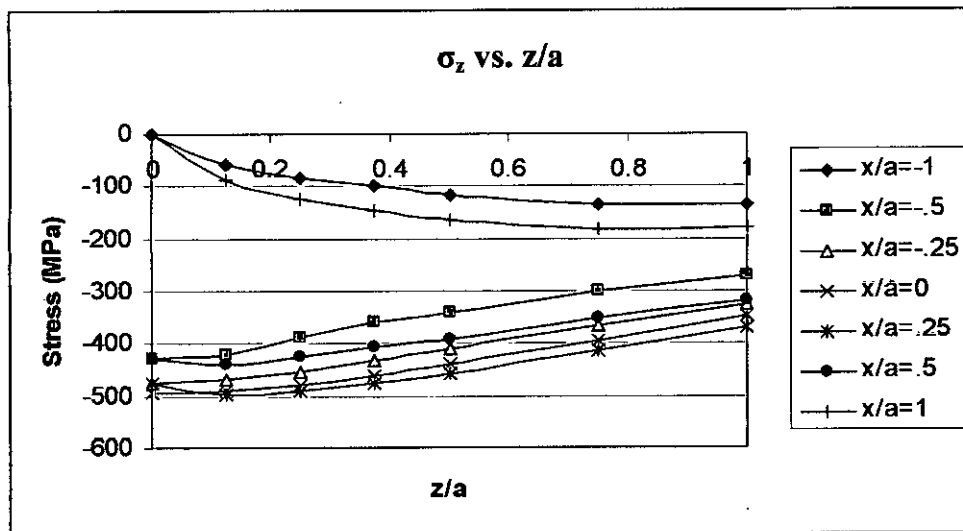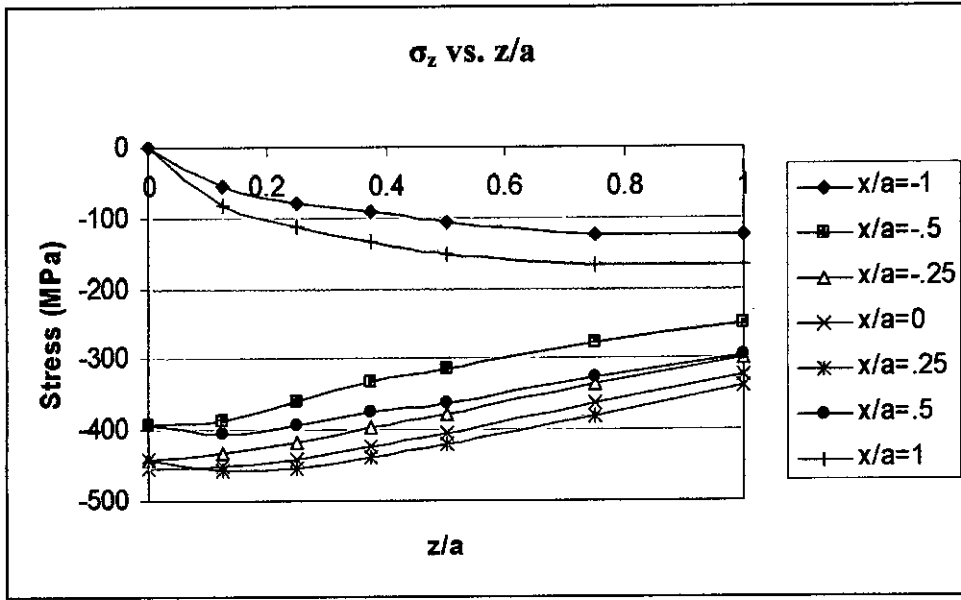

Figure 4.8.8: Stress Distribution vs. z/a for vertex angle 5° at t = 1*l* (Aluminum)
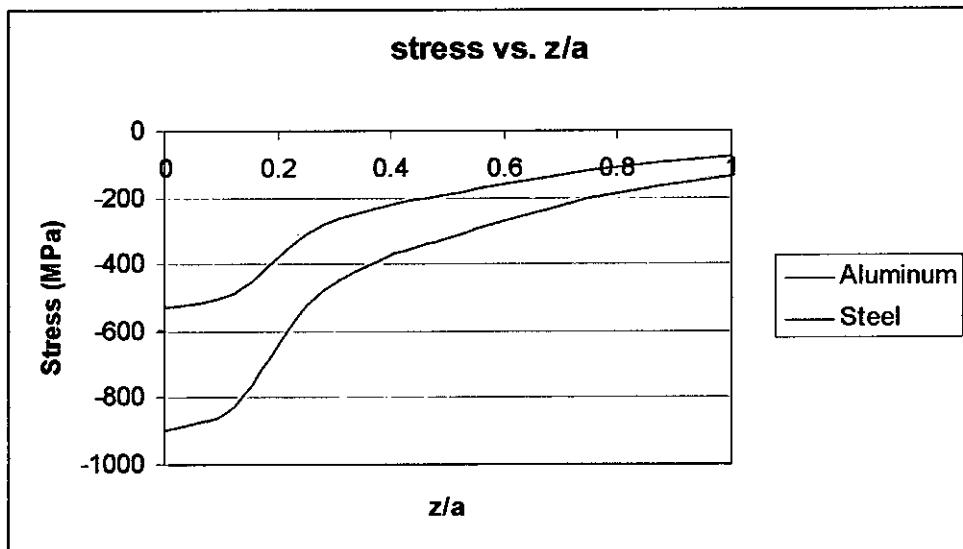
Figure 4.8.8: Stress Distribution vs. z/a for vertex angle 5° at t = 0.51 for different materials

4.2.4 Distribution σ_z at different vertex angle

The distribution of stress in X- direction also varies in value for different vertex angles. The variations of values depend on maximum pressure and half width length. As with increasing of vertex angle the half width length increase, hence maximum pressure decreases. So, the value of maximum stress decreases with increasing vertex angle, but the distribution is same according to approximation of Hertz theory. Here variations have shown for four different angles. Stress distributions along x/a for different vertex angle have been shown from figure 4.9.1 to 4.9.5.
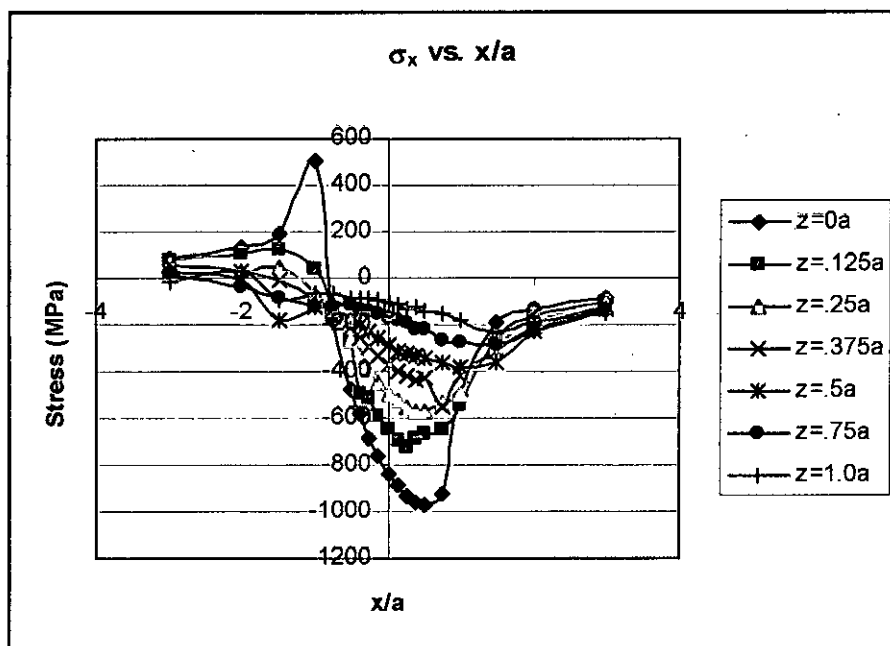
Figure 4.9.1: Stress Distribution vs. x/a for vertex angle 5° (Steel)
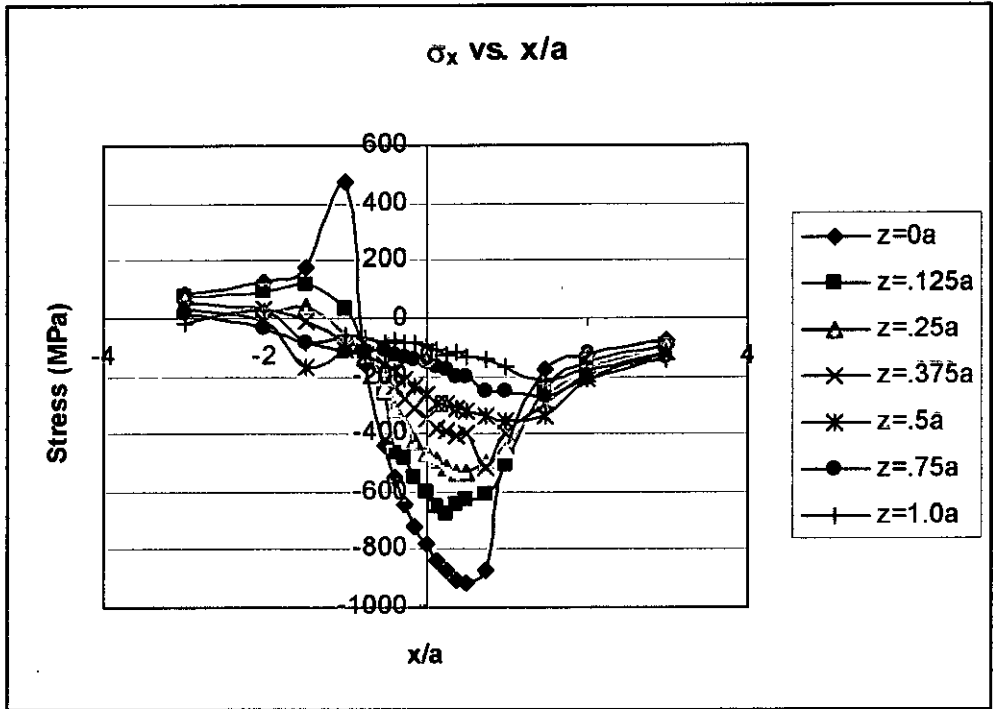
Figure 4.9.2: Stress Distribution vs. x/a for vertex angle 20° (Steel)
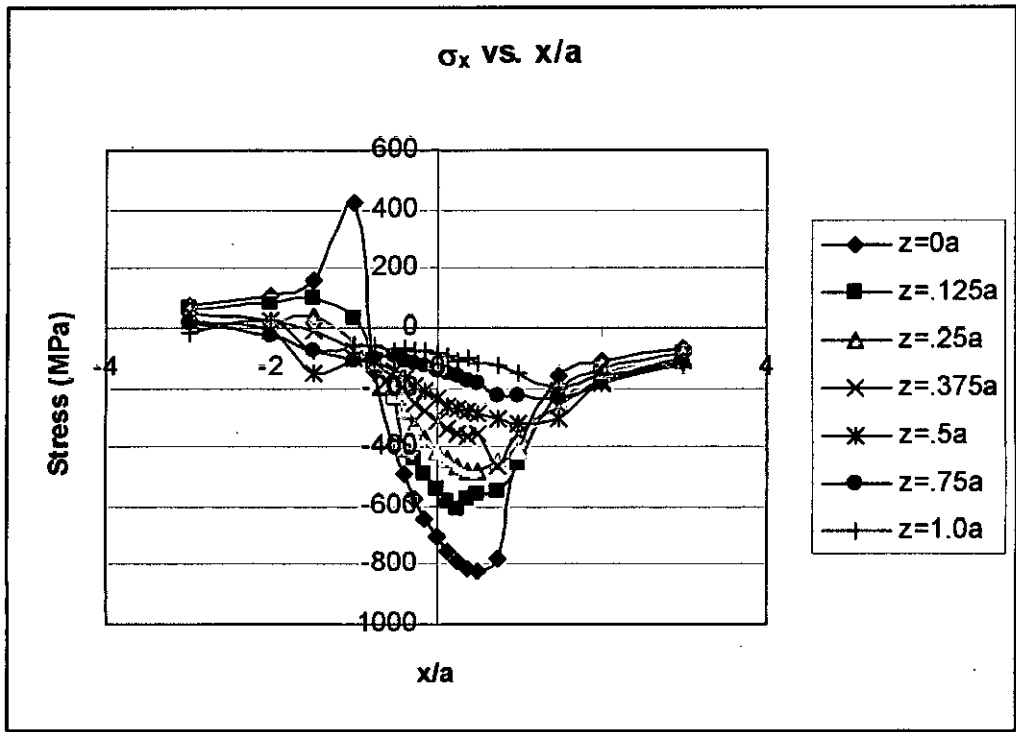
Figure 4.9.3: Stress Distribution vs. x/a for vertex angle 30° (Steel)
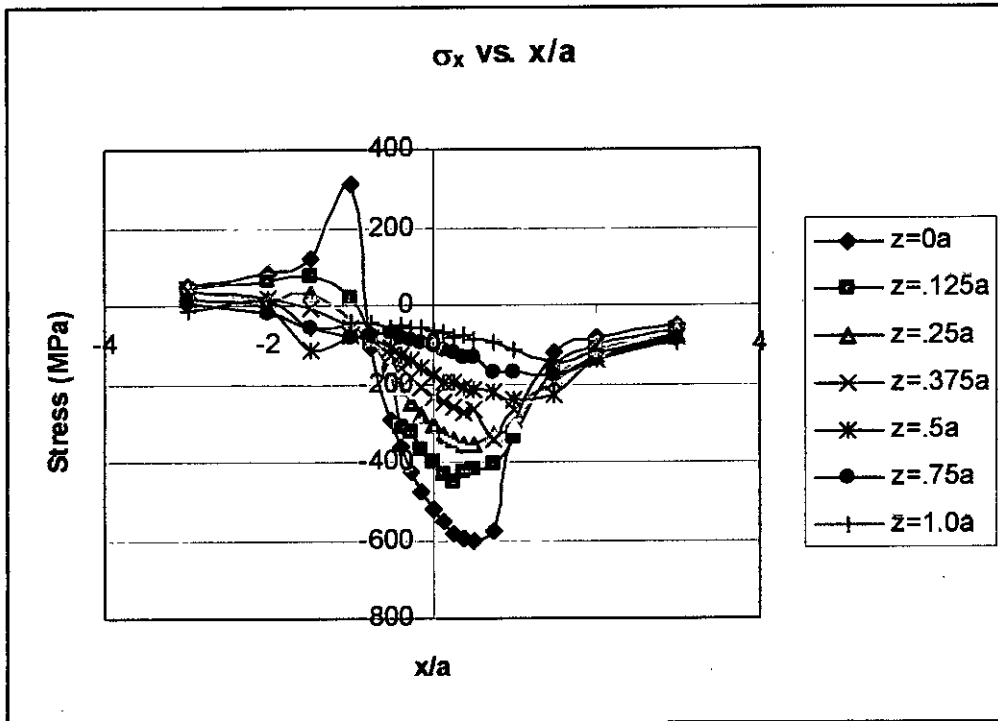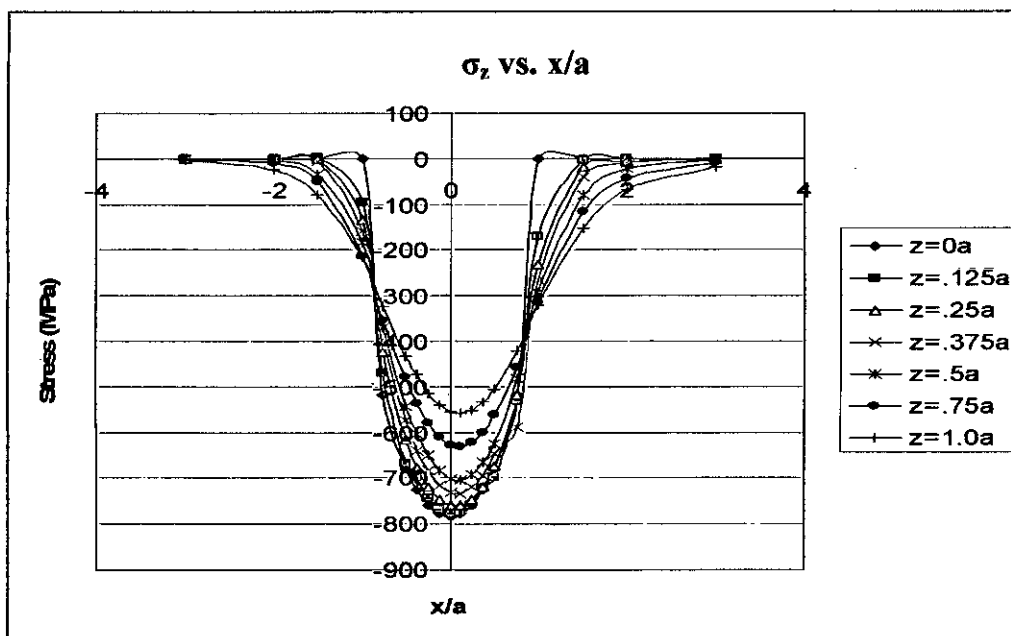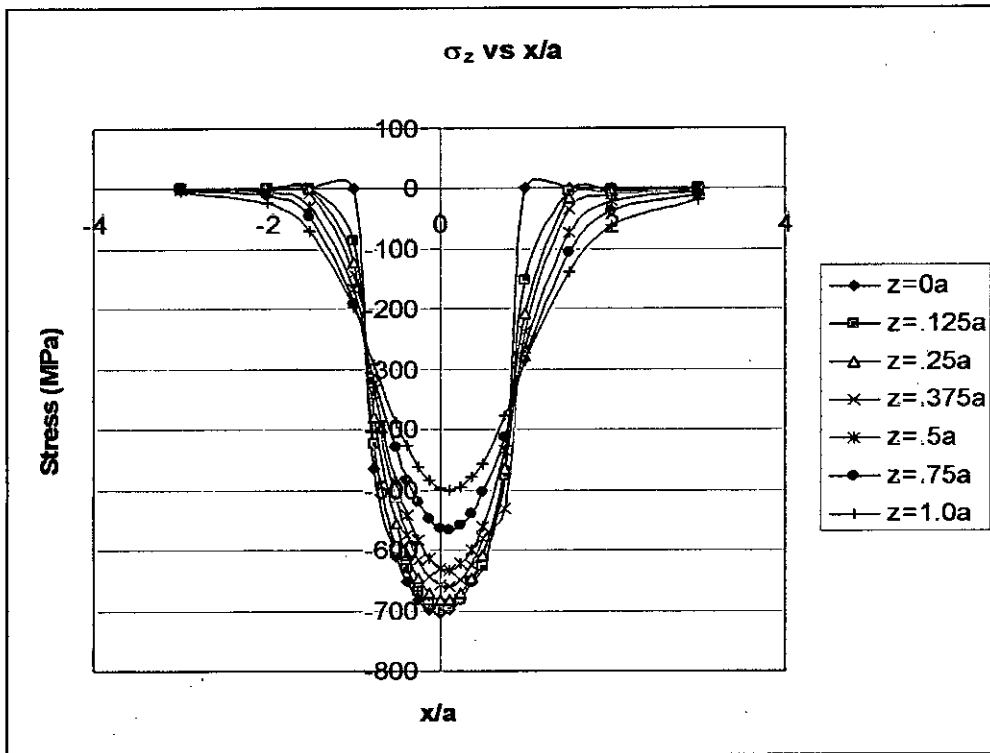
Figure 4.9.4: Stress Distribution vs. x/a for vertex angle 45° (Steel)
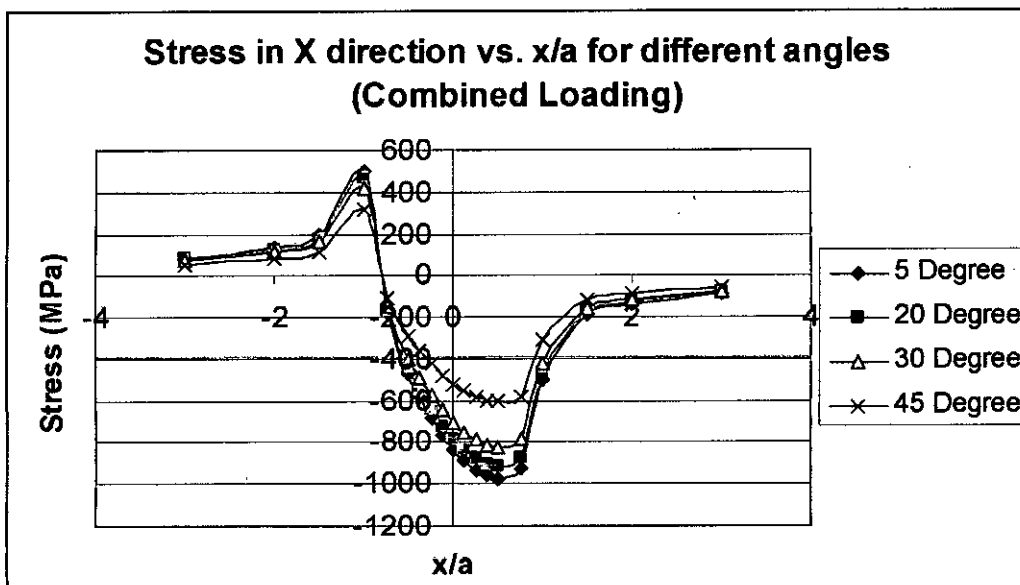
Figure 4.9.5: Stress distribution at in X axis at x/a=0 for different vertex angle at t=0

Combined loading

4.3 Stress in Z direction

Stress components in Z direction have been discussed from the following articles with variation of different contact geometries and vertex angle.

4.3.1 σ_z vs. x/a

Stress distribution in Z axis i.e. axis directed to solid vs. x/a shows that there is same distribution as pressure distribution for normal loading. The maximum stress ratio that is stress to maximum pressure has been found at x/a=0 and at the surface. With increasing of the distance from the surface it decreases. The maximum value of stress ratio is -1 that is exactly same what the value for maximum normal pressure.

The stress distribution (for tangential loading) vs. x/a shows linear relation. The stress ratio has very negligible value. It means by applying tangential load in X direction, stress components in Z axis don't vary so much. So, for combined loading the stress distribution has shown same like for normal distribution. The stress distribution in Z axis has been shown from figure 4.10 to 4.11. From figure 4.12.1 to 4.12.3 the stress distribution has been shown both in dimensionless form and for different materials.
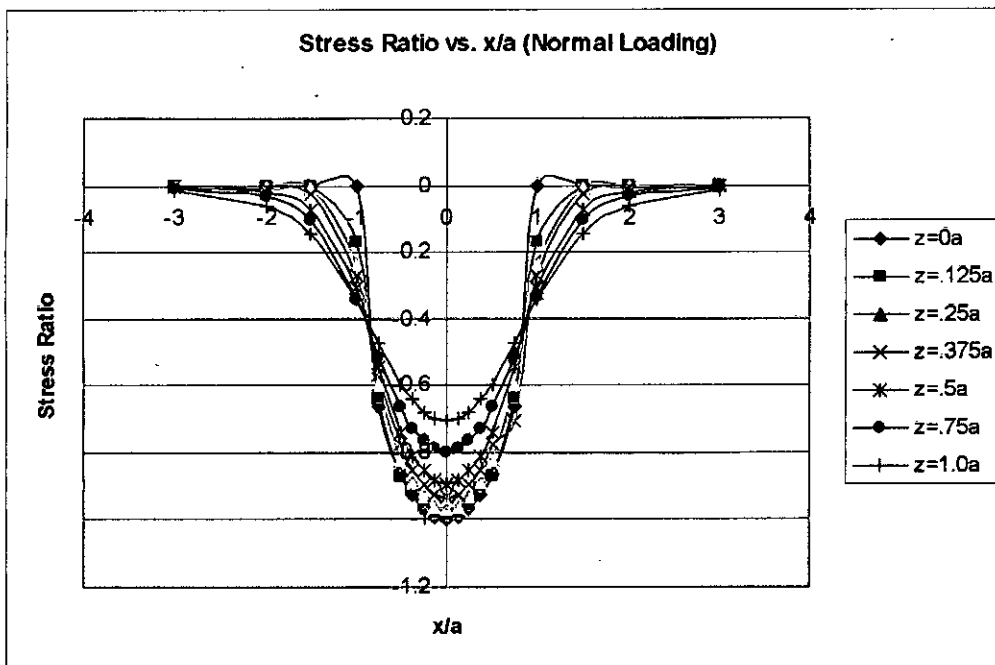
Figure 4.10: Stress distribution in Z axis vs. x/a for Normal loading
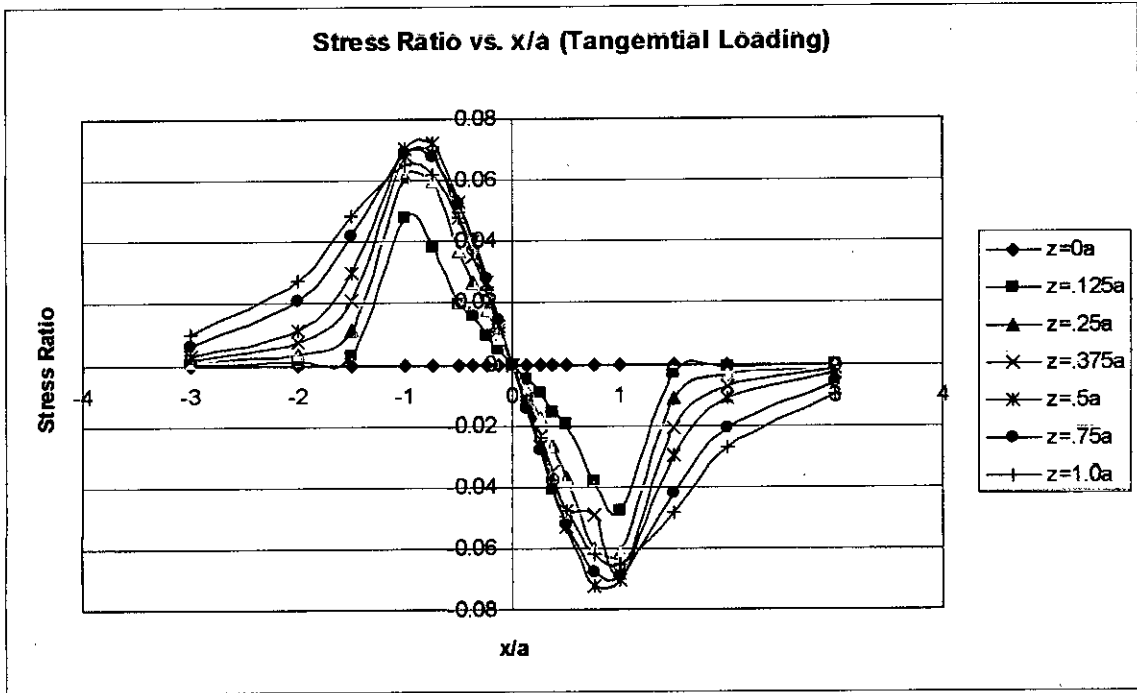
Figure 4.11: Stress distribution in Z direction vs. x/a for Tangential loading
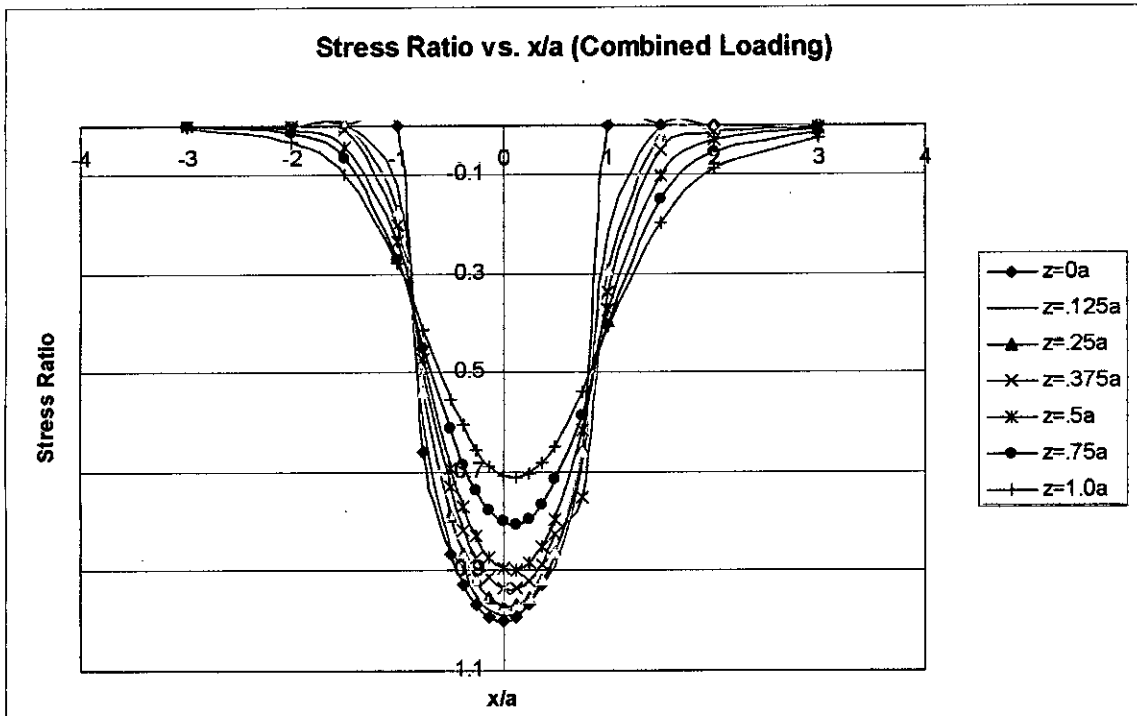
Figure 4.12.1: Stress distribution in Z direction vs. x/a for Combined loading
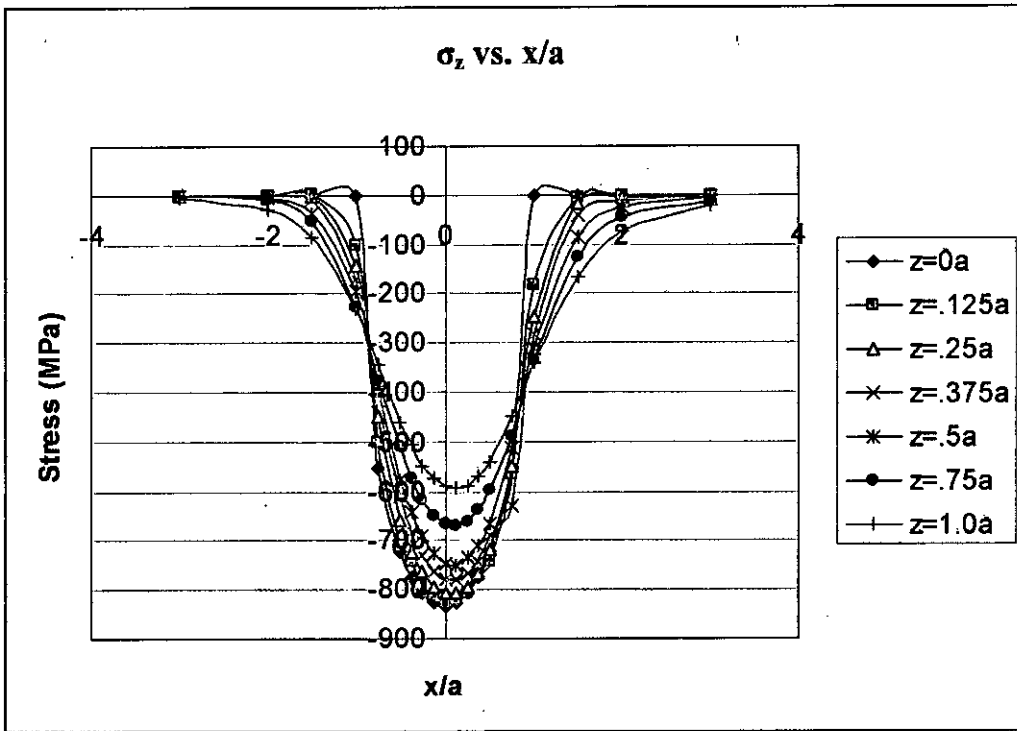
Figure 4.12.2: Stress distribution in Z direction vs. x/a for 5° vertex angle (Steel)
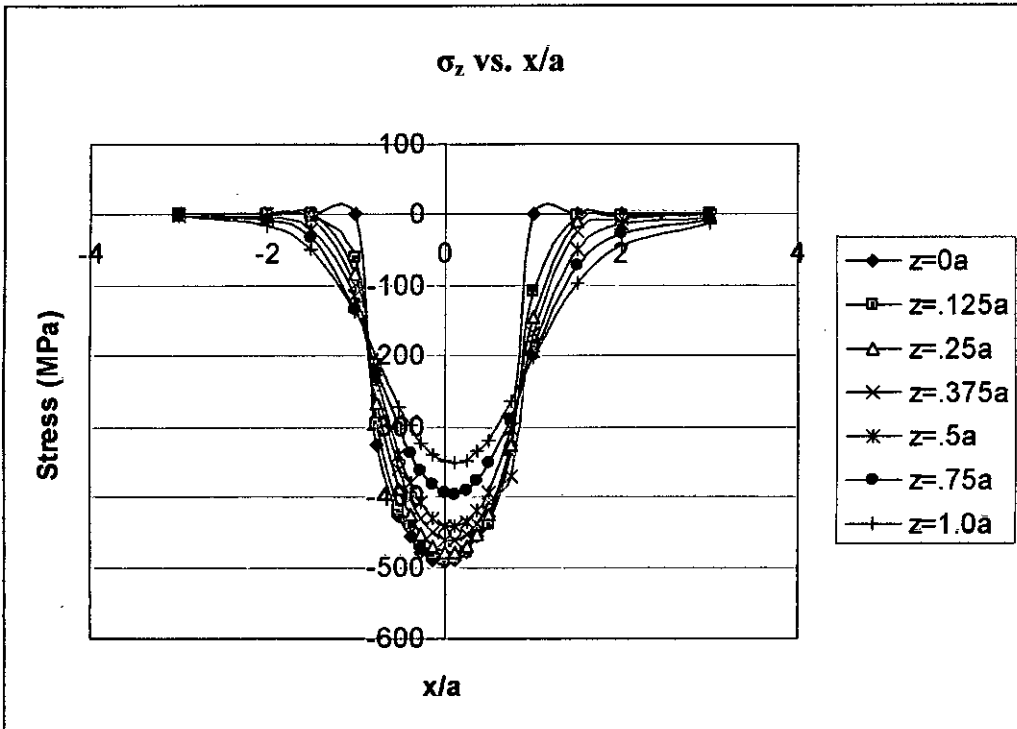
Figure 4.12.2: Stress distribution in Z direction vs. x/a for 5° vertex angle (Aluminum)

4.3.2 σ_z vs. z/a

From the stress distribution along z/a (for normal loading), it has been shown that the maximum stress has been found for x/a = 0 and it has a value of -1. For tangential loading it shows symmetric nature with respect to x/a = 0 line. For combined loading it has been found that maximum stress has been found for x/a=0.25. It means that, the maximum pressure will be found some value tilted towards leading edge of the conical rollers. The stress distribution vs. z/a for different loading conditions has been shown from figure 4.13-4.14. From figure 4.15.1 to 4.15.3 stress distribution vs. z/a has been shown both in dimensionless form and for different materials for combined loading.
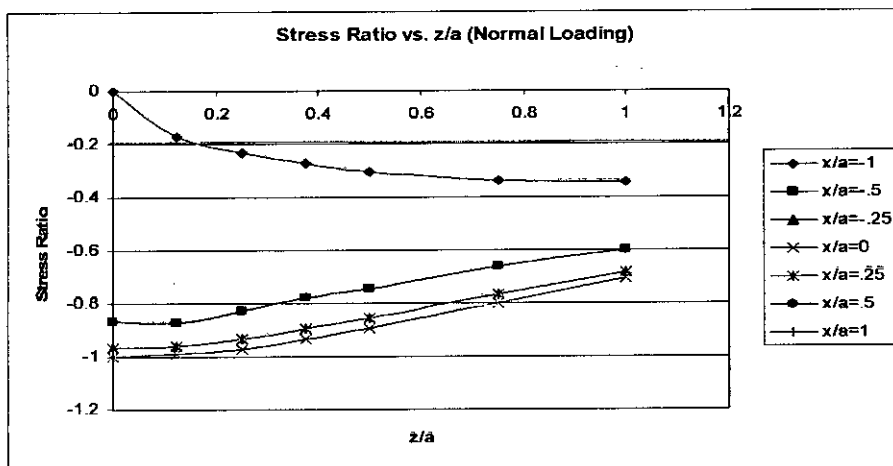
Figure 4.13: Stress distribution in Z axis vs. z/a for Normal loading
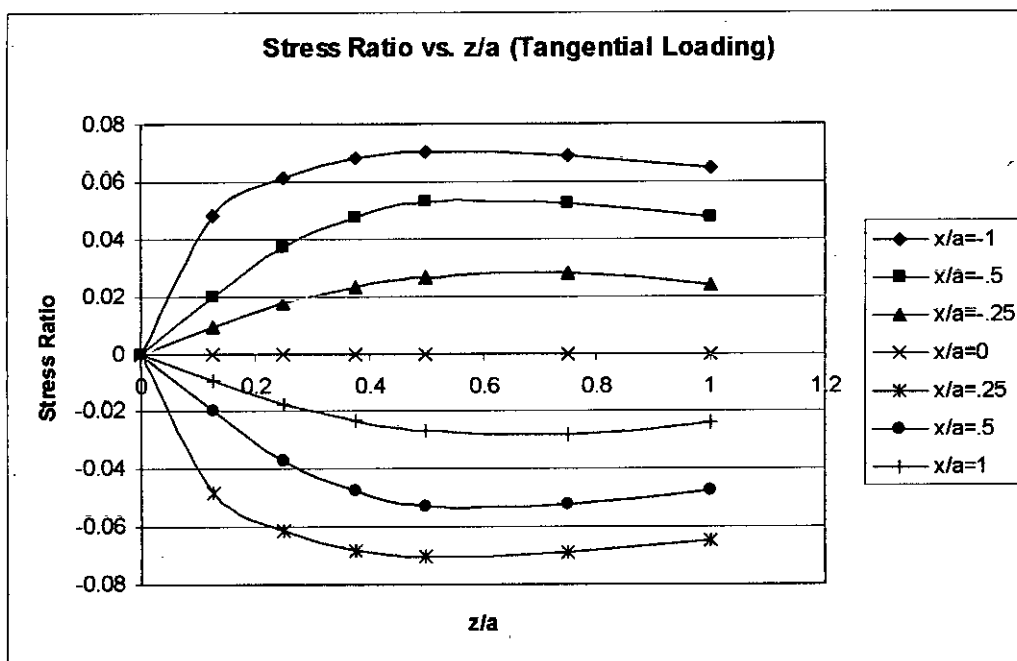
Figure 4.14: Stress distribution in Z axis vs. z/a for Tangential loading

57

Figure 4.15.1: Stress distribution in Z axis vs. z/a for Combined loading

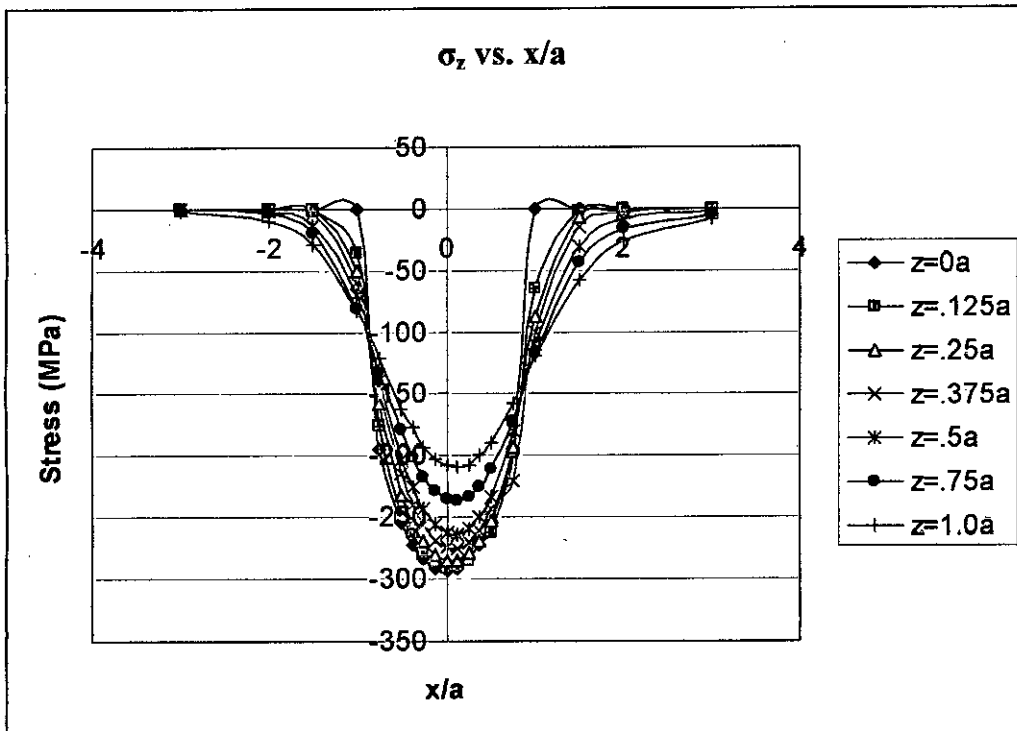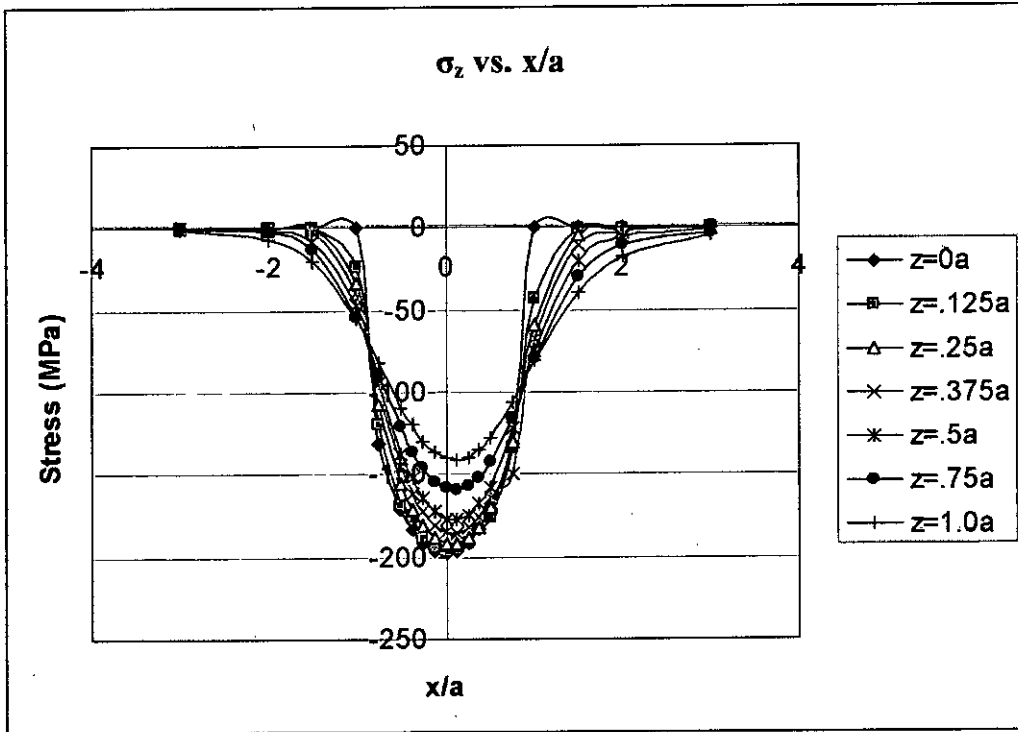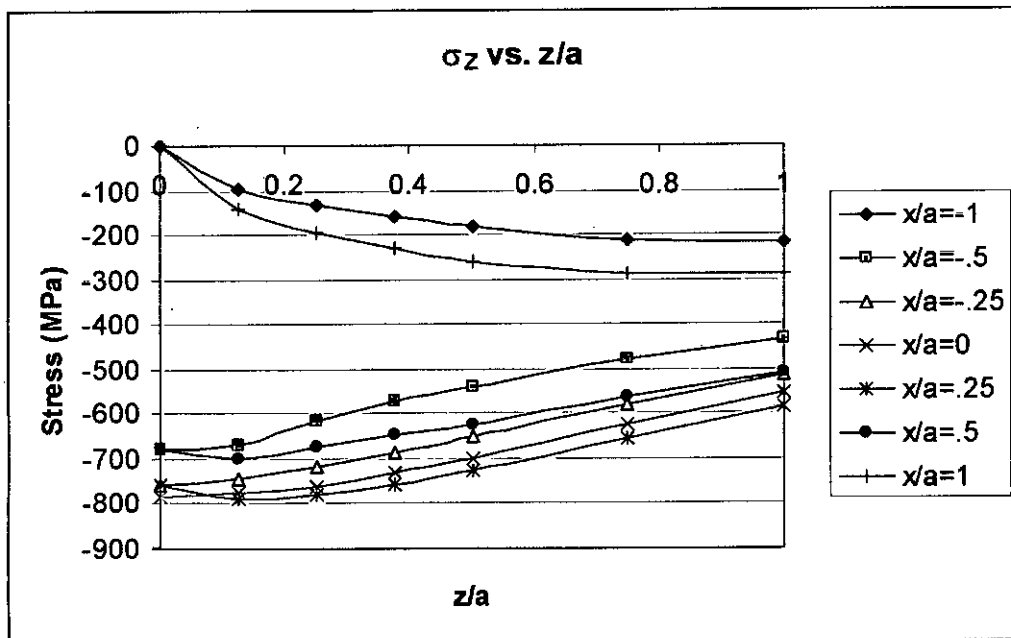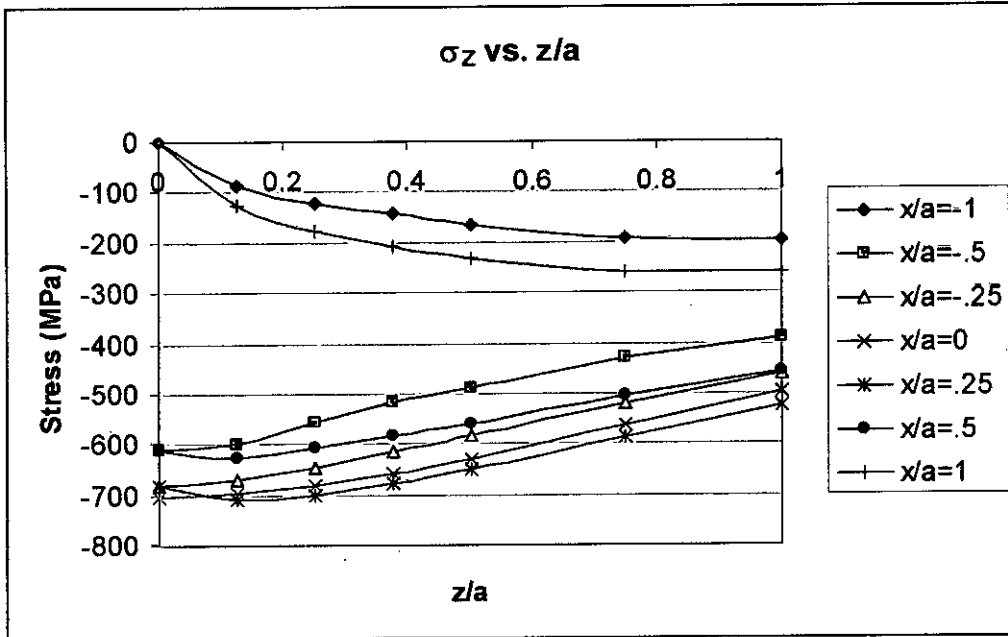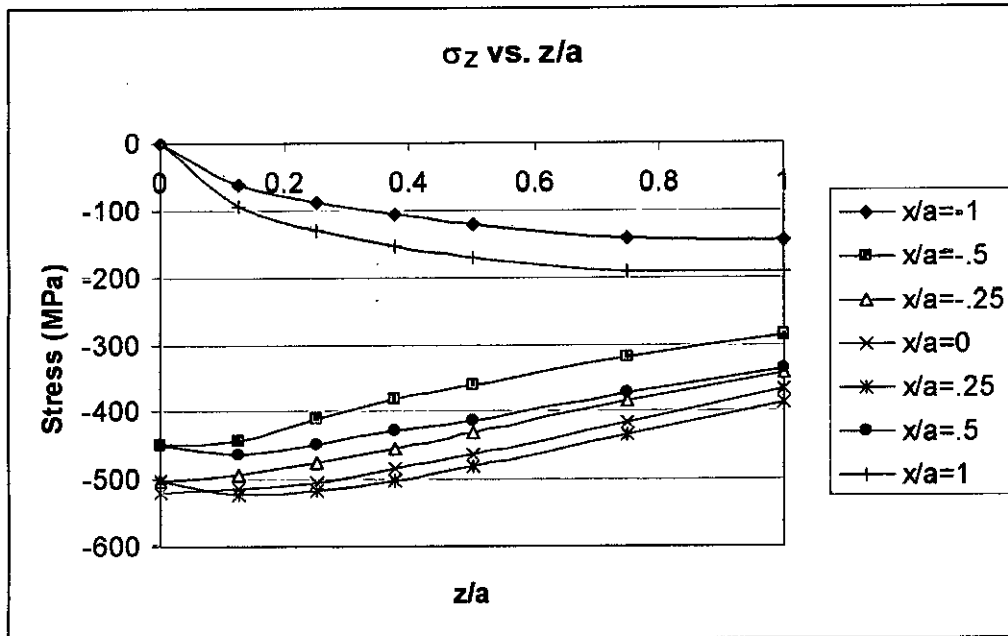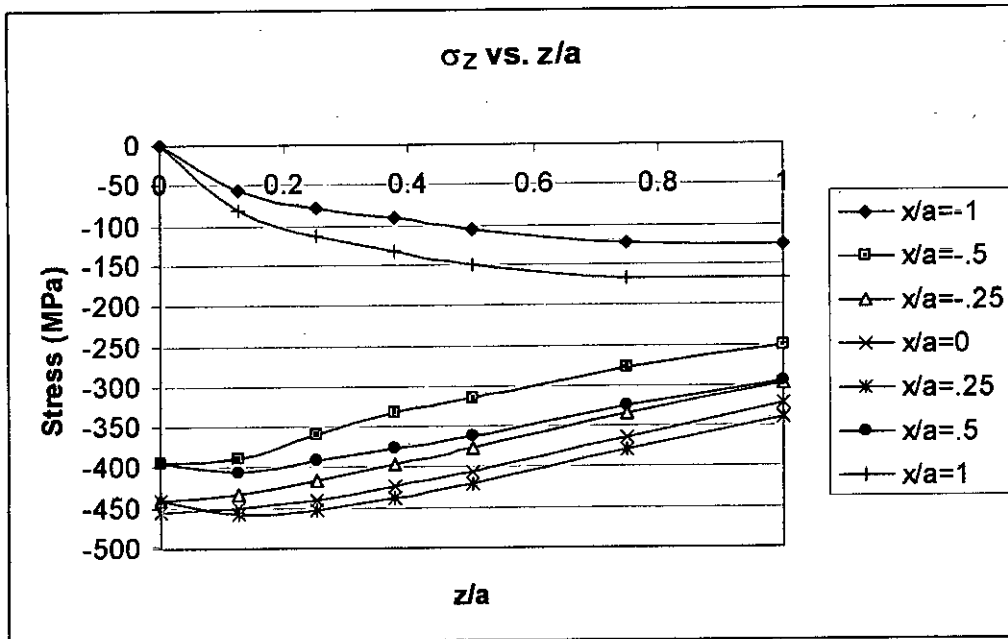Figure 4.15.2: Stress Distribution vs. z/a for vertex angle 5° at t = 0l (Steel)

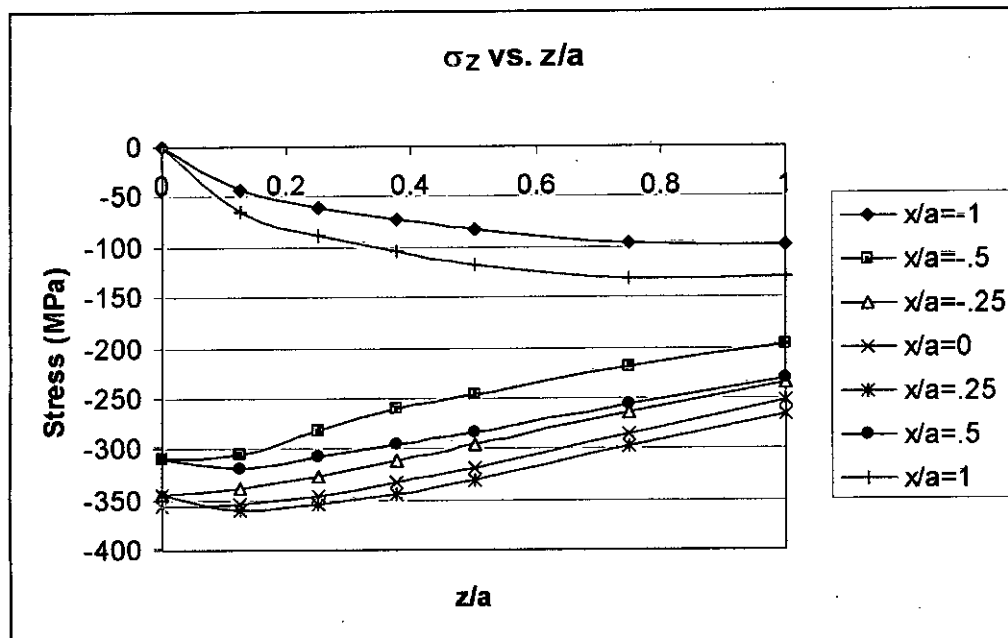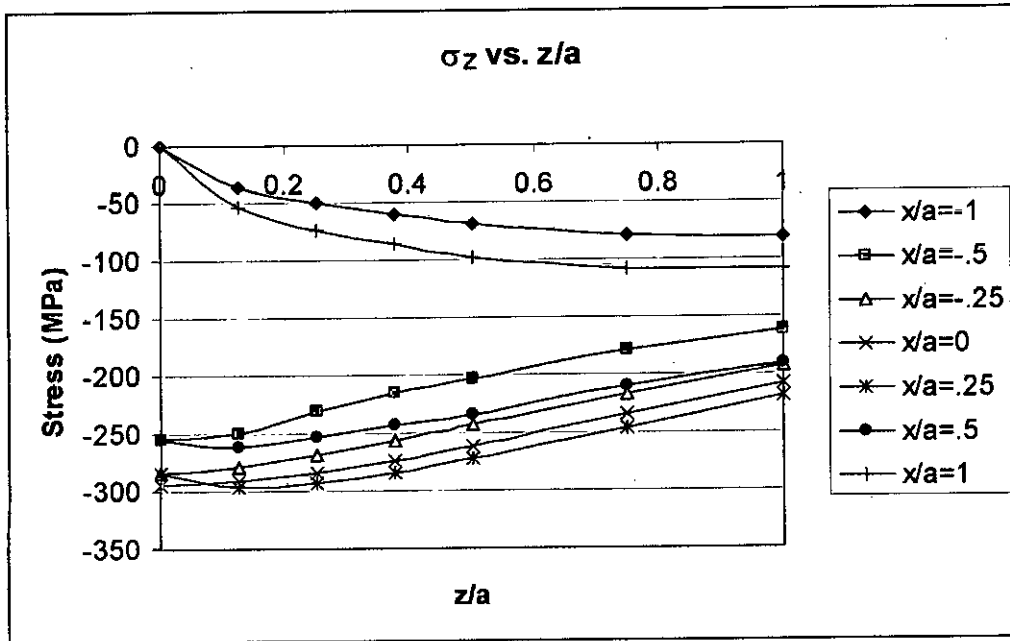Figure 4.15.3: Stress Distribution vs. z/a for vertex angle 5° at t = 0l (Aluminum)

4.3.3 Stress Distribution along with different length

Like stress distribution in X axis, stress in Z axis also varies with varying distance from tip. At the tip i.e. at t=0, the stress is maximum and its value decreases with increasing the distance from tip. The distribution does not vary except the value. The distribution has been shown in figure 4.16.1 to 4.6.10

Figure 4.16.1: Stress Distribution vs. x/a for vertex angle 5° at t = 0l (Steel)

Figure 4.16.2: Stress Distribution vs. x/a for vertex angle 5° at t = 0.25l (Steel)

Figure 4.16.3: Stress Distribution vs. x/a for vertex angle 5° at t = 0. 5l (Steel)

Figure 4.16.4: Stress Distribution vs. x/a for vertex angle 5° at t = 0. 75*l* (Steel)

Figure 4.16.5: Stress Distribution vs. x/a for vertex angle 5° at t = 1*l* (Steel)

Figure 4.16.6: Stress distribution in Z axis at different length at z/a=0 with vertex angle 5° for combined loading

Figure 4.16.6: Stress Distribution vs. x/a for vertex angle 5° at t = 0/ (Aluminum)

62

Figure 4.16.7: Stress Distribution vs. x/a for vertex angle 5° at t = 0.5*l* (Aluminum)

Figure 4.16.8: Stress Distribution vs. x/a for vertex angle 5° at t = 1*l* (Aluminum)
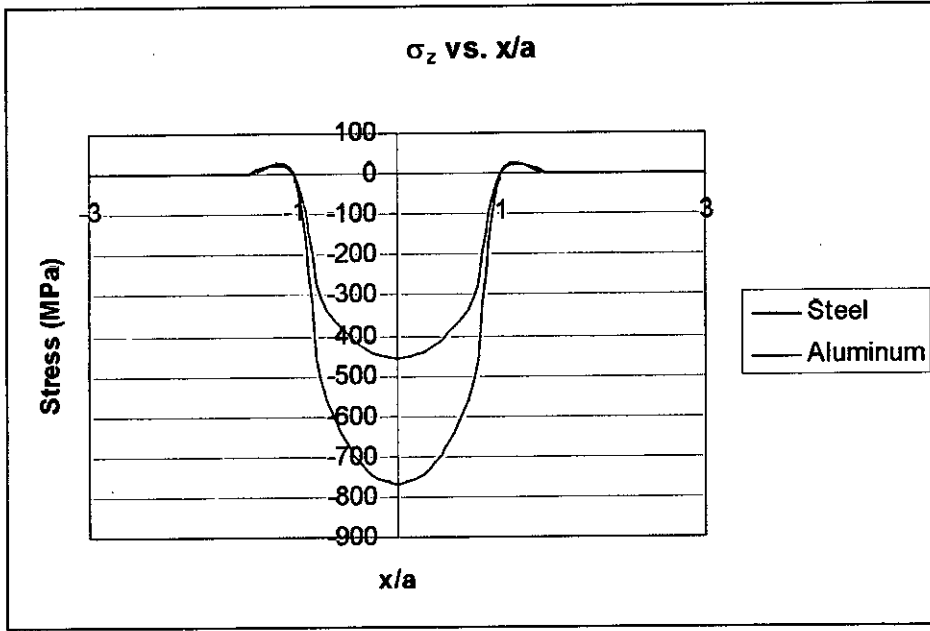
Figure 4.16.9: Stress Distribution vs. x/a for vertex angle 5° for different materials

Figure 4.17.1: Stress Distribution vs. z/a for vertex angle 5° at t = 0l (Steel)

Figure 4.17.2: Stress Distribution vs. z/a for vertex angle 5° at t = 0.25*l* (Steel)

Figure 4.17.3: Stress Distribution vs. z/a for vertex angle 5° at t = 0.5*l* (Steel)

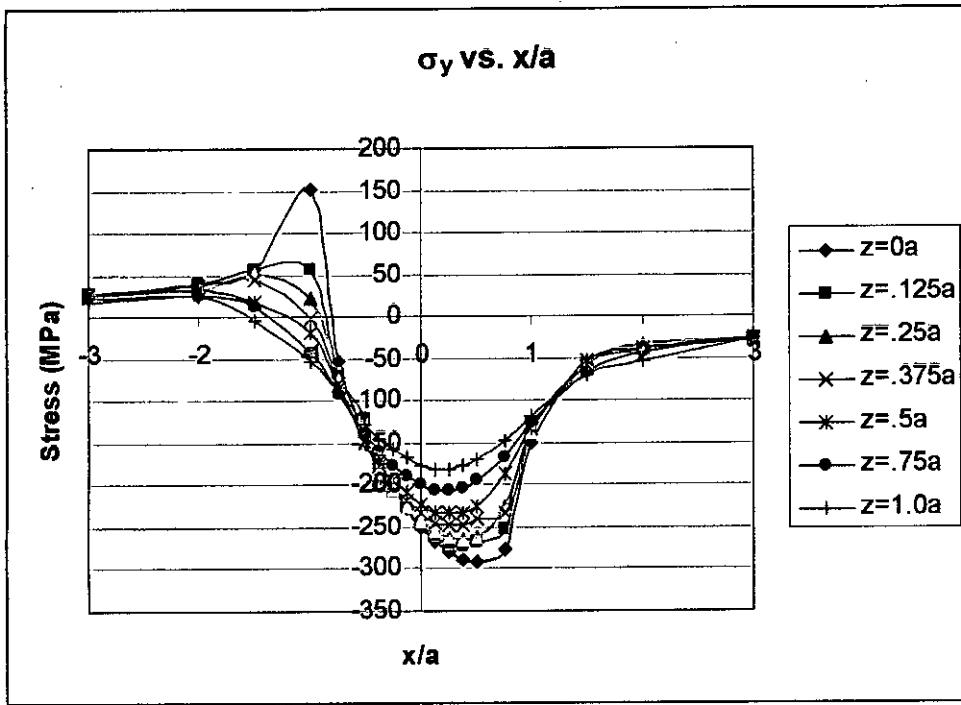Figure 4.17.4: Stress Distribution vs. z/a for vertex angle 5° at t = 0.75*l* (Steel)

Figure 4.17.5: Stress Distribution vs. z/a for vertex angle 5° at t = 1*l* (Steel)

Figure 4.17.6: Stress Distribution vs. z/a for vertex angle 5° at t = 0*l* (Aluminum)

66

Figure 4.17.7: Stress Distribution vs. z/a for vertex angle 5° at t = 0.5*l* (Aluminum)
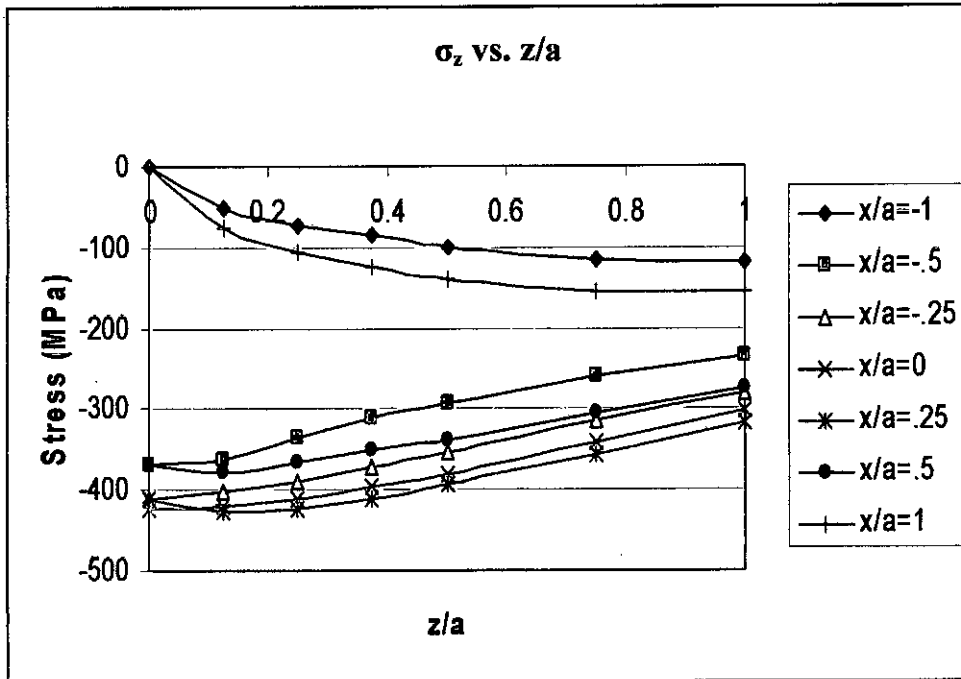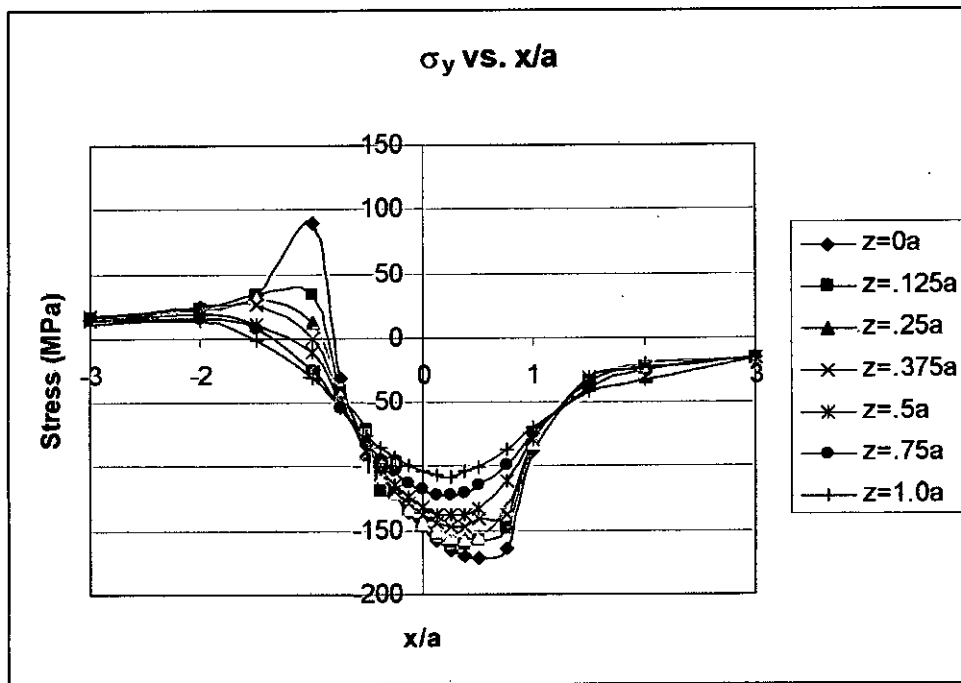

Figure 4.17.8 Stress Distribution vs. z/a for vertex angle 5° at t = 1*l* (Aluminum)
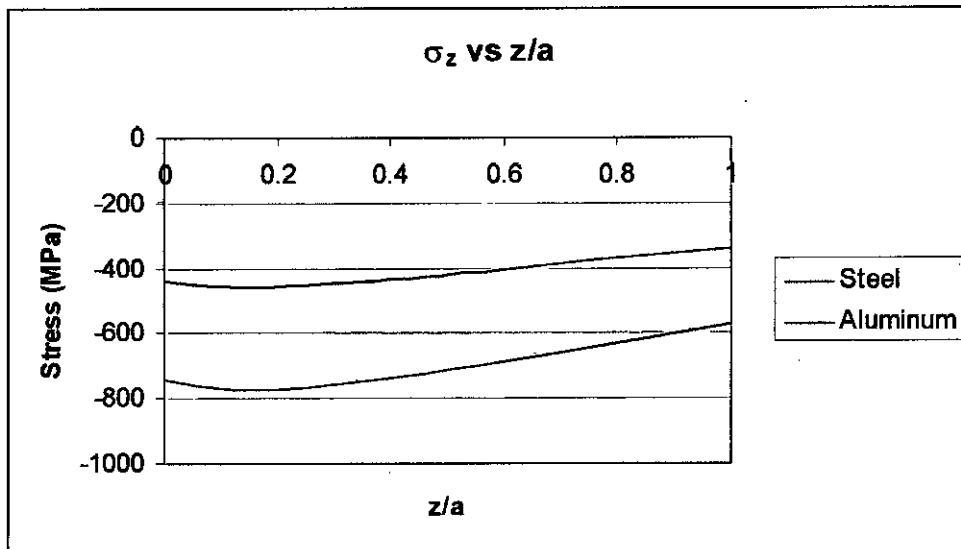
Figure 4.17.9 Stress Distribution vs. z/a for vertex angle 5° for different materials

4.3.4 Stress Distribution for different Vertex angles

From stress distribution with different vertex angle or vertex angle we have seen that, with increasing vertex angle the maximum value for stress decreases though distribution are same for all vertex angle. Here only stress at surface i.e. z=0 has been shown as it has higher value. The distribution has been shown from figure 4.18.1 to 4.18.9.

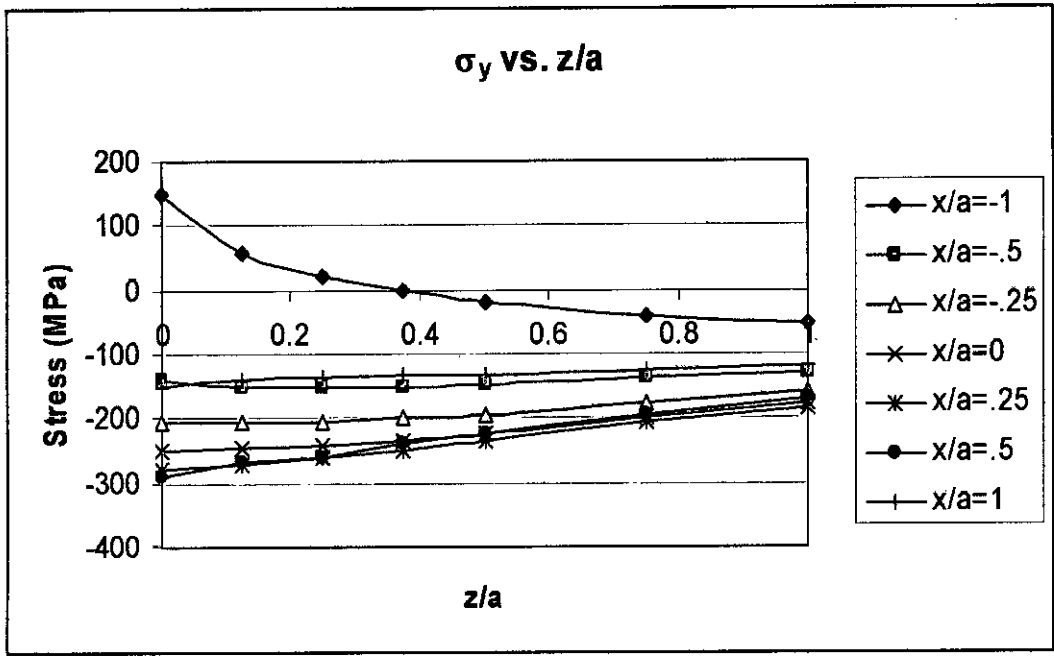Figure 4.18.1 Stress Distribution vs. x/a for vertex angle 5° at t=0 (Steel)

Figure 4.18.2 Stress Distribution vs. x/a for vertex angle 20° at t=0 (Steel)
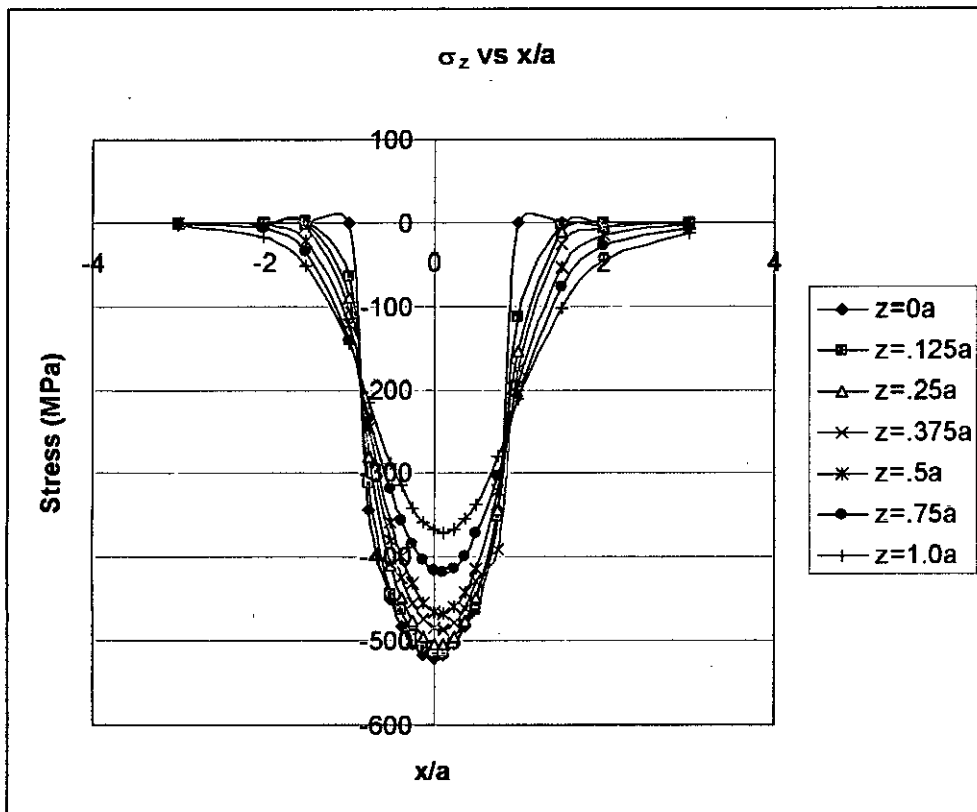
Figure 4.18.3 Stress Distribution vs. x/a for vertex angle 45° at t=0 (Steel)
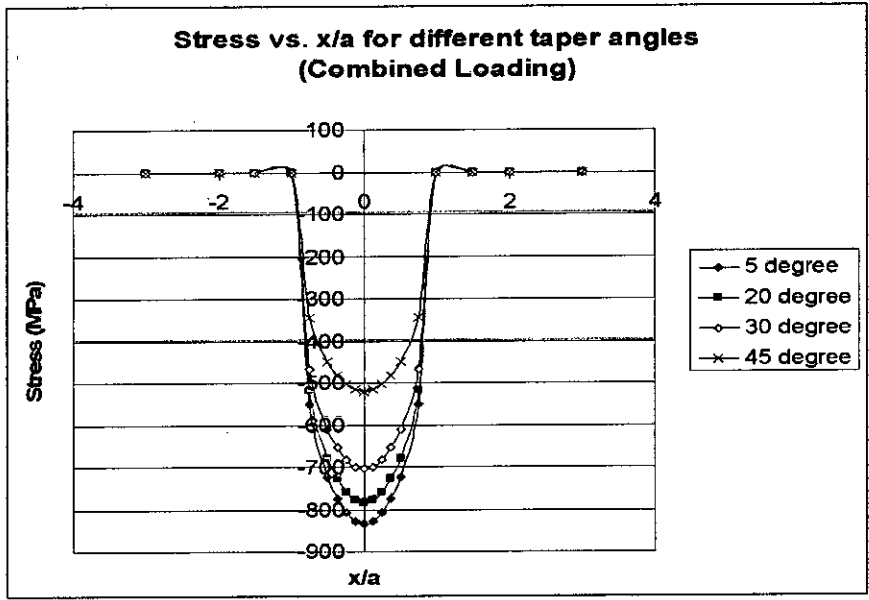
Figure 4.18.4: Distribution of Stress in Z direction (combined loading) vs. x/a for different vertex angle at t=0
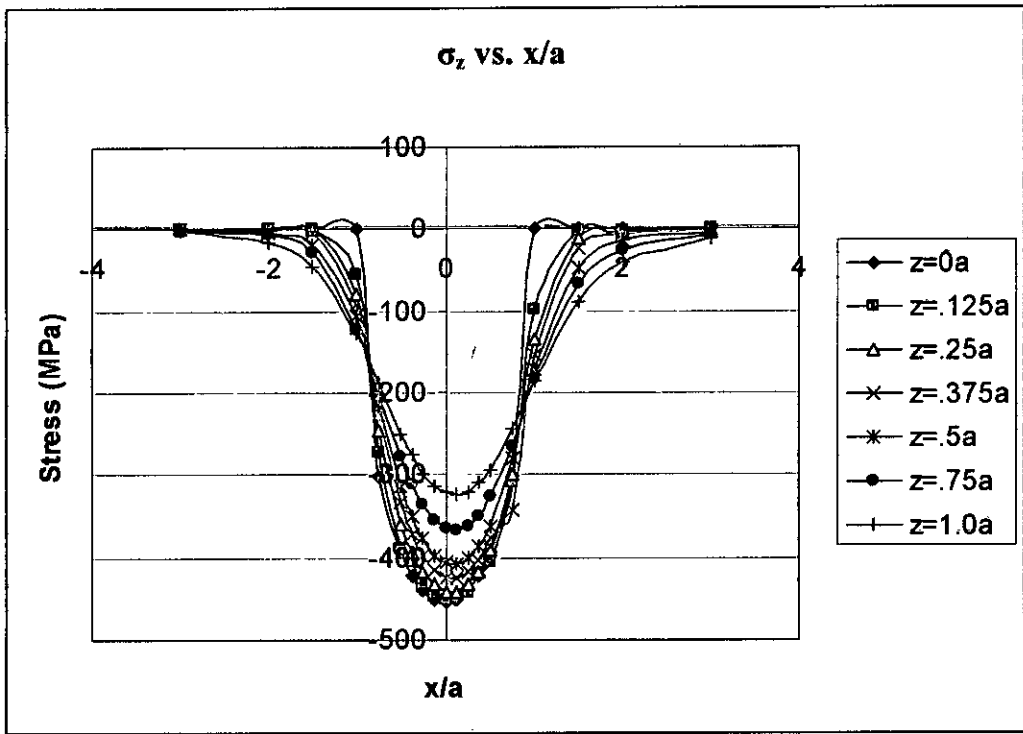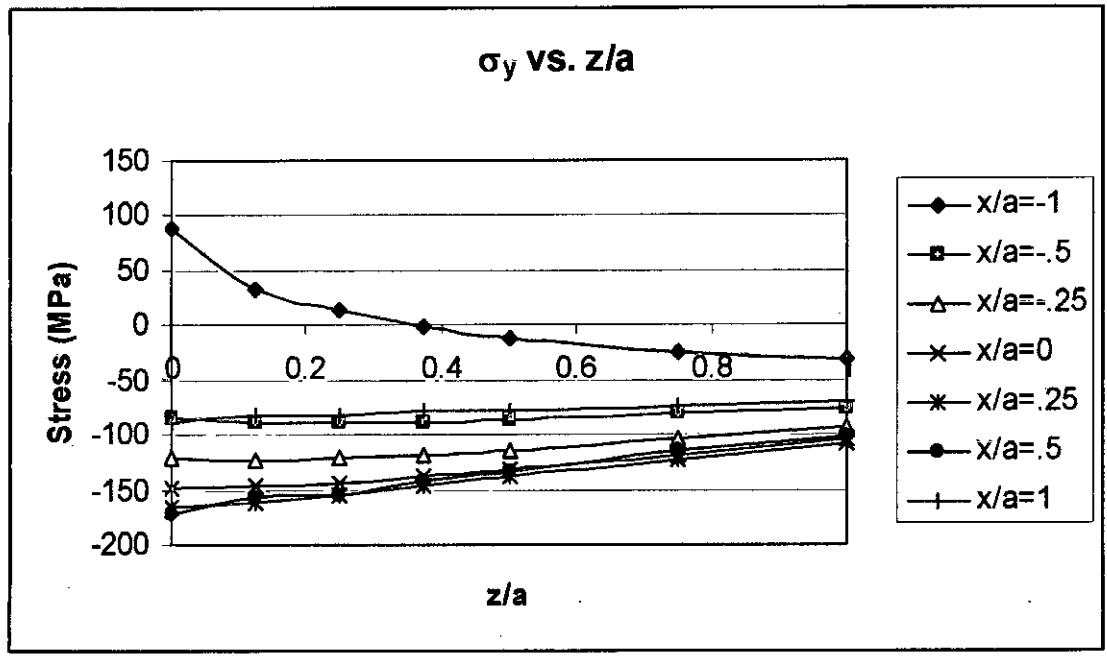

Figure 4.18.5 Stress Distribution vs. x/a for vertex angle 5° at t=0.5l (Aluminum)
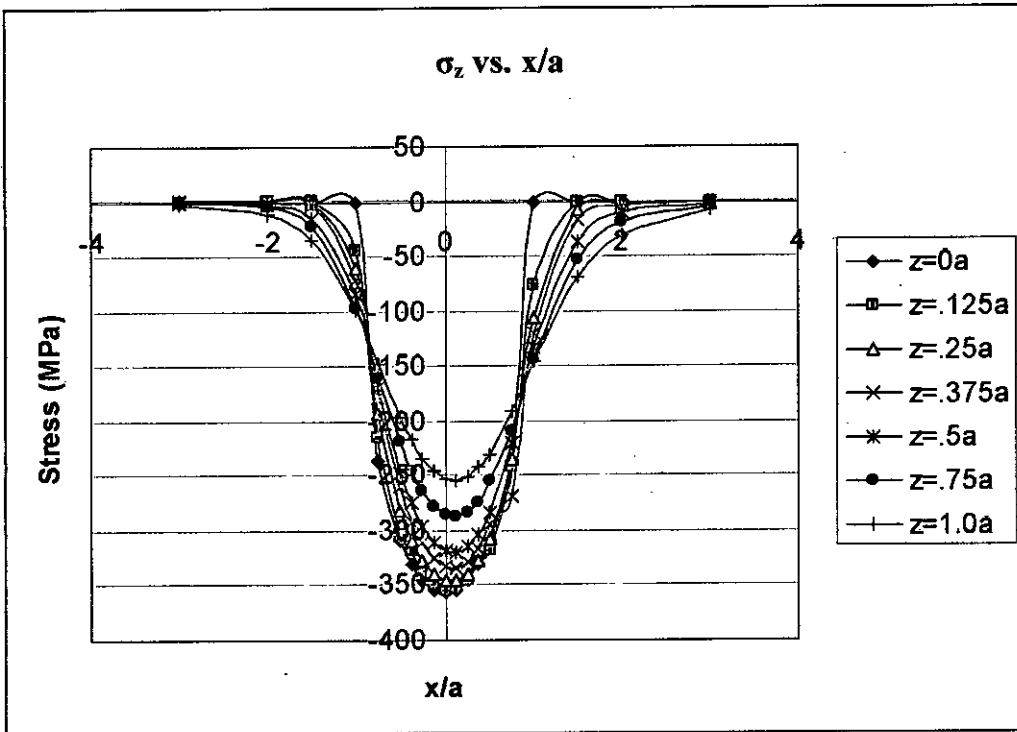
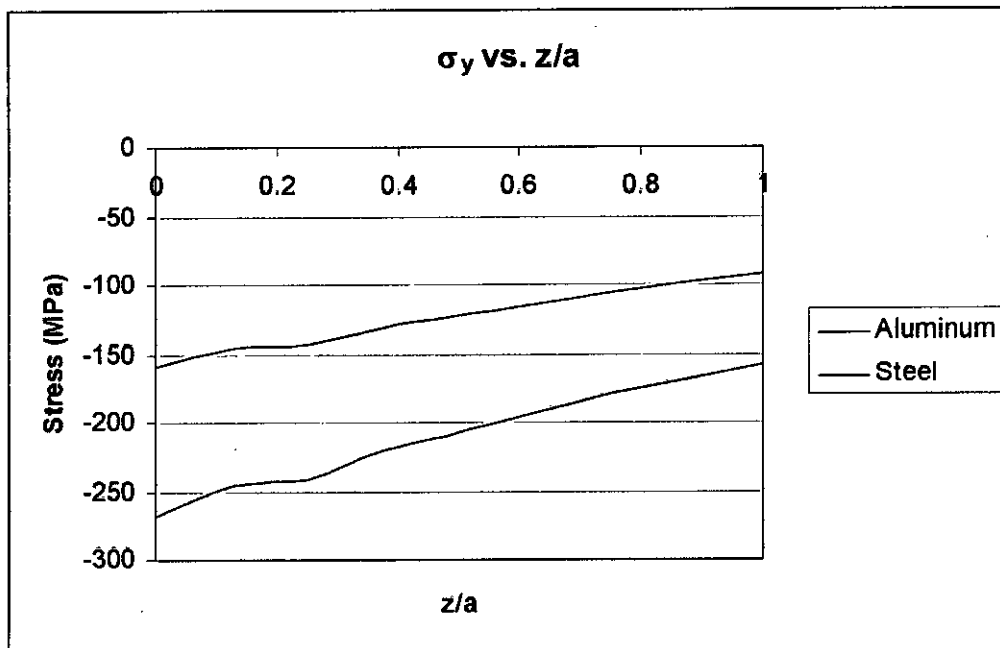Figure 4.18.6: Stress Distribution vs. x/a for vertex angle 20° at t=0.5l (Aluminum)

Figure 4.18.7: Stress Distribution vs. x/a for vertex angle 30° at t=0.5l (Aluminum)

Figure 4.18.8: Stress Distribution vs. x/a for vertex angle 45° at t=0.5l (Aluminum)
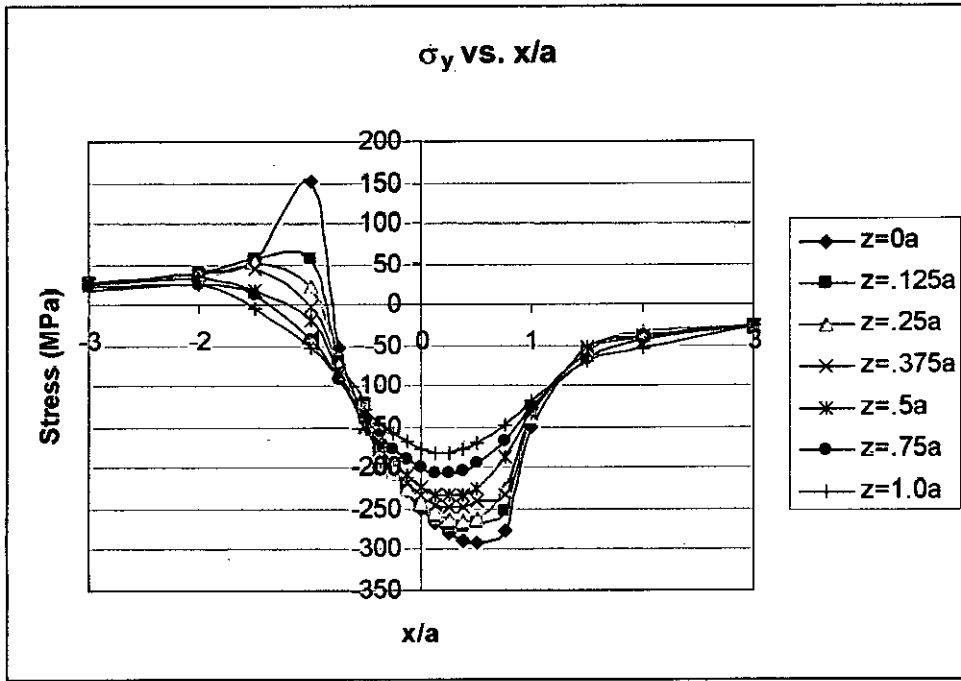

Figure 4.19.1: Stress Distribution vs. z/a for vertex angle 20° at t=0l (Steel)
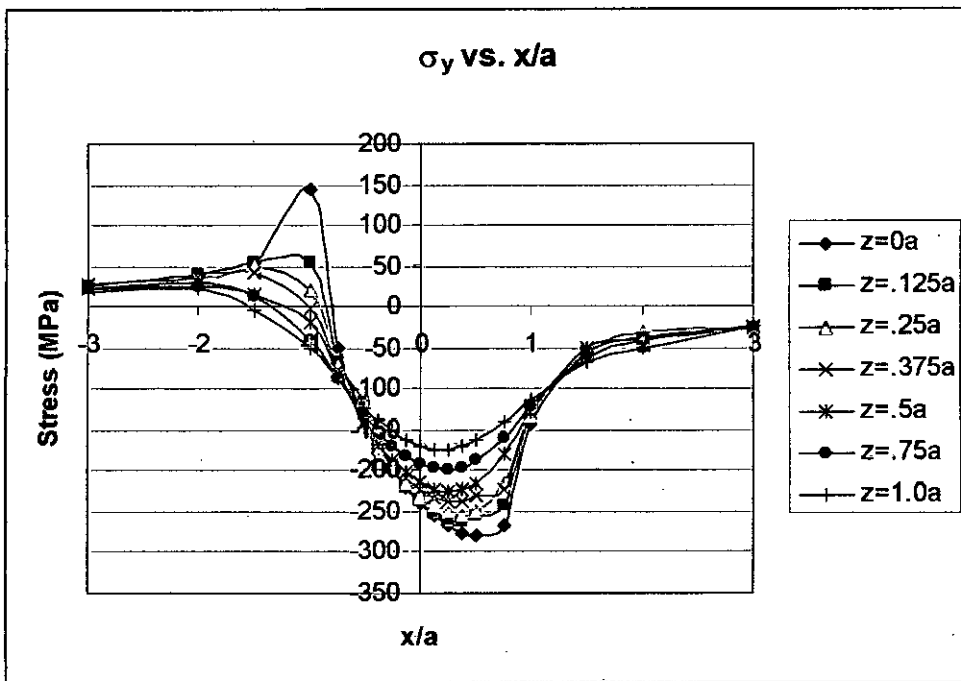
Figure 4.19.2: Stress Distribution vs. z/a for vertex angle 30° at t=0l (Steel)
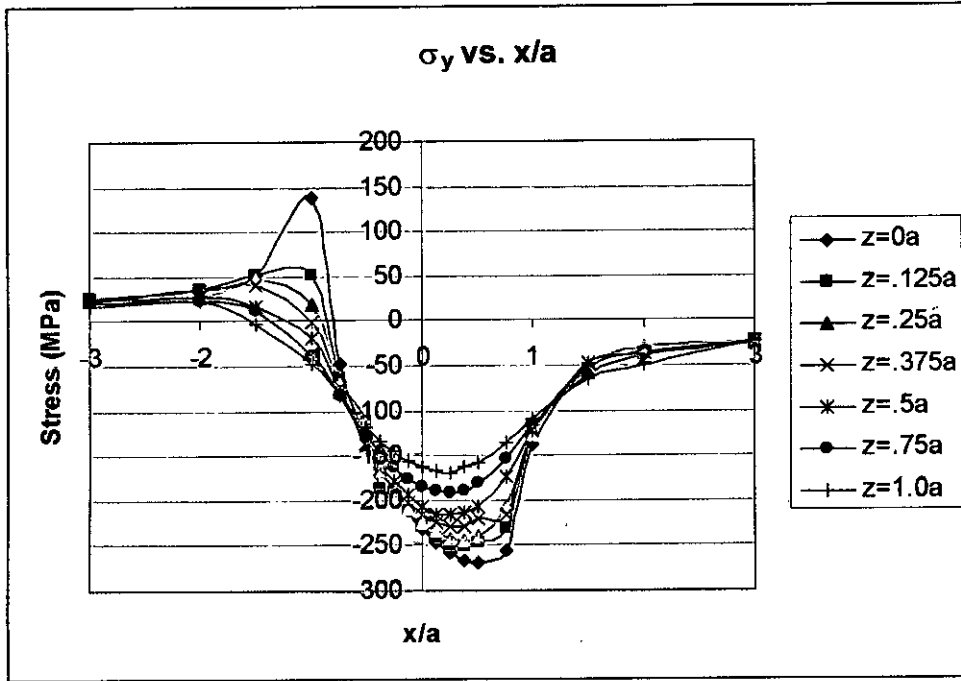

Figure 4.19.3: Stress Distribution vs. z/a for vertex angle 45° at t=0l (Steel)

Figure 4.19.4: Stress Distribution vs. z/a for vertex angle 5° at t=0.5l (Aluminum)

Figure 4.19.5: Stress Distribution vs. z/a for vertex angle 20° at t=0.5l (Aluminum)

Figure 4.19.6: Stress Distribution vs. z/a for vertex angle 30° at t=0.5l (Aluminum)
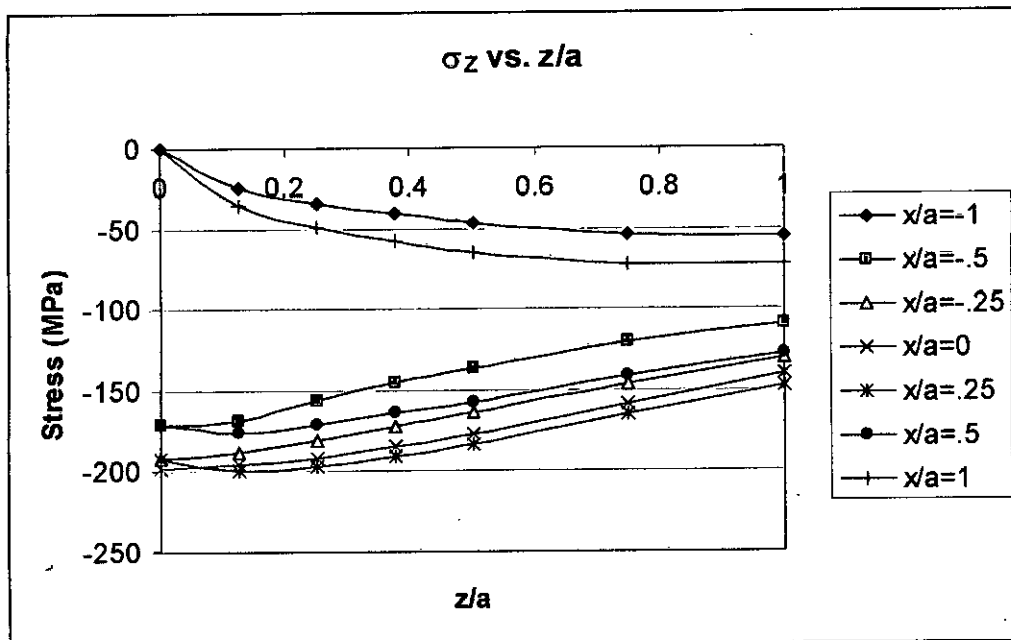
Figure 4.19.7: Stress Distribution vs. z/a for vertex angle 45° at t=0.5l (Aluminum)

4.4   Stress in Y axis

The stress components in Y axis have been found from plane strain approximation. In this case all stress components have been shown under combined loads i.e. presence of both normal and tangential load. We will discuss about stress distribution in this direction with variation of contact geometries, contact length and vertex angle for different materials.

4.4.1 σ_y vs. x/a

For case of plane strain, the third stress component is related with another stress component and poisson's ratio. As the stress has maximum value for combined loading, so third stress component are taken for combined loading. From the distribution of stress in Y axis, we have seen that the distribution is as like as that for X axis, i.e. maximum value has been found some value tilted towards leading edge. But value of stress ratio is 0.35 which is much lower than other two components. The location where maximum stress has been found is at contact surface ($z=0$) and at a distance (x/a=0.5) from line of symmetry. The stress distribution has been shown in figure 4.20.1 to 4.20.3 both in terms of stress ratio and for different materials.
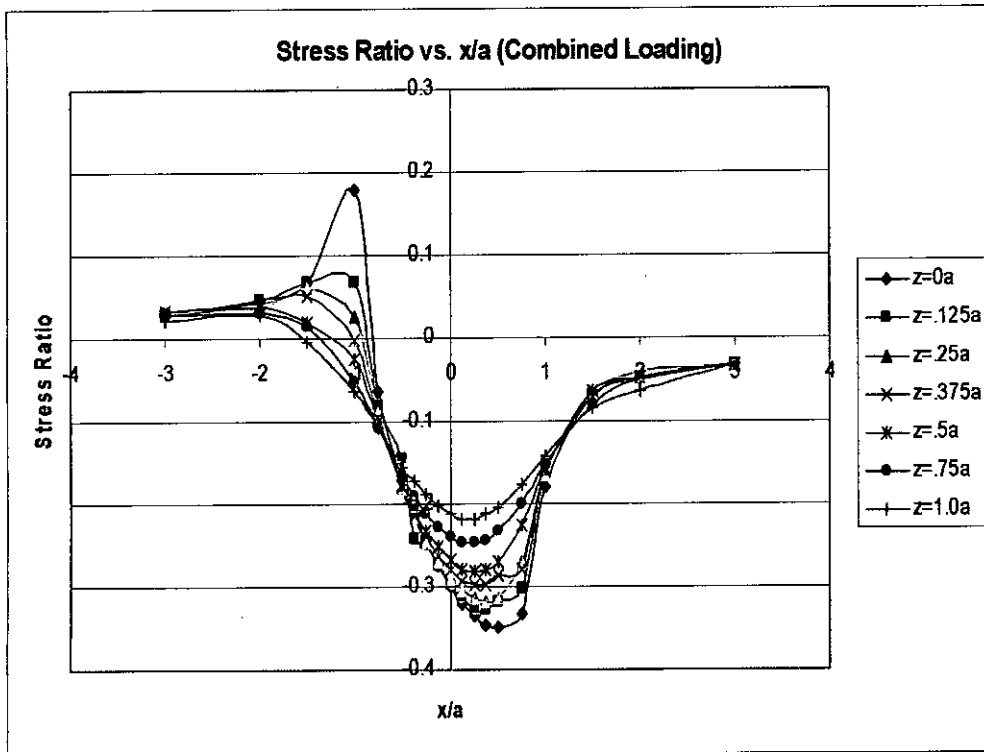
Figure 4.20.1: Stress distribution in Y axis vs. x/a

Figure 4.20.2: Stress Distribution vs. x/a for vertex angle 5° at t = 0*l* (Steel)

Figure 4.20.3: Stress Distribution vs. x/a for vertex angle 5° at t = 0*l* (Aluminum)
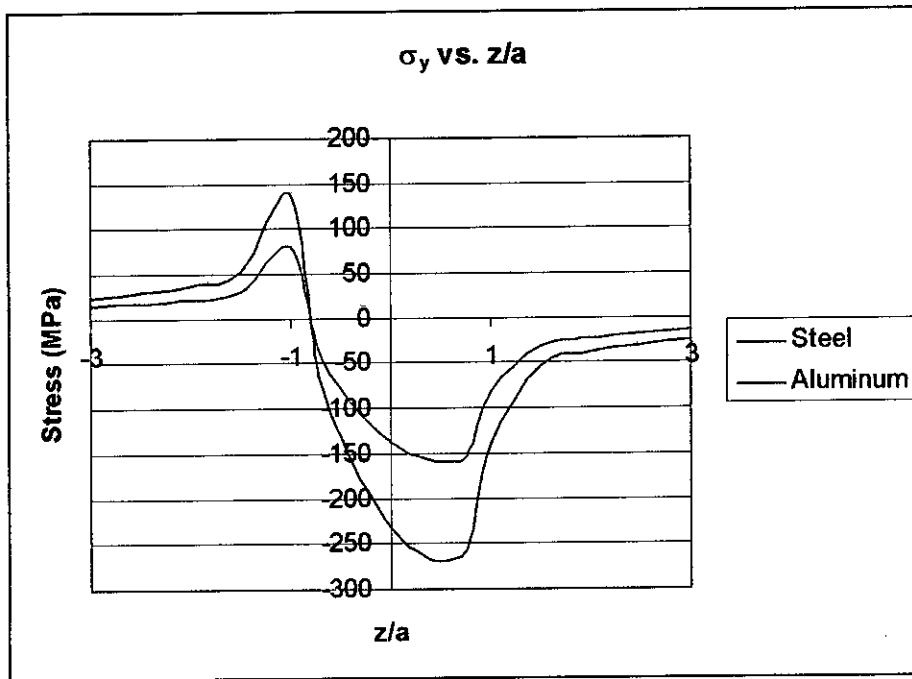
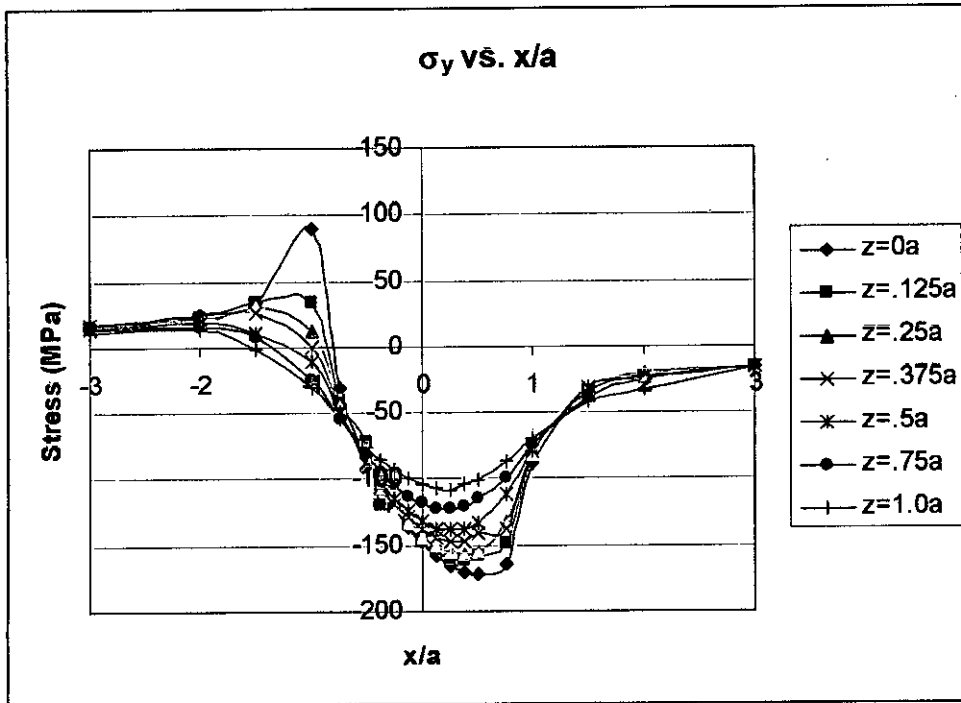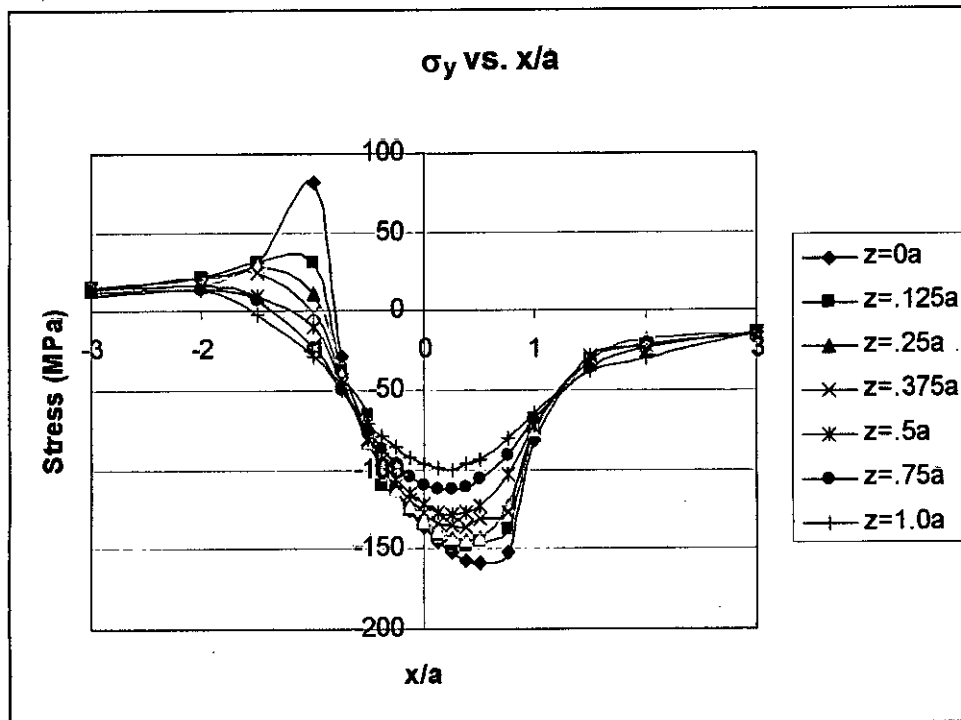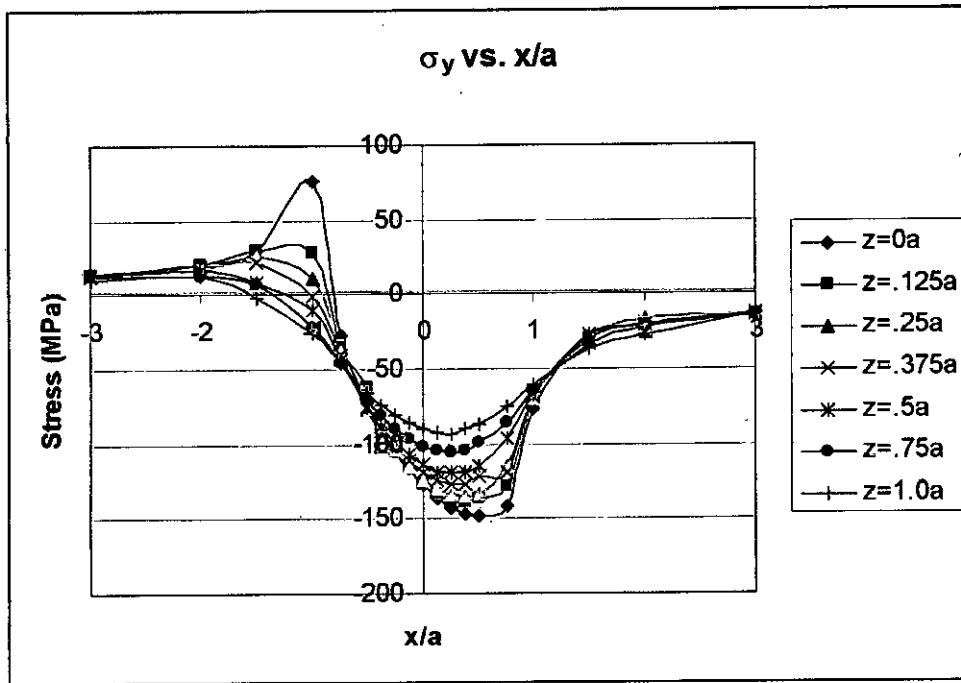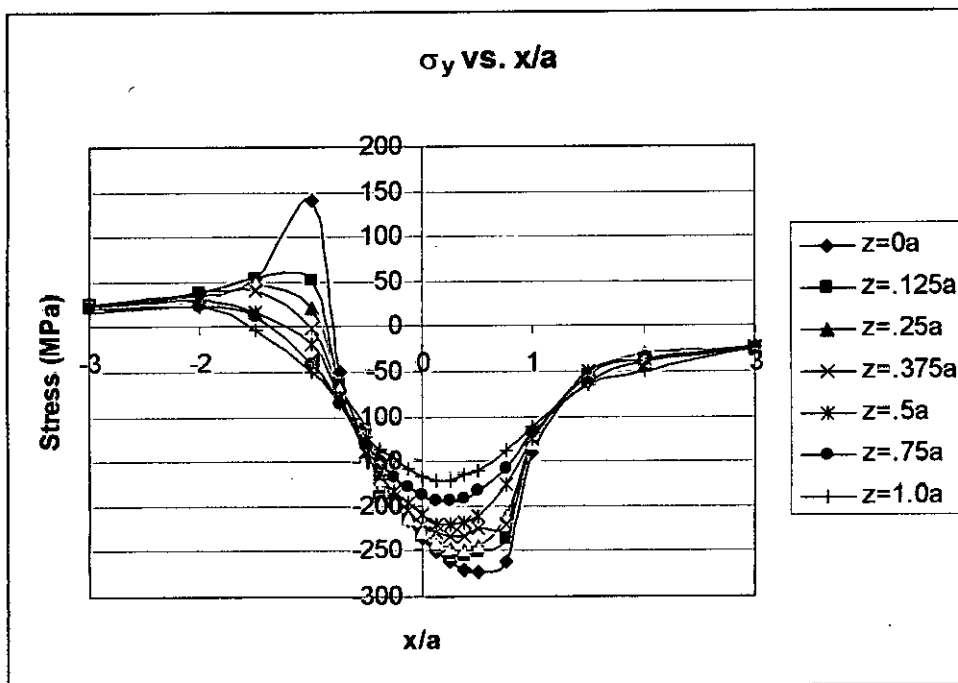Figure 4.20.4: Stress Distribution vs. x/a for vertex angle 5° for different materials

4.4.2 σ_y vs. z/a

From stress distribution in Y axis vs. z/a it has been shown that the maximum value of stress ratio has been found not at x/a = 0. And the maximum value is found at z=0 at i.e. at surface. Stress distribution for combined loading has been shown in figure 4.21.1 to 4.21.4
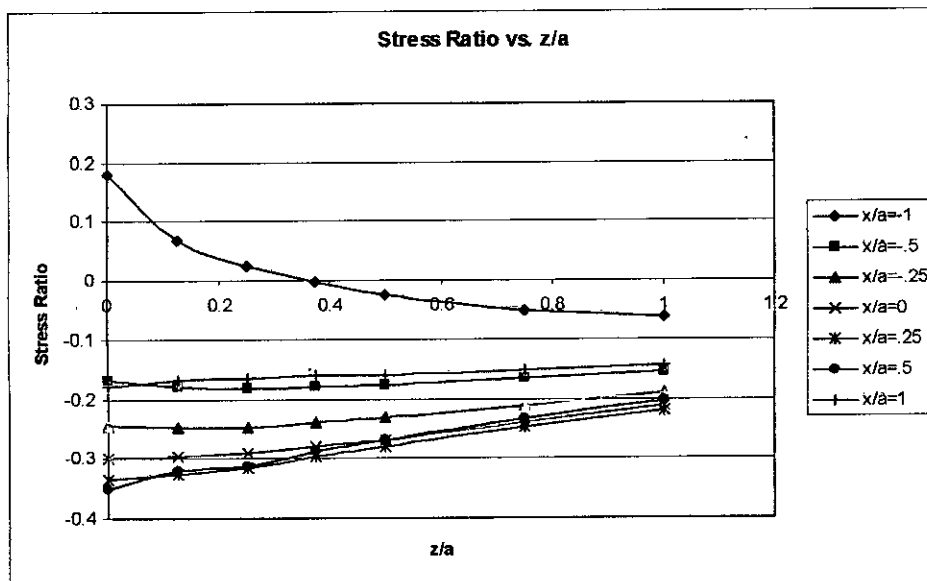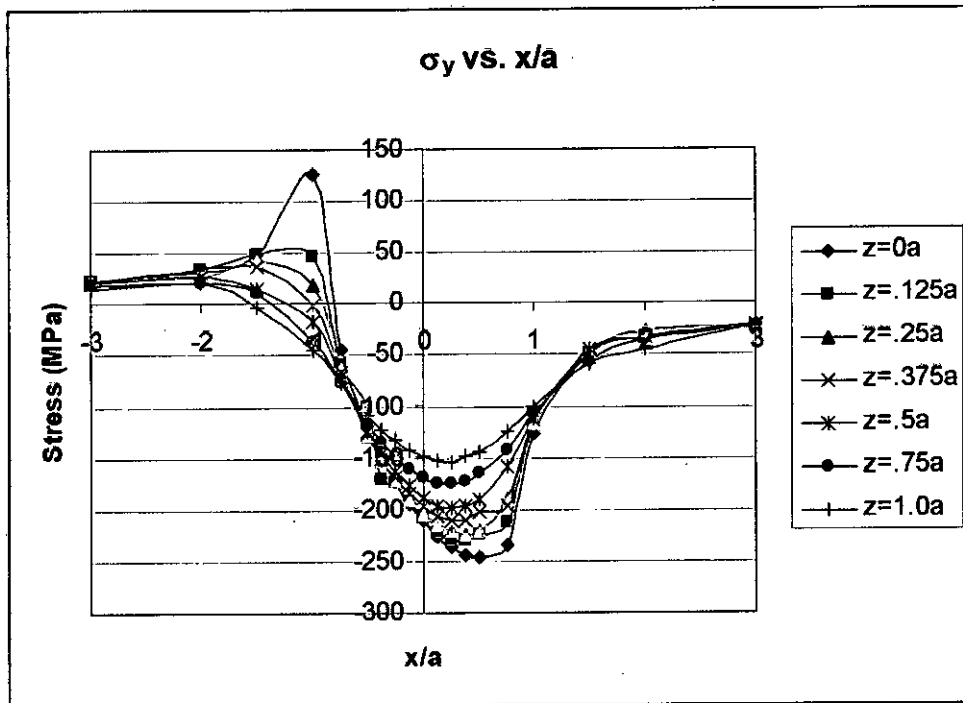

Figure 4.21.1: Stress distribution in Y axis vs. z/a

Figure 4.21.2: Stress Distribution vs. x/a for vertex angle 5° at t = 0*l* (Steel)

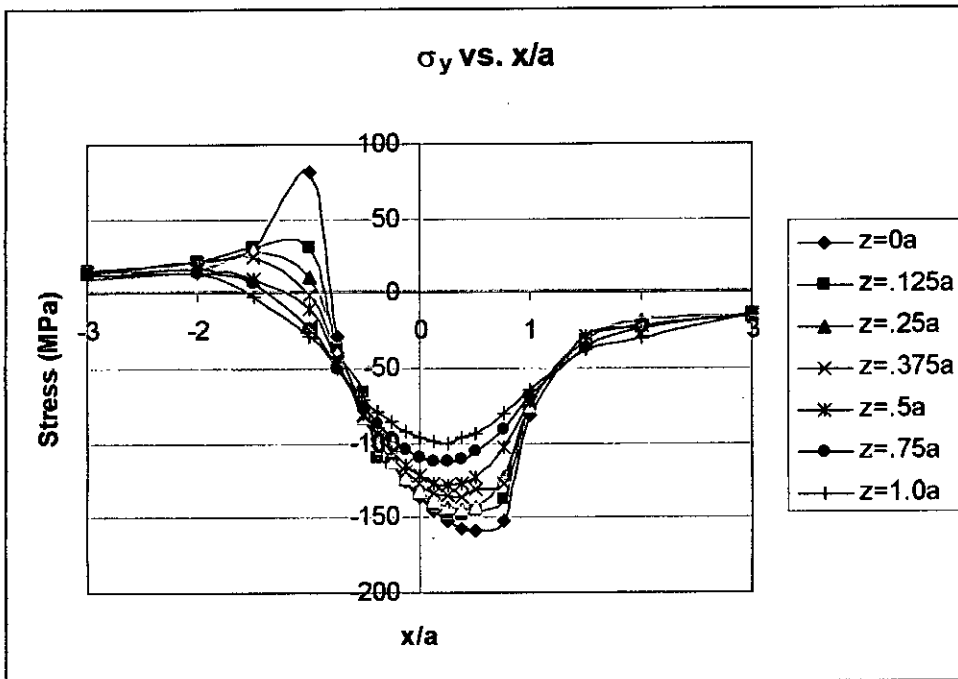Figure 4.21.3: Stress Distribution vs. x/a for vertex angle 5° at t = 0*l* (Aluminum)

Figure 4.21.4: Stress Distribution vs. x/a for vertex angle $5°$ at t = $0.5l$ for different materials

4.4.3 σ_y vs. x/a at different length and different vertex angle

From distribution of stress in Y axis vs. x/a at different length it has been shown that maximum stress has been found at the tip. With increasing of distance from tip, it decreases like other stress component. It has been shown from figure 4.22.1 to 4.22.9. With variation of vertex angle the distribution of stress is same though its maximum value varies. It varies such that with increasing of vertex angle it decreases. The distribution has been shown in figure 4.23.1 to 4.23.9.

Figure 4.22.1: Stress Distribution vs. x/a for vertex angle 5° at t = 0*l* (Steel)

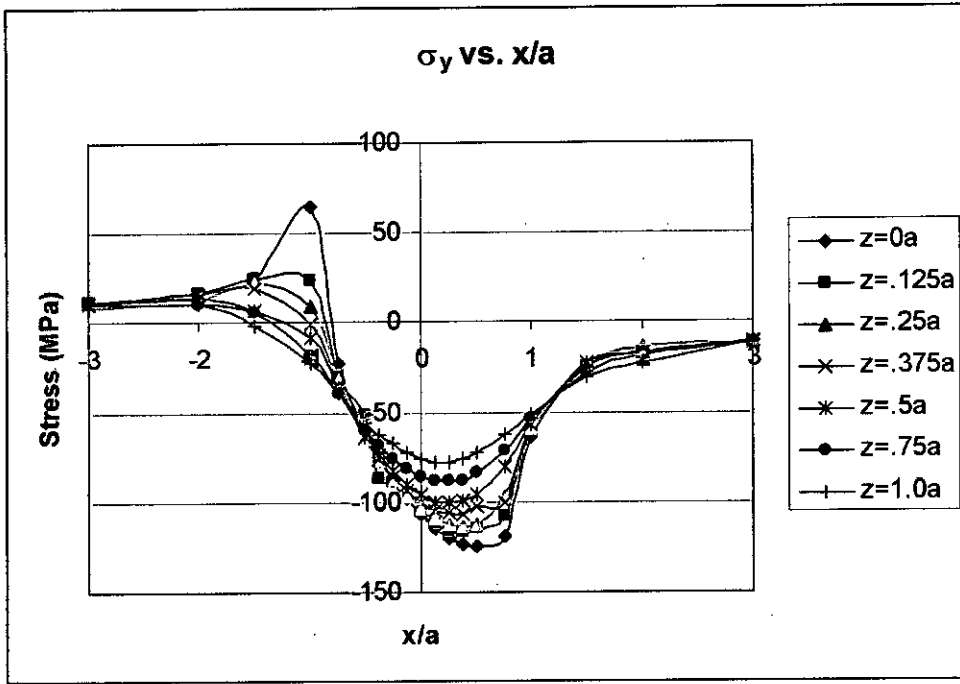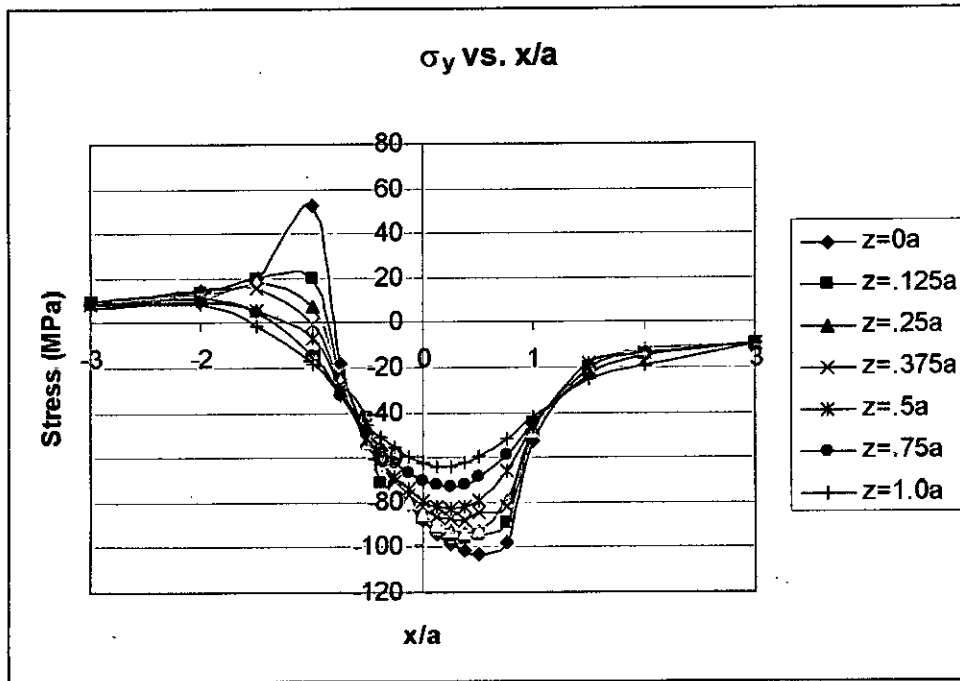Figure 4.22.2: Stress Distribution vs. x/a for vertex angle 5° at t = 0.25*l* (Steel)

Figure 4.22.3: Stress Distribution vs. x/a for vertex angle $5°$ at $t = 0.5l$ (Steel)
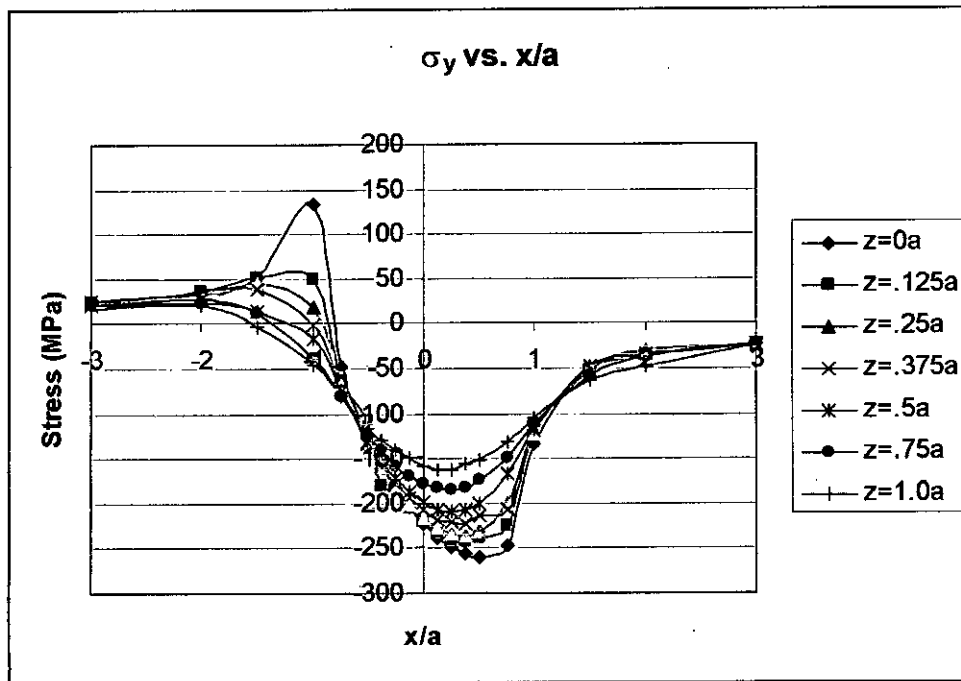
Figure 4.22.4: Stress Distribution vs. x/a for vertex angle $5°$ at $t = 0.75l$ (Steel)
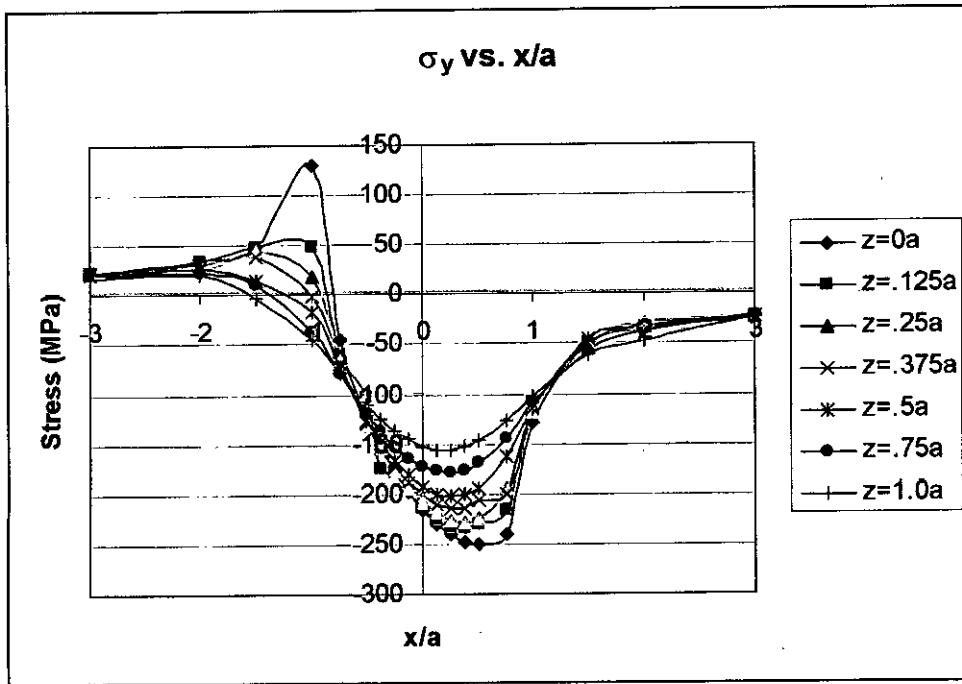
Figure 4.22.5: Stress Distribution vs. x/a for vertex angle 5° at t = 1*l* (Steel)
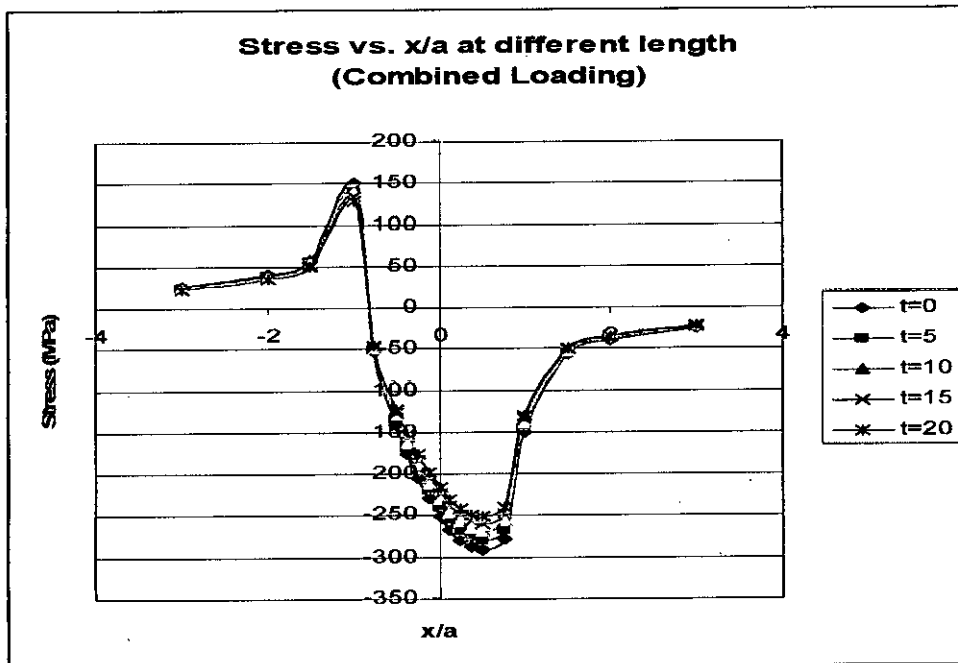
Figure 4.22.6: Stress distribution in Y axis at different length at z/a=0 with vertex angle 5° (Combined loading)

Figure 4.22.7: Stress Distribution vs. x/a for vertex angle 5° at t = 0*l* (Aluminum)

Figure 4.22.8: Stress Distribution vs. x/a for vertex angle 5° at t = 0.5*l* (Aluminum)

Figure 4.22.9: Stress Distribution vs. x/a for vertex angle 5° at t = 1*l* (Aluminum)

Figure 4.23.1: Stress Distribution vs. x/a for vertex angle 20° at t = 0*l* (Steel)

Figure 4.23.2: Stress Distribution vs. x/a for vertex angle $30°$ at t = $0l$ (Steel)
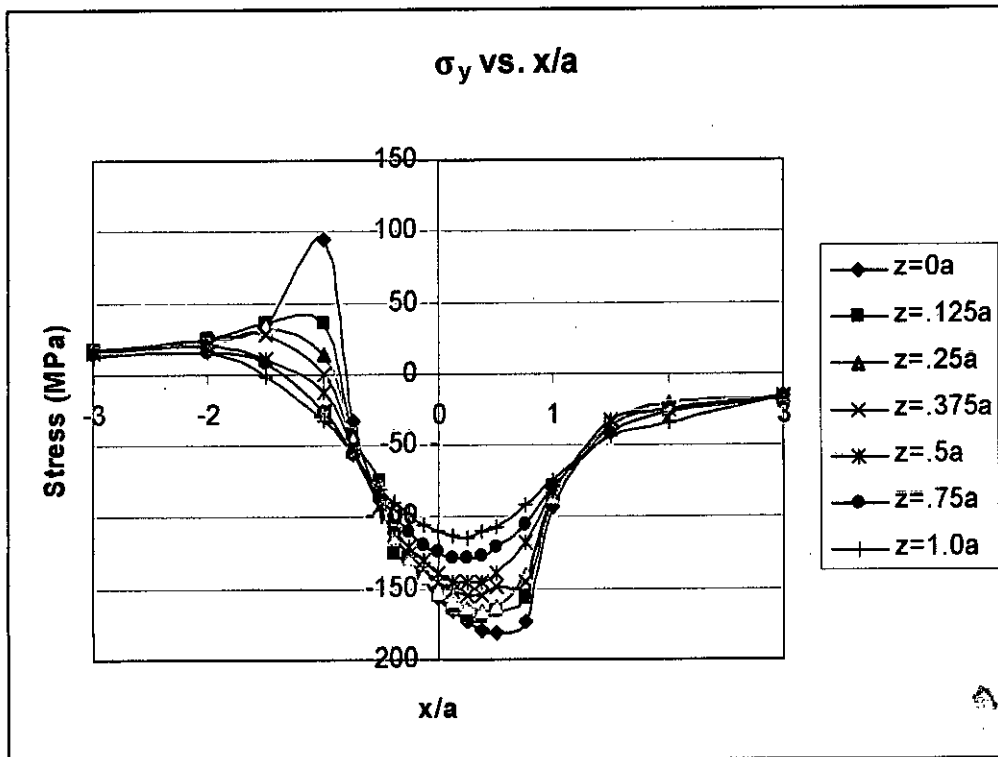
Figure 4.23.3: Stress Distribution vs. x/a for vertex angle $45°$ at t = $0l$ (Steel)
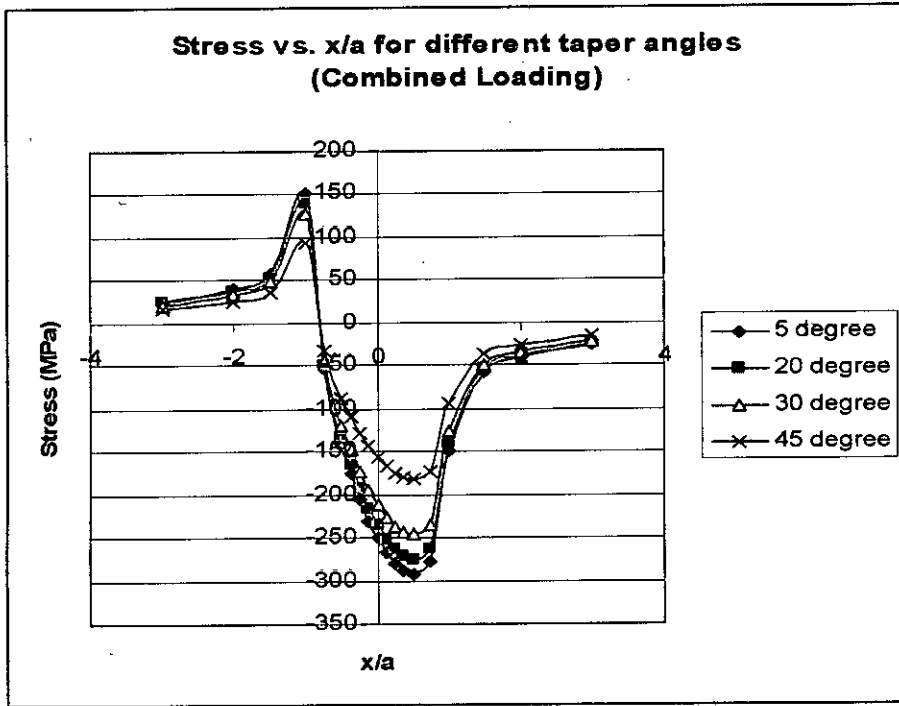
Figure 4.23.4: Distribution of Stress in Z direction (combined loading) vs. x/a for different vertex angle at t=0

Figure 4.23.5: Stress Distribution vs. x/a for vertex angle 5° at t = 0.5*l* (Aluminum)

Figure 4.23.6: Stress Distribution vs. x/a for vertex angle 20° at t = 0.5l (Aluminum)

Figure 4.23.7: Stress Distribution vs. x/a for vertex angle 30° at t = 0.5l (Aluminum)
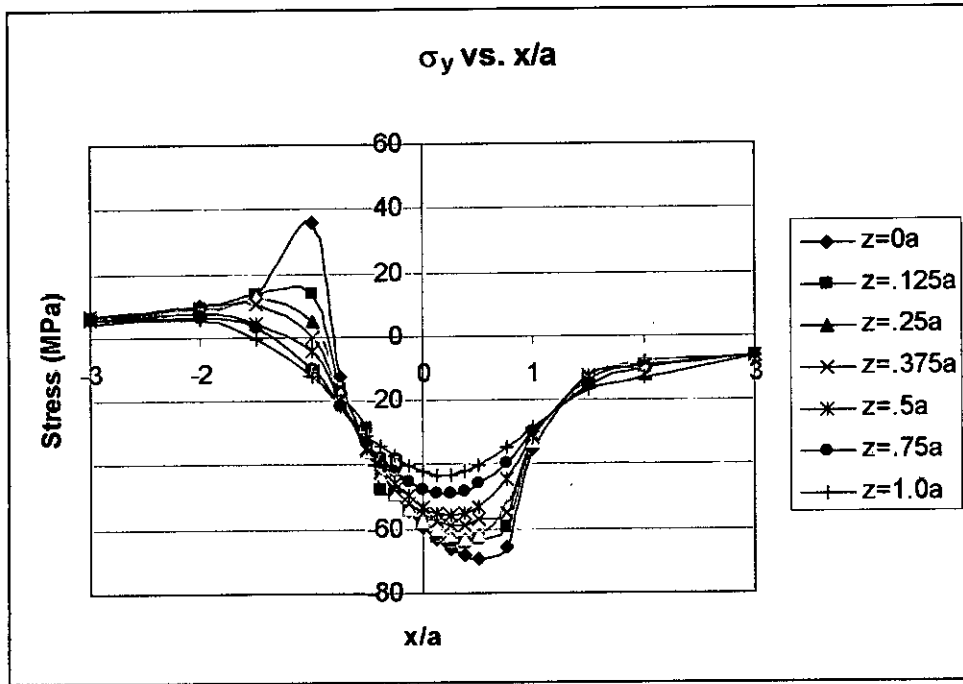
Figure 4.23.8: Stress Distribution vs. x/a for vertex angle 45° at t = 0.5*l* (Aluminum)

4.5.1 Shear Stress Distribution

The maximum shear stress has been found from Von Mises shear theory. So, it needs two normal stress components. From stress distribution for shear stress vs. x/a we have seen that maximum value for shear stress has been found that for z/a=.30 at it has been found at x/a=0 with a stress ratio of 0.4. At surface z=0 the value is not as high as that for z/a=0.30, though all other stress components are high at surface. The distribution of shear stress with variation of x/a and z/a have been shown from figure 4.24.1 to 4.24.4 and 4.25.1 to 4.25.4 respectively.
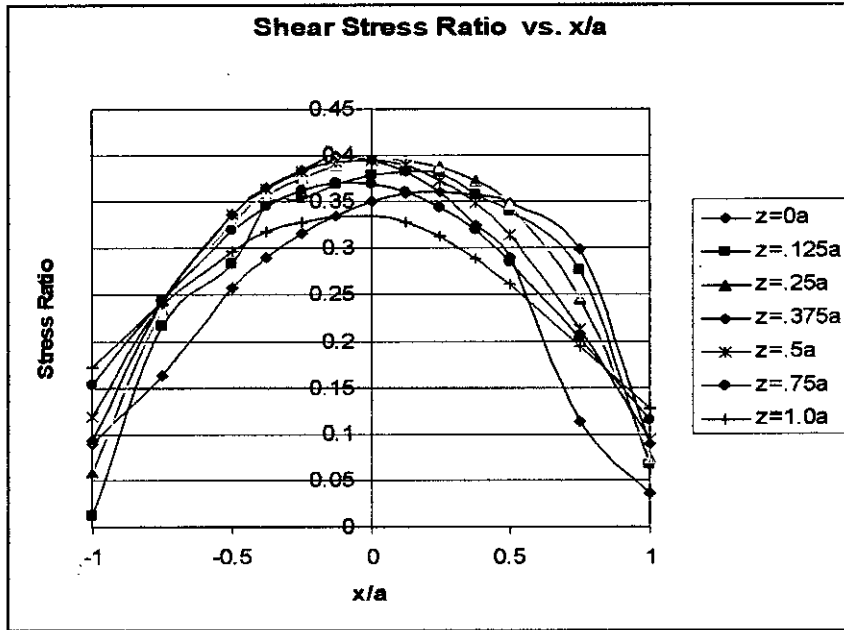
Figure 4.24.1: Shear Stress ratio vs. x/a
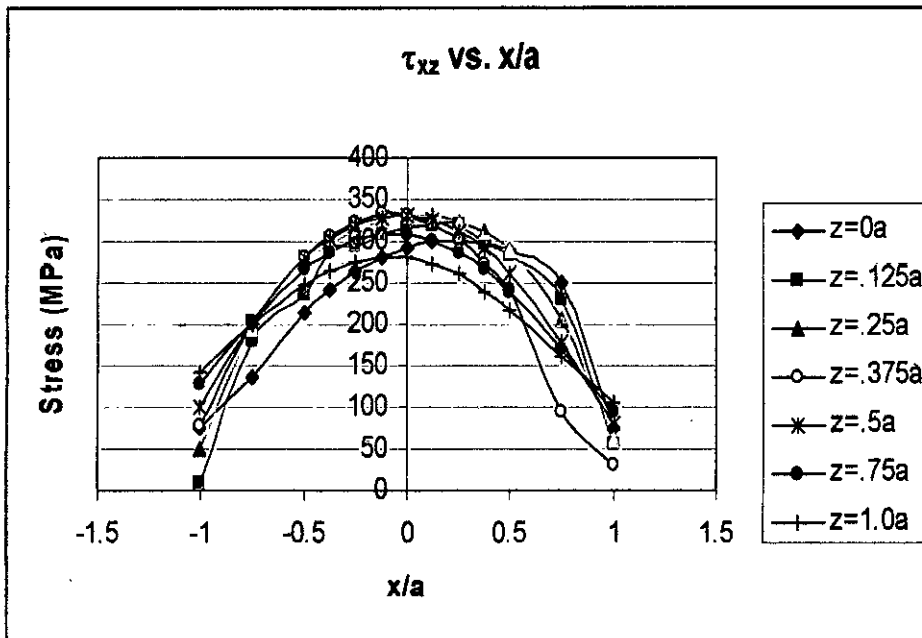
Figure 4.24.2: Shear Stress vs. x/a for vertex angle 5° at t=0*l* (Steel)
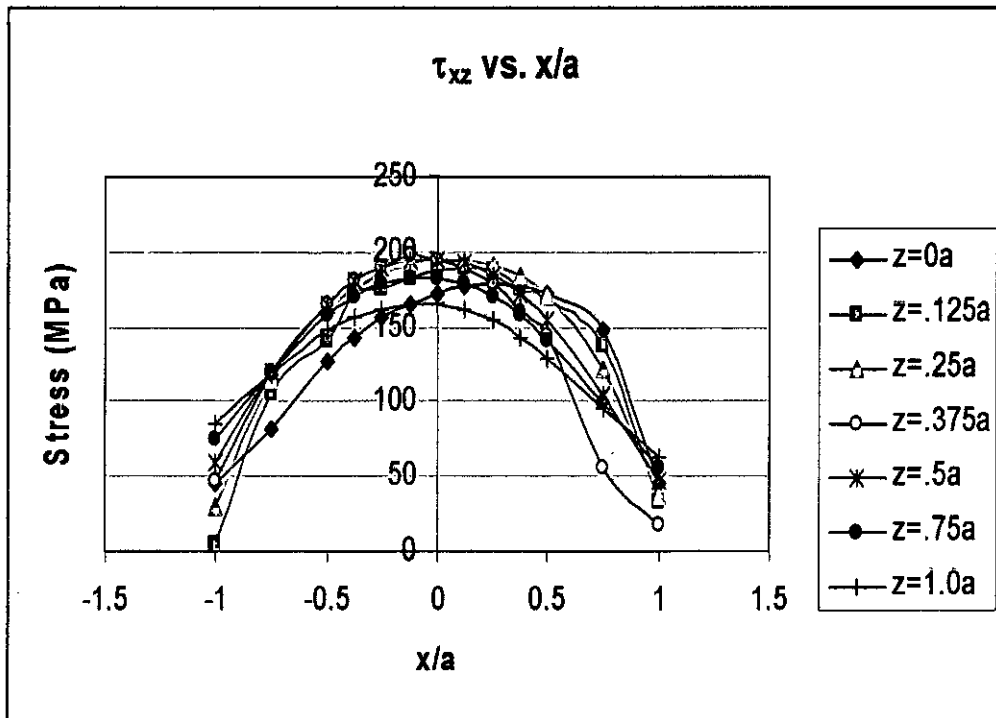
Figure 4.24.3: Shear Stress vs. x/a for vertex angle 5° at t=0*l* (Aluminum)
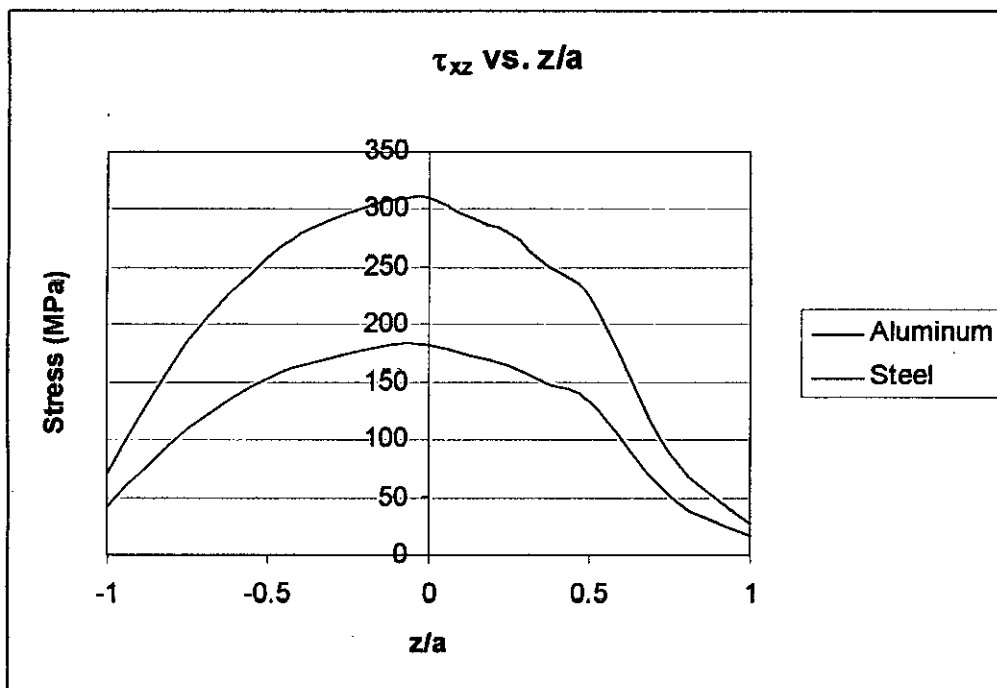
Figure 4.24.4: Shear Stress vs. x/a for vertex angle 5° with different materials
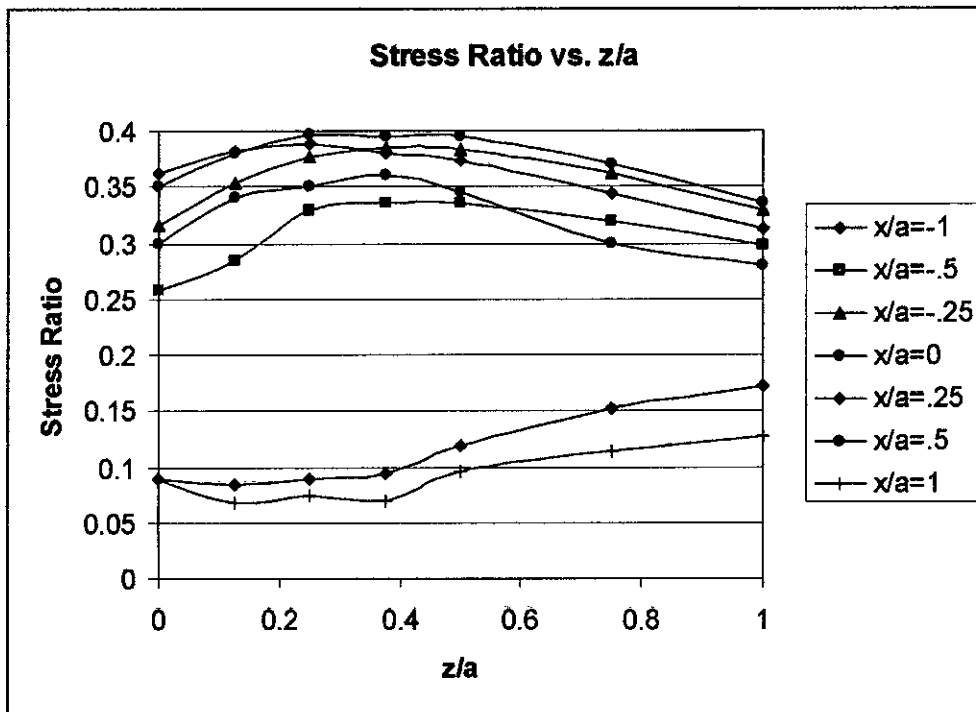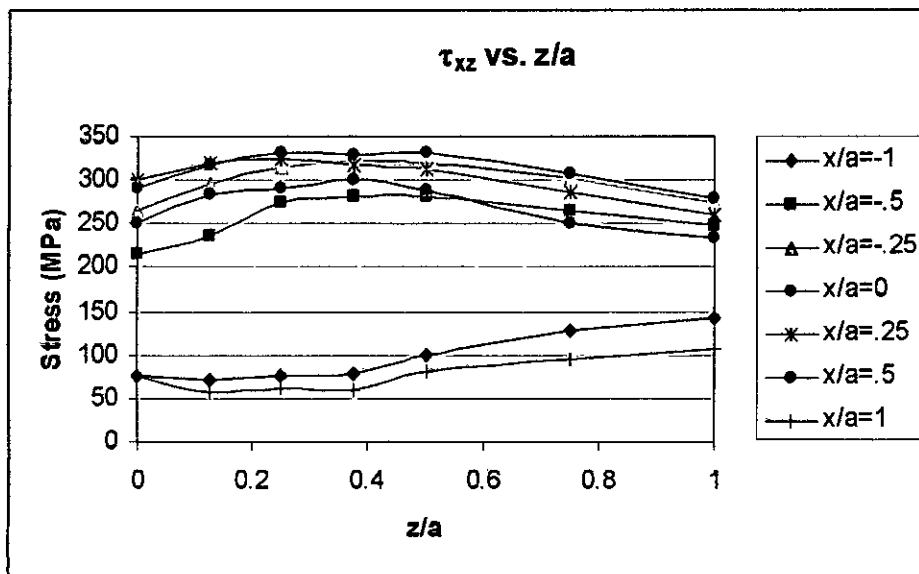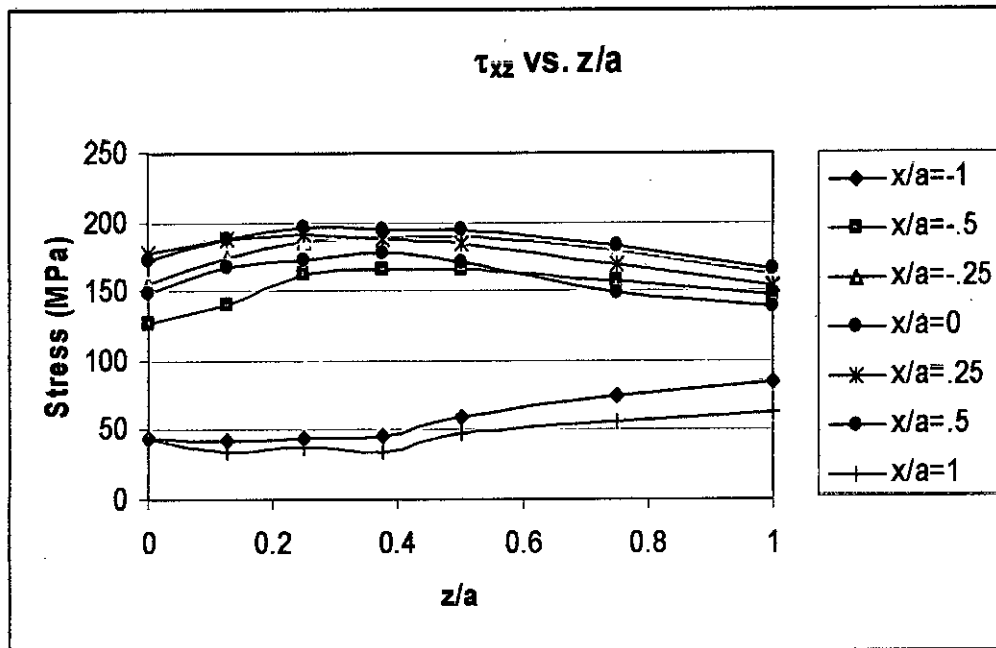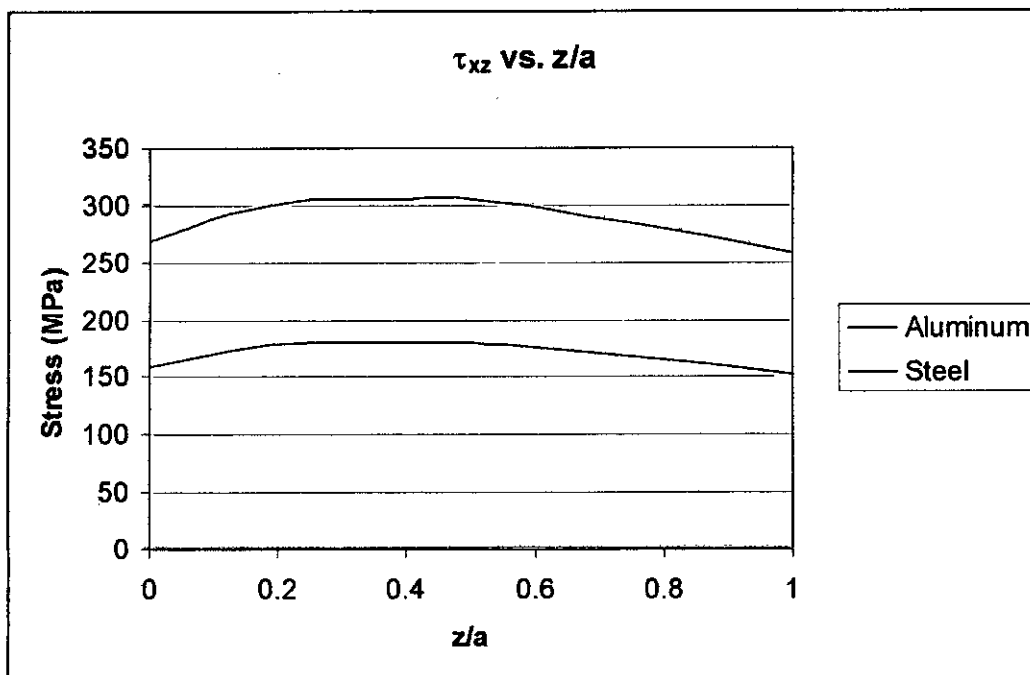
Figure 4.25.1: Shear Stress ratio vs. z/a
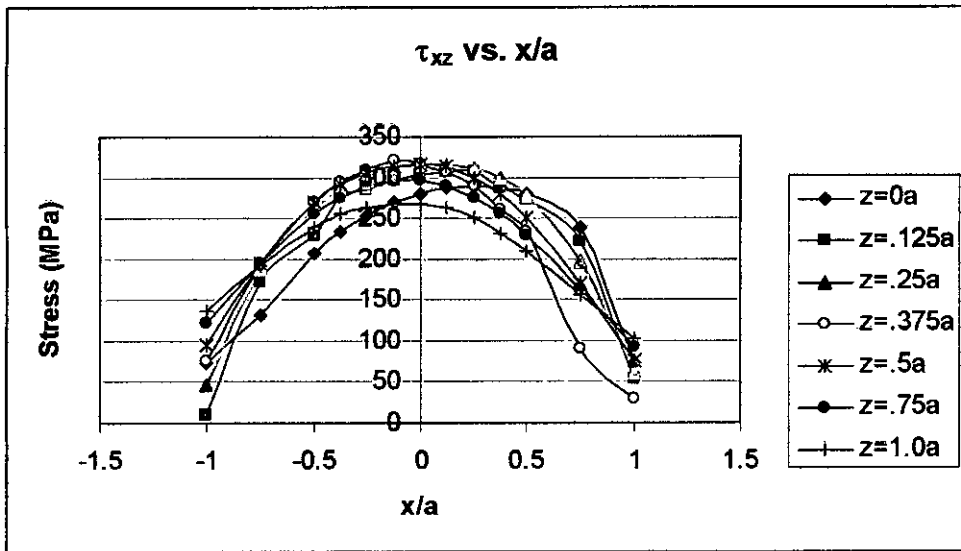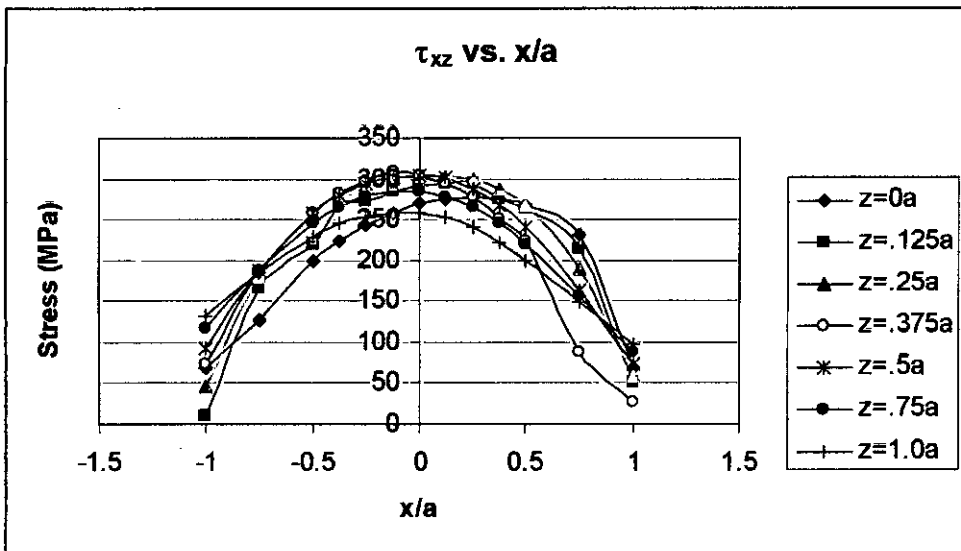

Figure 4.25.2: Shear Stress vs. x/a for vertex angle 5° at t=0*l* (Steel)

Figure 4.25.3: Shear Stress vs. x/a for vertex angle 5° at t=0*l* (Aluminum)

Figure 4.25.4: Shear Stress vs. z/a for vertex angle 5° with different materials

4.5.2 Shear stress at different length

Like other distribution of normal stress, shear stress has maximum value at tip of conical roller contact and it then decreases with increasing distance from tip. But distribution of stress remains same. On the other hand, for low vertex angle the shear stress has maximum value and it decreases in value with increasing vertex angle. The stress distribution has been shown form figure 4.26.1 to 4.26.9 with variation of x/a and that has been shown from figure 4.27.1 to 4.27.9 with variation of z/a.

Figure 4.26.1: Shear Stress vs. x/a for vertex angle 5° at t=0l (Steel)

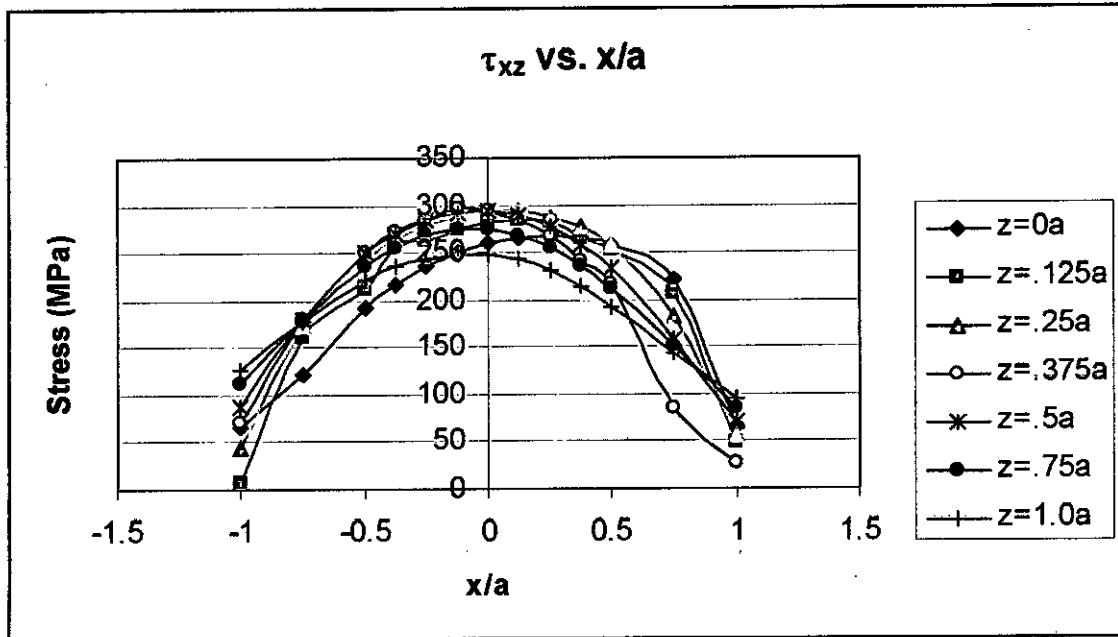Figure 4.26.2: Shear Stress vs. x/a for vertex angle 5° at t=0.25l (Steel)

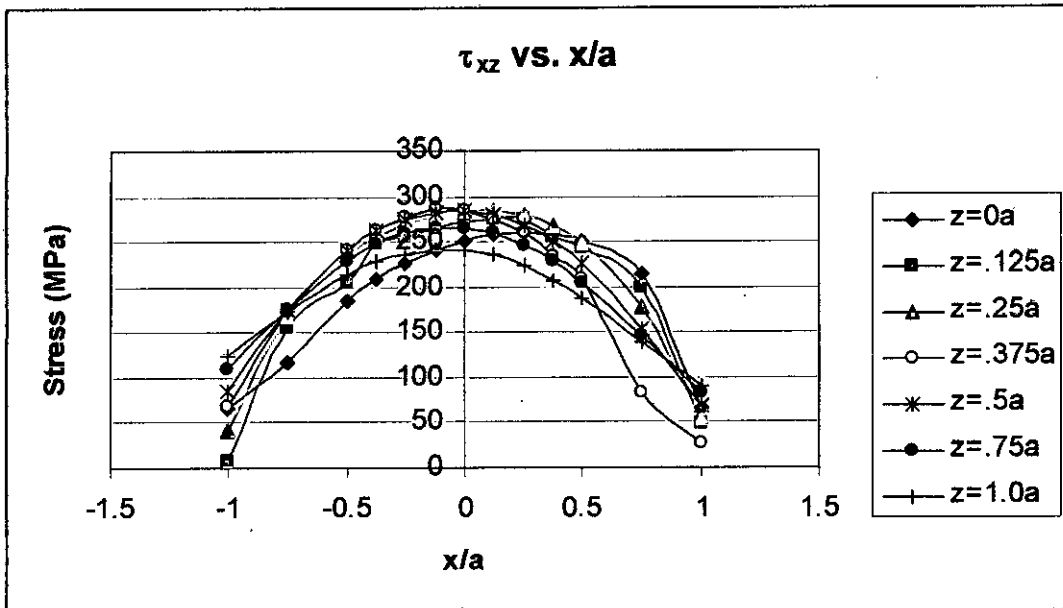Figure 4.26.3: Shear Stress vs. x/a for vertex angle 5° at t=0.5*l* (Steel)

Figure 4.26.4: Shear Stress vs. x/a for vertex angle 5° at t=0.75*l* (Steel)

95
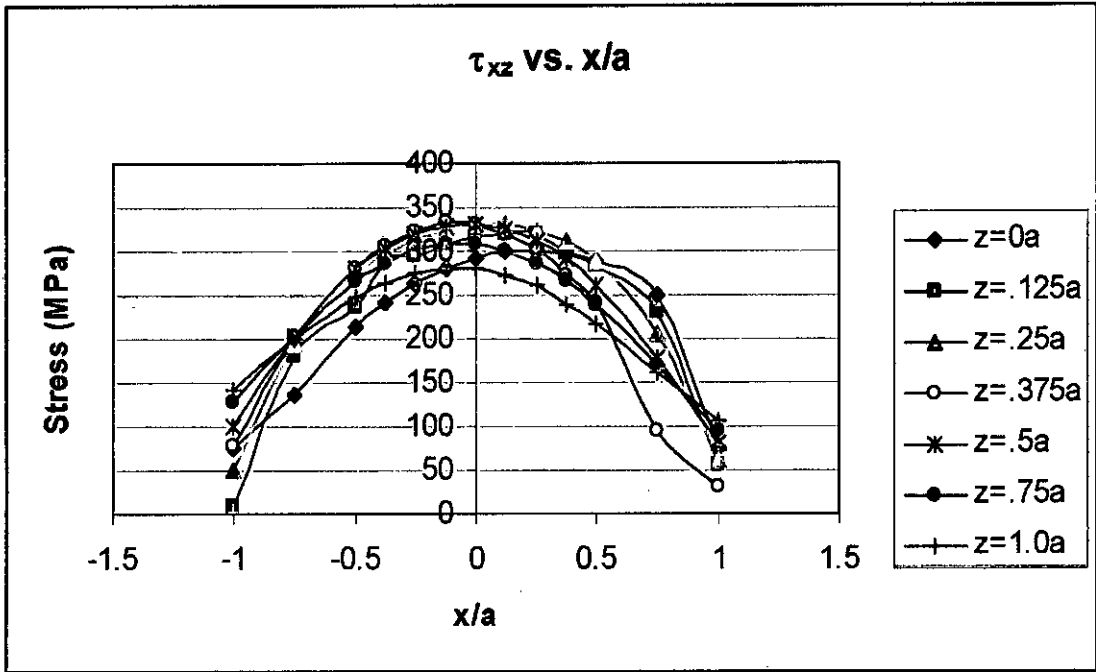
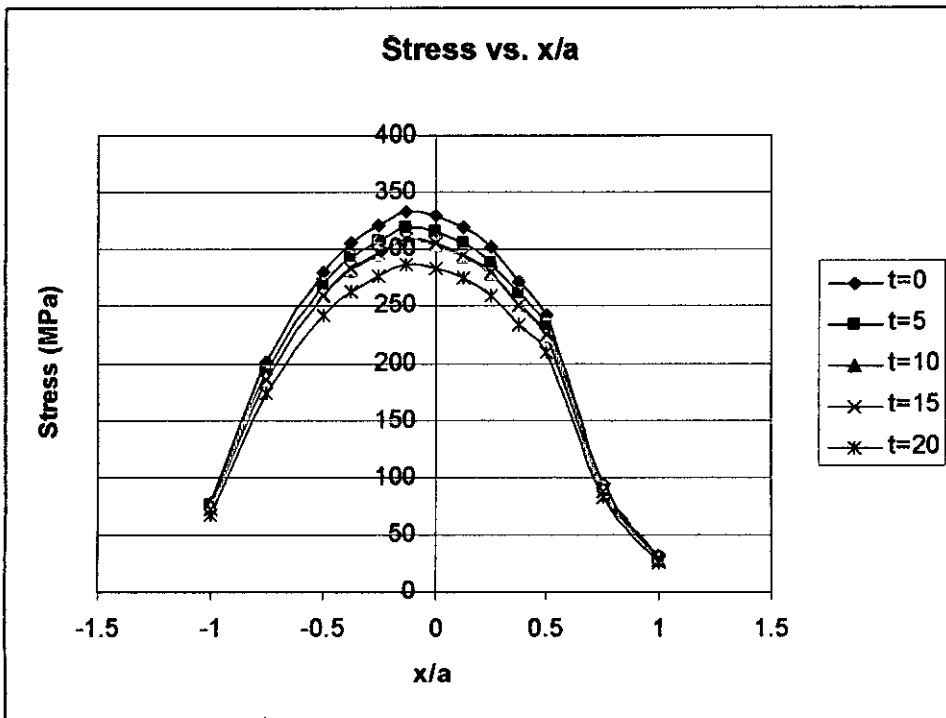Figure 4.26.5: Shear Stress vs. x/a for vertex angle 5° at t=1*l* (Steel)

Figure 4.26.6: Shear Stress at different length vs. x/a at z/a= .375 for vertex angle 5°
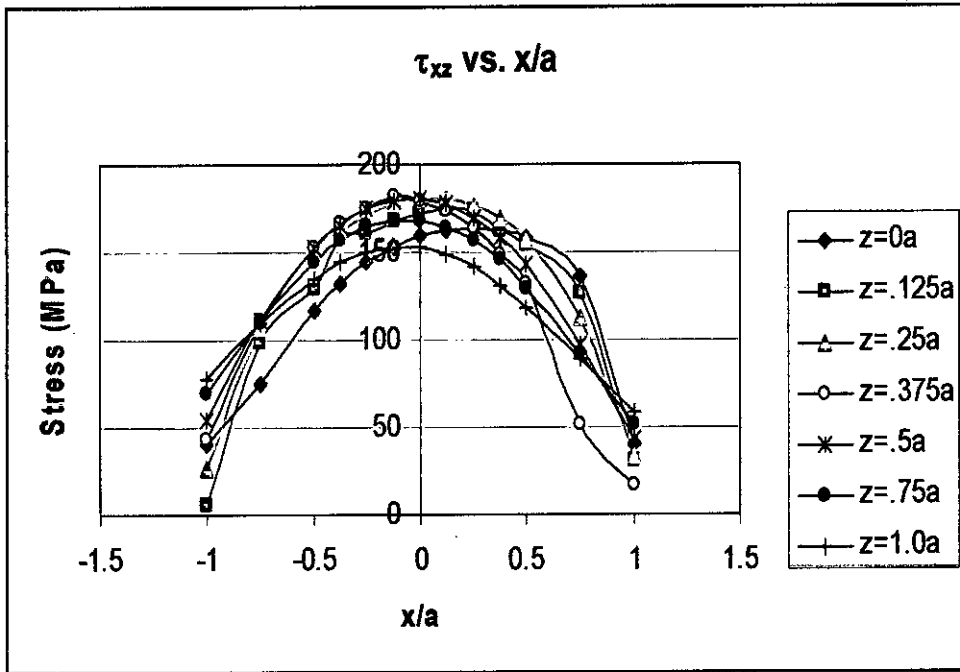
Figure 4.26.7: Shear Stress vs. x/a for vertex angle 5° at t=0*l* (Aluminum)

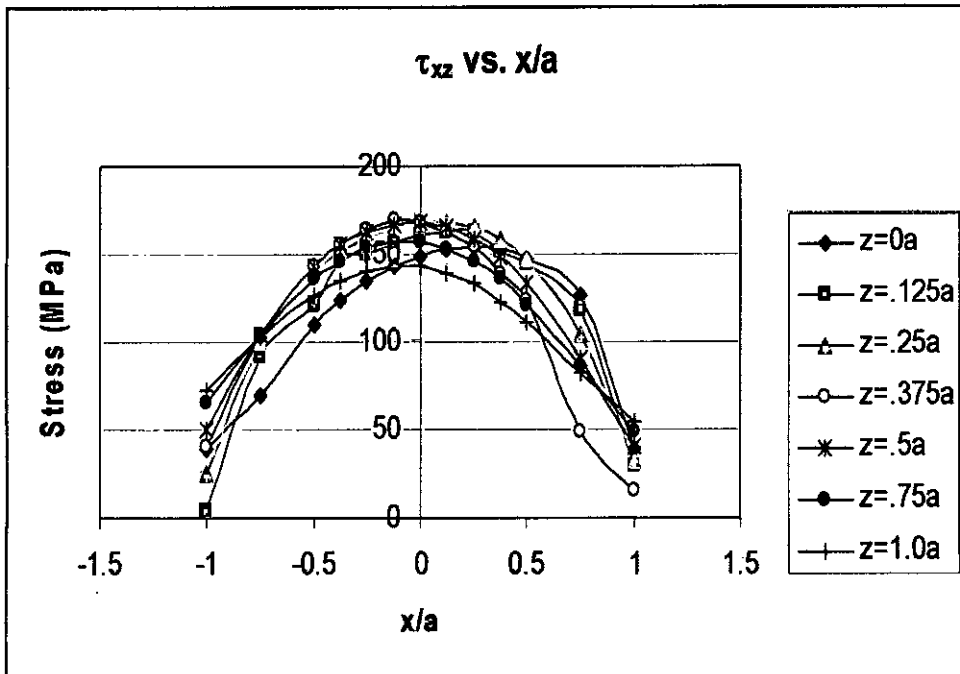Figure 4.26.8: Shear Stress vs. x/a for vertex angle 5° at t=0.5*l* (Aluminum)

Figure 4.26.8: Shear Stress vs. x/a for vertex angle 5° at t=1*l* (Aluminum)

Figure 4.27.1: Shear Stress vs. z/a for vertex angle 5° at t=0*l* (Steel)
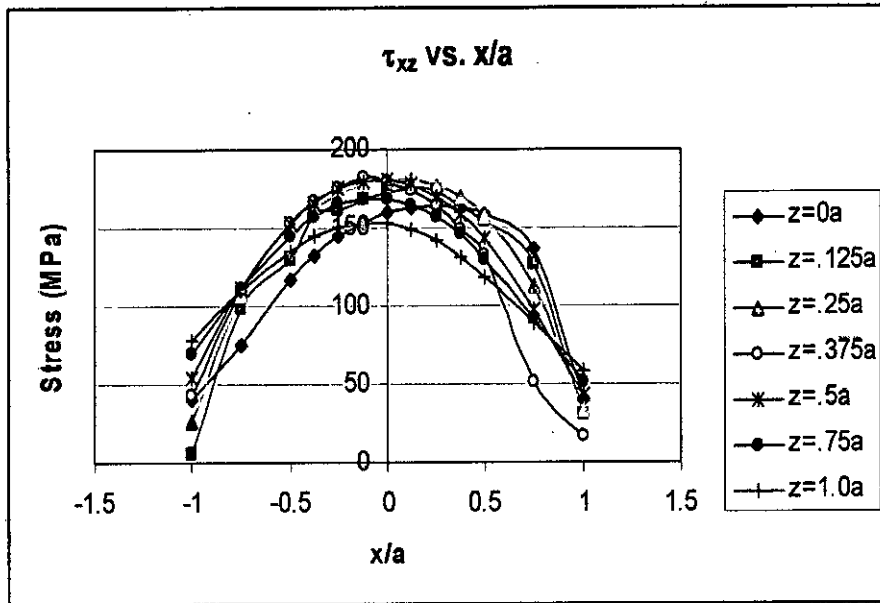
Figure 4.27.2: Shear Stress vs. z/a for vertex angle 5° at t=0.25l (Steel)

Figure 4.27.3: Shear Stress vs. z/a for vertex angle 5° at t=0. 5l (Steel)
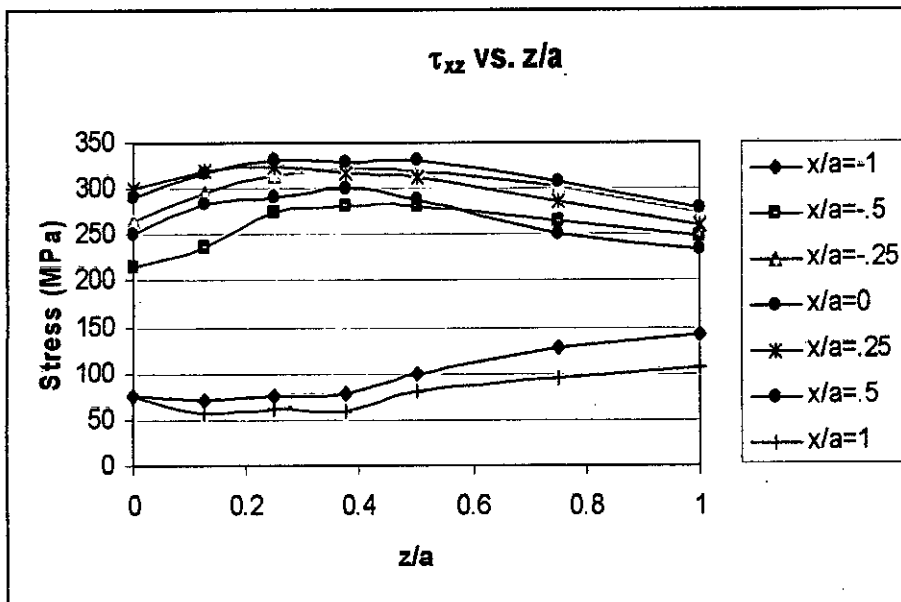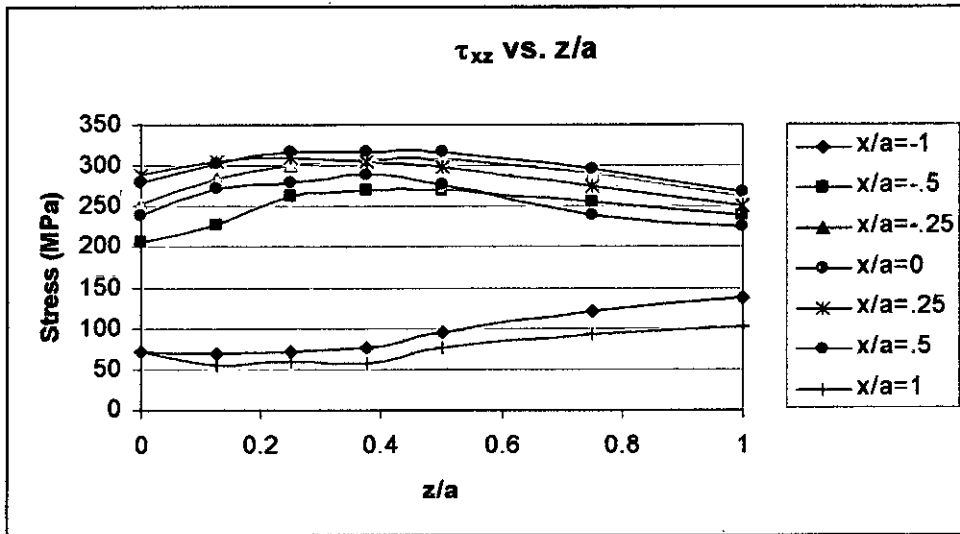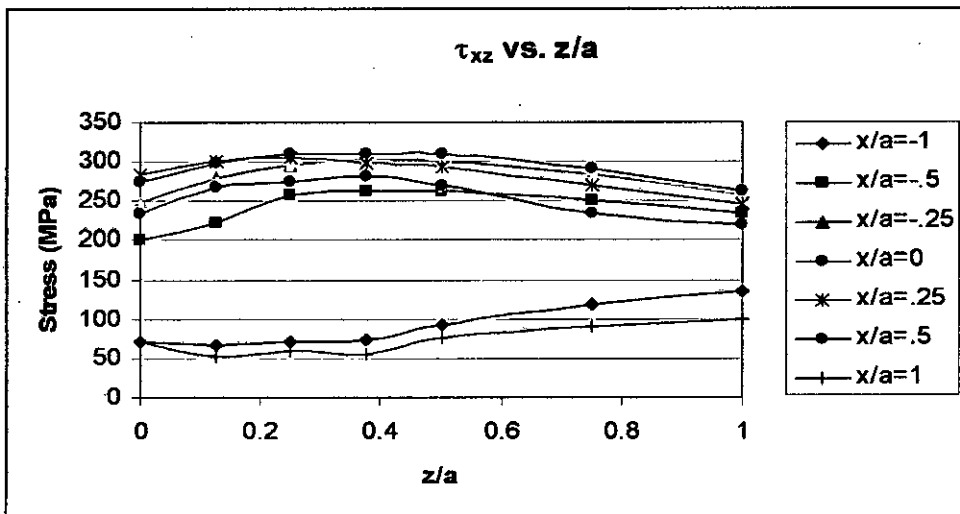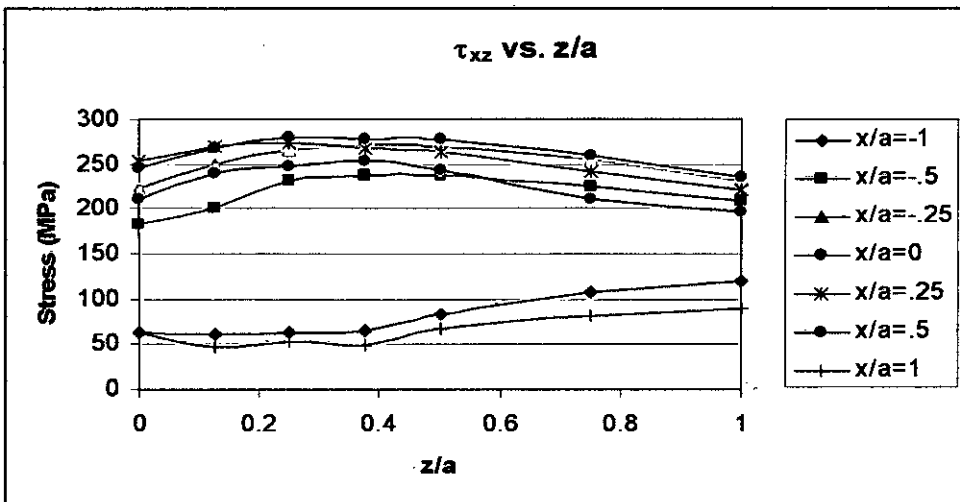

Figure 4.27.4: Shear Stress vs. z/a for vertex angle 5° at t=0.75l (Steel)

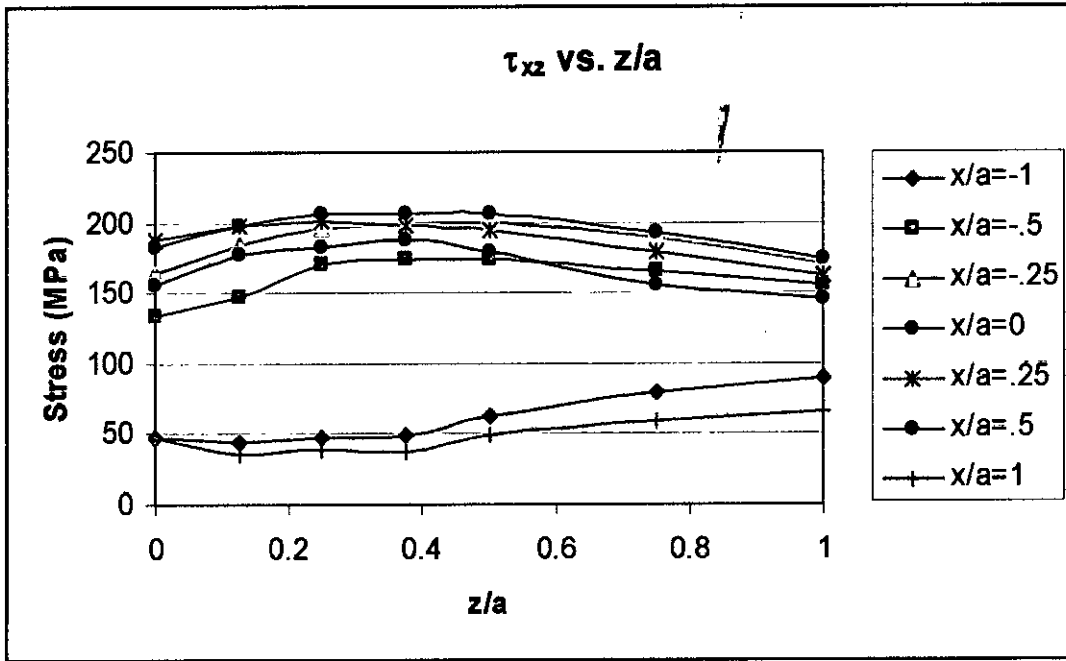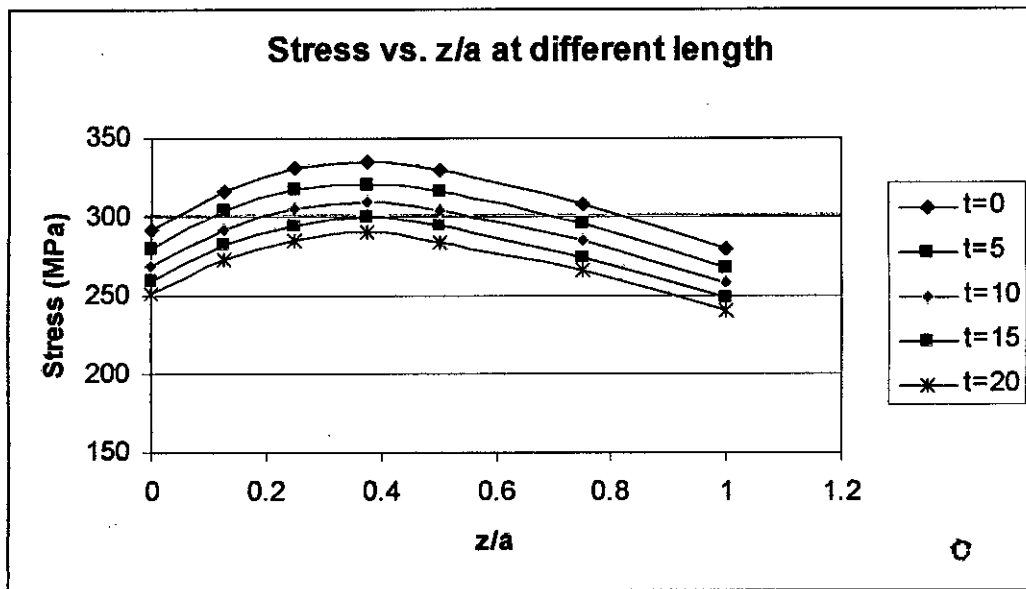Figure 4.27.5: Shear Stress vs. z/a for vertex angle 5° at t=1*l* (Steel)

Figure 4.27.6: Shear Stress at different length vs. z/a at x/a= 0 for vertex angle 5°
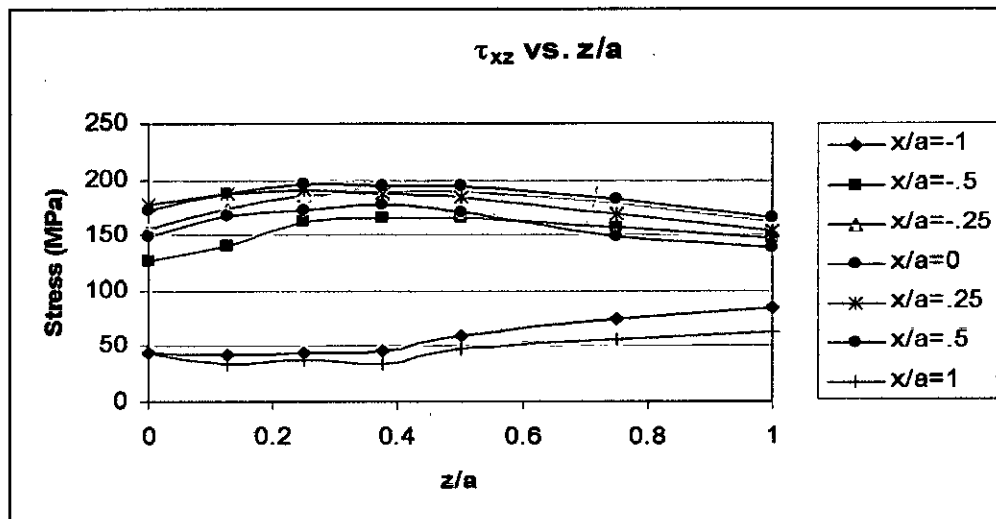
Figure 4.27.7: Shear Stress vs. z/a for vertex angle 5° at t=0 (Aluminum)

Figure 4.27.8: Shear Stress vs. z/a for vertex angle 5° at t=0.5*l* (Aluminum)
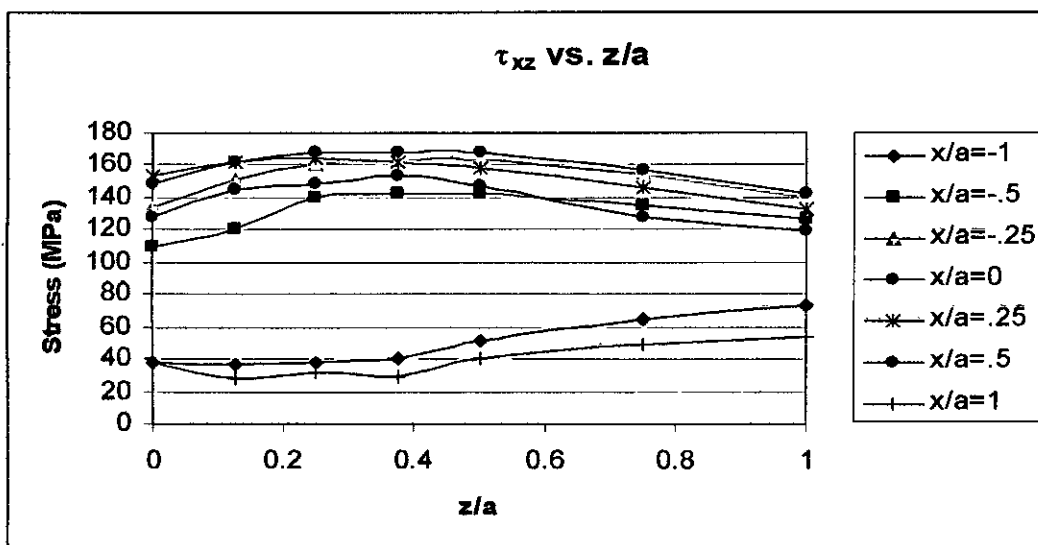
Figure 4.27.9: Shear Stress vs. z/a for vertex angle 5° at t=1*l* (Aluminum)

4.5.2 Shear stress distribution for different vertex angle

Shear stress varies with different vertex angle orientation. With increase of vertex angle shear stress decreases, but the distribution remain unchanged. The distribution vs. x/a and z/a has been shown from figure 4.28.1 to 4.28.7 and from figure 4.29.1 to 4.29.9 respectively.

Figure 4.28.1: Shear Stress vs. x/a for vertex angle 20° at t=0*l* (Steel)
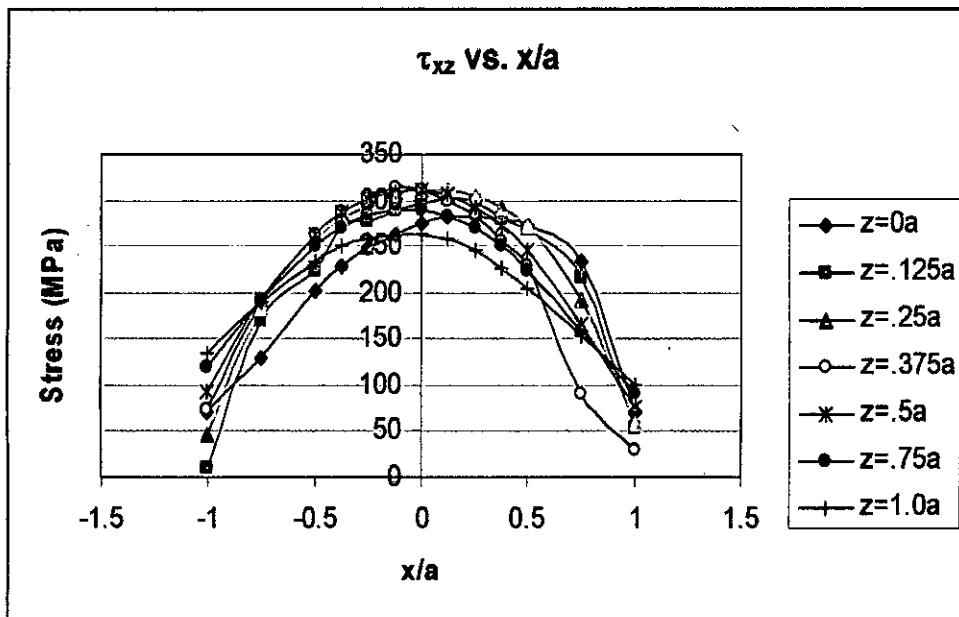
Figure 4.28.2: Shear Stress vs. x/a for vertex angle 30° at t=0*l* (Steel)

Figure 4.28.3: Shear Stress vs. x/a for vertex angle 45° at t=0*l* (Steel)
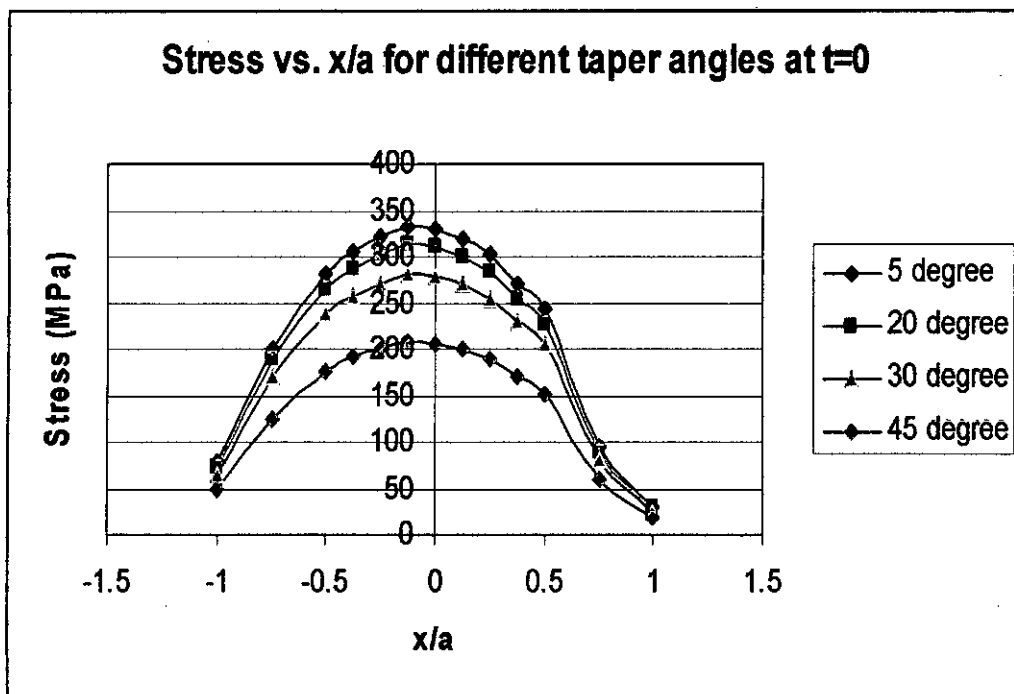
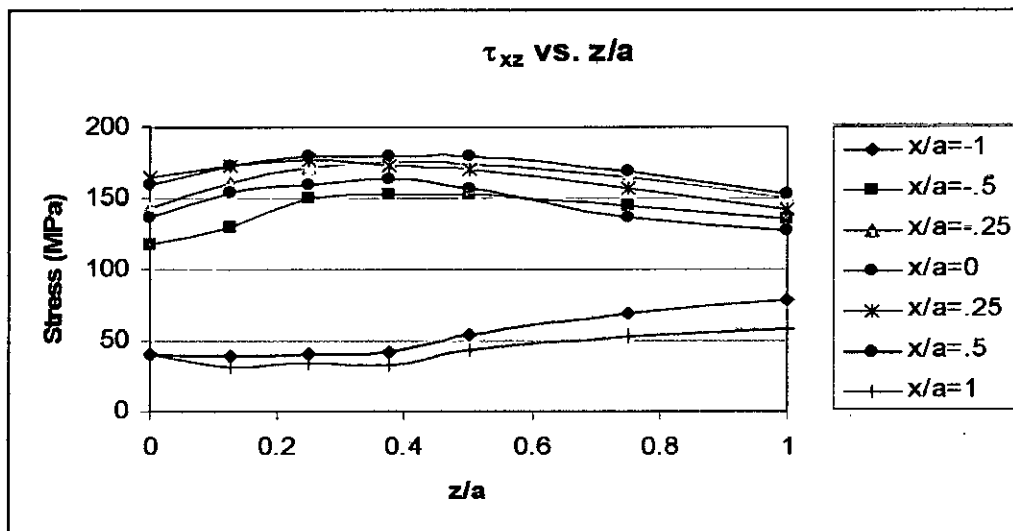Figure 4.28.4: Shear Stress at different length vs. x/a at z/a= .375 for different vertex

angle at t=0

Figure 4.28.5: Shear Stress vs. x/a for vertex angle 20° at t=0.5*l* (Aluminum)

Figure 4.28.6: Shear Stress vs. x/a for vertex angle 30° at t=0.5*l* (Aluminum)

104

Figure 4.28.7: Shear Stress vs. x/a for vertex angle 45° at t=0.5*l* (Aluminum)
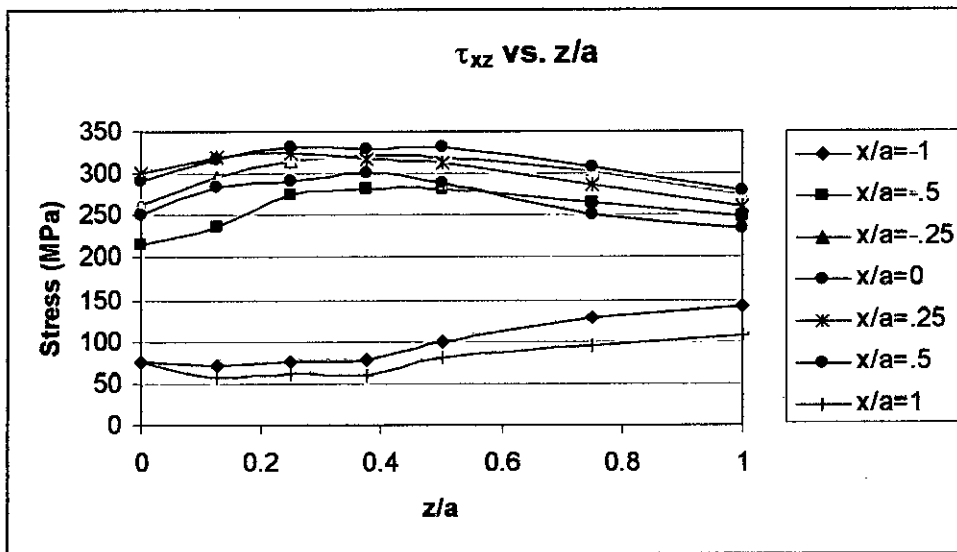
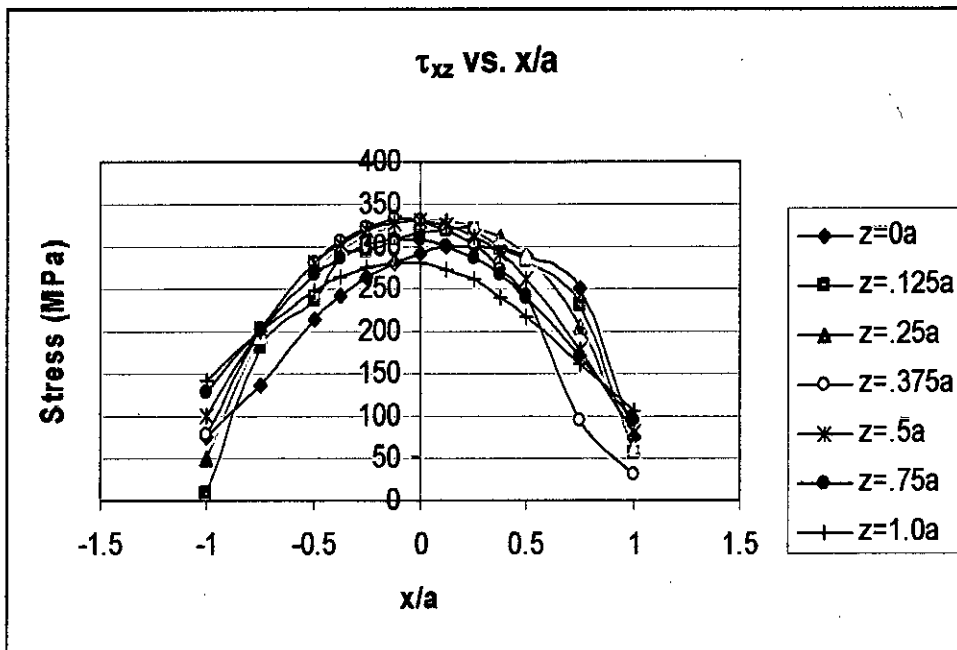
Figure 4.29.1: Shear Stress vs. z/a for vertex angle 5° at t=0*l* (Steel)
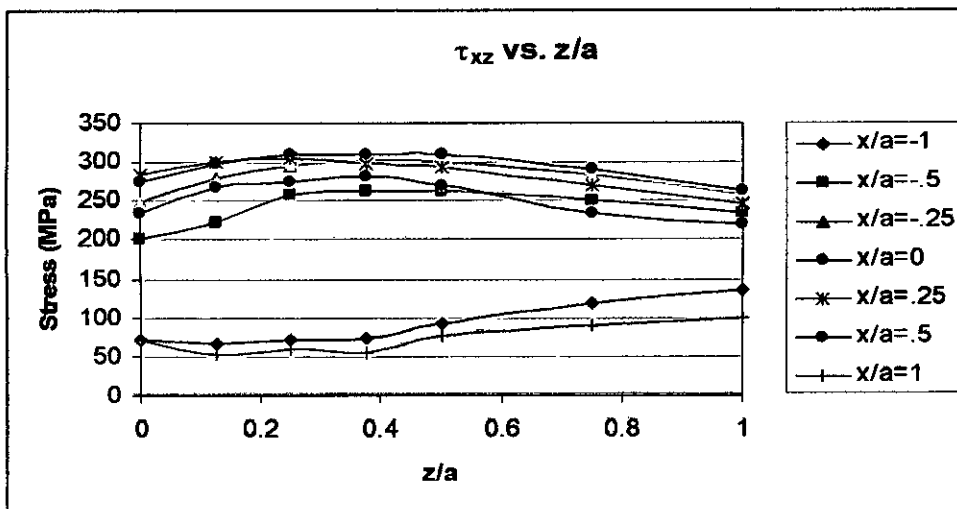
Figure 4.29.2: Shear Stress vs. z/a for vertex angle 20° at t=0*l* (Steel)
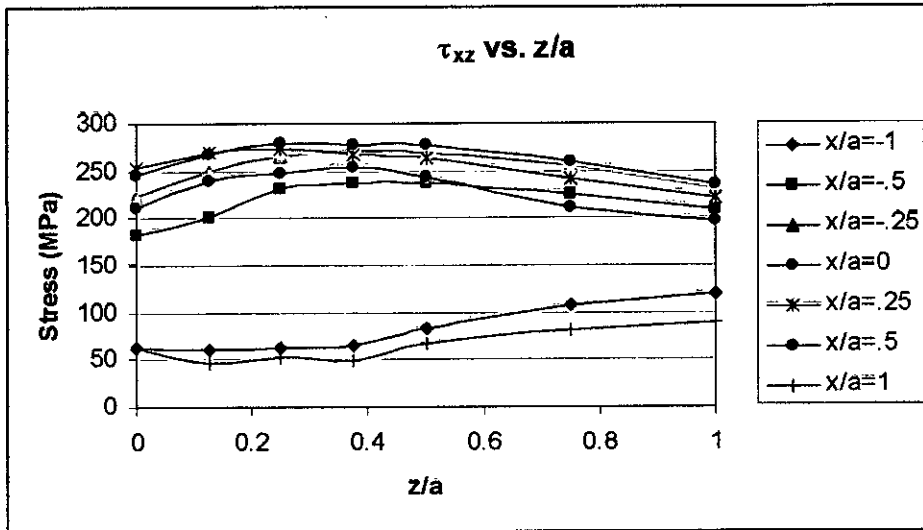
Figure 4.29.3: Shear Stress vs. z/a for vertex angle 30° at t=0*l* (Steel)
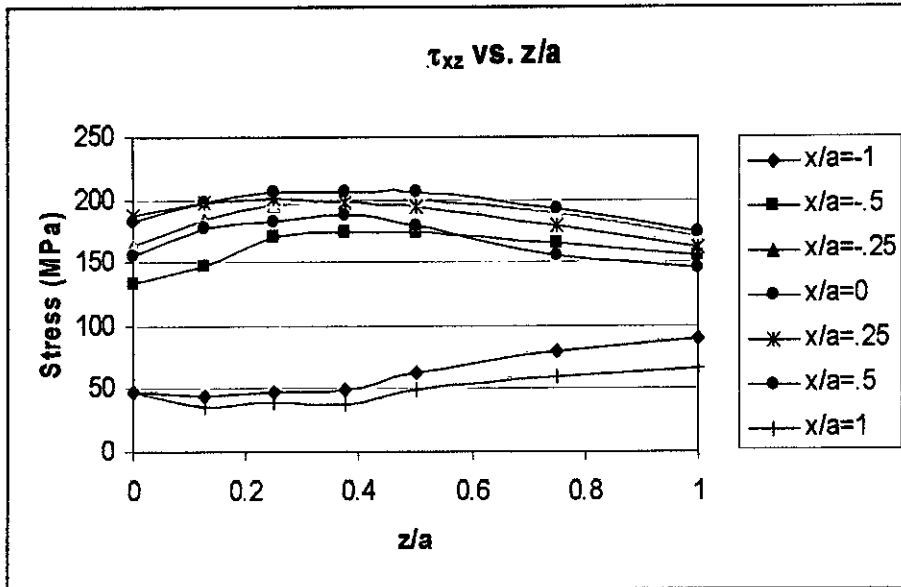
Figure 4.29.4: Shear Stress vs. z/a for vertex angle 45° at t=0*l* (Steel)
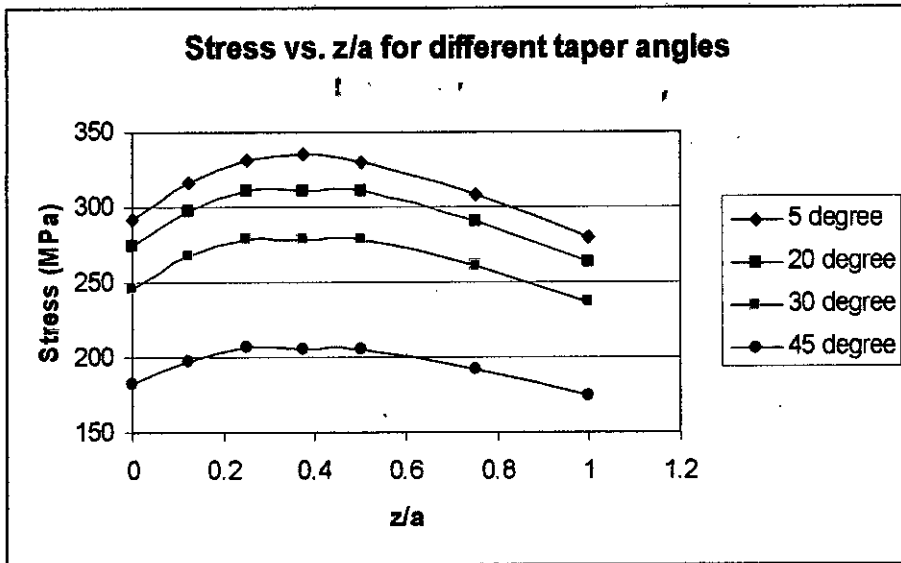
Figure 4.29.5: Shear Stress at different length vs. z/a at x/a= 0 for different vertex angle at t=0
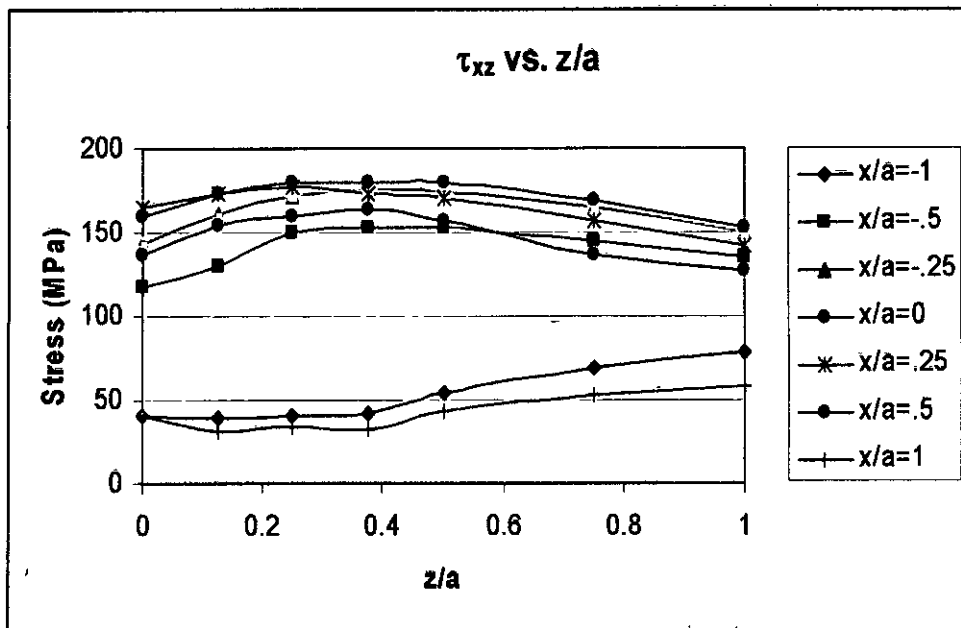
Figure 4.29.6: Shear Stress vs. z/a for vertex angle 5° at t=0.5l (Aluminum)
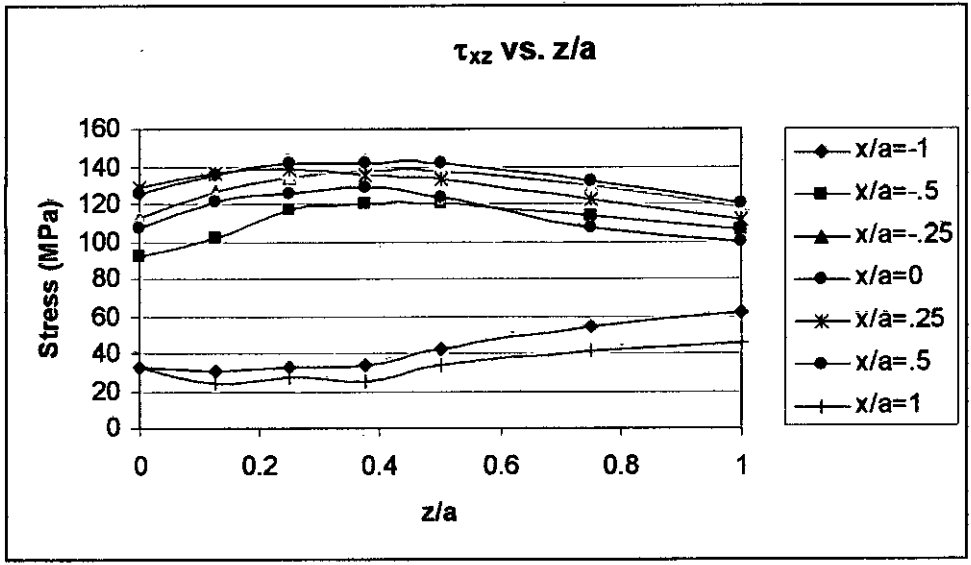
Figure 4.29.7: Shear Stress vs. z/a for vertex angle 20° at t=0.5*l* (Aluminum)
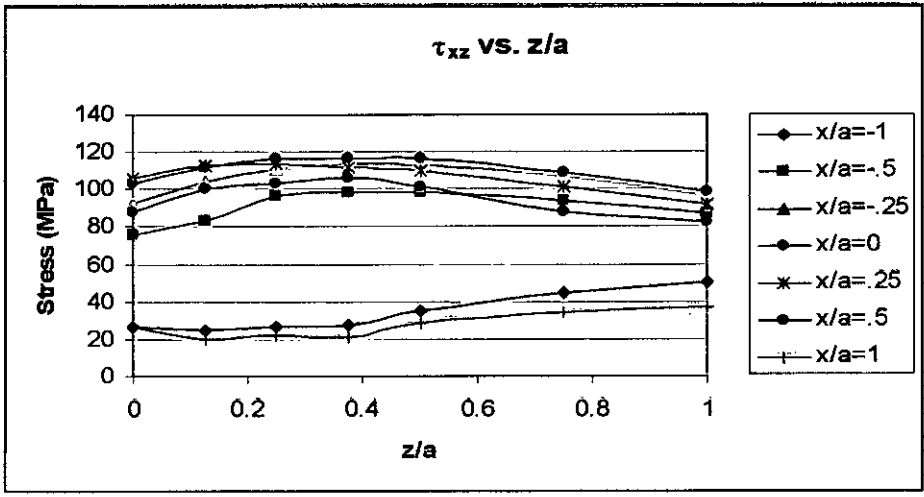
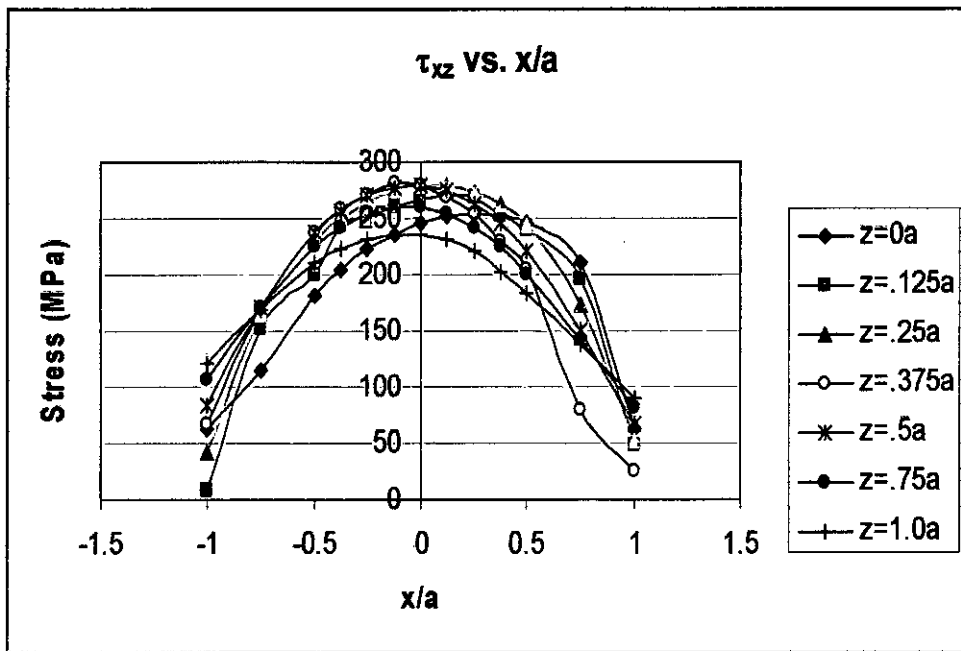

Figure 4.29.8: Shear Stress vs. z/a for vertex angle 30° at t=0.5*l* (Aluminum)

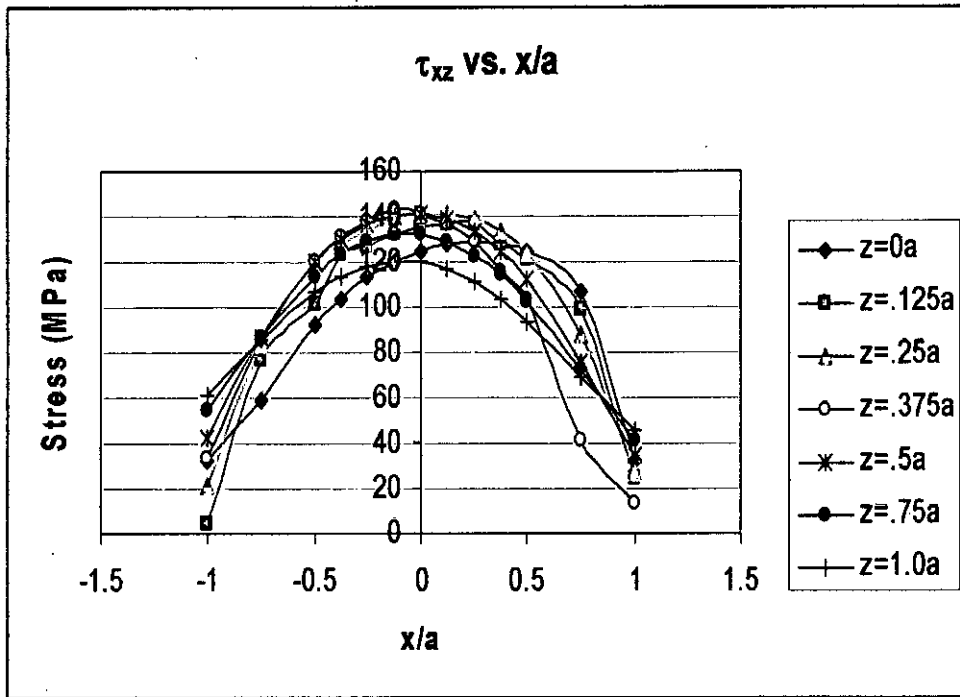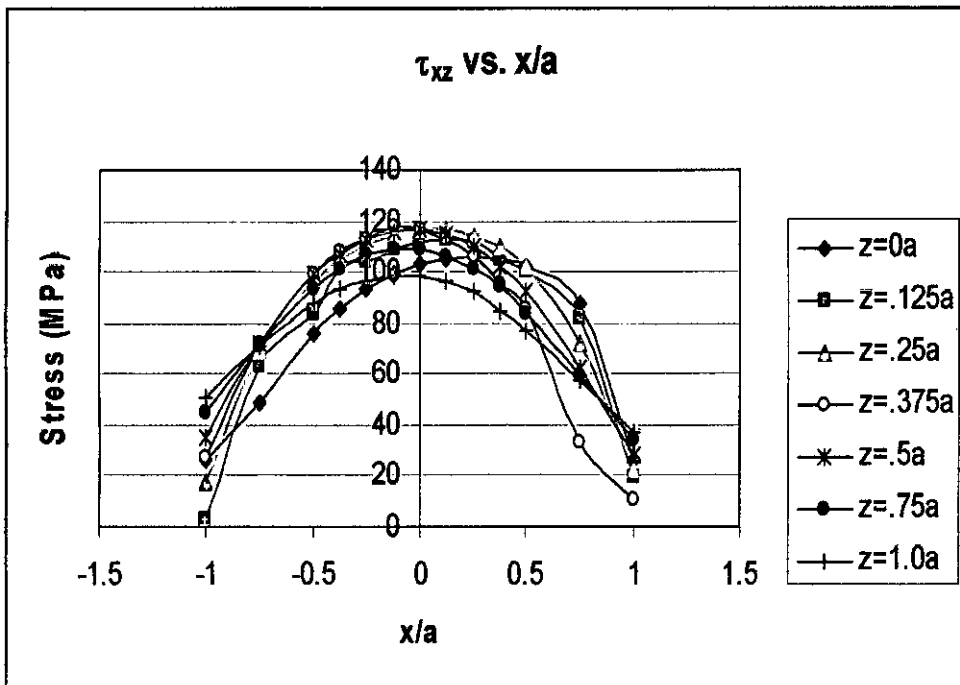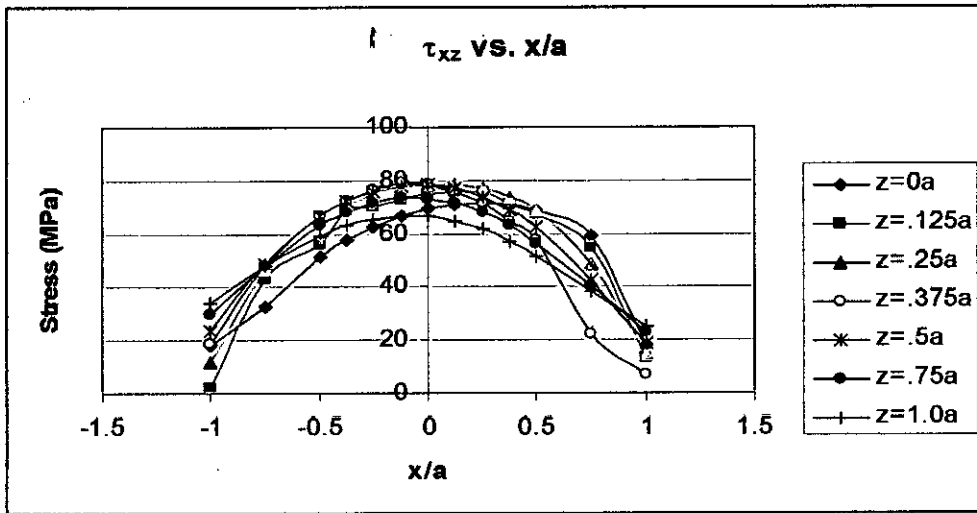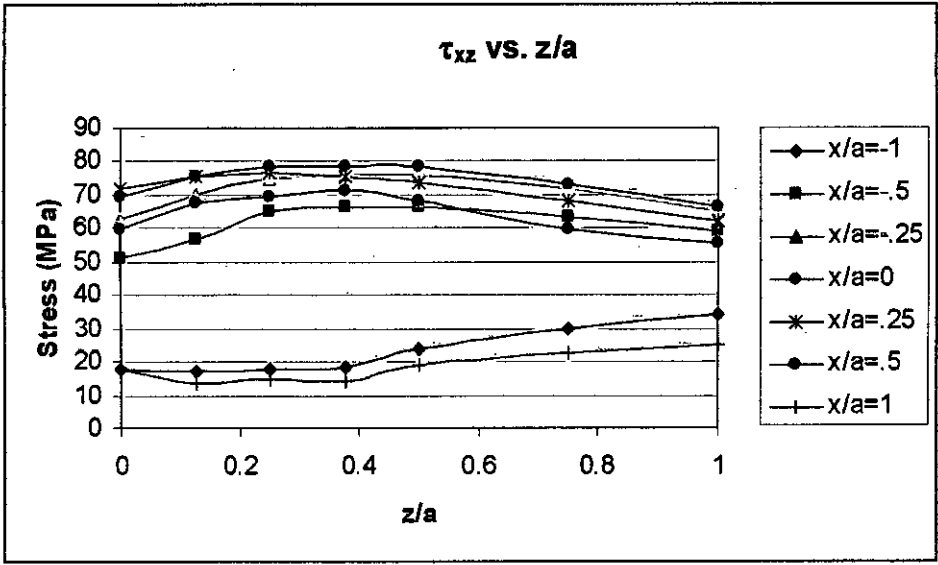Figure 4.29.9: Shear Stress vs. z/a for vertex angle 45° at t=0.5*l* (Aluminum)

4.6 Half width Distribution

In case of conical rollers in contact, the contact area is in form of trapezoid. So half width is not fixed like cylindrical contacts. The half width has same dimension with respect to line of symmetry. The variation of half width with respect to length has been shown in figure 4.31. It shows that, at tip the half width is minimum and it then increases. This is the reason, that by applying normal load, the half width is minimum at the tip, so stress component is higher at the tip. On the other hand, with increasing of vertex angle, half width length also increases. The half width length also varies with materials. For aluminum with low young modulus, the half width is higher. The variation of half width has been shown from figure 4.30.1 to 4.30.4.
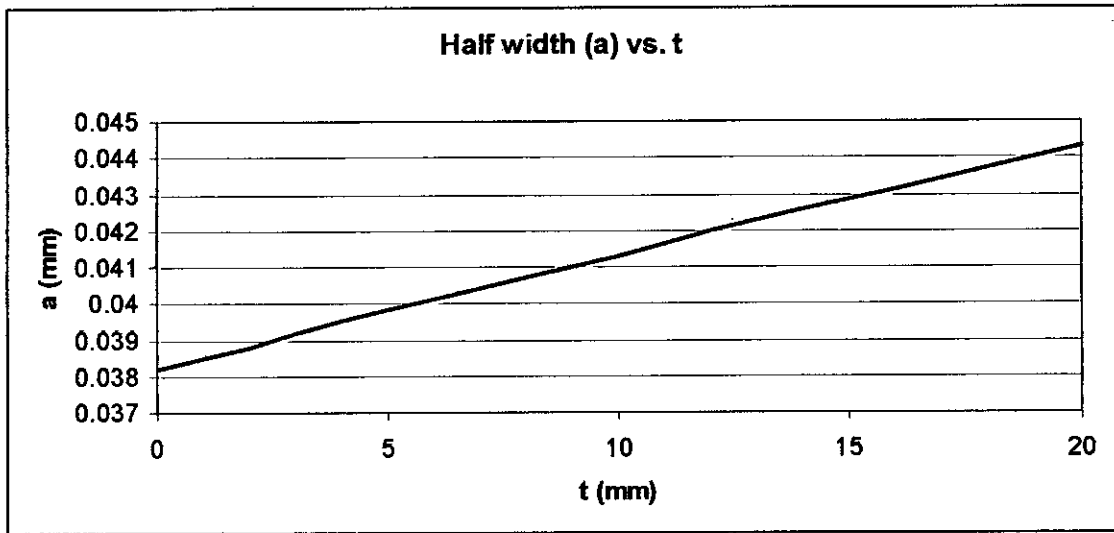
Figure 4.30.1: Half width vs. length (vertex angle 5°)
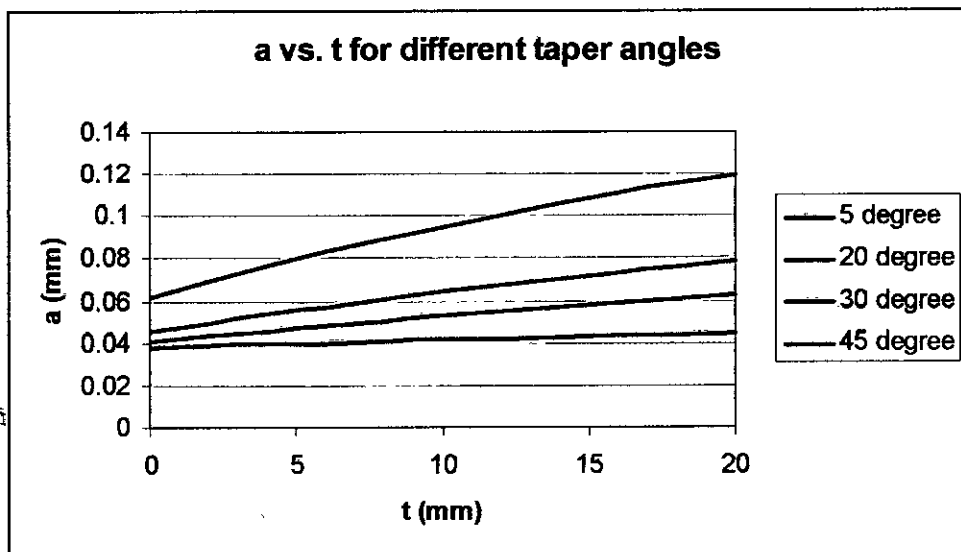
Figure 4.30.2: Half width vs. length for different vertex angle (Steel)
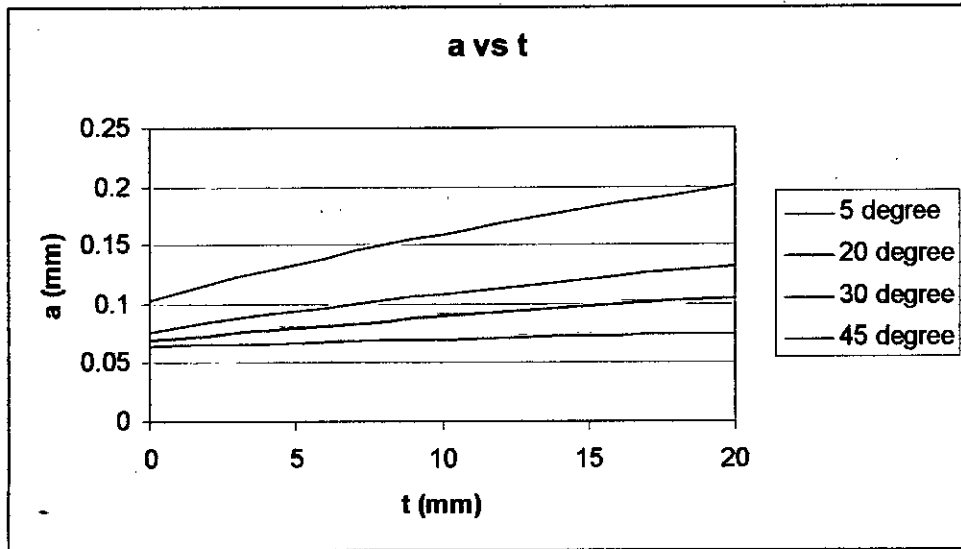
Figure 4.30.3: Half width vs. length for different vertex angle (Aluminum)
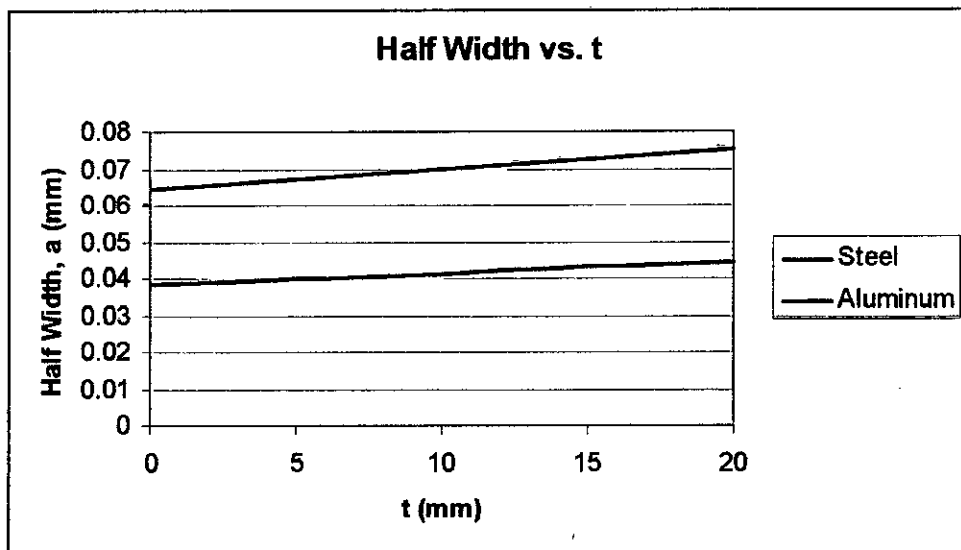
Figure 4.30.4: Half width vs. t for different materials (vertex angle 5°)

4.7 Maximum Pressure Distribution

As pressure distribution is assumed as Hertz Pressure distribution. So, it's distribution is elliptical with a maximum pressure. The distribution of maximum pressure along with different length has been shown from figure 4.31.1 to 4.31.4. It shows that the maximum pressure drops with increasing of length. And from distribution of

maximum pressure for different vertex angle we have seen that for $5°$ it has maximum value and it decreases with increasing of vertex angle.
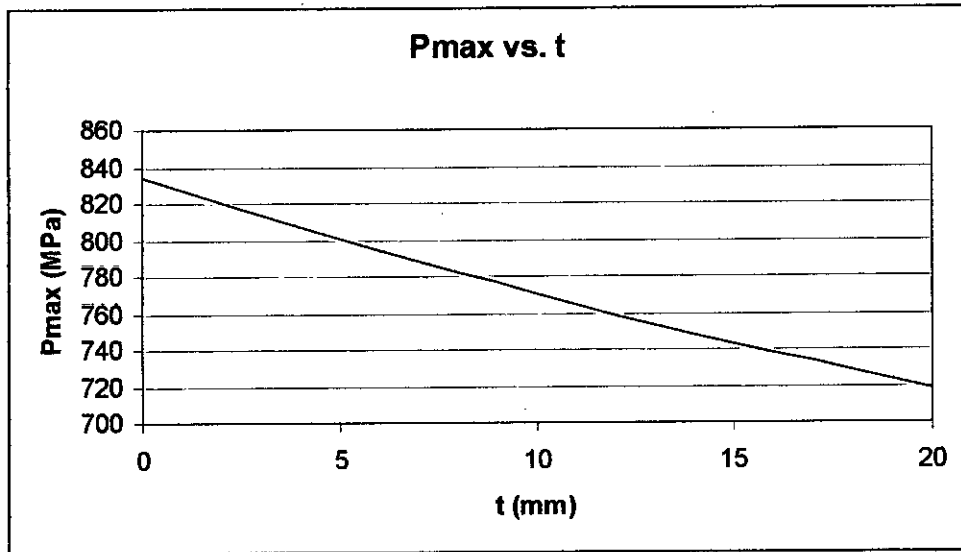
Figure 4.31.1: Maximum Pressure vs. length
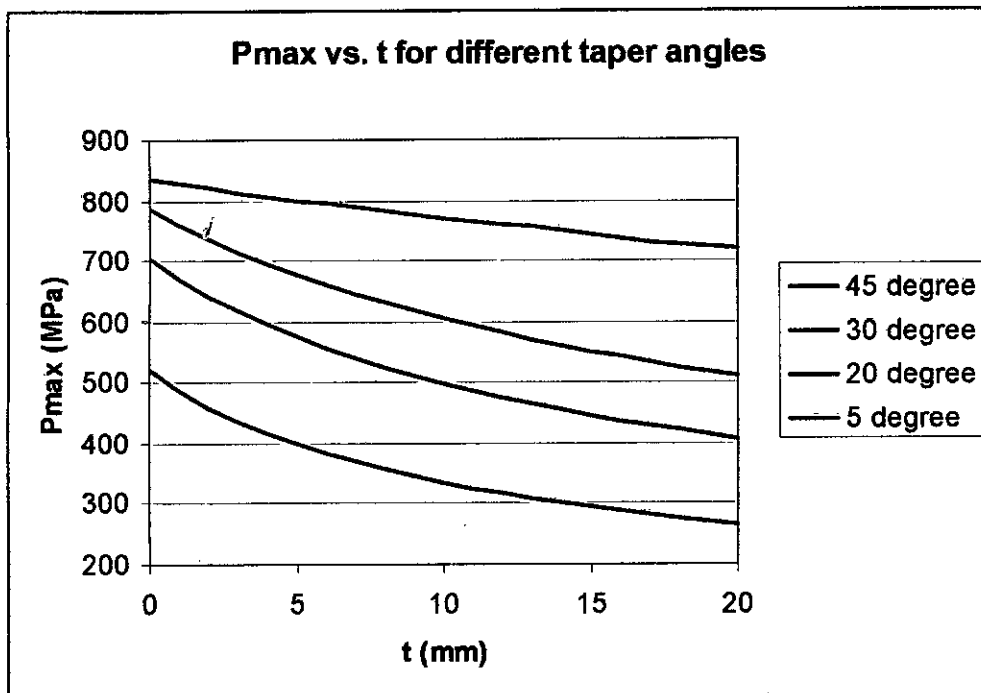
Figure 4.31.2: Maximum Pressure vs. length for different vertex angle (Steel)
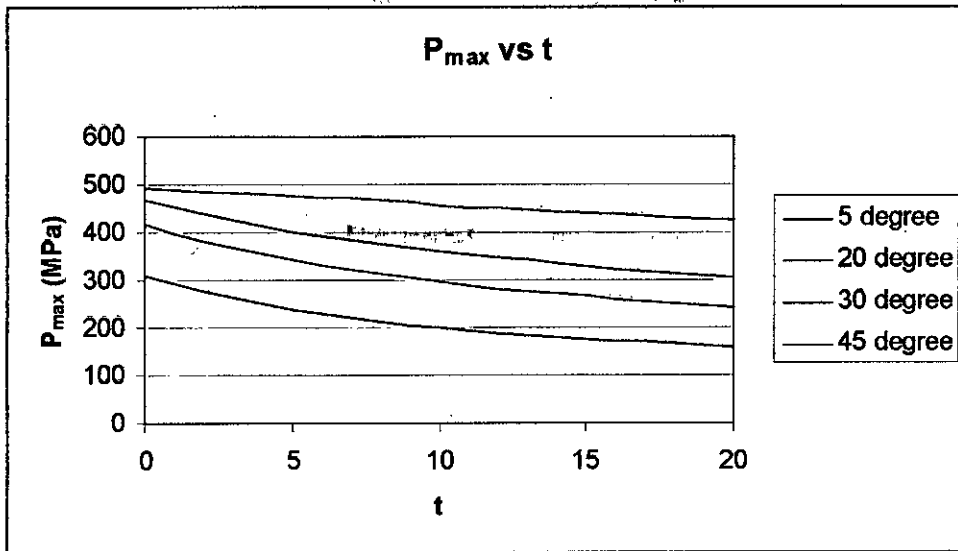
Figure 4.31.3: Maximum Pressure vs. length for different vertex angle (Aluminum)
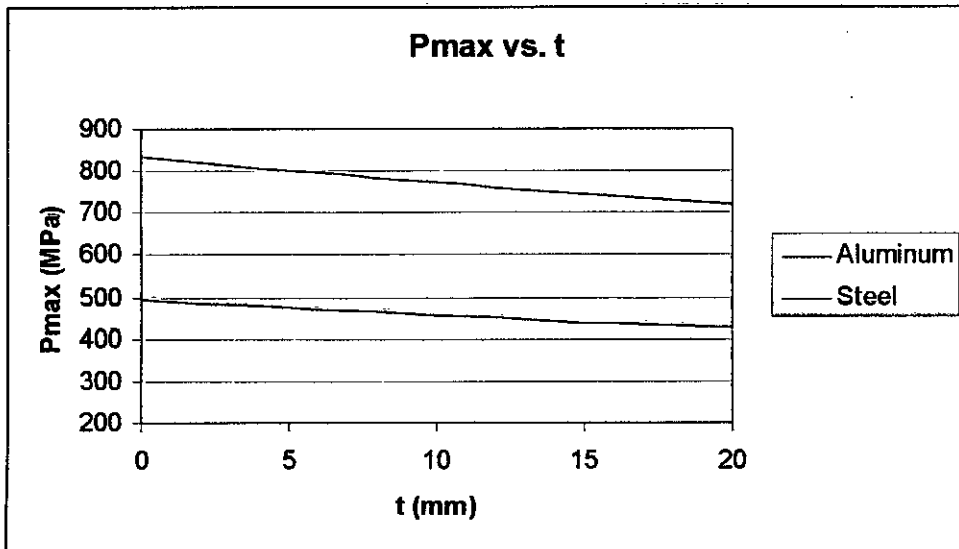
Figure 4.31.4: Maximum Pressure vs. length for different materials

(5° vertex angle)

4.8 Validation of results

To verify numerical results commercially available software has been used. The results those have been obtained from ANSYS are very close numerical solutions. Stress components in each direction are almost same with that of numerical results. The comparison of the results have been shown from figure 4.37 to 4.40.
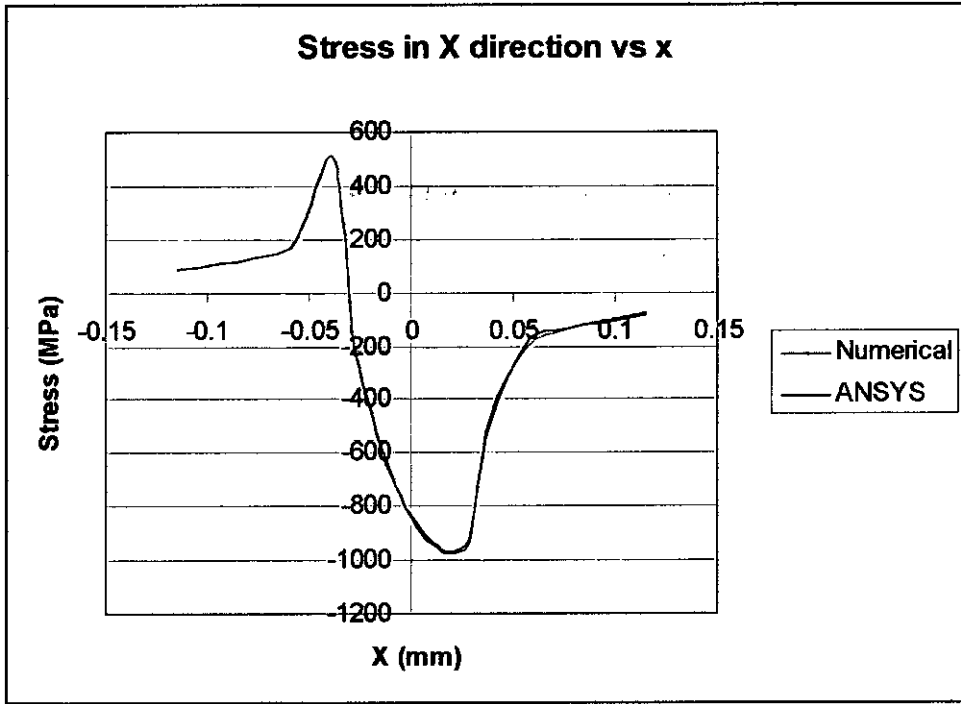
Figure 4.32.1: Comparison of stress in x direction vs x at t = 0*l* and vertex angle =5°
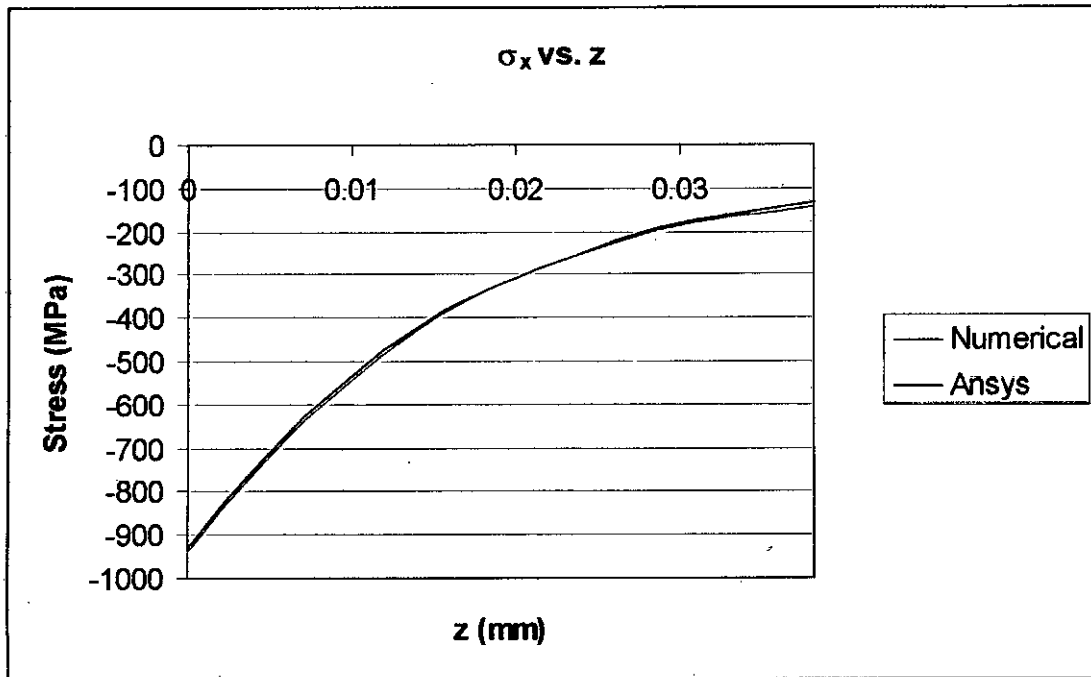
Figure 4.32.2: Comparison of stress in x direction vs z at t = 0*l* and vertex angle =5°
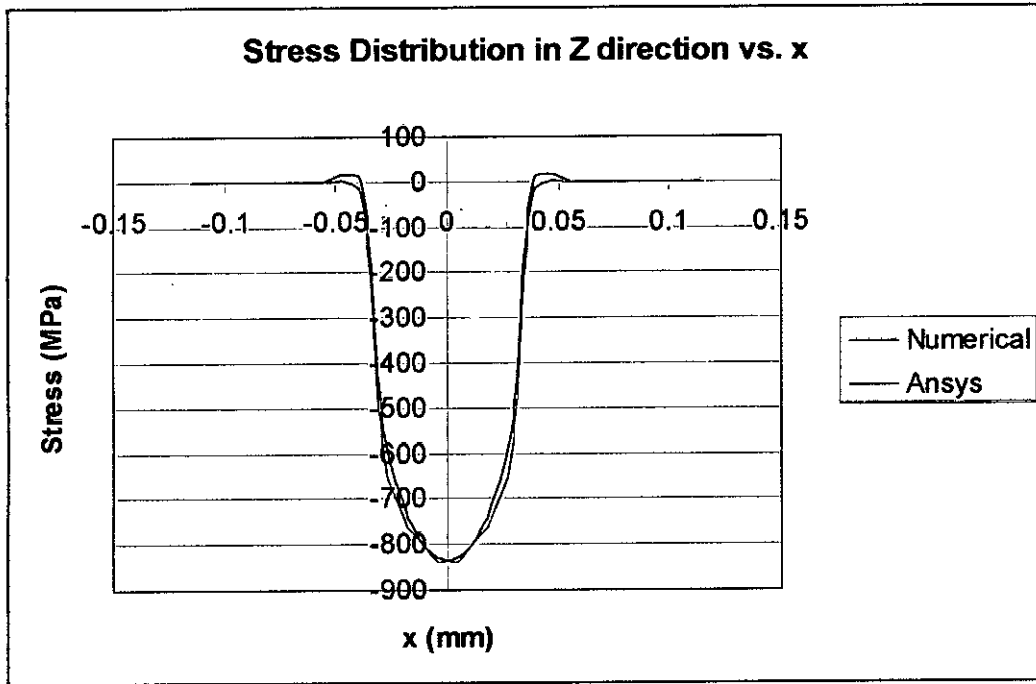
Figure 4.32.3: Comparison of stress in z direction vs. x at t = 0l and vertex angle =5°
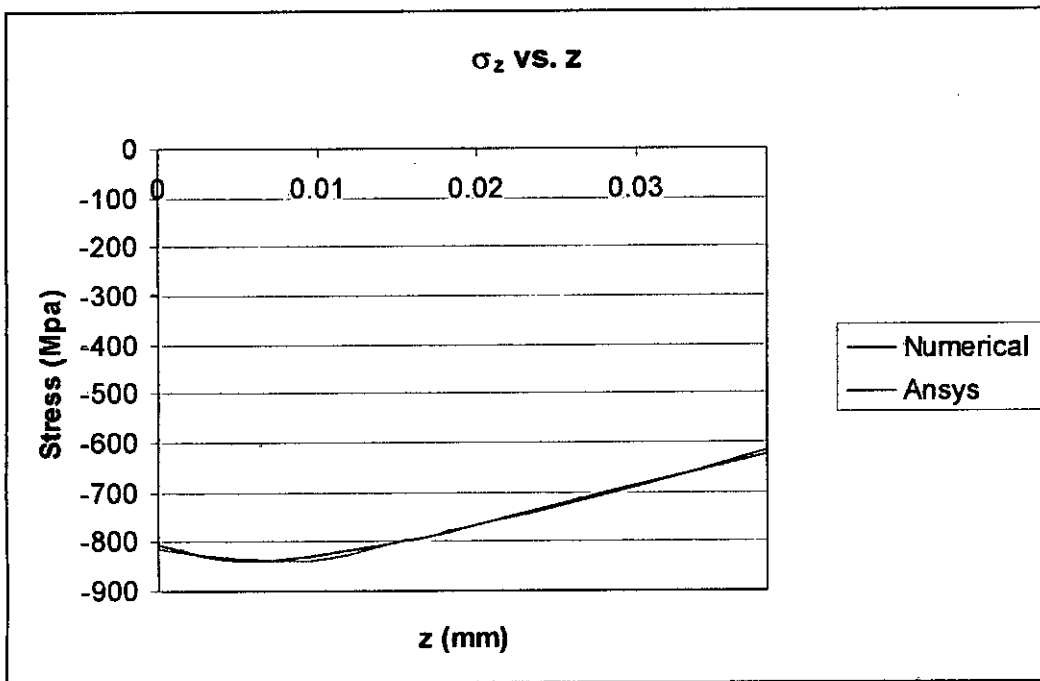
Figure 4.32.4: Comparison of stress in z direction vs. z at t = 0l and vertex angle =5°
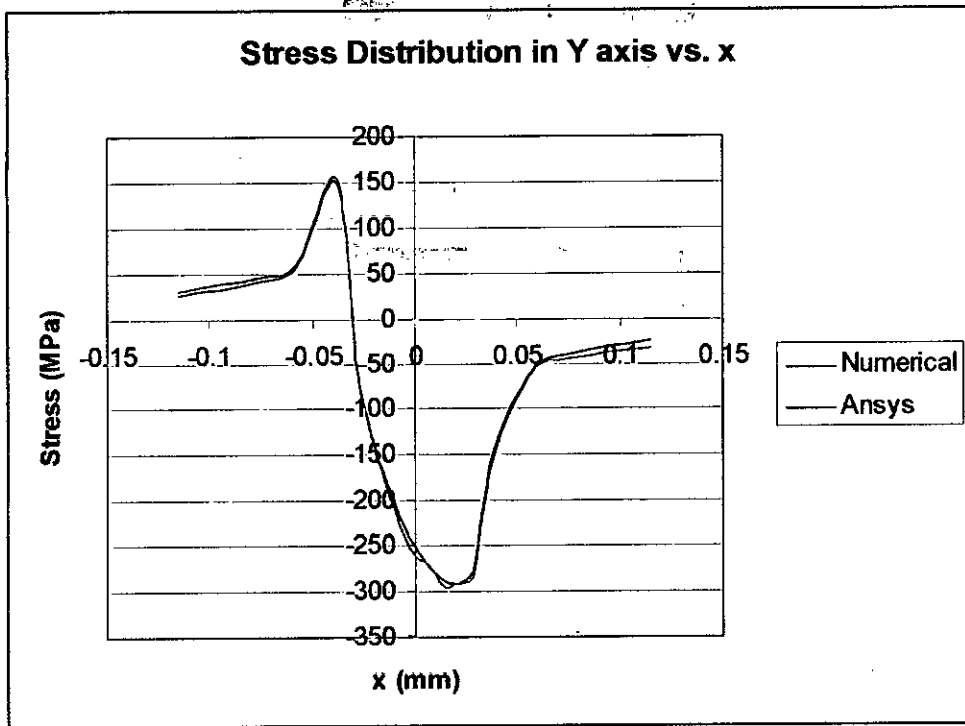
Figure 4.32.5: Comparison of stress in Y direction vs. x at t = 0l and vertex angle =5°
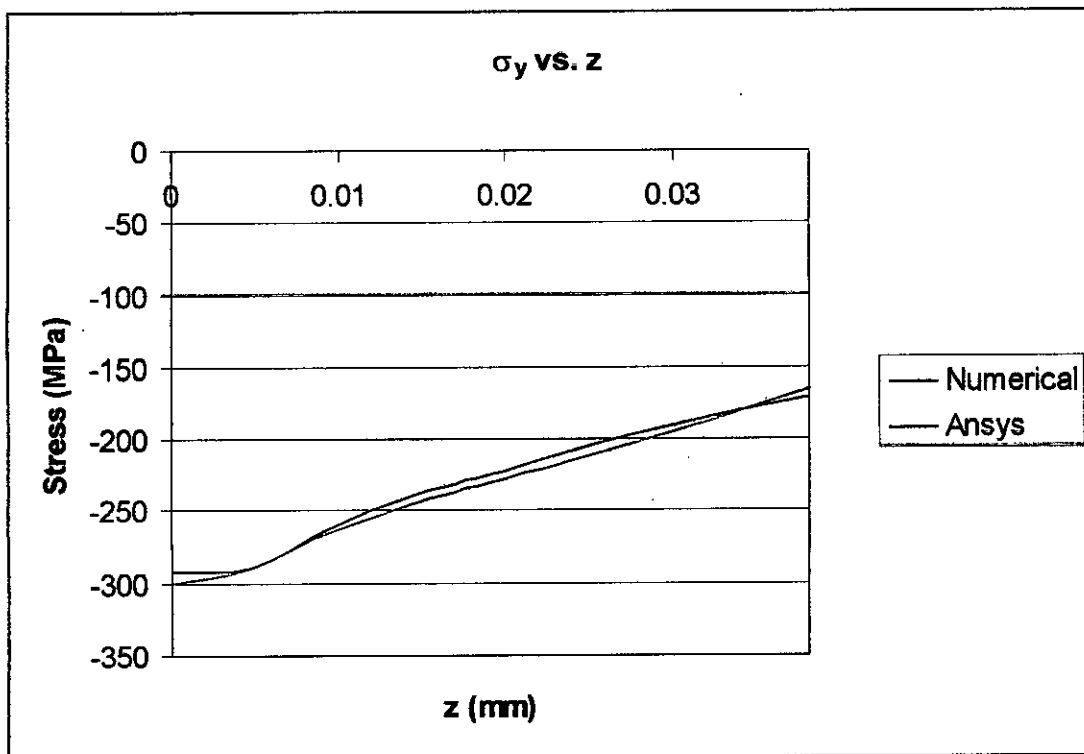
Figure 4.32.6: Comparison of stress in Y direction vs. z at t = 0l and vertex angle =5°
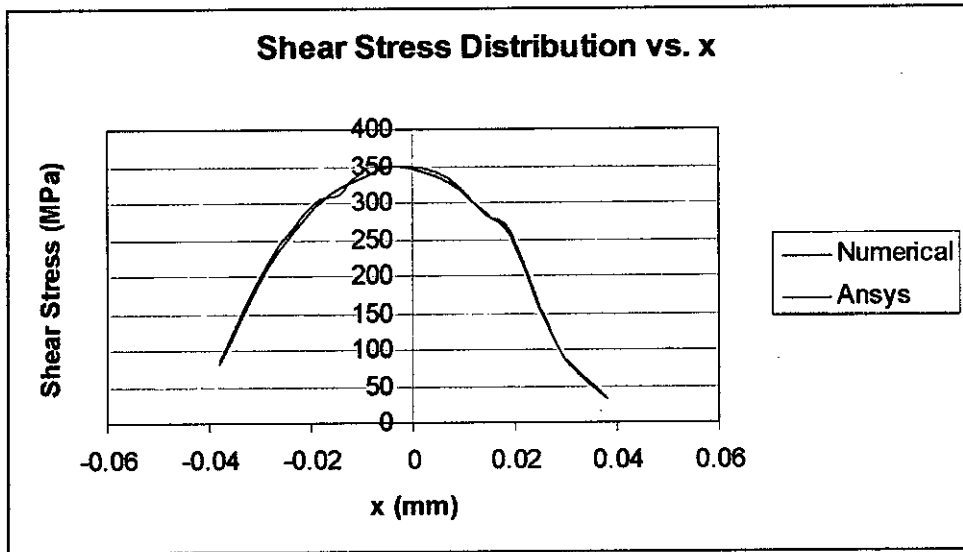
Figure 4.32.7: Comparison of Von Mises shear stress vs X at t = 0l and
vertex angle =5°
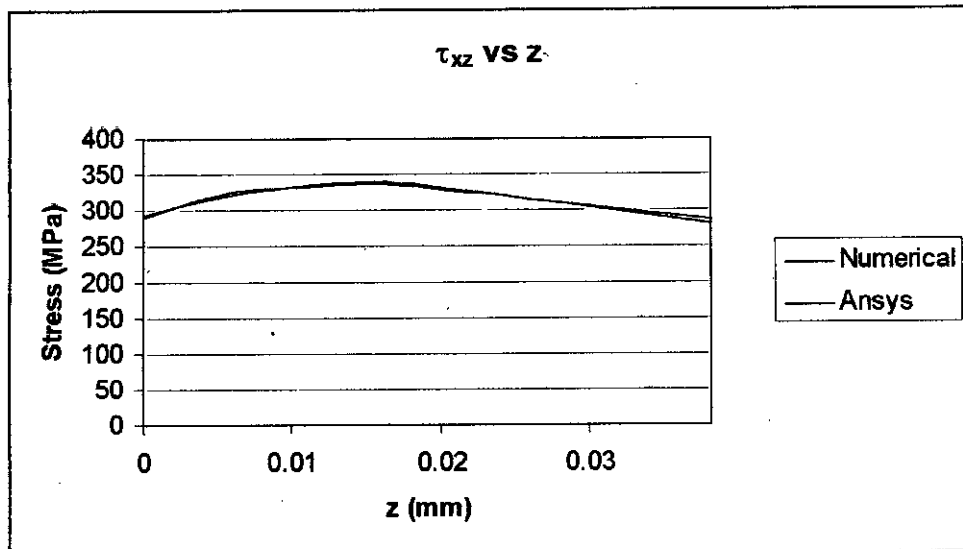
Figure 4.32.8: Comparison of Von Mises shear stress vs z at t = 0l and
vertex angle =5°

CHAPTER FIVE

CONCLUSIONS AND FURTHER RECOMMENDATIONS

5.1   General

Contact problems are very common in mechanical engineering design. Research on complex geometries like conical rollers in contact will offer more accurate results on stress fields among different engineering assemblies and contact. Through this work, by considering complex geometries rather than simple geometries, new researches on these complex geometries will be started. In this chapter, the summary of the present work with important conclusions have been stated. Also some recommendations have been passed forward for future works.

5.2 Conclusions

In this article we will discuss about the summary of the overall work in concise form as well the contribution of the present work

5.2.1 General Conclusions

♦ For simple geometries like sphere to sphere contact, cylinder to cylinder contact or cylinder to plane contact, the contact area or deformed area is either circular or rectangular based on type of contacts. But in present case, where two conical rollers are in contact, the deformed area is trapezoid. As for a rectangular half width is constant with respect to line of symmetric over the entire length. But in case of a trapezoid the half width is not constant over the entire length. So half width varies with distance (from smaller end) and vertex angles.

♦ In case of simple geometries the radius of curvature is constant through out the analysis. But for conical rollers in contact, the radius of curvature is not constant over the entire length. It varies with a function of vertex angle and distance (from smaller end). For analysis of varying radius of curvature a numerical technique has been used for iteration at each step of entire length.

♦ Stress fields in the contact area have been investigated by numerical technique. The stress components have been shown with different contact geometries. The numerical results have also been compared with the results from Ansys.

5.2.2 Contribution of this thesis

The results obtained from numerical technique have been considered as the contribution of this thesis. The numerical results have been also compared with ANSYS and have found that results from numerical technique are more consistent with that from ANSYS. The results are summarized below

♦ Stress distribution for X axis (σ_x) in case of normal loading has a maximum stress ratio i.e. σ_x / P_{max} is -1. It means the stress is compressive and maximum stress has a value same as maximum pressure. The maximum stress has been found at contact surface i.e $z/a=0$ and at $x/a = 0$ i.e. at line of symmetry. For the case of tangential loading, the distribution is linear. In leading edge i.e. where rolling starts, the stress type is compressive and in tailing edge it's type is tensile. The maximum stress ratio occurs at contact surface i.e. $z/a= 0$ and a value of 0.6. In leading edge it has been found compressive at $x/a=1$ i.e. where contact begins. In tailing edge it has been found tensile at $x/a= -1$ i.e. where contact ends. For combined loading, the maximum stress has been found at contact surface i.e. $z/a=0$ and it has been found at $x/a=0.5$ distance towards the leading edge with a value of -1.167. So in case of combined loading stress component in X direction has a value 16.7% higher that for normal loading and has been found 50% shifted towards the leading edge from symmetry.

♦ σ_x varies along the contact length. With increase of the distance from the apex of the roller σ_x decreases. The variation of stress between apex and larger end of the conical roller is 13.8% i.e. at the apex of the cone the stress is 13.8% higher than that at the large end. The stresses have been considered for combined loading. The stresses decrease along the length due to decrease of maximum pressure along the contact length. As stress components are related to maximum pressure P_{max}.

♦ For different vertex angle σ_x also varies. As there were four models with four different vertex angle. For vertex angle $5°$, σ_x has maximum value among four

model. The value of stress components (σ_x) decreases with increase of vertex angle orientation. Value of σ_x decreases about 5% with increase of 15° vertex angle from 5°. But this rate of decrease is higher with high vertex angle. With variation of 40° vertex angle stresses decreases up to 35% for same value of load.

♦ Stress components in Z direction (σ_z) for normal loading have distribution like the pressure distribution according to Hertz theory. The stress ratio is σ_z/P_{max} is -1 at z=0 and x/a=0 i.e. stress is compressive and it has been found at contact surface (z=0) and axis of symmetry (x/a=0). For tangential loading its distribution is linear along with X axis. For case of tangential loading compressive stresses have been found in the leading edge of rolling. On the tailing edge it has been found tensile stress. The maximum value of stress ratio for the case of tangential loading is .072 i.e. very negligible in compare with normal loading. So, for combined loading the distribution is almost like stress distribution for normal loading. In case of combined loading the stress ratio is -1 and it has been found as like as normal distribution i.e. at contact surface and in the line of symmetry of pressure distribution.

♦ From variation of σ_z vs. length of contact we can conclude that with increase of contact length from apex of the cone, value of maximum stress decrease. It decreases up to 14% (almost same value as that for σ_x) for combined loading.

♦ With variation of vertex angle σ_z also varies. For low vertex angle the σ_z is high. It decreases with increase of the vertex angle. For increasing 15° vertex angle it's value decrease up to 5% and for vertex angle variation of 40° stress decreases up to 25% in case of combined loading.

♦ Stress components in Y axis i.e. σ_y have been found from plane strain principle. For this case combined stresses have been considered. The stress ratio i.e. σ_y/P_{max} has a maximum value of -0.349 and it has been found at contact surface i.e. at z=0 and at a distance of x/a = 0.50 towards leading edge of the contact.

♦ From the variation of σ_y along the contact length we can conclude that like other two components of stress, this component also decrease with increase of contact length. The variation of stresses for combined loading between tip and end of the contact is up to 14.4%.

- For the case of contact problems, the main cause of the initiation and propagation of crack or cracks is the maximum value of shear stress. In this present work to predict maximum shear stress Von Mises Maximum Shear Stress principle has been used. The maximum value as well as location of that peak value is important. From this work, dor the case of combined loading we have found that the peak value of shear stress ratio i.e. ratio of maximum shear stress and maximum pressure is 0.39 which is 7.6% higher than that for only normal loading. For conical roller contact stress, the only researcher Al Zain has found for normal loading the value of stress ratio is 0.36. The location of the maximum shear stress has been found at $x/a=0$ i.e the line of symmetry and at $z/a=0.30$. Al Zain has found this value of 0.375. So from this two works it can be found that for combined loading the location of the maximum shear stress is 20% less deep from contact surface.

- Shear stress distribution varies along contact length. With increase of contact length value of maximum shear stress decreases. So, the apex of the cone is very critical for crack initiation or propagation. Similarly for low vertex angle shear stress has maximum value. Thus with low vertex angle and at the tip shear stress has maximum value.

- The stress distribution has higher value for steel than that for aluminum. The reason behind this is, the half width has higher value for aluminum. it means with application of load, the deformation in aluminum is higher that than for steel. So stress components at the contact surface and underneath of the contact surface are lower.

- Verification of numerical results has been done by using ANSYS. The results obtained from ANSYS have been found consistent with that of numerical results.

5.3   Further Recommendations

- In this work, only static normal loading has been considered. But fatigue loading and harmonic loading are sometimes seen in case of contact problems. So in future work, loads of these types may be in consideration.

- During contact there occurs some heat generation. So, contact geometries may be changed due to this heat generation. At that time the analysis will not be linear. It

120

will be non linear and hence non linear material properties should be given as input. So consideration of heat generation will be a good point for further research.

- In this work, very low sliding has been considered. If large sliding was considered then the problem would be more difficult, because at that time there was not simple relationship between normal and tangential loading.

- Both mating materials are same. That's why normal pressure distribution and half width dimension has not been altered. But if two materials are different then, the contact geometries will be changed. So, it may be another good point for further development of this work.

References and Bibliography

[1]   **Hertz, H**. Gesammelte Werke, Band I, 1895 (Basth, Leipzig) (English transl. Hertz J, H Miscellaneous papers, 1896 (Macmillan, London)

[2]   **Lunderberg, G.** Elastiche Beruehrung Zweier Halbraeume Forsch. Geb Ingenieurwesens A, 1936, 10, 201-211

[3]   **Smith, J.O. and Liu, C.K.** , Stresses due to tangential and normal loads on an elastic solid with application to some contact stress problems. Trans. ASME J. Appl. Mechanics, 1953, 75, 157-166

[4]   **Al-Zain, H.O.** Contact stresses in conical shaped rollers. Masters thesis, Department of Mechanical Engineering, Iowa State University, 2004.

[5]   **Ali M, Shakoor M, Fluggrad D and Qamhiyah** A. Cam optimization based on a fatigue life model. In proceedings of ASME 2006 International Design Engineering Technical Conferences and Computer and Information in Engineering Conference, Philadelphia, Pennsylvania, USA, 2006, pp 1- 8 (American Society of Mechanical Engineers, Newyork).

[6]   **Litvin, L. E. Fuentes A. and Hayasaka, K**. Design manufacture, stress analysis and experimental test of low noise high endurance bevel gears. Mechanism Mach Theory, 2006 41(1), 83 -118

[7]   **Borodich, F. M**. Hertz Contact Problem For Elastic Anisotropic Halfspace with Initial Stress, Plenum Publishing Corporation, 1990, 126-132.

[8]   **Timoshenko, S. and Goodier**, J. N., Theory of Elasticity, 3rd Ed., McGraw-Hill Book Company, New York, N. Y., 1979.

[9]   **Budynas, R. G.**, Advanced Strength and Applied Stress Analysis, 1979, McGraw-Hill, New York.

[10]   **Shigley, J.E.**, Mechanical Engineering Design, First Metric Edition, McGraw-Hill, New York

[11]   **Johnson, K. L.** Contact Mechanics, 1985 (Cambridge University Press)

[12]   **Robert D. Cook.** Finite Element Modeling for Stress Analysis, 1994, John Wiley and Sons, INC

[13]   **Norton, R. I.** Machine Design: an integrated approach, 3rd Edition, 2006 (McGraw-Hill, New York)

[14]   **ANSYS** user's manual, Version 10.0 , 2007